



## Part B

# Benchmarking of aerodynamic and aeroelastic models

## Contribution to deliverable 2.21

Agreement no.:	308974
Duration	60 months from 1st November 2012
Co-ordinator:	Mr Peter Hjuler Jensen
Supported by:	EU 7th Framework Programme

Support by:



---

### PROPRIETARY RIGHTS STATEMENT

This document contains information, which is proprietary to the "INN WIND.EU" Consortium. Neither this document nor the information contained herein shall be used, duplicated or communicated by any means to any third party, in whole or in parts, except with prior written consent of the "INN WIND.EU" consortium.

---

## Document information

<b>Document Name:</b>	Part B: Benchmarking of aerodynamic and aeroelastic models
<b>Confidentiality Class</b>	PU
<b>Document Number:</b>	D2.21 Benchmarked aerodynamic-structural design methods
<b>Editors:</b>	Vasilis Riziotis, Dimitris Manolas, Leonardo Bergami, Georg Pirrung, Helge Aagaard Madsen, Alessandro Croce, Miquel Rura, Carlos Pizzaro De La Fuente, David Gimenez
<b>Review:</b>	Flemming Rasmussen
<b>Date:</b>	June 2015
<b>WP:</b>	WP2 LIGHT WEIGHT ROTOR
<b>Task:</b>	Task 2.1: Aerodynamic concepts for high speed, low solidity offshore rotors

## TABLE OF CONTENTS

TABLE OF CONTENTS .....	3
SUMMARY OF CONCLUSIONS .....	4
INTRODUCTION .....	5
CODE TO CODE COMPARISON RESULTS .....	6
1.1    Isolated blade model validation. ....	6
1.1.1    Modal frequencies and shape validation. ....	6
1.1.2    Static load cases .....	13
1.2    Rotor aeroelastic validation.....	29
1.3    Full wind turbine aeroelastic validation .....	37
1.3.1    Step-up and step-down cases .....	37
Time series: stiff WT step-up case.....	44
Time series: stiff WT step-down case .....	46
Time series: flexible WT step-up case .....	48
Time series: flexible WT step-down case.....	55
Time series statistics vs. wind speed .....	62
Time series: flexible WT step-up case .....	69
Time series: flexible WT step-down case.....	75
1.3.2    Turbulent wind cases at 8m/s (Mann model) .....	81
1.3.3    Turbulent wind cases at 8m/s and 18m/s (Veers mode) .....	103
BIBLIOGRAPHY.....	112

## SUMMARY OF CONCLUSIONS

In view of supporting design activities towards large wind turbines and acquiring more confidence in the simulated results, a cross comparison of state-of-the-art aeroelastic tools is performed within the INN WIND.EU project. The results of this cross comparison activity are presented herein. The comparison concerns the 10 MW scale Reference Wind Turbine (RWT) designed by DTU at a size beyond the current commercial scale. Aiming at identifying possible shortcomings, variants of the standard modeling context are tested. In addition to Blade Element Momentum (BEM) aerodynamics, elaborate wake models are considered while for the structural part different multi-body representations of the blade and a generalized Timoshenko beam model are cross checked.

The load case matrix consists of eigenvalue calculations considering the straight isolated blade, static calculations at which a flapwise load or a twisting moment are applied, time domain aeroelastic simulations of the isolated rotor and time domain aerodynamic and aeroelastic simulations for the prebent rotor considering either a step up and a step down ramp of the uniform wind or a turbulent inflow.

With respect to mode results, all aeroelastic tools (Timoshenko beam models) are found to compare well to NISA 3D FEM up to the seventh mode. Strong coupling effects are consistently predicted and a fair overall agreement is obtained. The beam models predict a similar torsion mode, but compared to the 3D FEM the torsion angle as well as the coupled flapwise component are underpredicted.

In the static calculations considering a flapwise load, the bending-torsion geometric nonlinear effect is triggered due to the high flapwise deflections (about 10% of the blade length). In general good agreement is found. Out of the different sensors chosen, the torsion angle has the highest uncertainty (about  $0.2^\circ$  at the tip). In the twisting moment static case the overall agreement is good.

The overall agreement in the step up and step down cases is good. The tower top moments and especially the yawing moment as well as the blade root pitching moment and the torsion angle are the sensors with the highest differences.

The agreement in the turbulent inflow conditions is considered satisfactory. In the stiff rotor results, the deviations are due to the wake dynamics. Cylindrical wake modeling in BEM is found to over-filter the response compared to more elaborate ones while free wake results are in between. In the fully coupled cases, in open loop operation significant deviations are seen in the 1P & 2P flapwise responses which are attributed to the different dynamic inflow modeling. When the controller is switched on, the agreement in the flapwise predictions slightly improves which is attributed to the controller. In the same case the 2<sup>nd</sup> symmetric edgewise mode is differently predicted, probably due to different modeling of the bending-torsion coupling.

## INTRODUCTION

The up-scaling of modern turbines towards the 20 MW size, a target set by the wind community (Sieros, 2012) in the past years, imposes weight requirements for the blades and calls for improved aerodynamic performance of the rotor with the aim to balance subsequent increase in costs for example of the tower and the underwater support structure. The design of innovative large scale, flexible, low induction rotors that comply with the reduced weights and optimized aerodynamic performance requirements is the main focus of Work Package 2. In this framework and with the aim to evaluate the new innovative concepts in terms of specific performance indicators (PI) a number of state-of-the-art aeroelastic design tools have been employed. A cross comparison of these tools is performed herein on the Innwind.eu reference 10 MW wind turbine (Bak, 2013).

Under WP2 of Innwind.eu project the targets of defining, assessing and demonstrating new innovative lightweight blade and rotor concepts have been set. These new concepts will integrate new aerodynamic and structural design opportunities as well as innovative control strategies for reduced loads and weights. New non-conventional airfoil shapes suitable of low induction rotors, light weight internal structures, passive and active control methods are some of the options investigated in the project. The ultimate goal is to evaluate these design options in terms of specific PIs and qualify the most promising ones for further investigation. This is done by means of state-of-the art aeroelastic tools. From the point of view of the structural analysis, such tools must be able to predict non-linear geometric coupling effects due to large deflections as the proposed designs are expected to be lightweight and therefore very flexible. Also they must be able to account for structural coupling effects due to structural tailoring of the inner structure as for example twist-bending coupling effect. On the other hand, from the point of view of the aerodynamics they must be able to handle new aerodynamic challenges stemming from the up-scaling of the rotor as for example dynamic inflow effects due to 1P excitation which in case of up-scaled rotors becomes more pronounced as the rotational frequency is getting closer to the frequency that the wind spectrum exhibits its maximum energy.

The structural part of the aeroelastic tools employed in the present work is based on Timoshenko beam modeling of the turbine components either formulated on a multi-body context (Larsen T J, 2004), (Bottasso, 2006-2015), (Manolas D.I., 2014) or through generalized Timoshenko approximations formulated with respect to the deflected (curved) elastic axis (Gérardin M., 2001). So, by definition the models can handle light-weight flexible structures. As concerns rotor aerodynamics, various Blade Element Momentum (BEM) type models are available as well as more advance free wake vortex models (Voutsinas, 2006) or prescribed wake hybrid models (Pirrung, 2014).

Structural and aerodynamic load predictions of the abovementioned tools are cross compared on a reference 10 MW wind turbine with the aim to identify possible shortcomings of the applied methodologies mainly in relation to the scale of the turbine analyzed.

## CODE TO CODE COMPARISON RESULTS

The code-to-code comparison work is divided into the following parts:

- a) isolated blade analysis,
- b) rotor aeroelastic analysis,
- c) full wind turbine aeroelastic analysis

Results from the following codes of different complexity are compared:

Code name	Institute	Code type
Cp-Lambda	PoliMi	Multibody
HAWC2	DTU	Multibody
hGAST	NTUA	Multibody
NEREA (GT)	GAMESA	Generalized Timoshenko
NEREA (modal)	GAMESA	Modal (Craig-Bampton)

**Table 1: Codes participating in the benchmark comparison.**

### 1.1 Isolated blade model validation.

In this part the validation of the isolated blade model is presented. Validation is based on the cross comparison of the results of different beam models as well as on the comparison against advanced 3D or shell FEM codes. In selected cases simulations for both the **straight** and the **pre-bent** blade are presented in order to highlight the effect of the blade prebending on the results.

#### 1.1.1 Modal frequencies and shape validation.

The predicted natural frequencies of the isolated blade are presented in Table 2 for vacuum conditions and zero structural damping. The frequencies are listed in order of magnitude from lower to higher values. They are compared against predictions from 3D FEM codes (Lekou & Chortis, 2013). It is noted that no torsion mode frequency and shape are provided by Cp-Lambda code, because this tool identifies the first torsion mode outside the range of frequencies presented in the table. GAMESA simulations have been performed with NEREA (GT). The agreement between the different beam codes is fair both comparing beam models but also in comparison to 3D FEM models. Overall 3D F.E.M models seem to predict slightly higher frequencies of the first five modes. Higher deviations are noted in the predictions of the second flapwise mode (mode 3). The shape of the second flapwise mode is presented in Figure 3 (CRES predictions). It is seen that all beam models underestimate the coupling with the torsion direction predicted by the 3D F.E.M model (NISA model, CRES predictions). Some high deviations are also noted in the frequency of the torsional mode (mode 6). The highest torsional frequency (6.60 Hz) is predicted by HAWC2 code. This is higher than the upper bound of the 3D FEM codes predictions. It is clear that at least three modes lie in the frequency range of [5-6.5 Hz] which indicates a strong coupling between directions of deflection in these modes. On the other hand, the abovementioned small deviations in the torsional mode do not affect the full wind turbine natural frequencies that are also provided in Table 3 for vacuum conditions and zero structural damping (presented also in version 1 of D 2.21).

The corresponding mode shapes are shown in Figure 1-Figure 8 (up to the 4<sup>th</sup> flapwise mode). The results of the different aeroelastic tools are compared against predictions of NISA shell type model

provided by CRES (Lekou & Chortis, 2013). Results for the straight blade are only presented in the sequel. This is because the available NISA mode shapes correspond to the blade without prebend.

Cross comparison of the different codes indicates:

- The edgewise modal displacement in the 1<sup>st</sup> flapwise mode (structural pitch coupling effect) is slightly underestimated by all beam models (Figure 1).
- Similarly the flapwise component is under-predicted in the 1<sup>st</sup> edgewise mode (Figure 2)
- NISA predicts a small torsion component in the 2<sup>nd</sup> flapwise mode which is not predicted by any of the beam models (see Figure 3).
- 2<sup>nd</sup> edgewise and 3<sup>rd</sup> flapwise modes are predicted well by all codes (Figure 4, Figure 5).
- In the 1<sup>st</sup> torsion mode NISA predicts higher torsion rotations all along the blade span, as well as a very strong flapwise component which is not predicted by any of the beam models (Figure 6).
- A relatively good agreement is obtained in the 3<sup>rd</sup> edgewise between beam models and NISA code. NEREA slightly under-predicts the edgewise displacement component. In fact NEREA predicts a higher flapwise component in the respective mode (Figure 7).
- Good agreement is also obtained in the 4<sup>th</sup> flapwise mode. Again NEREA seems to over-predict the edgewise displacement in the mode (Figure 8).

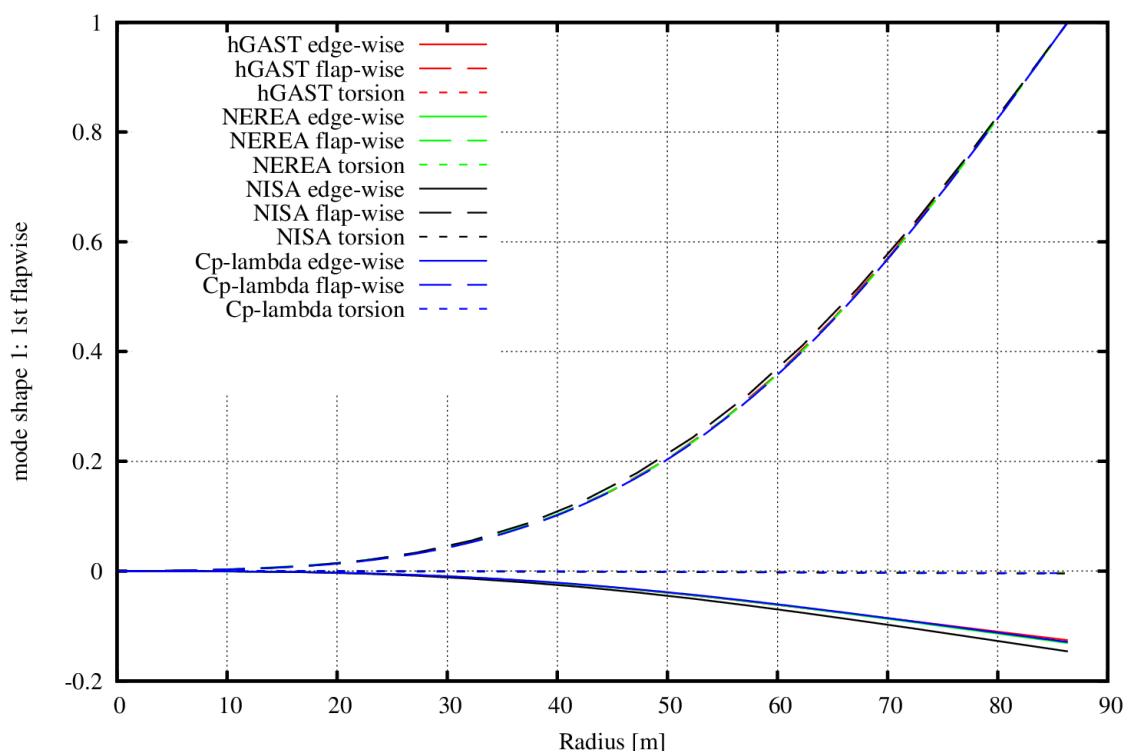


**Figure 1: Shape of the 1st flapwise mode – straight blade - normalized modal deflections, bending displacements [m/m] and torsion angle [rad/m]**

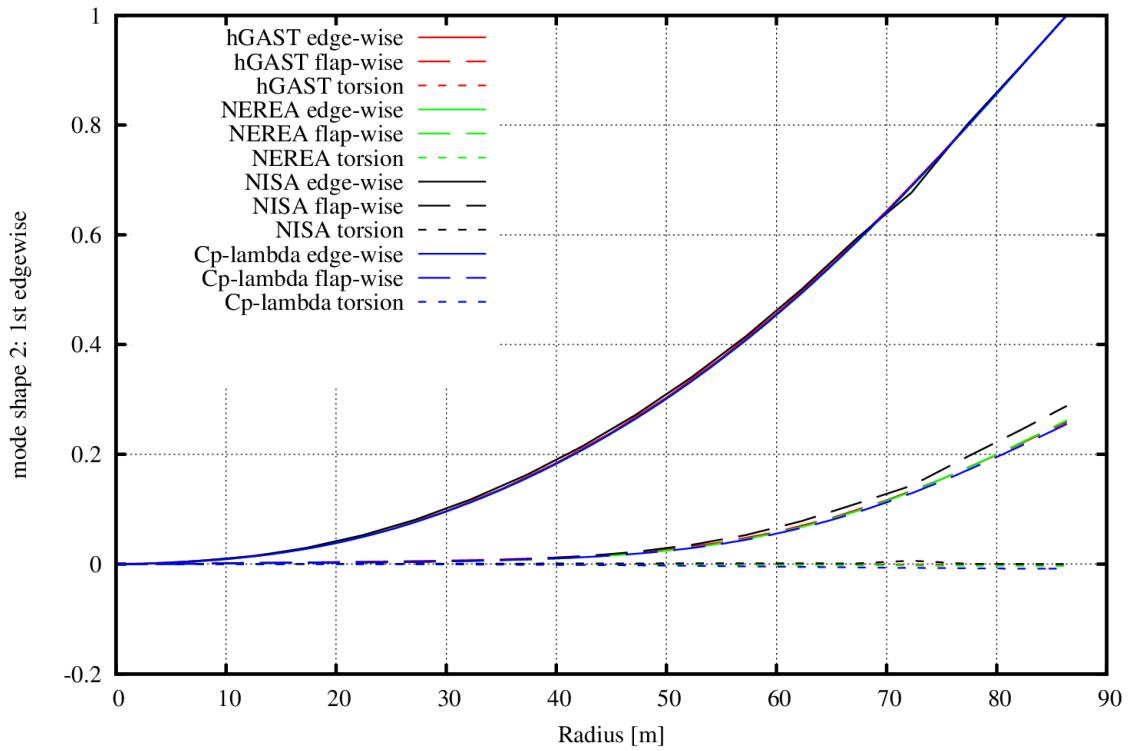


Figure 2: Shape of the 1st edgewise mode - straight blade

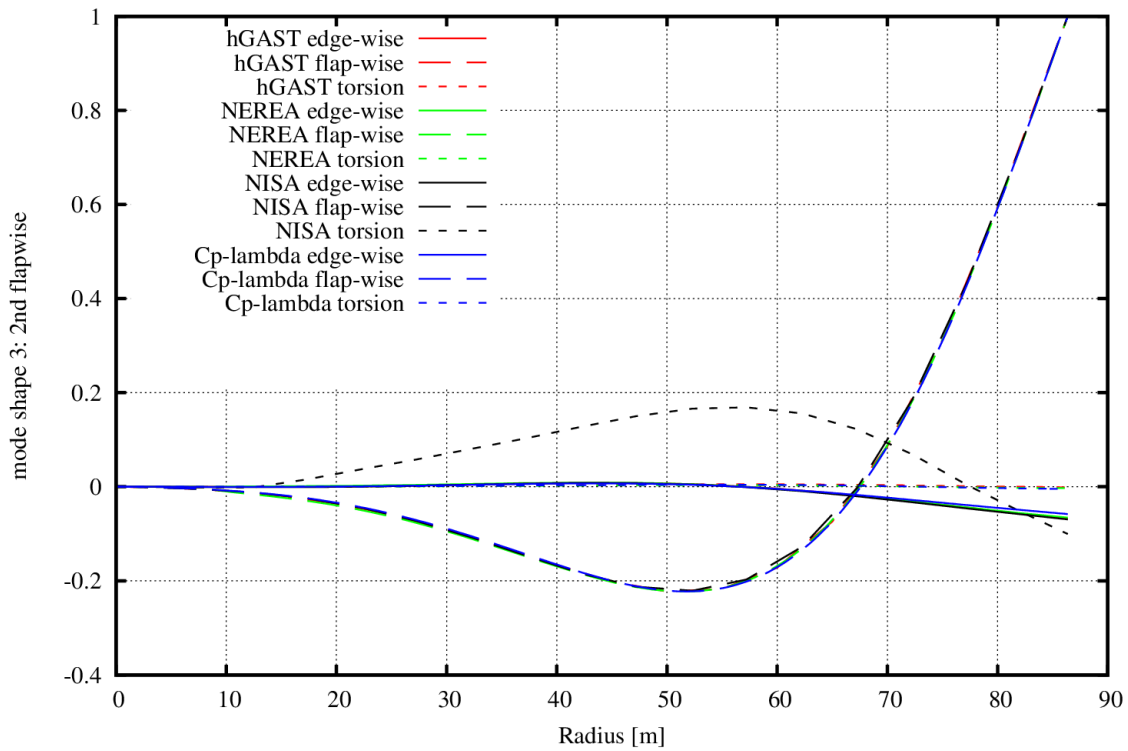


Figure 3: Shape of the 2nd flapwise mode - straight blade

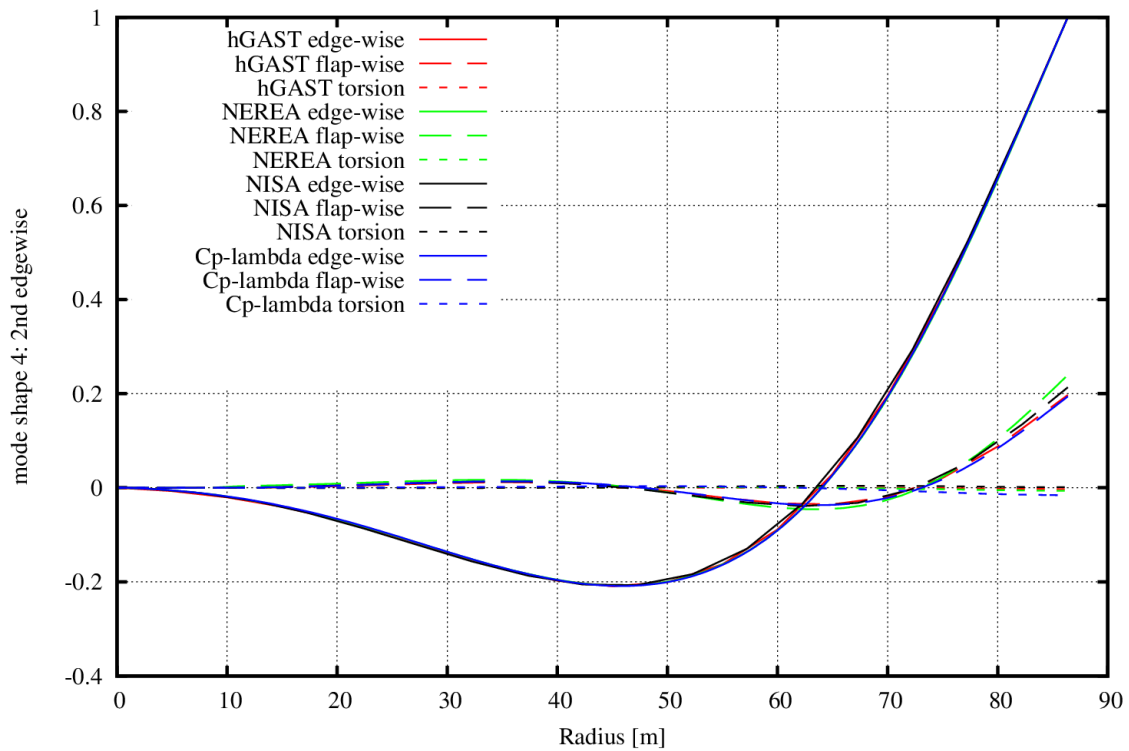


Figure 4: Shape of the 2nd edgewise mode – straight blade

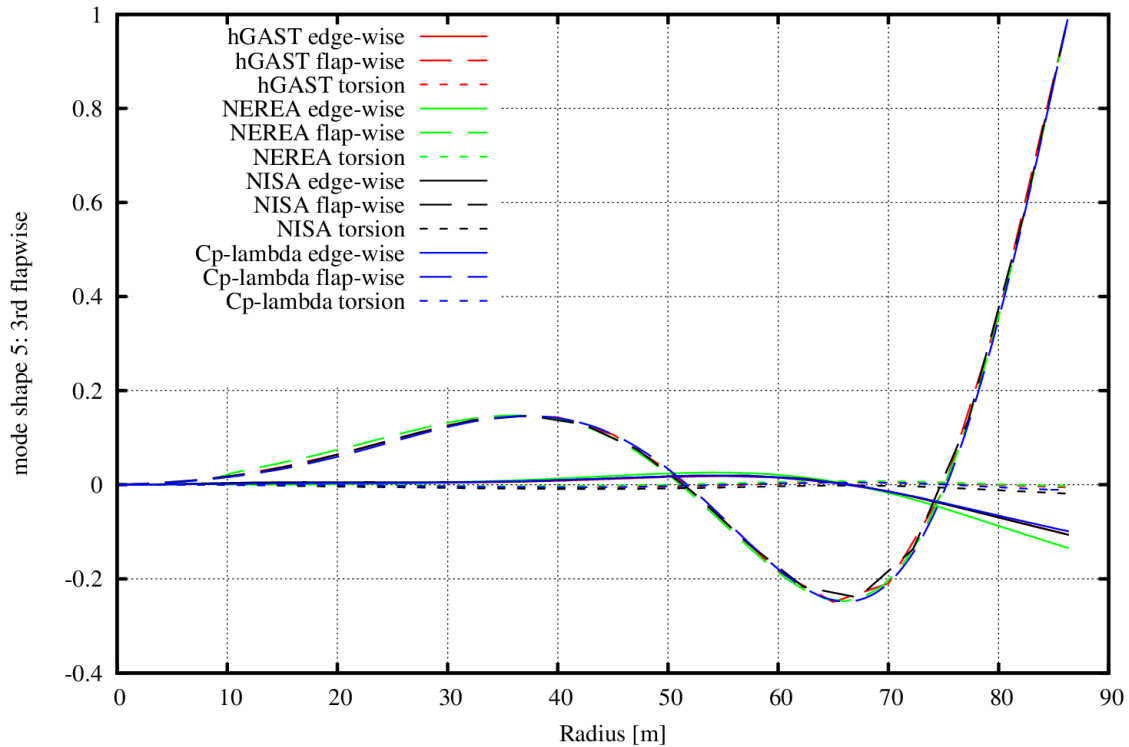


Figure 5: Shape of the 3rd flapwise mode – straight blade

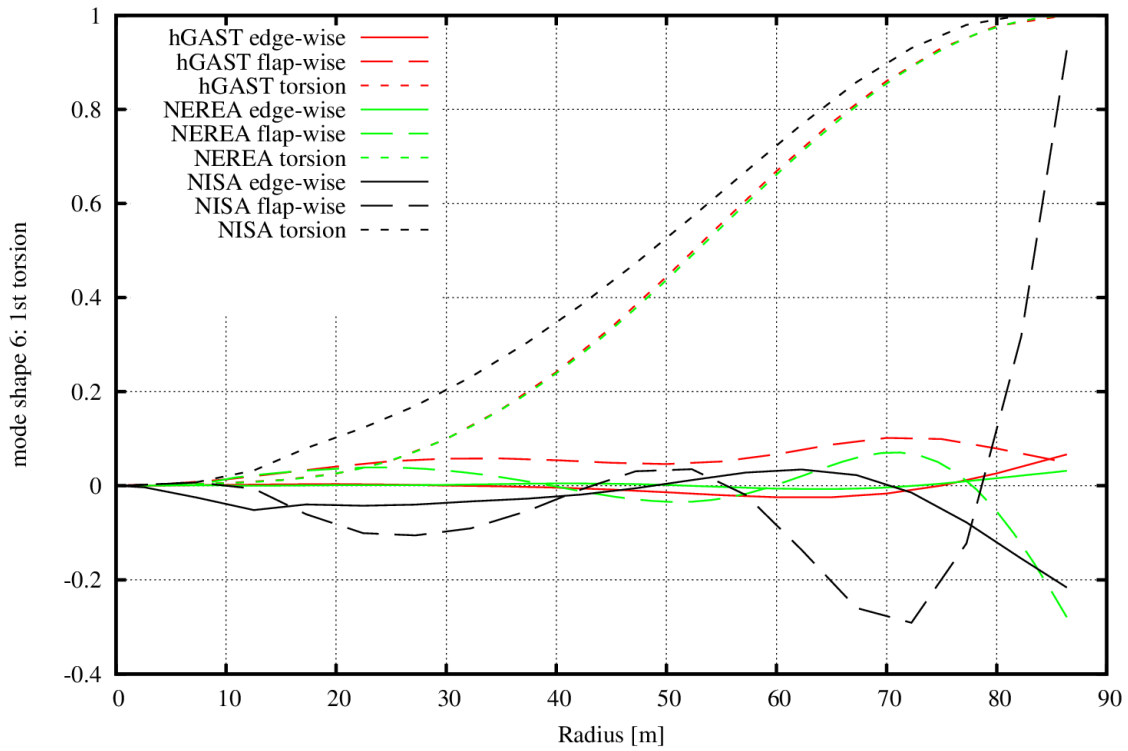


Figure 6: Shape of the 1st torsion mode – straight blade

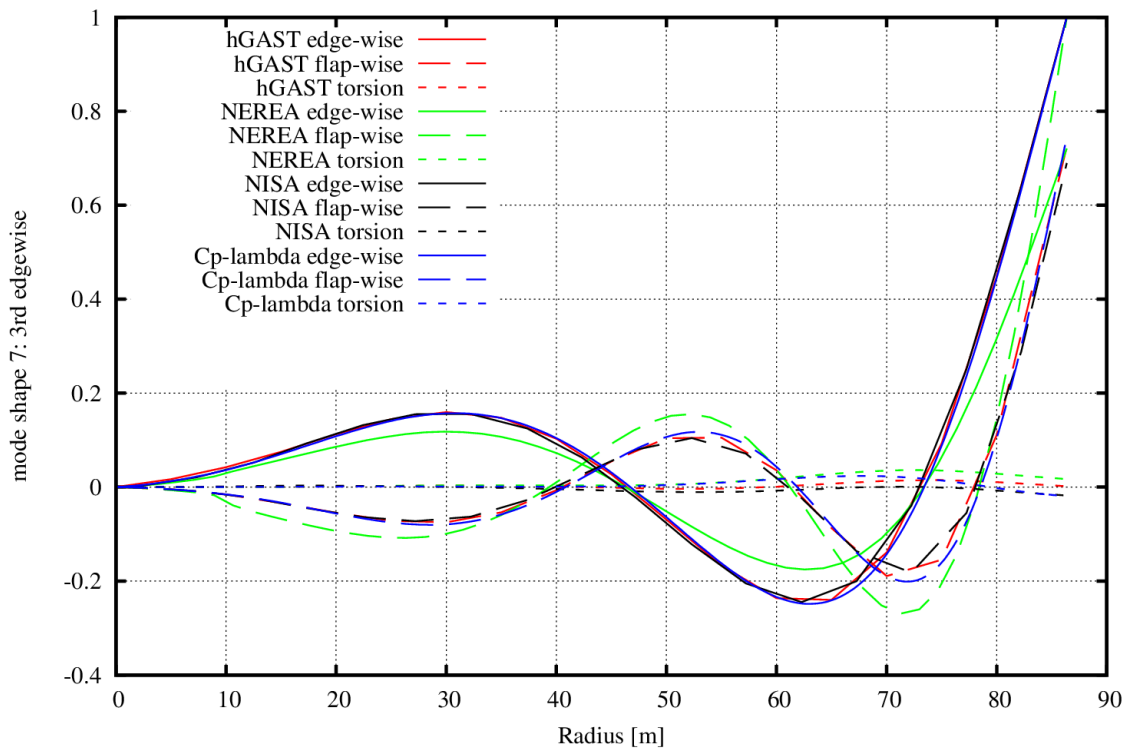


Figure 7: Shape of the 3rd edgewise mode – straight blade

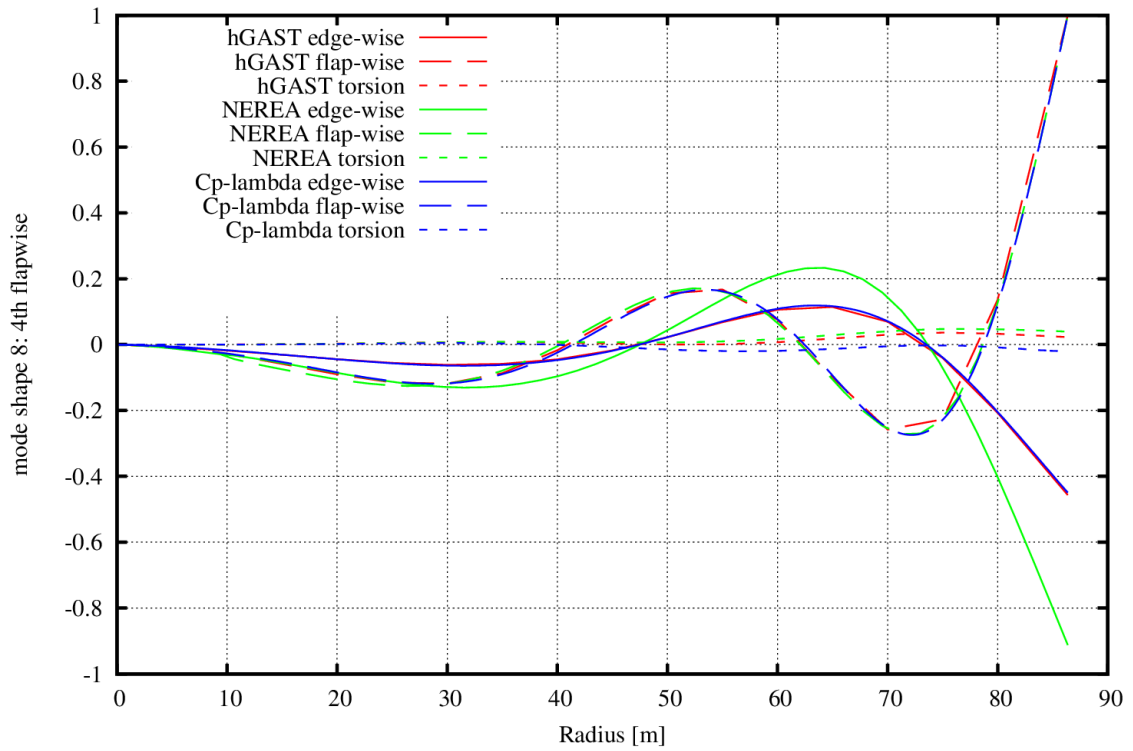


Figure 8: Shape of the 4th flapwise mode – straight blade

#	mode	Beam models				3d-FEM models					
		hGAST	NEREA	Cp-lambda	HAWC2	CRES	CENER	DTU	POLIMI	UPAT	WMC
1	1st flap	0.62	0.62	0.62	0.61	0.64	0.62	0.62	0.61	0.61	0.62
2	1st edge	0.94	0.94	0.94	0.93	0.96	1.01	0.98	0.91	0.95	0.97
3	2nd flap	1.76	1.74	1.76	1.74	1.85	1.80	1.75	1.74	1.75	1.80
4	2nd edge	2.80	2.79	2.80	2.77	2.86	3.02	2.89	2.77	2.83	2.98
5	3rd flap	3.59	3.52	3.60	3.57	3.76	3.77	3.53	3.55	3.57	3.77
6	1st torsion	5.40	5.36	-	6.60	6.01	6.24	5.49	5.67	5.55	6.17
7	3rd edge	5.73	5.61	5.74	5.70	5.82					
8	4th flap	6.09	6.03	6.11	6.11						

**Table 2: Blade natural frequencies. Comparison of predictions of Beam model and 3D FEM models (vacuum and zero structural damping)**

nr.	Mode:	Frequency at Stand-still [Hz]			
		Cp-Lambda	HAWC2	HStab2	hGAST
1	1st Tower FA	0.250	0.249	0.251	0.250
2	1st Tower SS	0.253	0.251	0.256	0.253
3	DT fixed-free	0.504	0.502		0.512
4	1st Asym.Flapp Yaw	0.558	0.547	0.546	0.548
5	1st Asym.Flapp Tilt	0.603	0.590	0.590	0.593
6	1st Coll. Flap	0.640	0.634	0.630	0.648
7	1st Asym.Edge Heave	0.925	0.922	0.922	0.930
8	1st Asym.Edge SS	0.939	0.936	0.935	0.945
9	2nd Asym. Flap. Yaw	1.405	1.376	1.368	1.374
10	2nd Asym. Flap. Tilt	1.603	1.551	1.548	1.531
11	2nd Coll. Flap	1.777	1.763	1.759	1.795
12	2nd Coll. Edge (DT)	1.984	1.970	1.803	2.000
13	3rd Asym. Flap. Tilt	2.302	2.248	2.237	2.295

**Table 3: Wind turbine natural frequencies at standstill (vacuum and zero structural damping).**

### 1.1.2 Static load cases

The following static loading cases were simulated:

- s1 - z – force:** Flapwise force of 9000 N/m uniformly distributed along the blade span
- s2 - y – moment:** Torsion moment of 7500 kN/m uniformly distributed along the blade span
- s3 - z – force:** Flapwise point force of 100 kN acting at the tip of the blade
- s4 - y – moment:** Torsion point moment of 80 kNm acting at the tip of the blade

Forces and moments are applied on the pitch axis.

The compared output results are:

- 1) radial distribution of deflections and torsion angle.
- 2) radial distribution of internal moment.

Simulations are performed both for the **straight** and the **prebent** blade. All simulations are performed with the non-linear (multibody and generalized Timoshenko) codes.

The axes of the blade coordinate system are defined as follows:

Blade coordinate system fixed at zero twist (not rotated by twist along the blade), x axis in the chordwise direction (for zero twist section) pointing towards the TE, y axis in the radial direction pointing towards the tip and z perpendicular to the chord (flatwise) direction pointing towards the suction side.

Figure 9 - Figure 14 present results of the simulation case **s1** for the **straight** blade.

Overall the agreement of the results of the codes compared in this case is good (hGAST, NEREA(GT) and Cp-Lambda). Higher differences are seen in the torsion angle (Figure 14). The applied load leads to a maximum flapwise deflection of about 9 m (see Figure 11). Under such a high flapwise deflection bending torsion coupling is triggered. The maximum predicted torsion angle ranges from  $-1.2^{\circ}$  to  $-1.6^{\circ}$ . Clearly hGAST underestimates the torsion angle all along the blade span. NEREA (GT) and Cp-Lambda compare well up to the radius of 60 m. Then deviations begin in the outer part of the blade. However, maximum deviation between the two codes does not exceed  $0.2^{\circ}$ .

Figure 15-Figure 16 present results of the simulation case **s2** for the **straight** blade.

A good agreement is obtained between the 3 codes in the predicted pitching moment (Figure 15). However, Cp-Lambda slightly underestimates the torsion (twisting) angle (Figure 16). This indicates that probably a higher torsional stiffness is considered in Cp-Lambda simulations, which is also consistent with the natural frequencies prediction (table 2).

Figure 17-Figure 22 present results of the simulation case **s1** for the **prebent** blade.

A small deviation between the 3 codes in the predicted flapwise deflection is observed in this case (Figure 19). Also hGAST seems to slightly overestimate the blade extension (Figure 21). The results for the torsion angle (Figure 22) are quite similar to those of the straight blade case (see Figure 16).

Figure 23-Figure 27 present results of the simulation case **s3** for the **straight** blade.

The agreement between the 2 codes compared in this case (HAWC2 and hGAST) in the flapwise bending moment is almost perfect (Figure 23). Some differences are seen in the torsion moment which in HAWC2 results appears to be wavy while hGAST predicts a smooth distribution along the span (probably due to different reference axis with respect to which the moment is calculated) (Figure 24). The flapwise deflections slightly differ at the outmost part of the blade (very close to the tip) (Figure 25). A difference close to the tip is also seen in the torsion angle. The predictions of the two codes slightly deviate near the tip. HAWC2 predicts a sudden drop of the torsion angle close to the tip (to about  $-1^\circ$ ) which also appears in hGAST but to a much smaller extent (Figure 27).

Figure 28-Figure 29 present results of the simulation case **s4** for the **straight** blade.

An about  $1^\circ$  difference is noted at the very tip of the blade however, the shape of the distribution is very similar up to the radius of 72 m (Figure 29). The difference at the tip is probably due to different resolution of the structural grid towards the tip. At the very tip, the rate of the increase of the torsion angle is very high and therefore predictions are expected to be sensitive to the density of the structural grid.

Figure 30-Figure 34 present results of the simulation case **s3** for the **prebent** blade.

A similar agreement between the two codes is obtained for the prebent blade. Also in this case a sudden drop of the torsion angle appears in HAWC2 predictions close to the tip region (Figure 34).

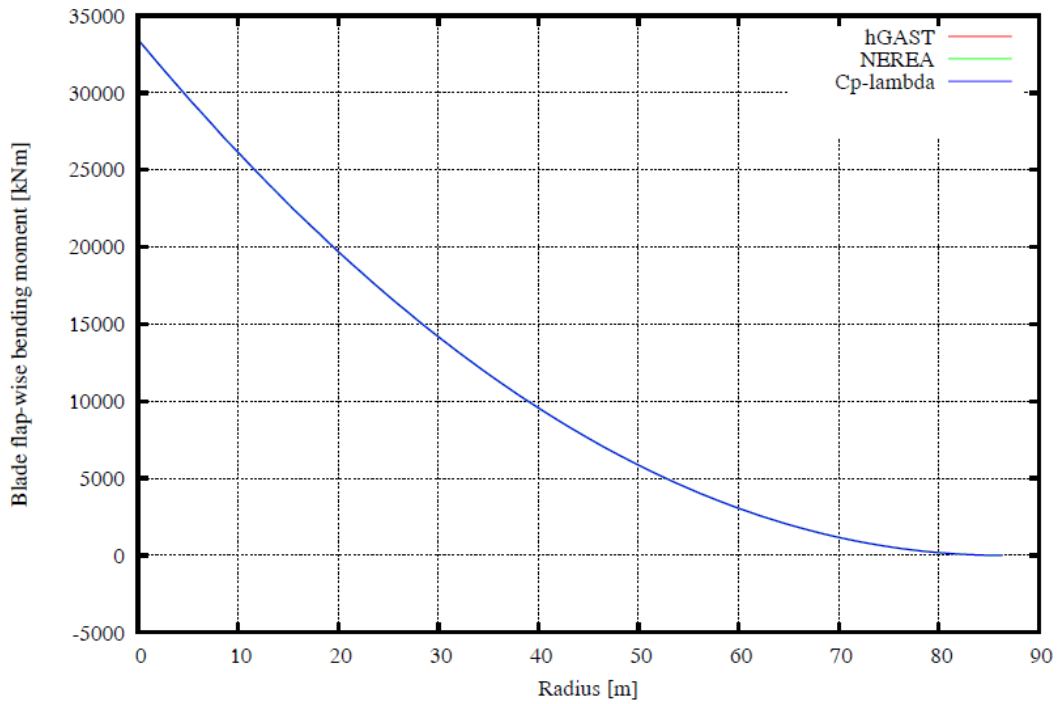


Figure 9: Flapwise bending moment distribution– flapwise force  $F_z=9000$  N/m - straight blade

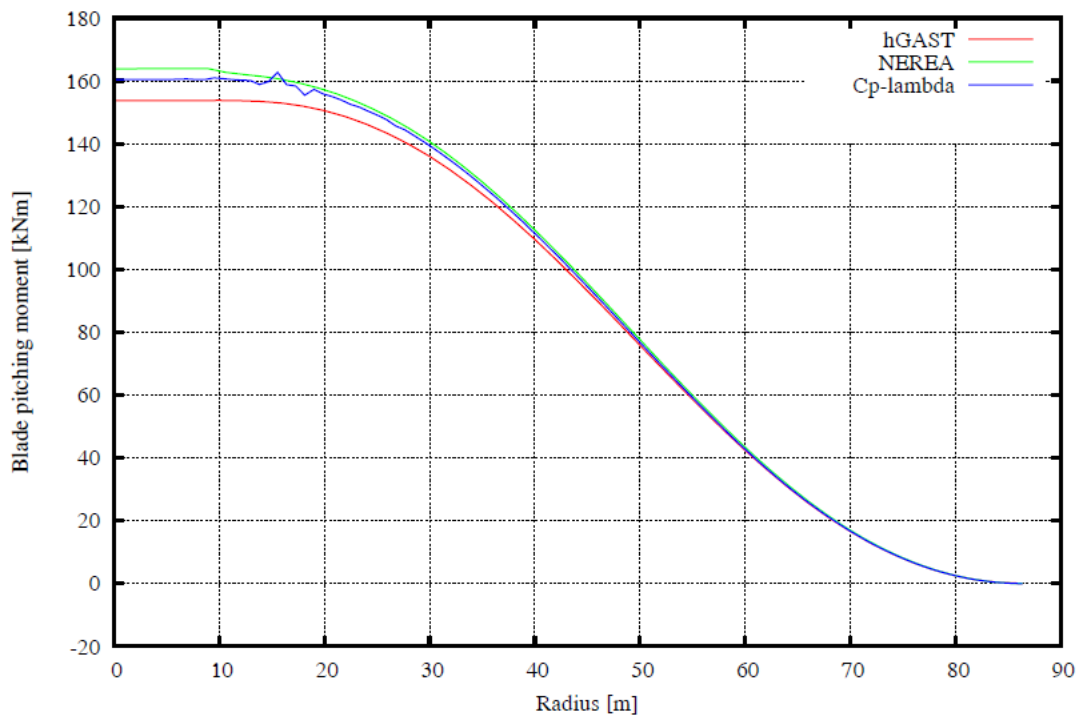


Figure 10: Pitching moment distribution – flapwise force  $F_z=9000$  N/m - straight blade

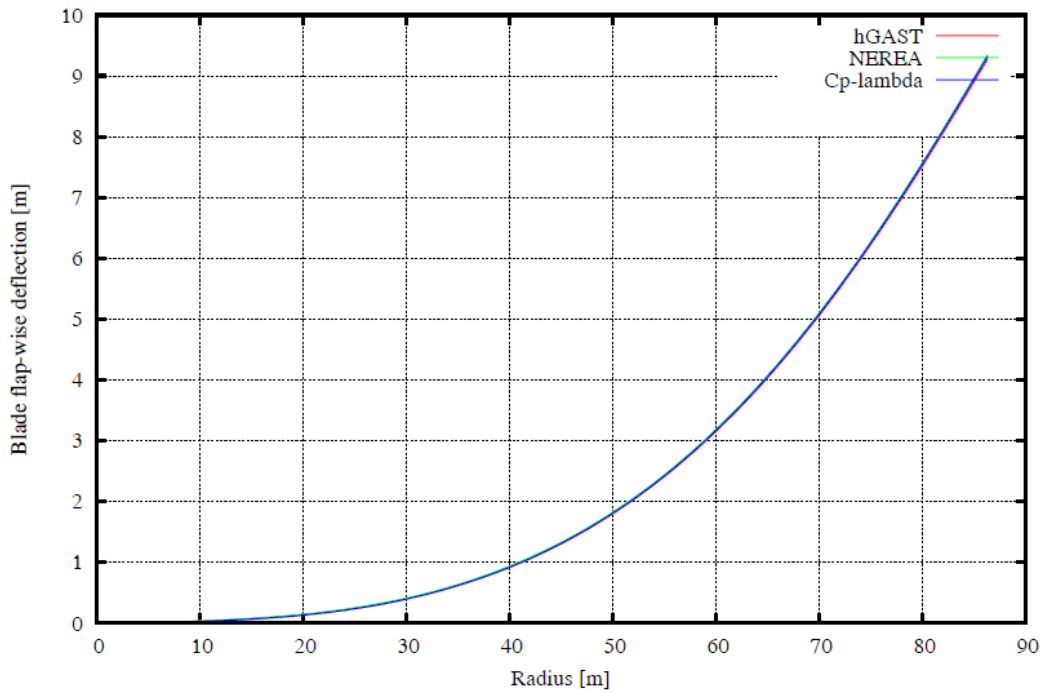


Figure 11: Flapwise deflection distribution – flapwise force  $F_z=9000$  N/m - straight blade

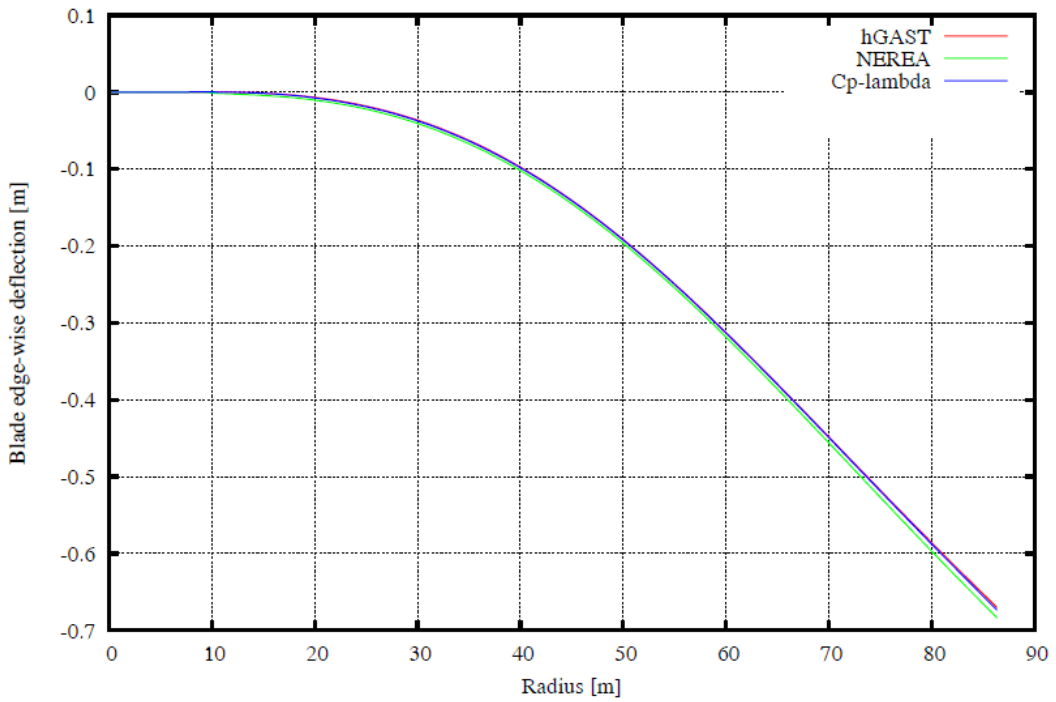


Figure 12: Edgewise deflection distribution – flapwise force  $F_z=9000$  N/m - straight blade

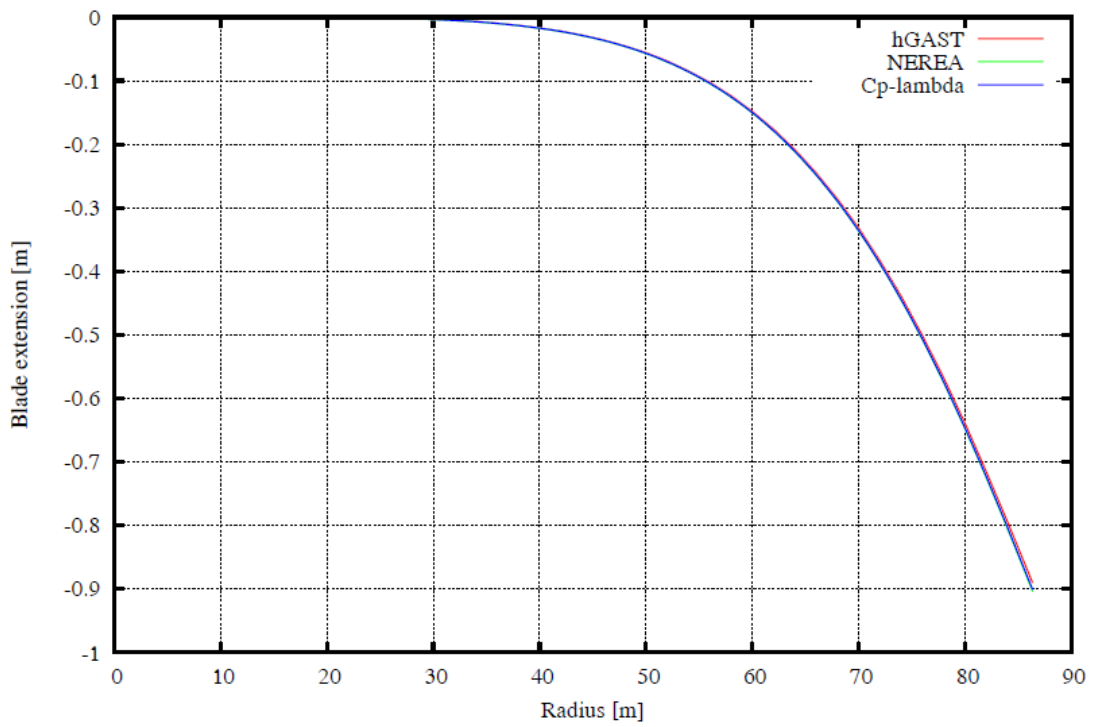


Figure 13: Extension distribution - flapwise force  $F_z=9000$  N/m - straight blade

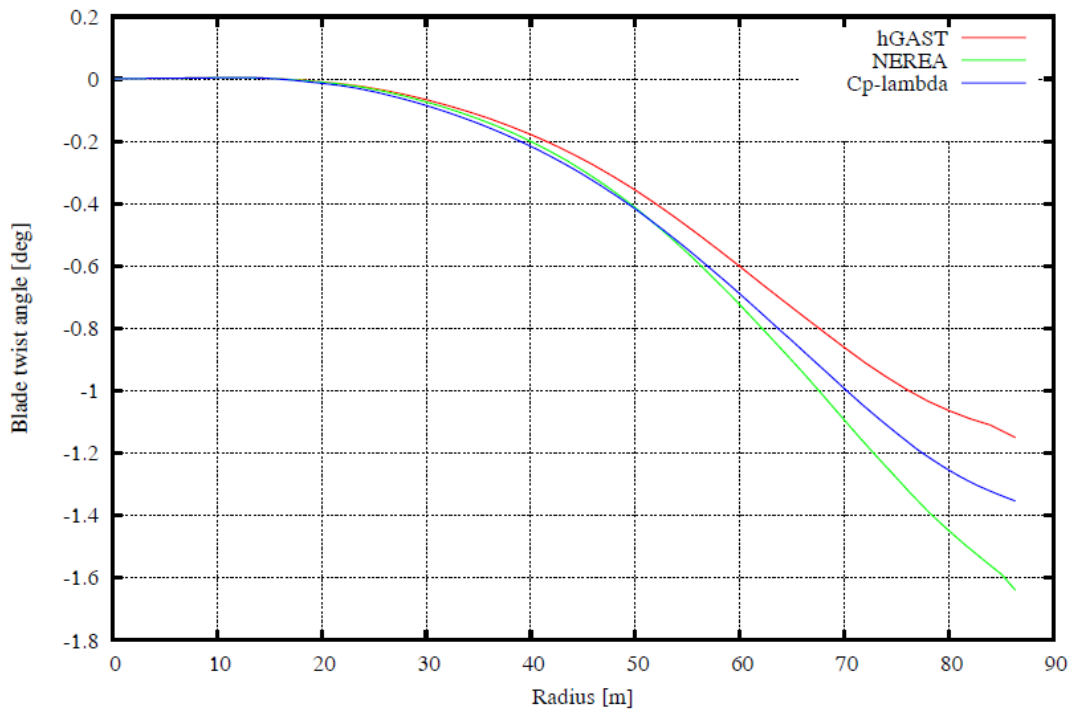


Figure 14: Twist distribution - flapwise force  $F_z=9000$  N/m - straight blade

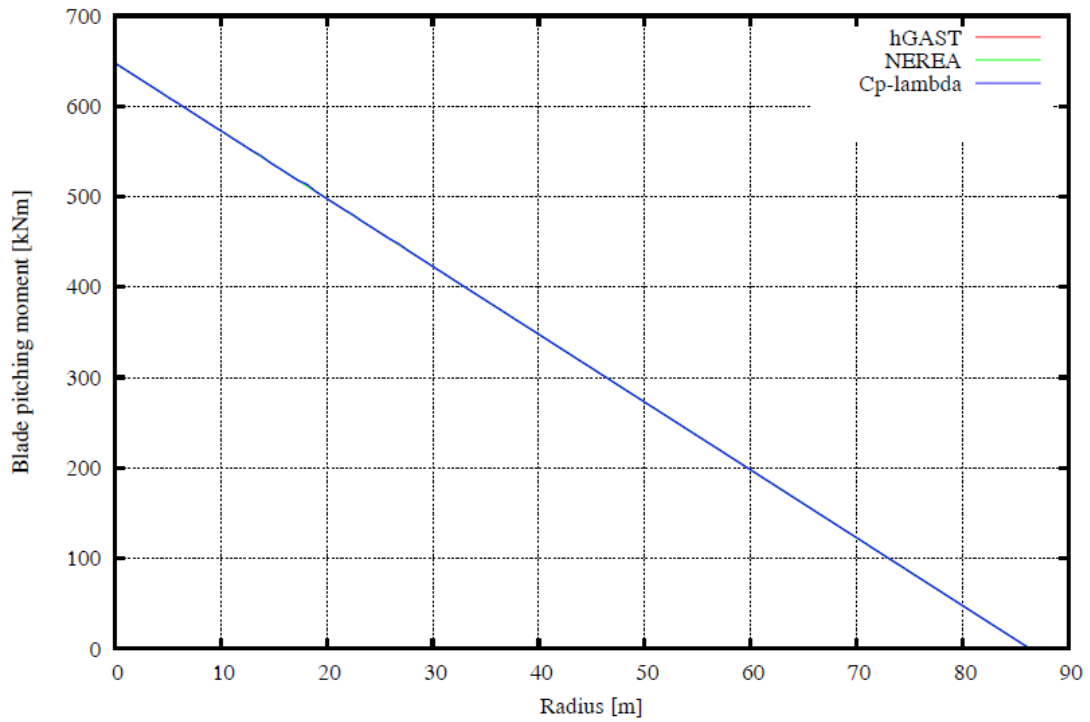


Figure 15: Pitching moment distribution – torsion moment  $M_y=7500 \text{ Nm/m}$  - straight blade

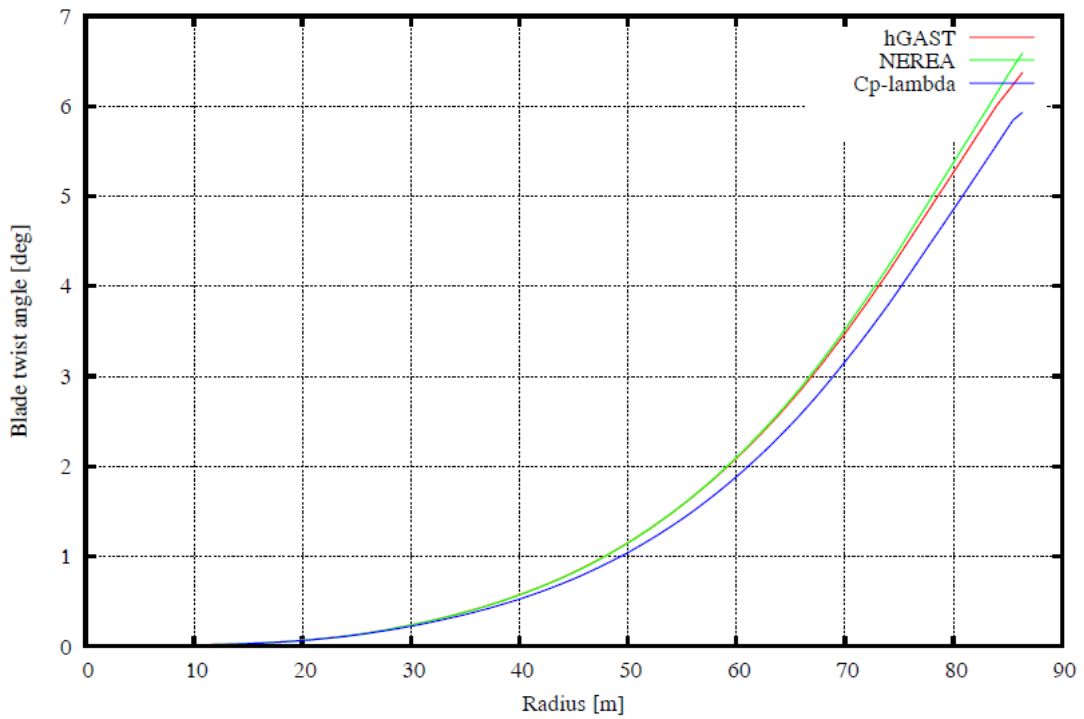


Figure 16: Twist distribution – torsion moment  $M_y=7500 \text{ Nm/m}$  - straight blade

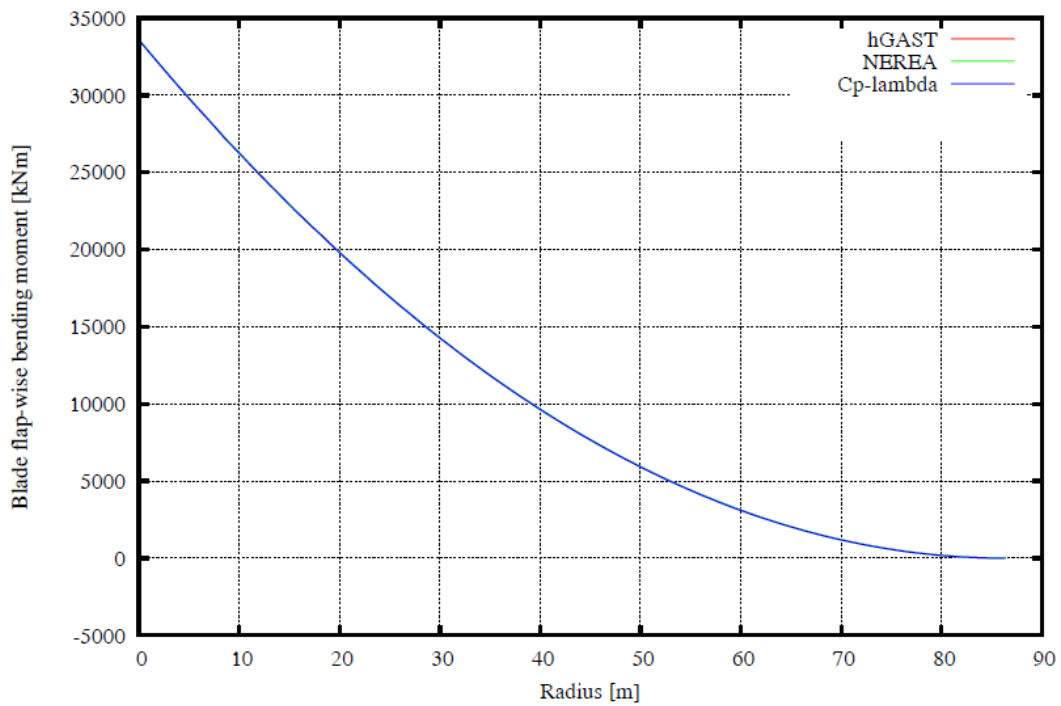


Figure 17: Flapwise bending moment distribution – flapwise force  $F_z=9000$  N/m - prebent blade

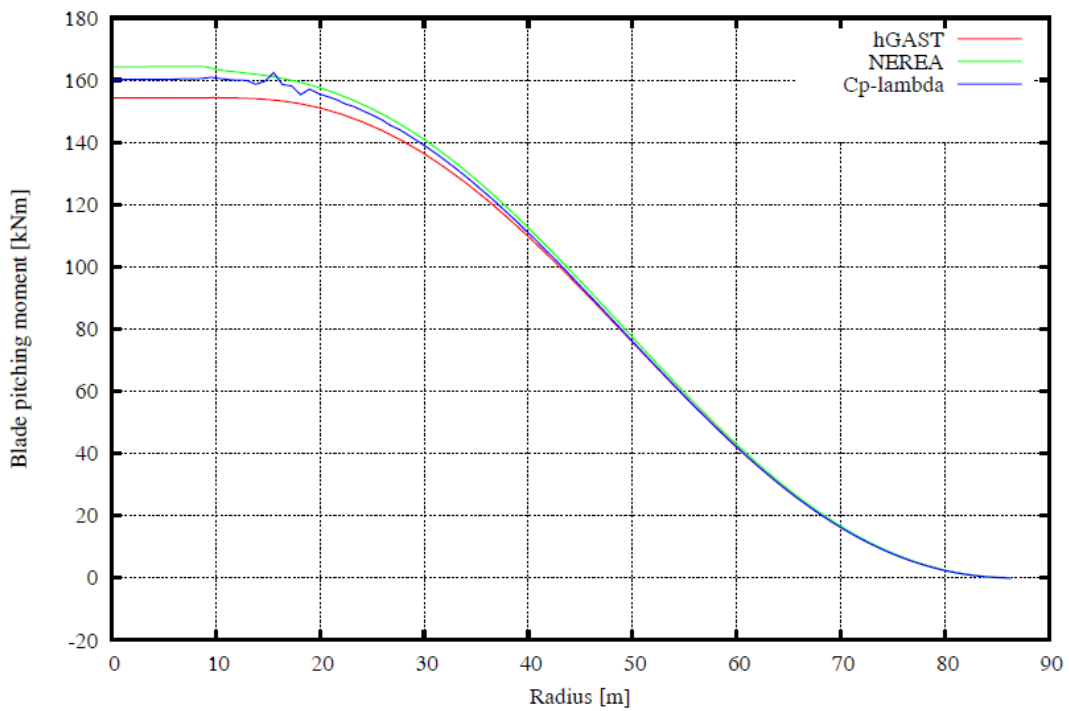


Figure 18: Pitching moment distribution – flapwise force  $F_z=9000$  N/m - prebent blade

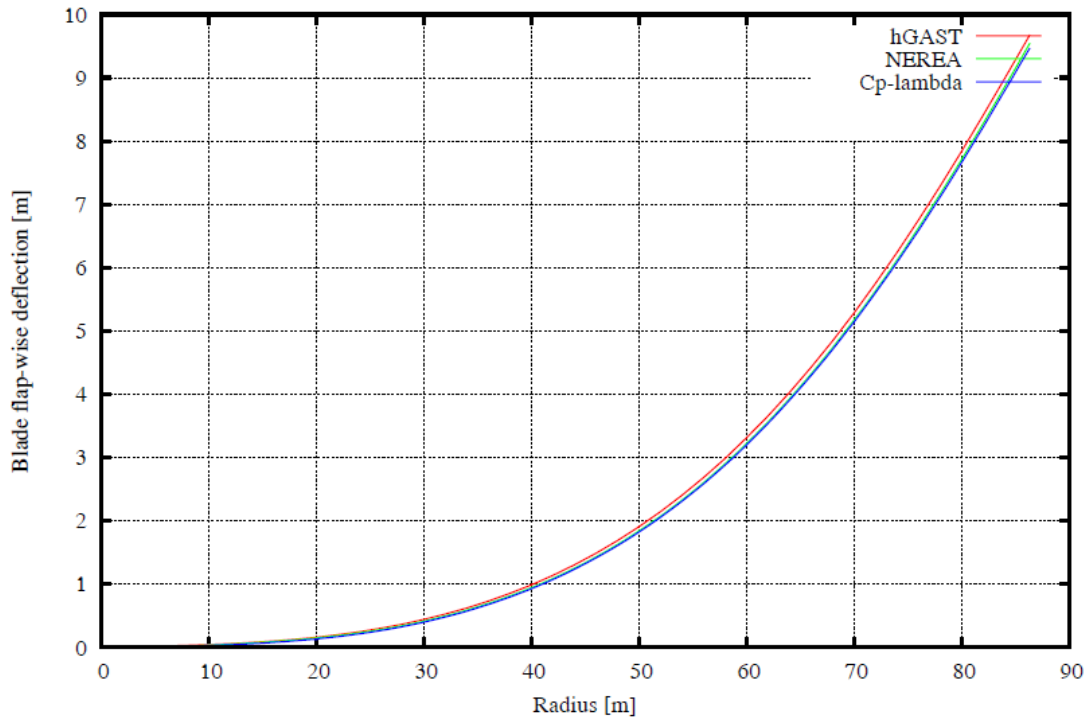


Figure 19: Flapwise deflection distribution – flapwise force  $F_z=9000$  N/m - prebent blade

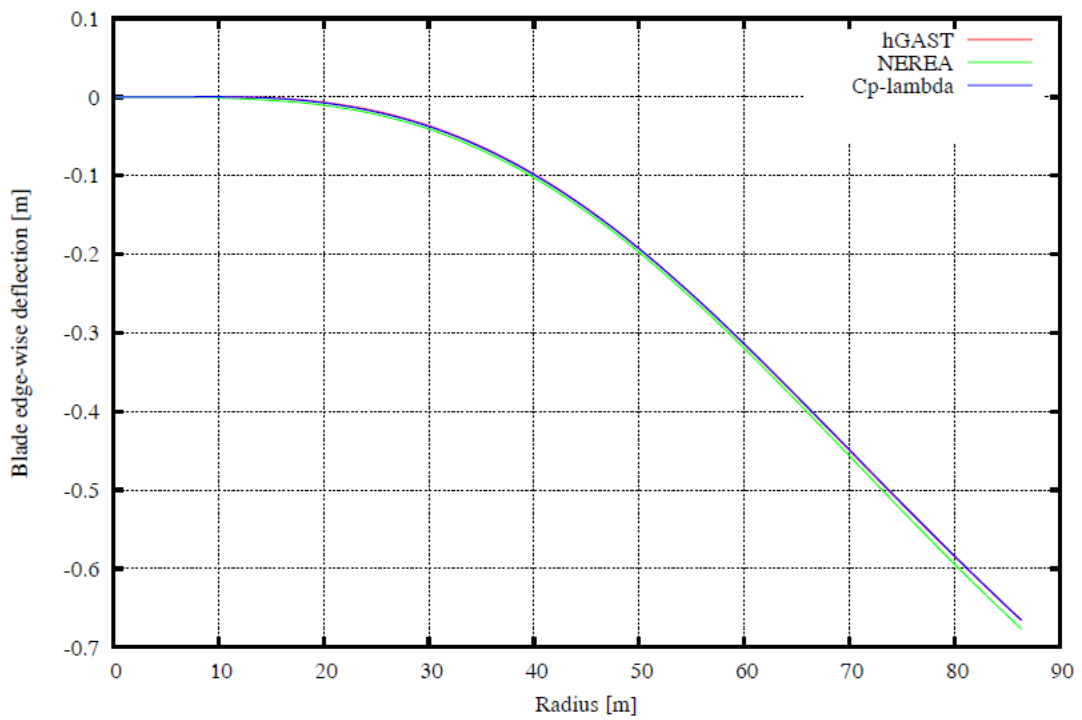


Figure 20: Edgewise deflection distribution – flapwise force  $F_z=9000$  N/m - prebent blade

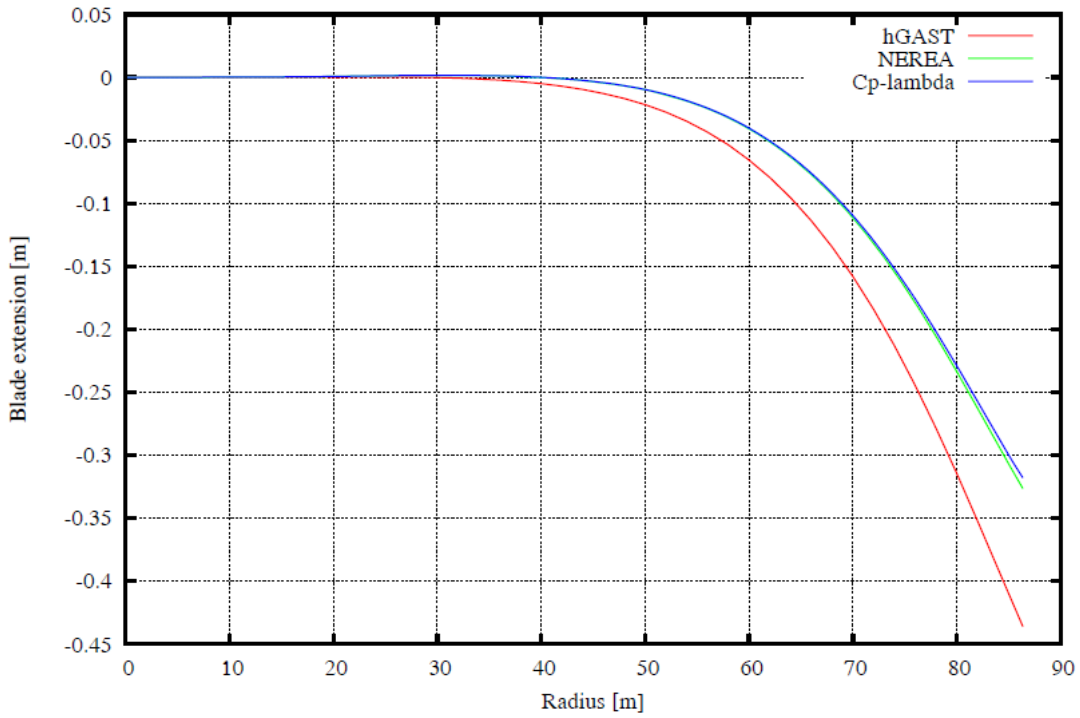


Figure 21: Extension distribution - flapwise force  $F_z=9000$  N/m - prebent blade

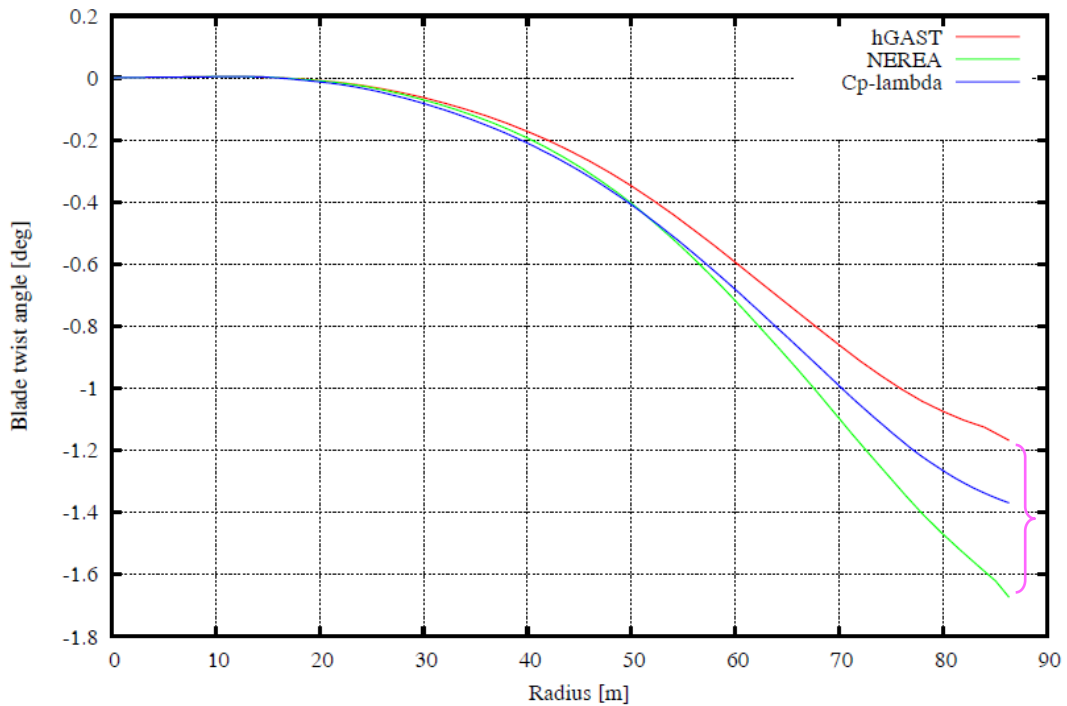


Figure 22: Twist distribution - flapwise force  $F_z=9000$  N/m - prebent blade

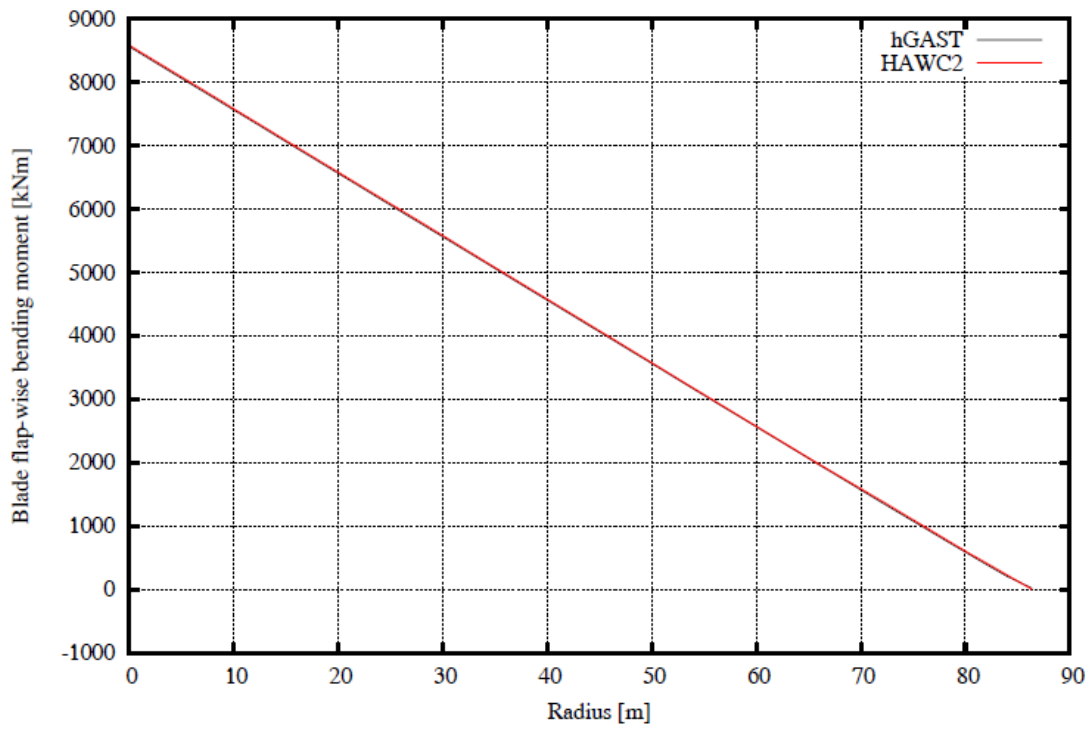


Figure 23: Flapwise bending moment distribution – flapwise tip force  $F_z=100$  kN - straight blade

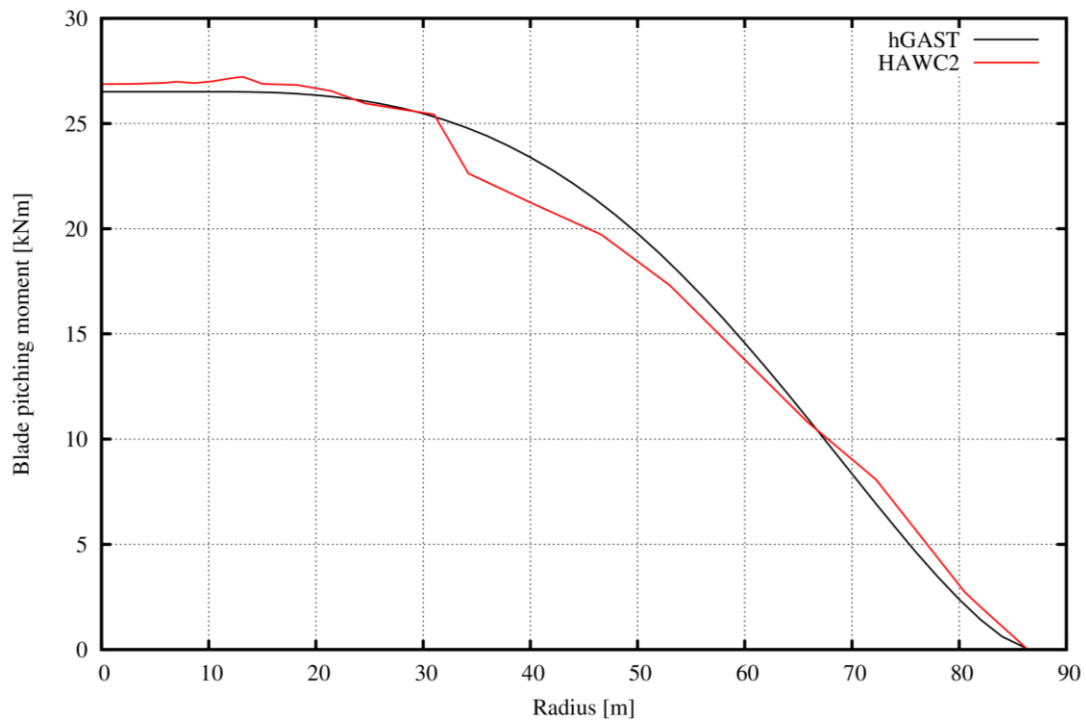


Figure 24: Pitching moment distribution – flapwise tip force  $F_z=100$  kN - straight blade

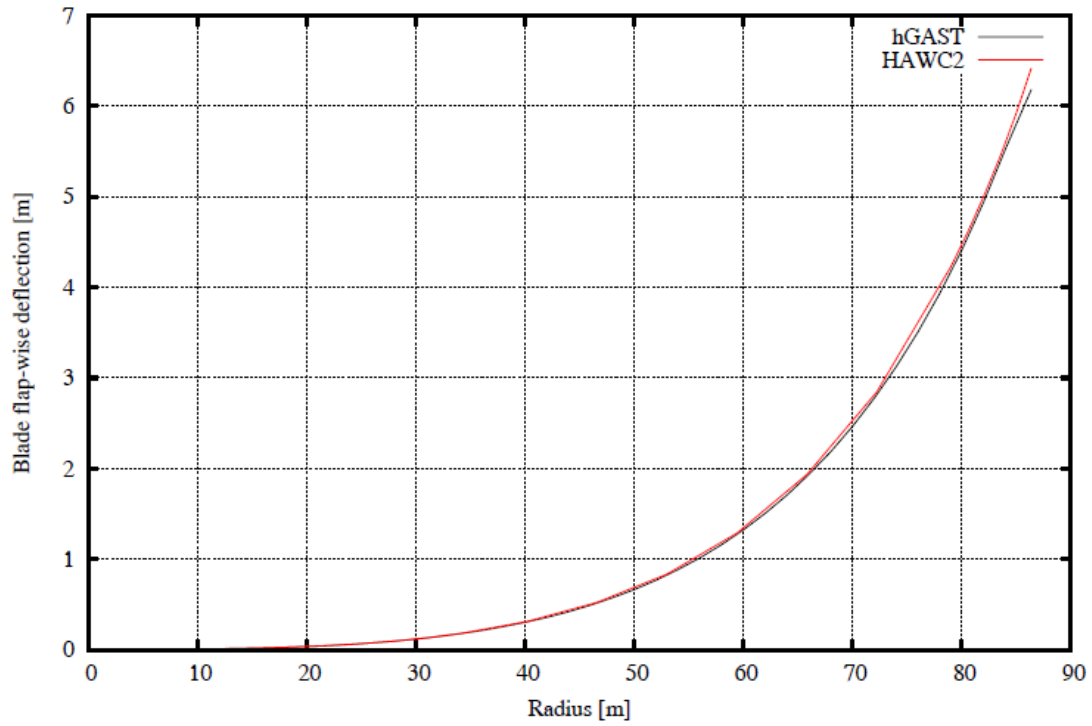


Figure 25: Flapwise deflection distribution – flapwise tip force  $F_z=100$  kN - straight blade

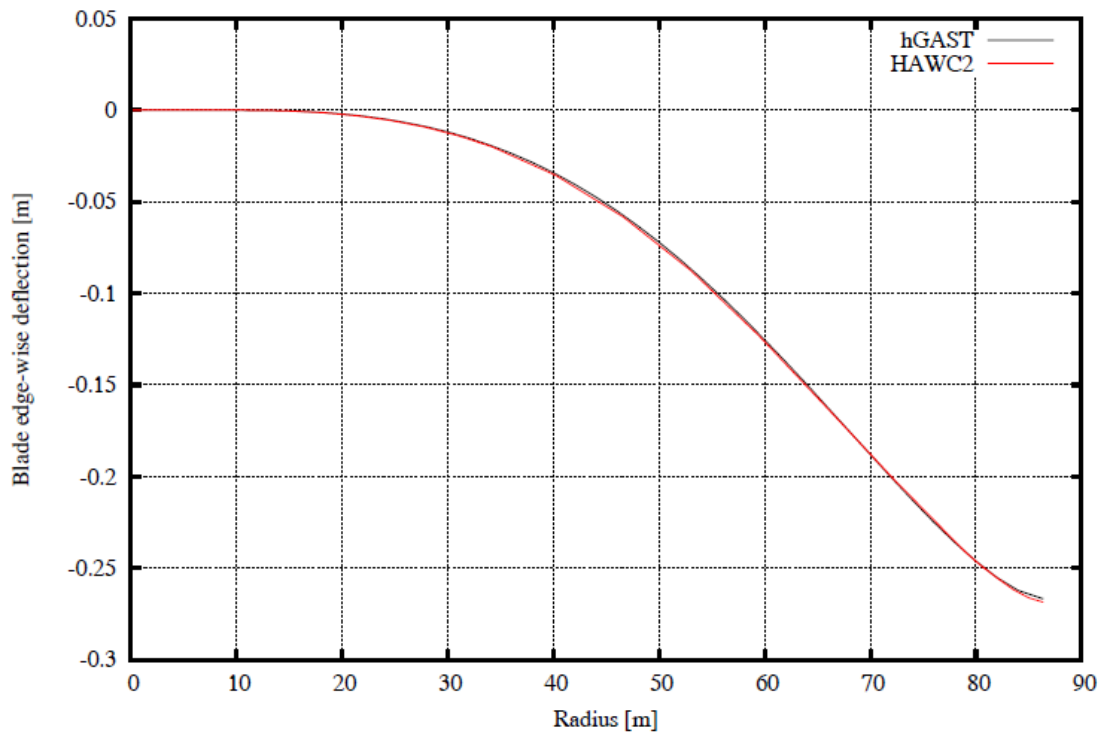


Figure 26: Edgewise deflection distribution – flapwise tip force  $F_z=100$  kN - straight blade

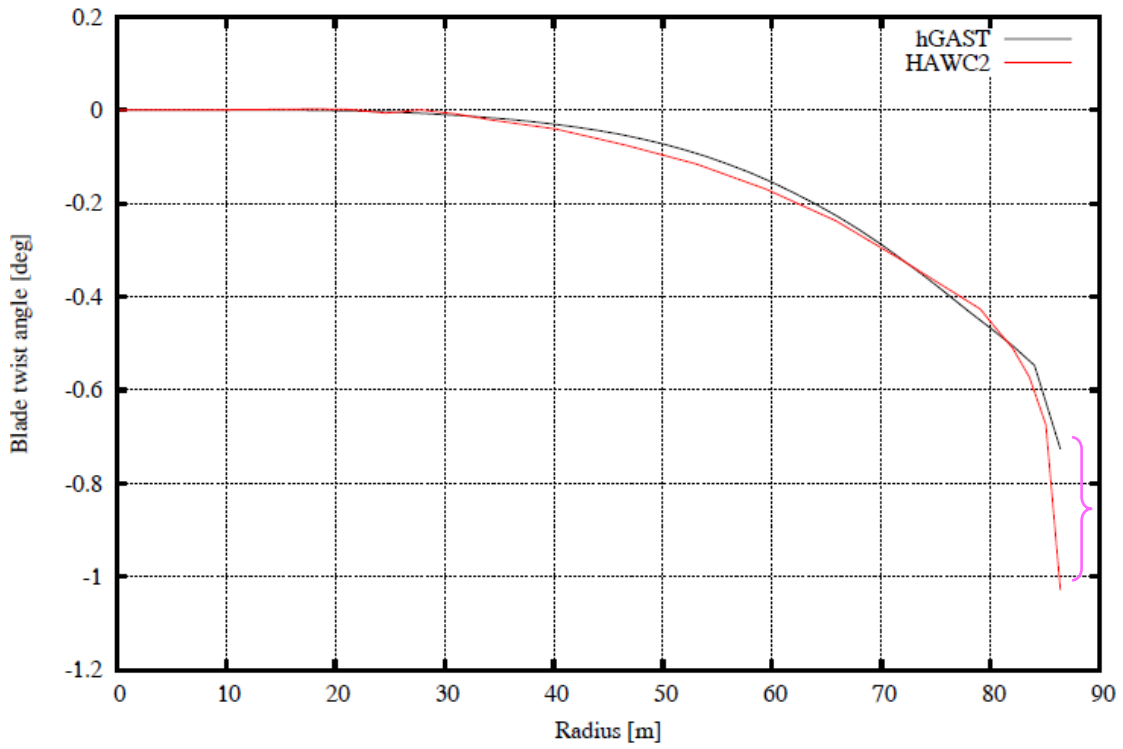


Figure 27: Twist distribution – flapwise tip force  $F_z=100$  kN - straight blade

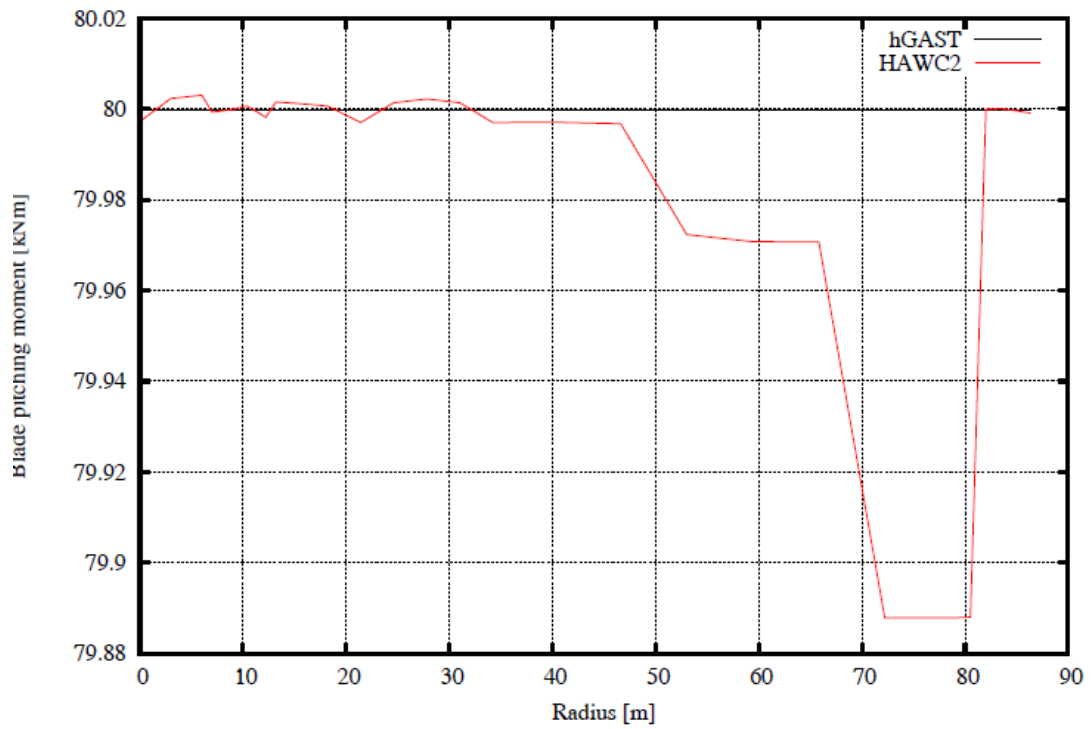


Figure 28: Pitching moment distribution – torsion tip moment  $M_y=80$  kNm - straight blade

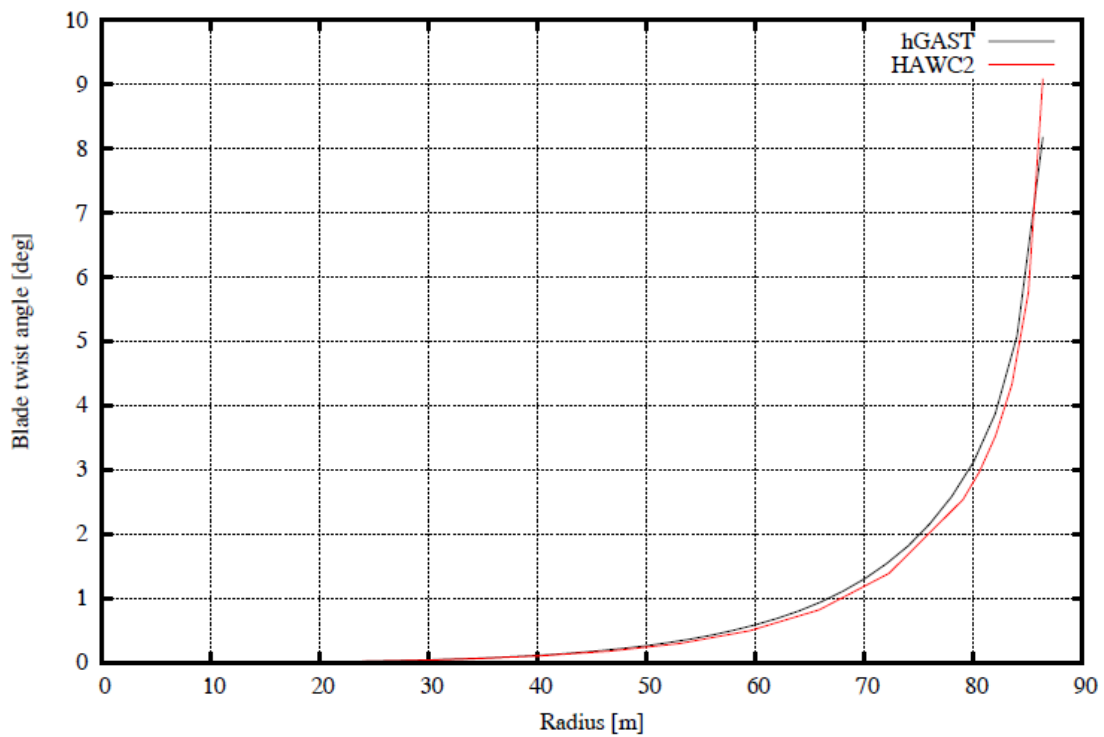


Figure 29: Twist distribution – torsion tip moment  $M_y=80$  kNm - straight blade

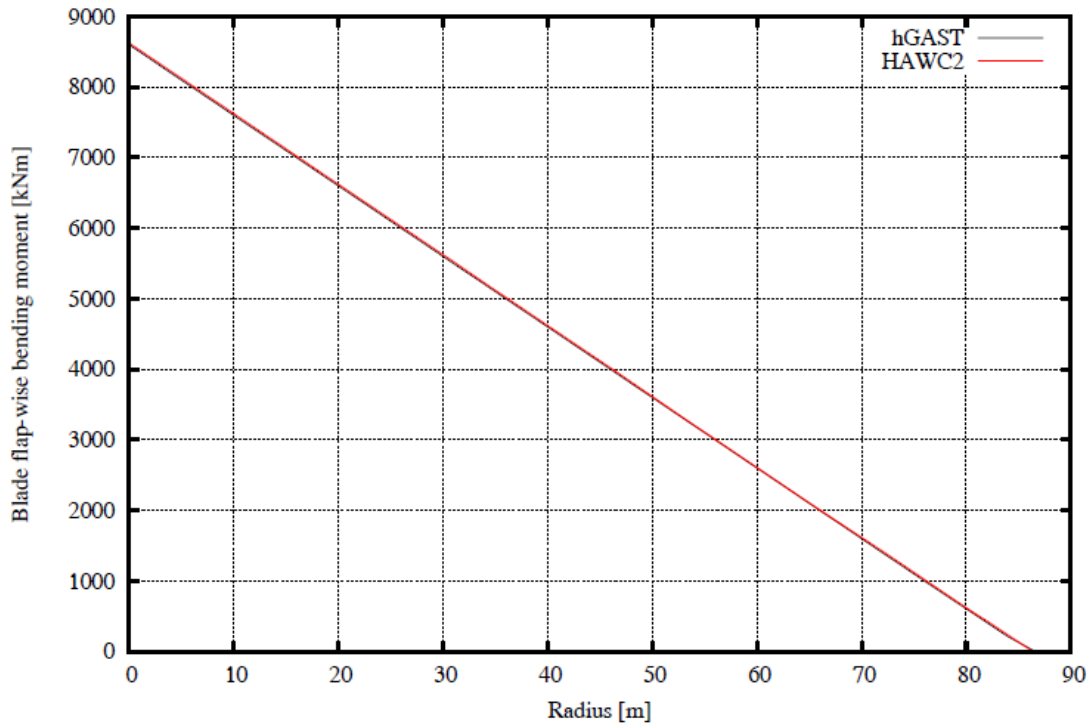


Figure 30: Flapwise bending moment distribution – flapwise tip force  $F_z=100$  kN - prebent blade

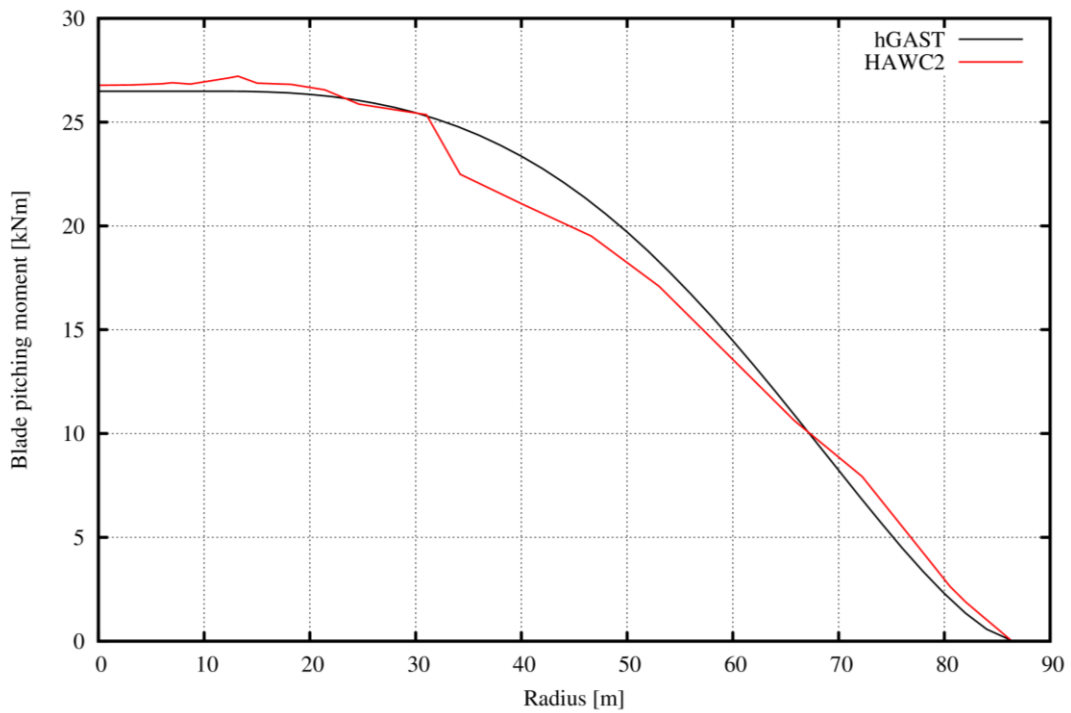


Figure 31: Pitching moment distribution – flapwise tip force  $F_z=100$  kN - prebent blade

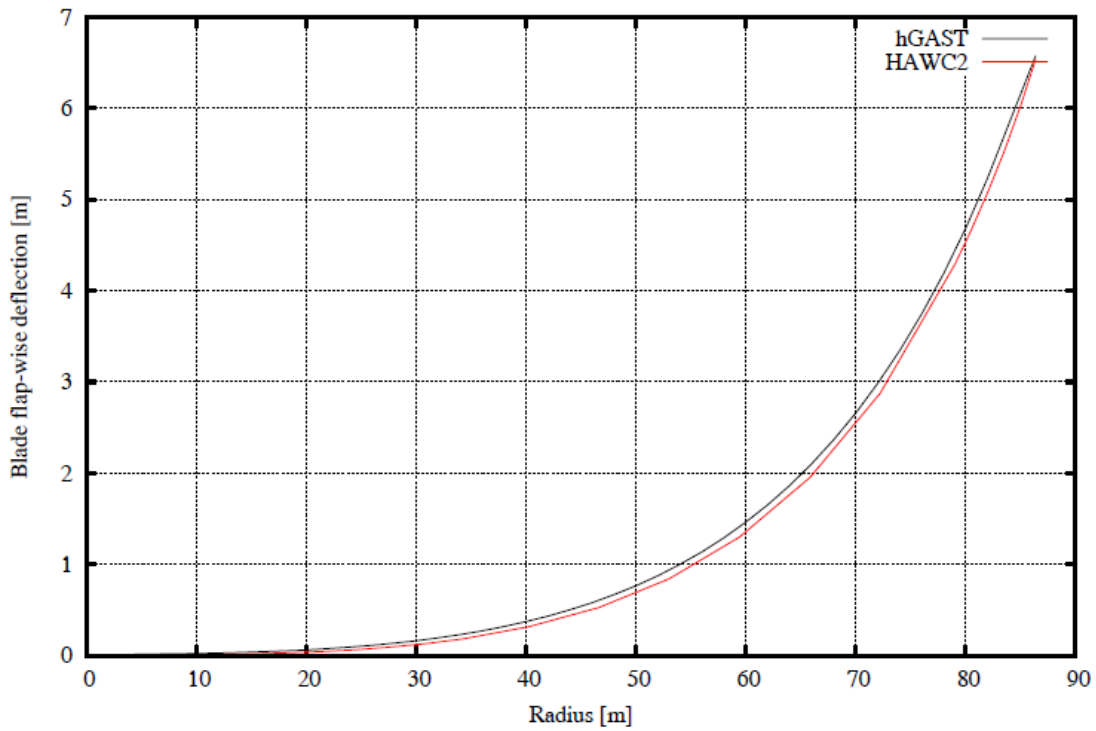


Figure 32: Flapwise deflection distribution – flapwise tip force  $F_z=100$  kN - prebent blade

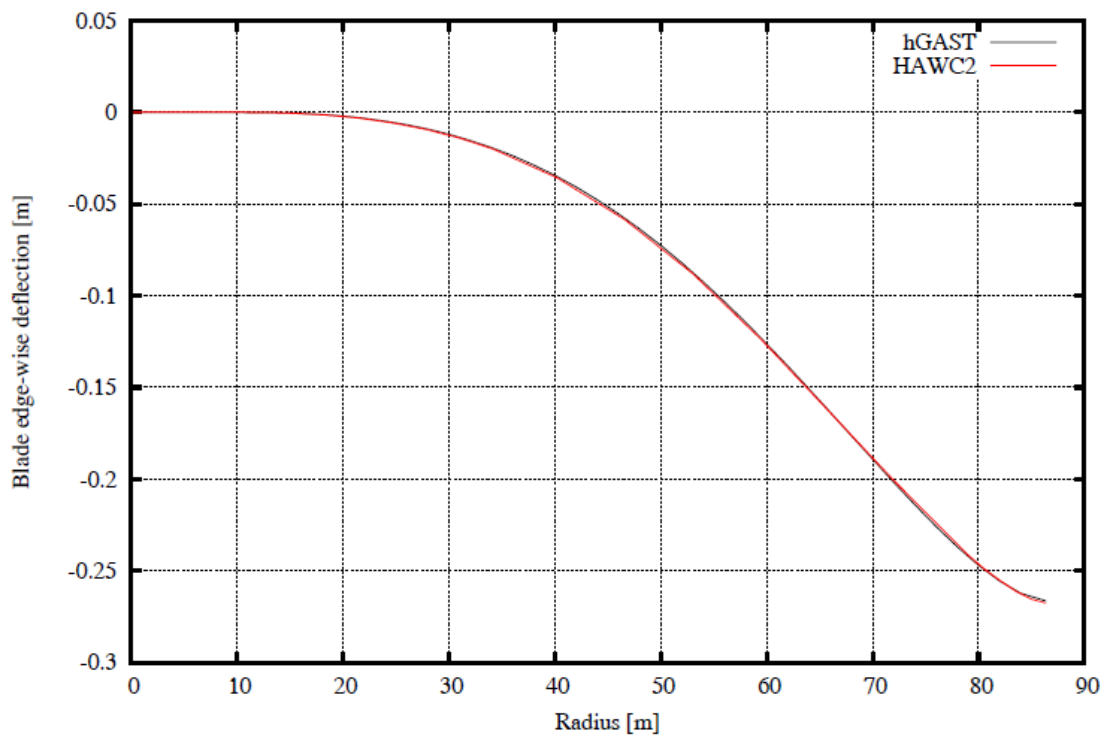


Figure 33: Edgewise deflection distribution – flapwise tip force  $F_z=100$  kN - prebent blade

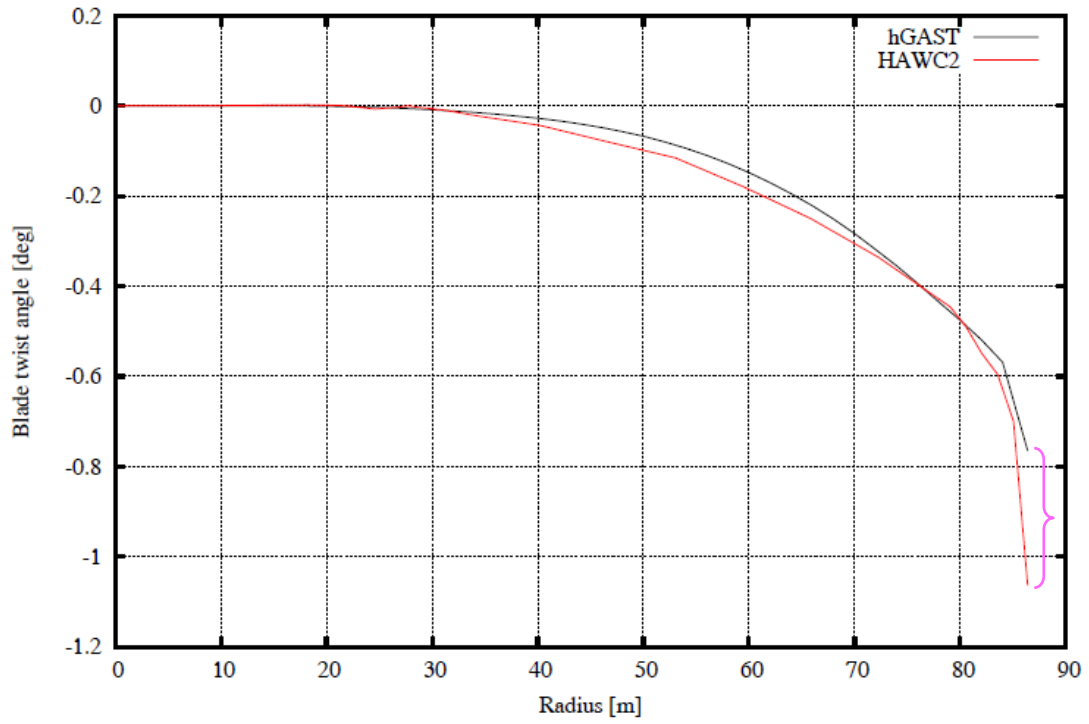


Figure 34: Twist distribution – flapwise tip force  $F_z=100$  kN - prebent blade

## 1.2 Rotor aeroelastic validation

The isolated rotor system in uniform wind conditions and without the controller operating is validated in this section. Simulations are performed for the **prebent** blade. Simulations results of hGAST and NEREA (modal) are compared. NEREA (modal) represents the typical fast aeroelastic tool used by the industry while hGAST is a non-linear tool that accounts for geometric non-linearity effects.

Uniform wind simulations, at the wind speeds of 8 m/s (partial load) and at the wind speed of 18 m/s (full load) are performed for the isolated rotor system (the rest of the wind turbine is considered stiff).

Operational characteristics (rotor speed and pitch angle) are considered constant during the simulation (controller not active) and are taken from the table below.

**Table 4: Operational data for rotor benchmarking**

Wind Speed	Pitch [deg.]	RPM
4	2.751	6.000
5	1.966	6.000
6	0.896	6.000
7	0.000	6.000
8	0.000	6.426
9	0.000	7.229
10	0.000	8.032
11	0.000	8.836
12	4.502	9.600
13	7.266	9.600
14	9.292	9.600
15	10.958	9.600
16	12.499	9.600
17	13.896	9.600
18	15.200	9.600
19	16.432	9.600
20	17.618	9.600
21	18.758	9.600
22	19.860	9.600
23	20.927	9.600
24	21.963	9.600
25	22.975	9.600

Time-series of the following quantities are compared after periodicity of the loads and deflections is reached.

1. Time [s]
2. Blade root out-of-plane bending moment [kNm]
3. Blade root twisting moment [kNm]

4. Blade root in-plane bending moment [kNm]
5. Blade tip out-of-plane deflection [m]
6. Blade tip in-plane deflection [m]
7. Blade tip twisting (torsion) angle [deg]

Bending moments and structural deformations are defined according to the reference system sketched in Figure 35.

In addition it is noted that:

The air density is constant and equal to  $\rho = 1.225 \text{ kg/ m}^3$ .

The blade deflections and root bending moments are referred to the rotor plane coordinate systems (in-plane and out-of-plane), as opposed to the blade coordinate system (edgewise and flapwise) and they are calculated with respect to the blade pitch axis (centerline at blade root). The two systems coincide for zero pitch angles and the blade coordinate system rotates as the blade pitches, whereas the rotor plane coordinate system does not.

The blade tip torsion angle is instead referred to the blade local deflected elastic axis. The time series of the blade tip torsion do not include the effects of the whole blade pitching while the structural pitch angle is either not included.

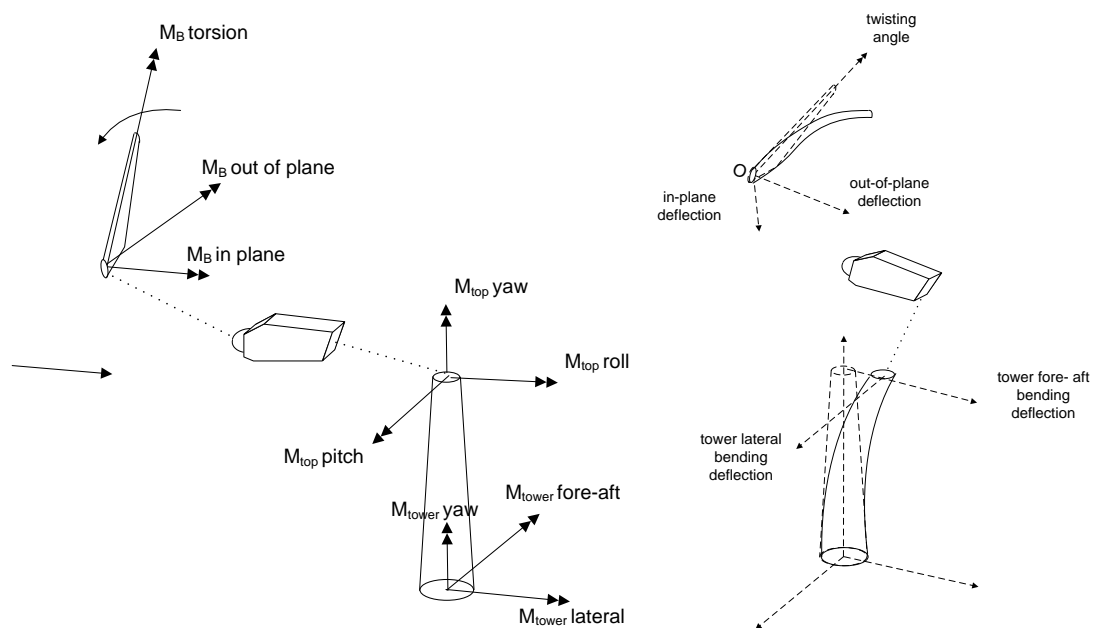


**Figure 35: Reference systems for the wind turbine aeroelastic computations**

Results for 3 periods of rotation are presented in Figure 36-Figure 40 for the wind speed of 8 m/s and in Figure 41-Figure 45 for the wind speed of 18 m/s.

At the wind speed of 8 m/s :

- NEREA predicts a higher range of the variation of the out-of-plane bending moment. Also, there is a clear phase shift between the two time series and a smaller level shift of about 2% (Figure 36)

- The in-plane moments are not shown in the figures because as they are driven by the weight of the blade they perfectly agree.
- The agreement in the pitching moment is good both in terms of ranges and phase. Slightly smaller ranges are predicted by hGAST (Figure 37).
- A higher level shift is seen in the out-of-plane deflection (about 10%) which is related to the lower torsion angle predicted by hGAST (Figure 38). The phase shift is similar to the one seen in the out-of-plane bending moment (see Figure 36).
- An about 0.5 m level shift is seen in the edgewise deflection at the blade tip. NEREA predicts an almost zero mean while hGAST predicts a mean deflection of 0.5 m (leading) (Figure 39). The non-zero mean in-plane deflection predicted by hGAST is due to a non-linear geometric coupling related with the very high out-of-plane deflection of the blade. A similar coupling has been also seen in the static load cases when the out-of-plane deflection gets too high.
- A  $0.5^\circ$  level difference is noted in the torsion angle. hGAST predicts a nose down torsion deformation while NEREA gives the opposite trend (Figure 40).

At the wind speed of 18 m/s the results are quite similar to those of 8 m/s:

- The amplitude of the out-of-plane bending moment is higher in NEREA predictions. Again, there is a phase shift between the two time series (Figure 41).
- The agreement in the pitching moment is again satisfactory (Figure 42).
- A big level shift is seen in the out-of-plane deflection (Figure 43) which is again related to the  $1^\circ$  difference in the torsion angle.
- An about 0.5 m level shift is seen in the in-plane deflection at the blade tip (Figure 44).

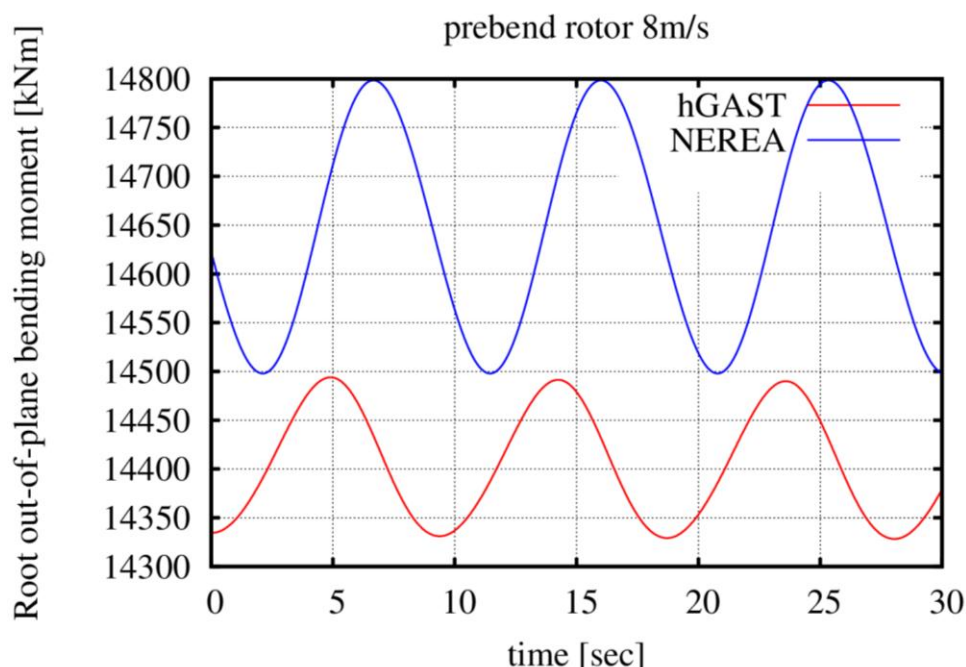


Figure 36: Blade root out-of-plane bending moment – wind speed 8 m/s - prebent blade

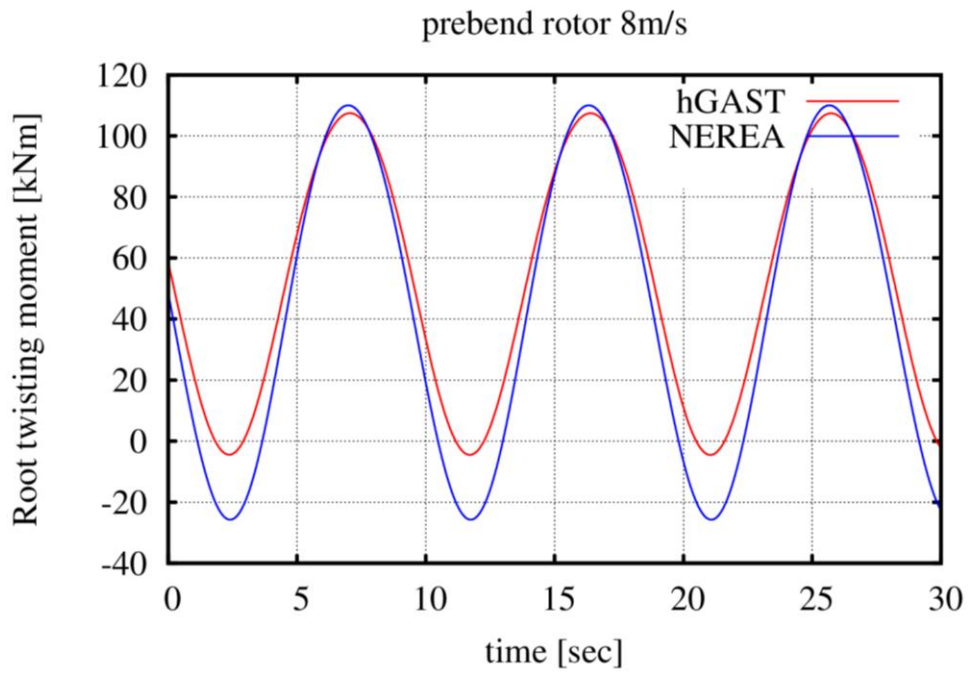


Figure 37: Blade root twisting moment – wind speed 8 m/s - prebent blade

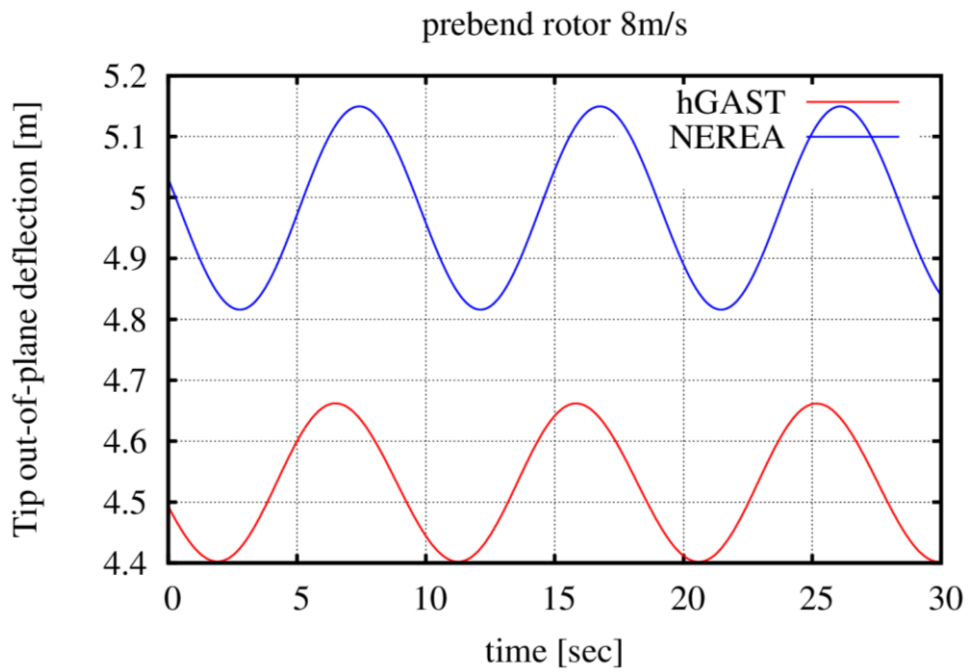


Figure 38: Blade tip out-of-plane deflection – wind speed 8 m/s - prebent blade

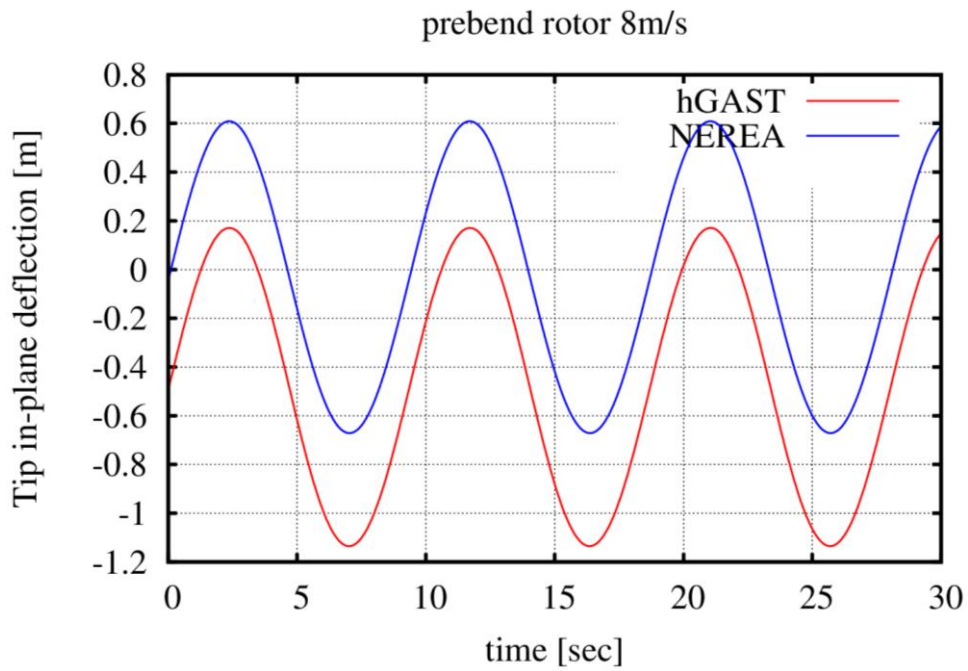


Figure 39: Blade tip in-plane deflection – wind speed 8 m/s - prebent blade

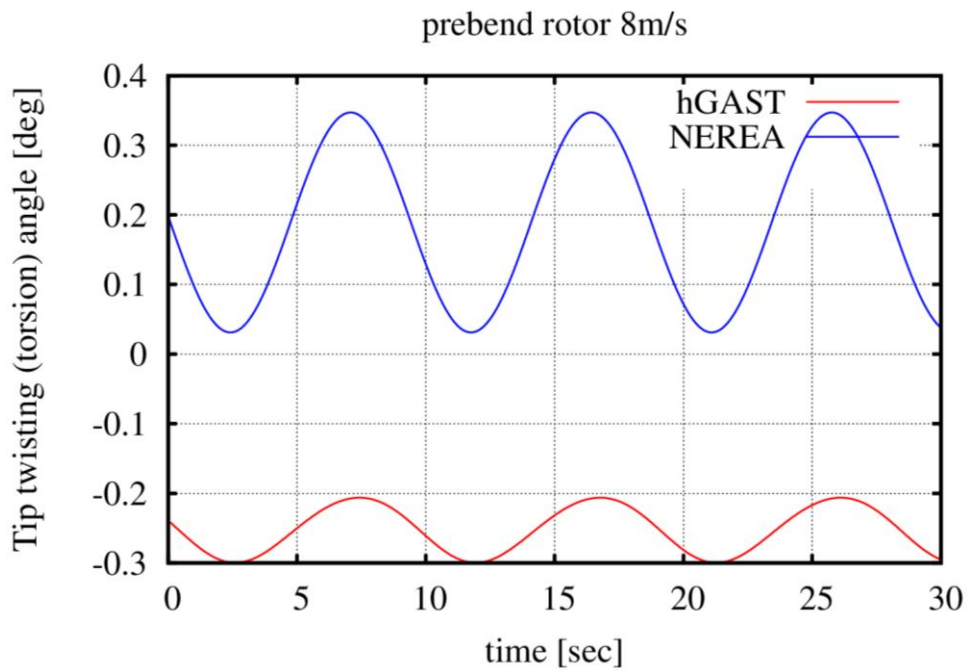


Figure 40: Blade tip twisting angle– wind speed 8 m/s - prebent blade

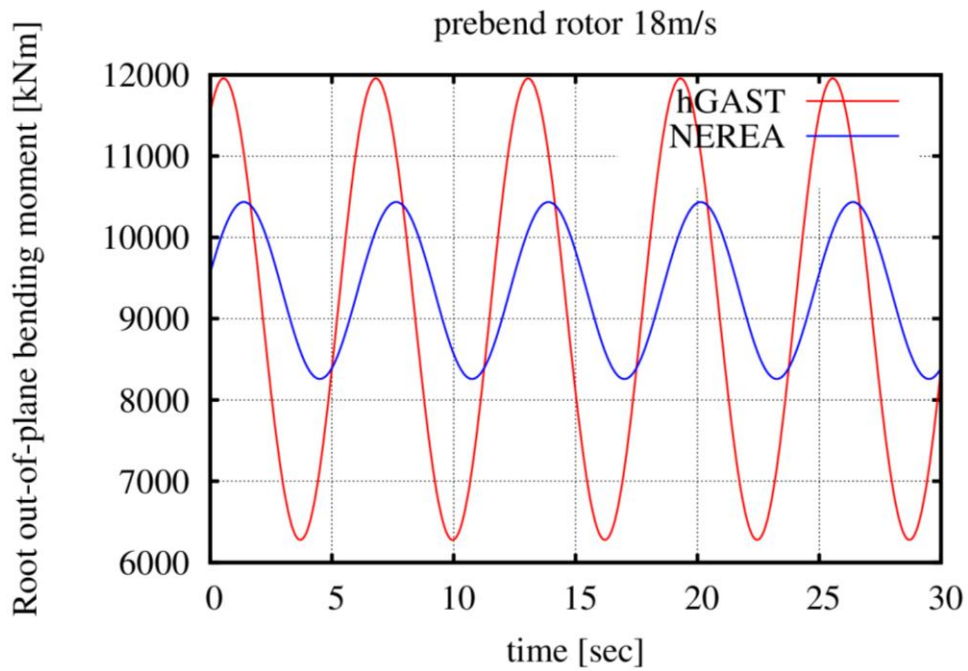


Figure 41: Blade root out-of-plane bending moment – wind speed 18 m/s - prebent blade

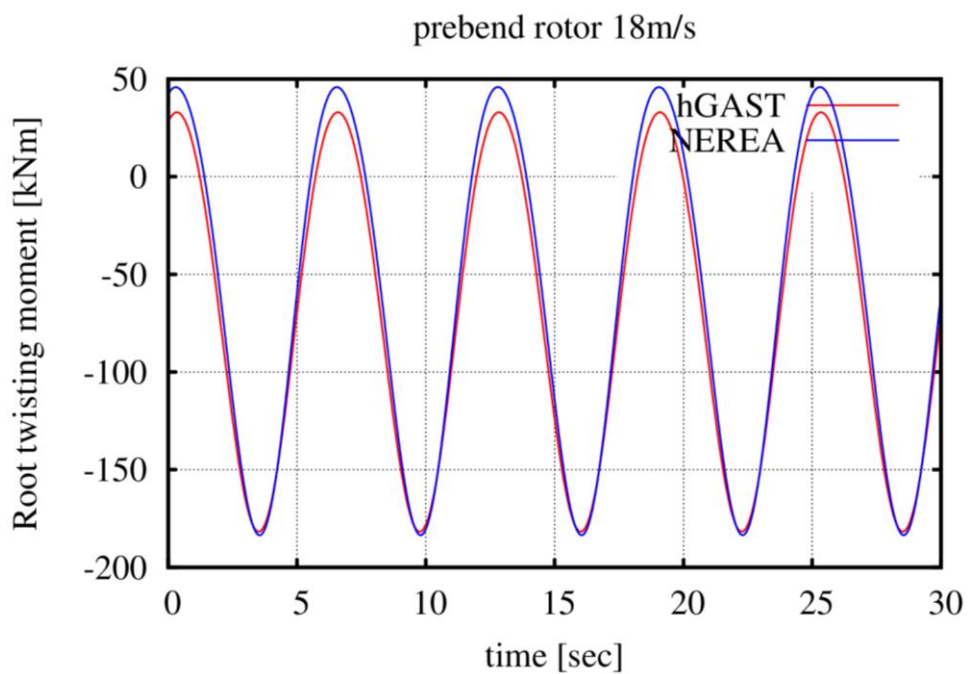


Figure 42: Blade root twisting moment – wind speed 18 m/s - prebent blade

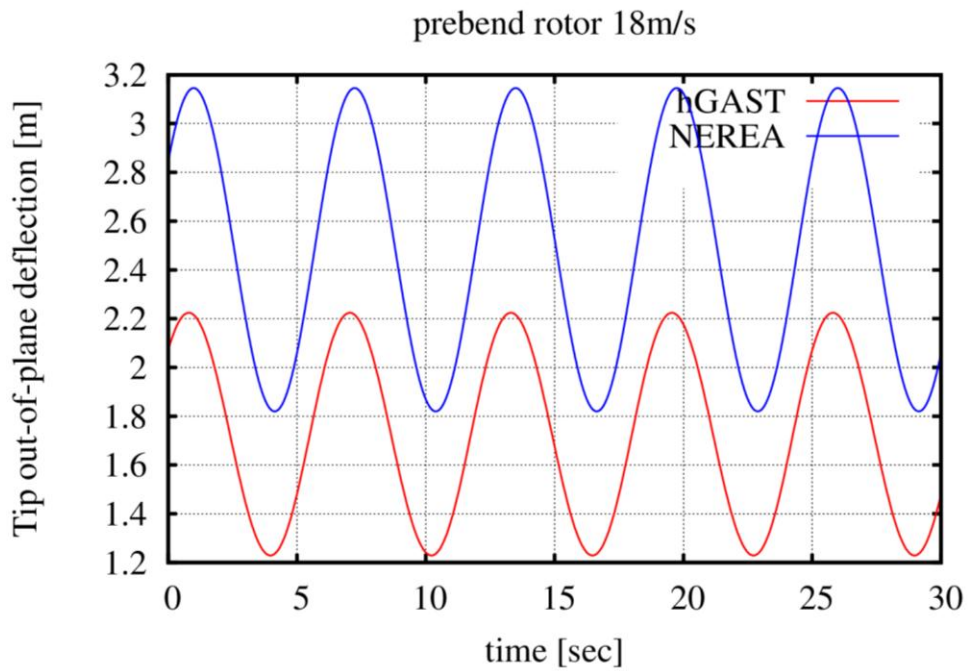


Figure 43: Blade tip out-of-plane deflection – wind speed 18 m/s - prebent blade

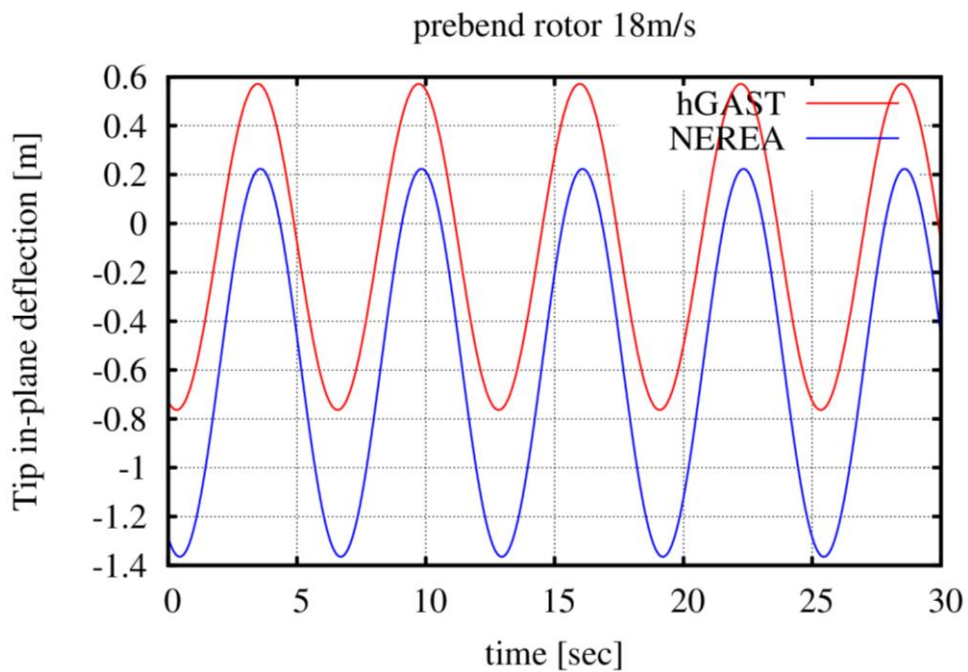


Figure 44: Blade tip in-plane deflection – wind speed 18 m/s - prebent blade

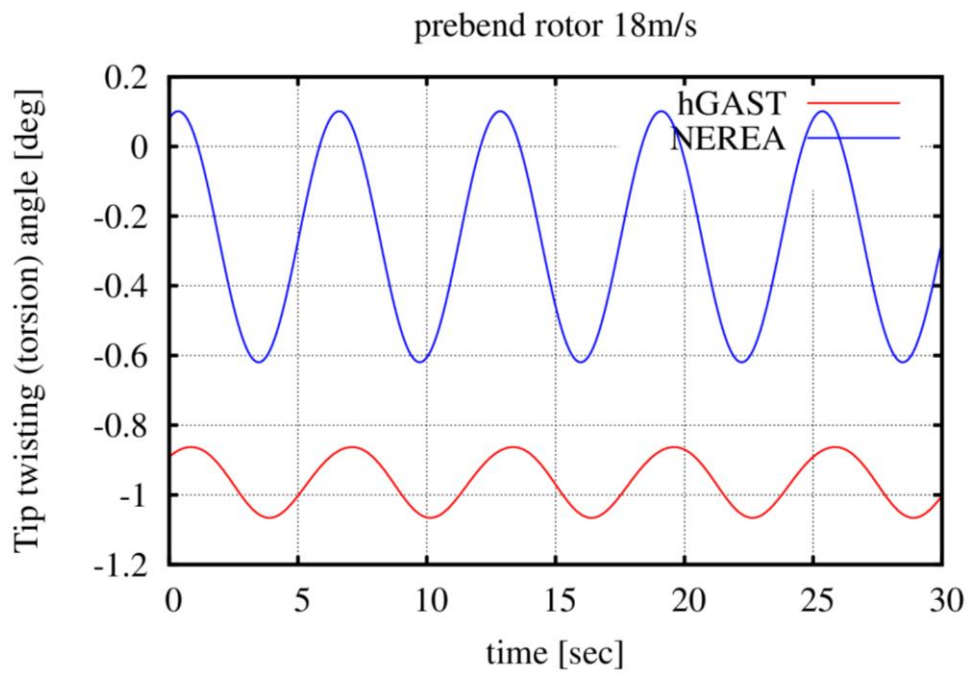


Figure 45: Blade tip twisting angle– wind speed 18 m/s - prebent blade

### 1.3 Full wind turbine aeroelastic validation

Simulations of the full wind turbine system are performed in this section for the **prebent** blade.

Analysis consists of the following test cases:

- Wind step-up and step-down cases, as defined in D 2.21 (Zahle, Riziotis, Bergami, & Madsen, 2013)), for the stiff and the flexible turbine are simulated from the cut-in to the cut-out wind speeds (4-25m/s). **Updated/additional results with respect to those shown in version 1 of D 2.21 are provided herein.**
- 10min simulations considering turbulent inflow defined either using the Mann model or the Veers model.

#### 1.3.1 Step-up and step-down cases

Wind conditions: Uniform inflow,

Definitions: In the step-up case, starting from the cut-in speed of 4 m/s, 1 m/s steps of the wind speed are simulated up to the cut-out wind speed of 25 m/s. The wind speed rises within 1 s linearly and remains constant for 100 s (see Table 5 and Figure 46), while for the step-down case starting from the cut-out speed of 25 m/s, 1 m/s steps of the wind speed will be simulated down to the cut-in wind speed of 4 m/s. The wind speed drops within 1 s linearly and remains constant for 100 s (see Table 6).

**Table 5 . Definition of the wind speed step-up cases**

t[s]	Wind speed [m/s]
0	4
100	4
101	5
201	5
202	6
302	6
303	7
.....	.....

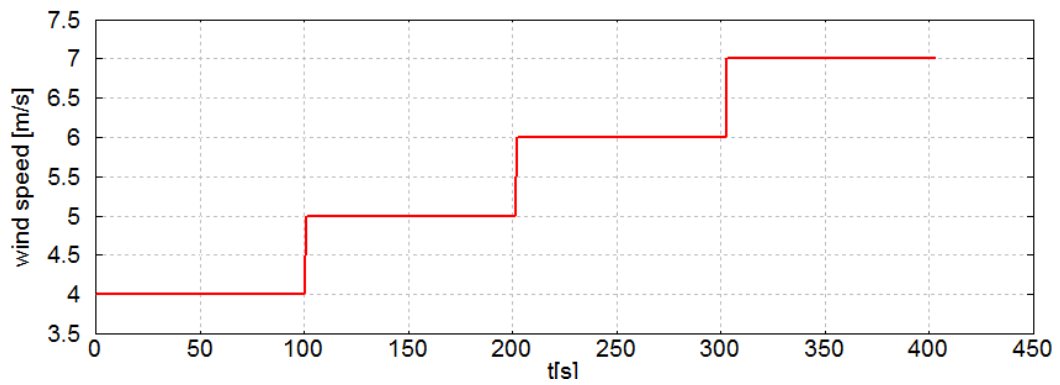


Figure 46: Example of horizontal wind time series for the wind turbine aeroelasticity comparison.

Table 6: Definition of the wind speed step down cases

t[s]	Wind speed [m/s]
0	25
100	25
101	24
201	24
202	23
302	23
303	22
.....	.....

Output:

Time-series of:

1. Time [s]
2. Rotor speed [Rpm]
3. Generator speed [Rpm]
4. Generator torque [kNm]
5. Blade collective pitch [deg]
6. Blade root out-of-plane bending moment [kNm]
7. Blade root twisting moment [kNm]
8. Blade root in-plane bending moment [kNm]
9. Tower top pitching moment [kNm]
10. Tower top rolling moment [kNm]
11. Tower top yawing moment [kNm]
12. Tower base fore-aft moment [kNm]
13. Tower base lateral moment [kNm]
14. Tower base yaw moment [kNm]
15. Blade tip out-of-plane deflection [m]
16. Blade tip in-plane deflection [m]
17. Blade tip twisting (torsion) angle [deg]
18. Tower top fore-aft deflection [m]
19. Tower top lateral deflection [m]

The aeroelastic bending moments, and structural deformations, are given according to the reference system sketched in Figure 35.

In addition it is noted that:

The air density is constant and equal to  $\rho = 1.225 \text{ kg/ m}^3$ .

The blade pitch angle is positive for the blade pitched to feather, i.e. positive pitch angles reduce the angles of attack along the blade.

The blade deflections and root bending moment are referred to the rotor plane coordinate systems, as opposed to the blade coordinate system. The two systems coincide for zero pitch angles and the blade coordinate system rotates as the blade pitches, whereas the rotor plane coordinate system does not.

The blade tip torsion angle is instead referred to the blade coordinate systems, i.e. the time series of the blade tip torsion do not include the effects of the whole blade pitching; the structural twist angle is not included either.

The tower top sensor is defined at the yaw bearing position, at the last node of the tower, below the nacelle element, hence at a distance from the ground of  $z = 115.63 \text{ m}$ .

### Aerodynamic simulations (Time series of the stiff rotor) - HAWC2 and GAST simulations

The rotor speed, the blade collective pitch, the generator's torque and the aerodynamic thrust and power are compared for the stiff step up and step down cases in Figure 47 and Figure 48 respectively. The agreement between GAST and HAWC2 is fine. Very small differences are seen in the variable speed part (7-11m/s) in which GAST predicts slightly reduced rotor speed and slightly increased blade pitch which results in an overall reduced torque, thrust and power as compared to HAWC2 predictions.

### Aeroelastic simulations (Time series of the flexible turbine and statistics) – Cp-Lambda, HAWC2 and GAST simulations

In Figure 49 and Figure 50 predictions provided by the aeroelastic tools Cp-Lambda, HAWC2 and GAST are compared for the step up and step down cases for the flexible turbine. Overall the agreement is fine, although differences are reported for some of the sensors. In addition the statistics (min, max and mean values) for the step up case are presented in (Figure 51) as functions of the corresponding wind speed. In order to limit the effects of the time transient following the step change in wind speed, the statistics are performed on the time series portions corresponding to the last three full rotor revolutions of each wind speed step. It is observed that:

- The agreement in the prediction of the rotor speed seems to be good. Below rated conditions HAWC2 returns slightly higher aerodynamic torque, resulting in higher rotational speed and higher generator torque and power output as compared both to GAST and to Cp-Lambda. This is due to different computation of the torsion deformation with direct influence on AOA and thus on aerodynamic loading, as explained next.

This disagreement of the torsional deformation appears to be a difference in output of the torsion, as opposed to a difference in the aeroelastic computation of the blade torsion. The HAWC2 results are obtained using entries of the transformation matrix from blade system to the deformed element system to compute the torsional deflection. This computation of the torsion is affected by high out-of-plane blade deflections and therefore the disagreement to the other codes is largest at high thrust. To obtain an alternative output of the tip torsion, a modified torsion sensor has been implemented. This sensor uses the rotation vector from the undeformed to the deformed element coordinate system. The projection of that rotation vector on the pitch axis results in a torsion output that is less sensitive to out-of-plane deflection than the original sensor in HAWC2. This modified torsional output is compared to the original HAWC2 torsion output in Figure 49a. Clearly the modified torsional output is in better agreement with the GAST and Cp-Lambda results shown in Figure 49, which indicates that the differences in the tip torsion are due to different methods of outputting the torsion rather than different aeroelastic torsion computations.

So below rated wind speed HAWC2 predicts increased generator torque, rotor speed and generator speed, while above rated speed this difference is masked by the controller through the slight increase in the collective pitch angle.

- Good agreement is observed in the blade root moments. Expected differences below rated wind speed in HAWC2 are explained by the abovementioned increase in the rotor speed, HAWC2 predicts slightly increased mean value of the blade root pitching moment while GAST clearly predicts reduced amplitude for the same signal.
- The tower top tilting and rolling moments show similar trends. In the tower top tilting moment a slight mean value shift appears in Cp-Lambda predictions as compared to the other two codes. A small difference appears also in the predictions of HAWC2 and GAST in

the vicinity of the rated wind speed. A good agreement is reported on the tower top rolling moment. The slight over-prediction of the moment below the rated speed by HAWC2 is in line with the rotor speed.

- An overall good agreement is reported in the tower bottom fore-aft and side-to-side bending moments. All codes predict oscillations in the tower side-to-side moment. Clearly the initial transient is included in GAST and Cp-Lambda simulations, while in HAWC2 it has been eliminated. GAST predicts larger load oscillations at low wind speeds while HAWC2 at high wind speeds for the same signal.
- The yawing moments along the tower predicted by the GAST and HAWC2 codes have close mean values, but slightly different trends, with HAWC2 predicts a milder increase of the moment above rated conditions. HAWC2 and Cp-Lambda present a better agreement as regards the slope of the curve above the rated speed but they also exhibit higher mean value differences.
- The blade tip out-of-plane displacement exhibits a good agreement between the three codes above the rated power, while below rated conditions HAWC2 reports higher tip deflections for the wind speed range from 7-11 m/s due to the higher rotational speed.
- The blade tip in-plane displacement shows a good agreement below rated conditions, but significantly different trends above rated. The differences between hGAST and the other two codes are caused by different choices of reference coordinate systems. GAST provides the deflections with respect to the blade coordinate system (following the pitch angle rotation), while HAWC2 and Cp-Lambda provide the deflections with respect to the rotor plane.
- The torsion angle difference between HAWC2 and the other codes is already discussed. Moreover although torsion angle prediction by Cp-Lambda and GAST follows a similar trend, a different mean value is obtained in case of high flapwise deflections (above rated wind speed). This is mainly attributed to the bending-torsion coupling effect which is triggered when the bending deflections get high. A denser FEM grid should be used in GAST.
- A good agreement between the codes is reported for the tower top displacement in the fore-aft direction, whereas in the side-to-side direction the differences reported on the bending moments are also reflected on the deflection.
- HAWC2 and GAST codes report a good agreement in the predicted aerodynamic thrust force, while Cp-Lambda predicts higher values. A good agreement is also reported in the aerodynamic power between all three codes, with the exception of the below rated conditions at which HAWC2 predicts increased power due to the increased rotor speed.

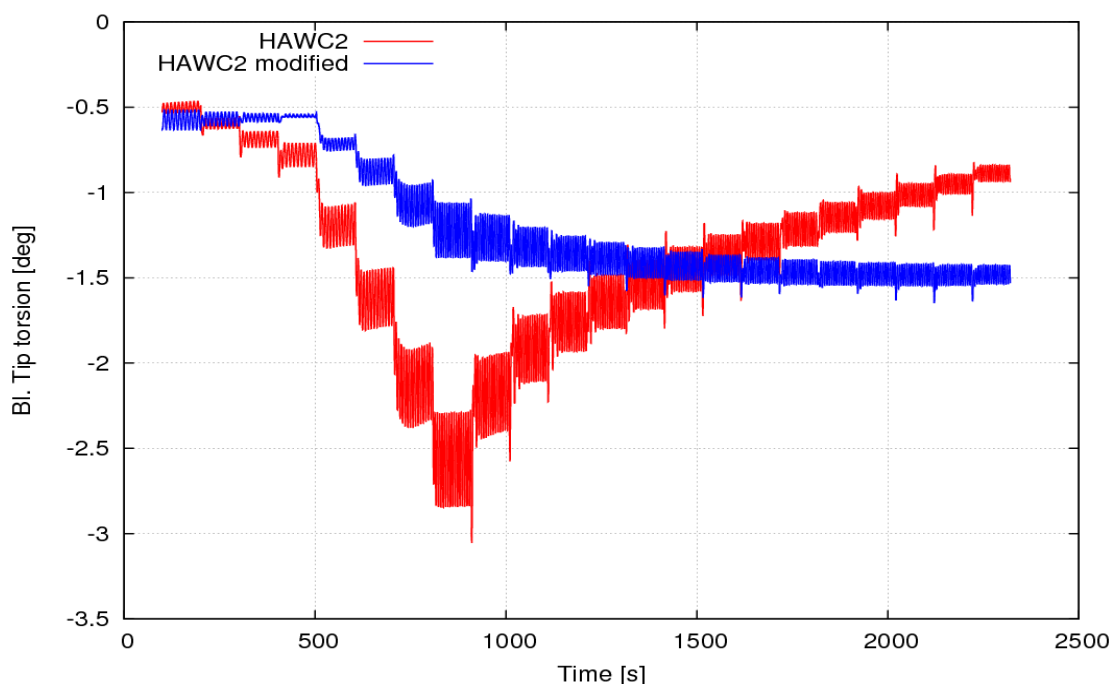


Figure 49a: Comparison of HAWC2 output sensors for blade tip torsion in the wind step up case.

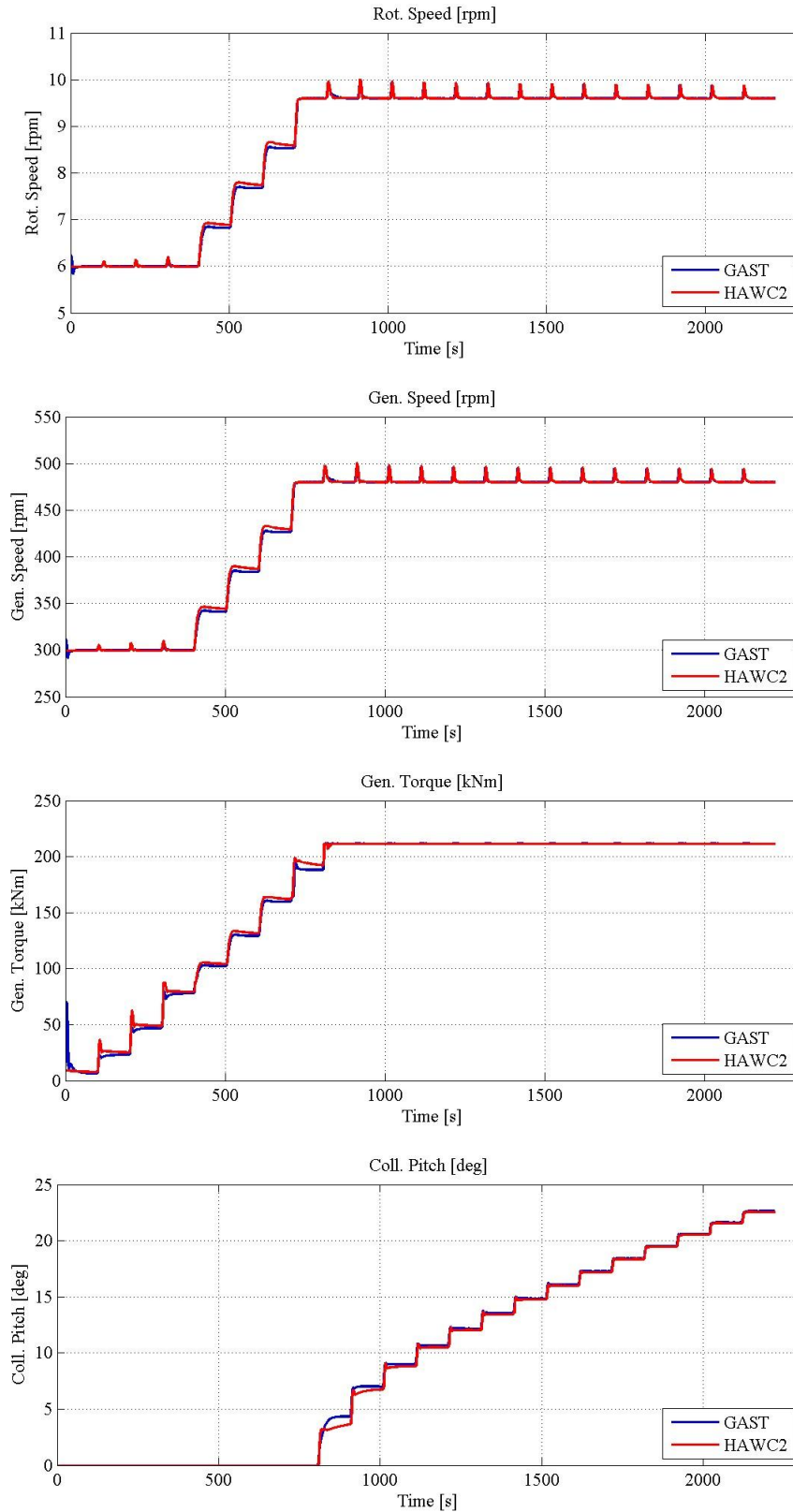
#### Aeroelastic simulations (Time series of the flexible turbine) - hGAST and NEREA simulations

In Figure 52 and Figure 53 predictions provided by the aeroelastic tools hGAST and NEREA are compared for the same step up and step down cases. It is observed that:

- The agreement in the prediction of the rotor speed and the generator torque is good.
- The pitch angle is consistently predicted with an offset by NEREA due to the absence of the torsion degree of freedom.
- The blade root moments are overall in good agreement. hGAST predicts reduced blade root pitching moment in line with the previous findings (see Figure 49, Figure 50).
- The trend in the tower top moments is consistent, while small differences are seen mainly in the mean values. It is noted that the tower top moments are very sensitive to the aerodynamic loading, so the differences seen could be attributed to the different aerodynamic modeling. Mean values of the fore-aft moment are in good agreement, while differences near the rated wind speed are noted. NEREA predicts a mean value drift of the side-to-side moment above rated wind speed. The mean value drift of the yawing moment is similarly predicted by hGAST and NEREA, while NEREA predicts slightly higher mean values for the same signal.
- Good agreement of the tower bottom fore-aft and side-to-side moments is obtained. hGAST predicts slightly lower fore-aft moment for high wind speed while both codes exhibit similar behavior in the lateral direction, as also depicted in the side-to-side bending moment signal.
- Differences are reported in the blade tip deflections. NEREA predicts higher out-of-plane deflections and close to zero torsion angles, while the in-plane deflection is overall in good agreement.

- Good agreement is observed in the tower top fore-aft and side-to-side deflections. The slightly increased fore-aft deflection predictions by NEREA for high wind speeds are in line with the tower bottom fore-aft moment results.

### Time series: stiff WT step-up case



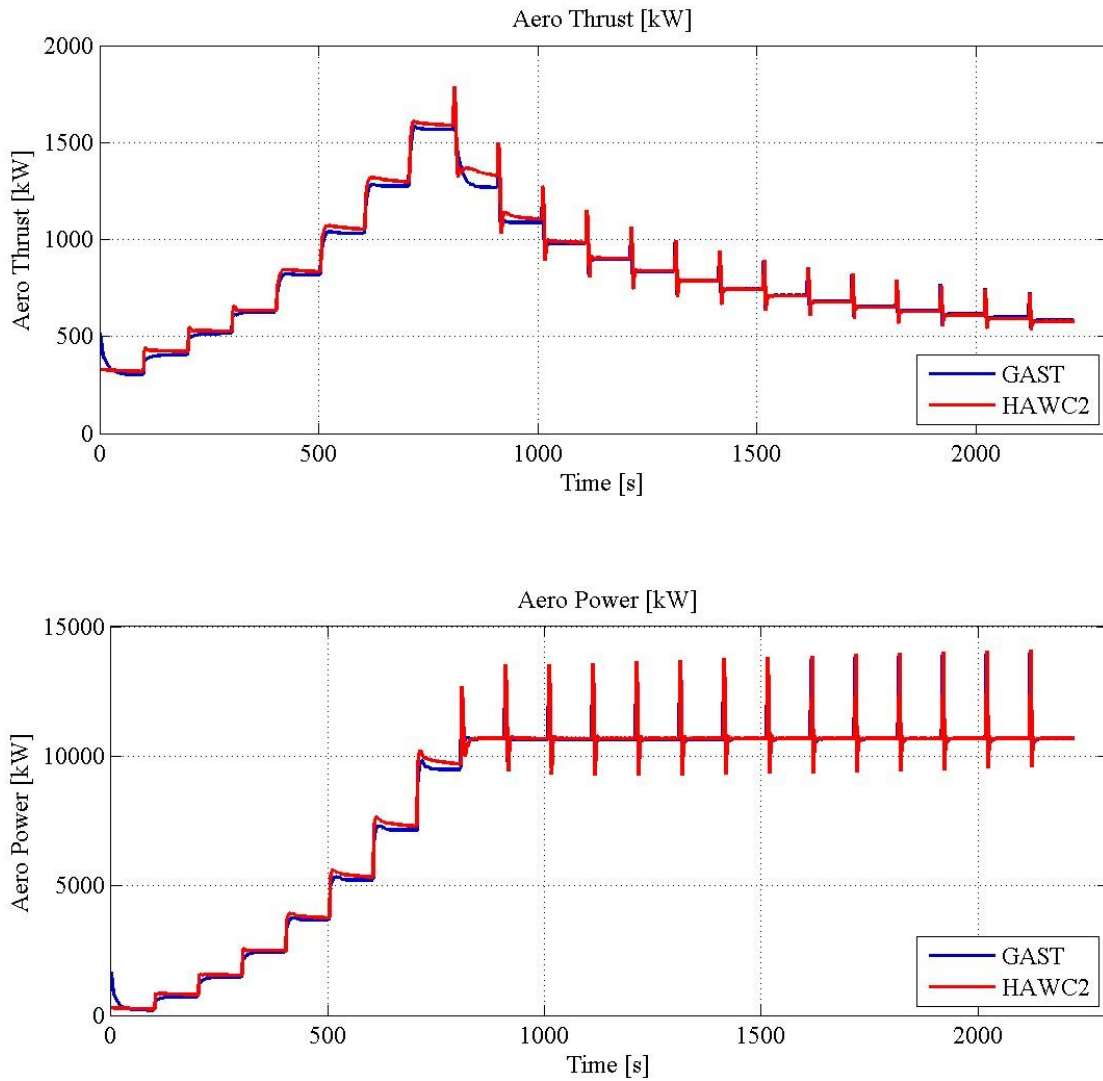
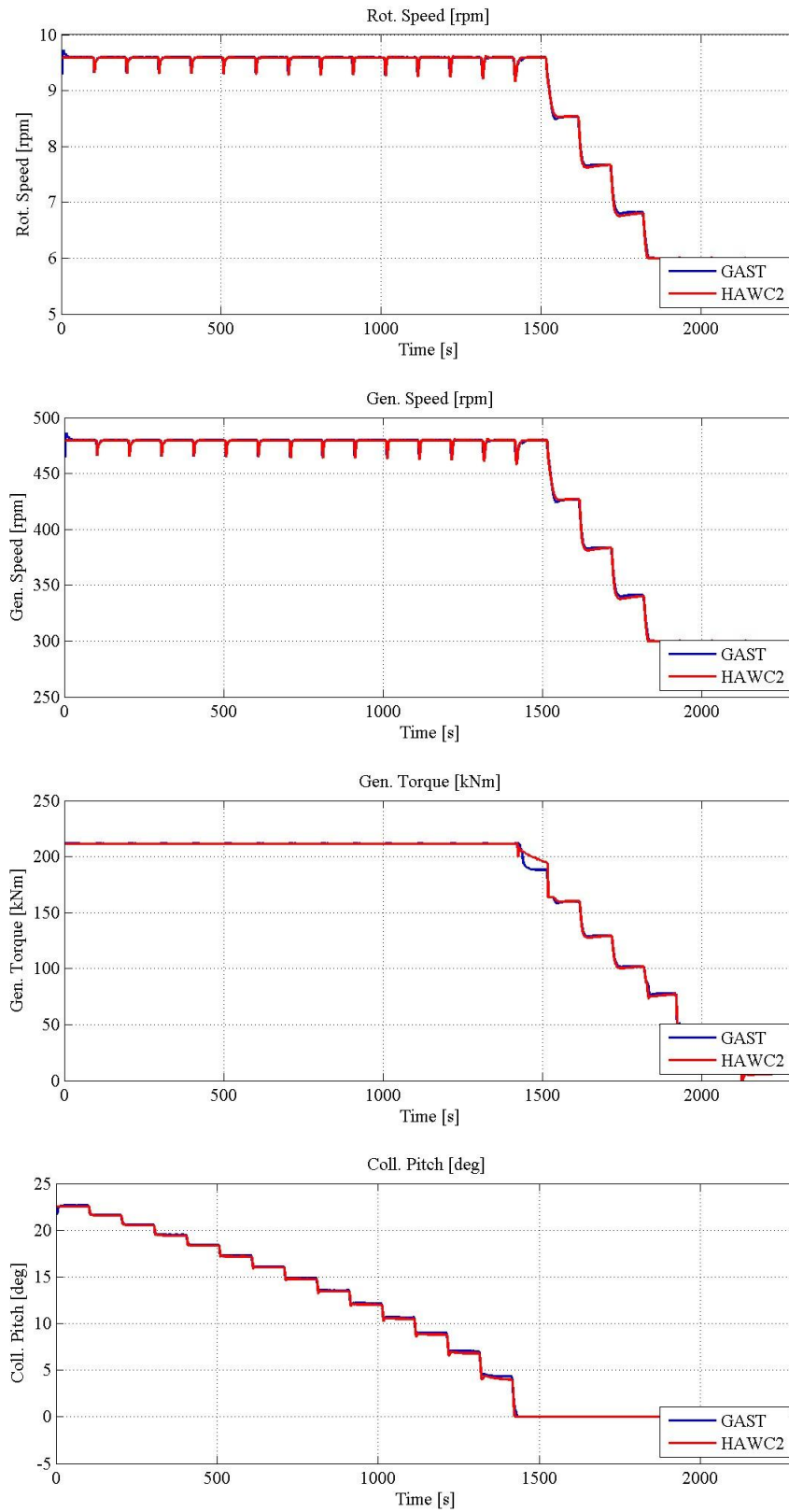


Figure 47: Step up rigid turbine

### Time series: stiff WT step-down case



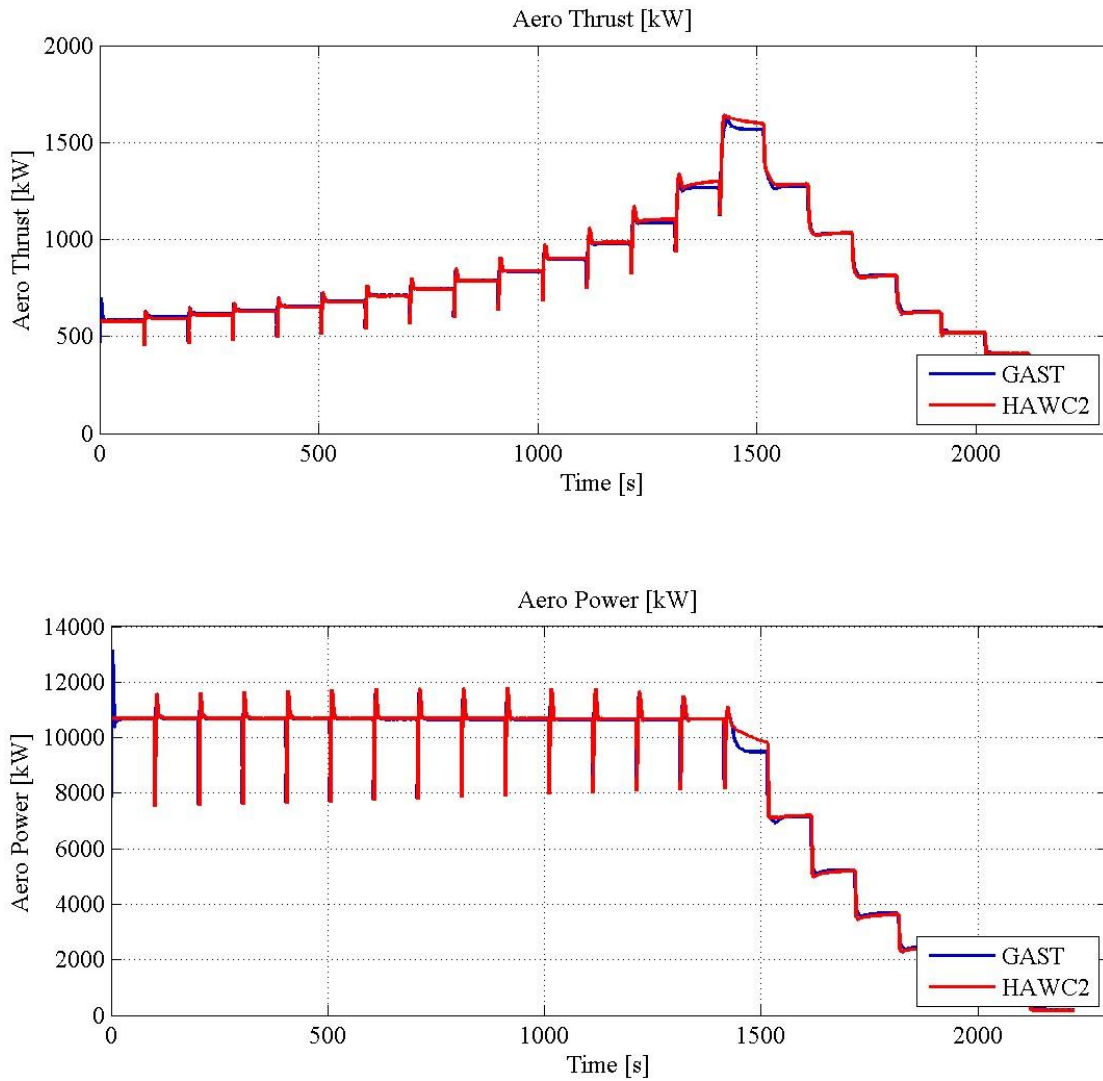
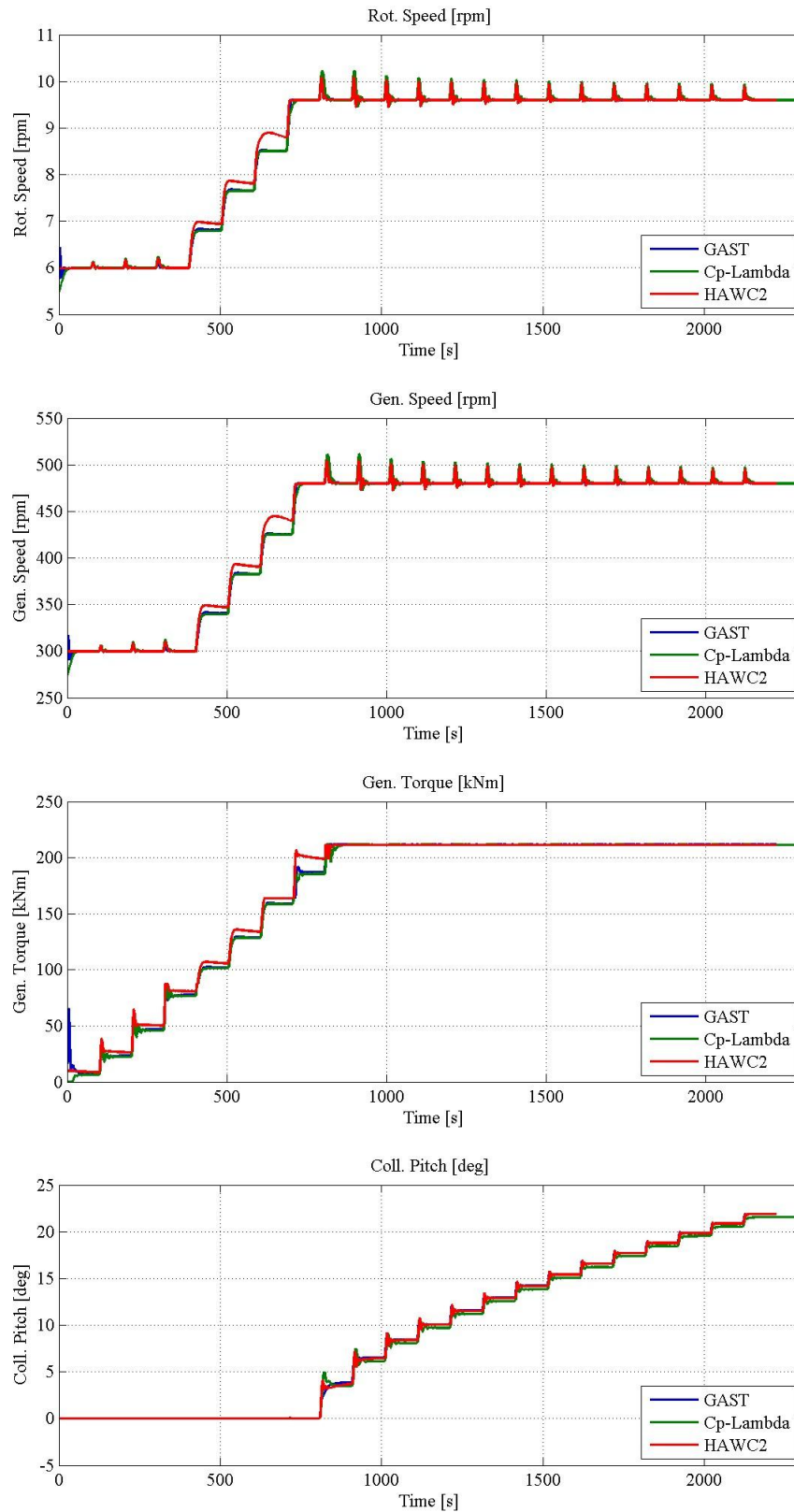
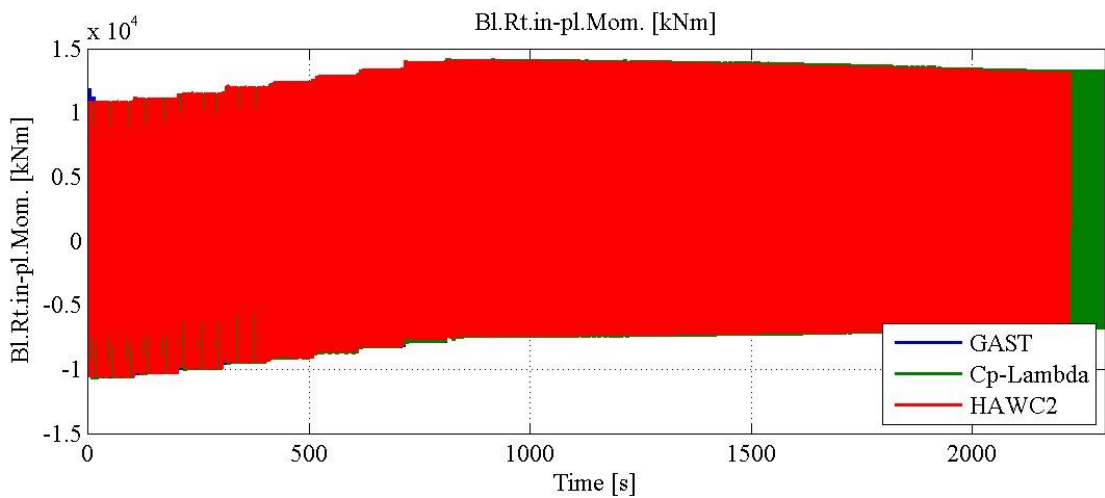
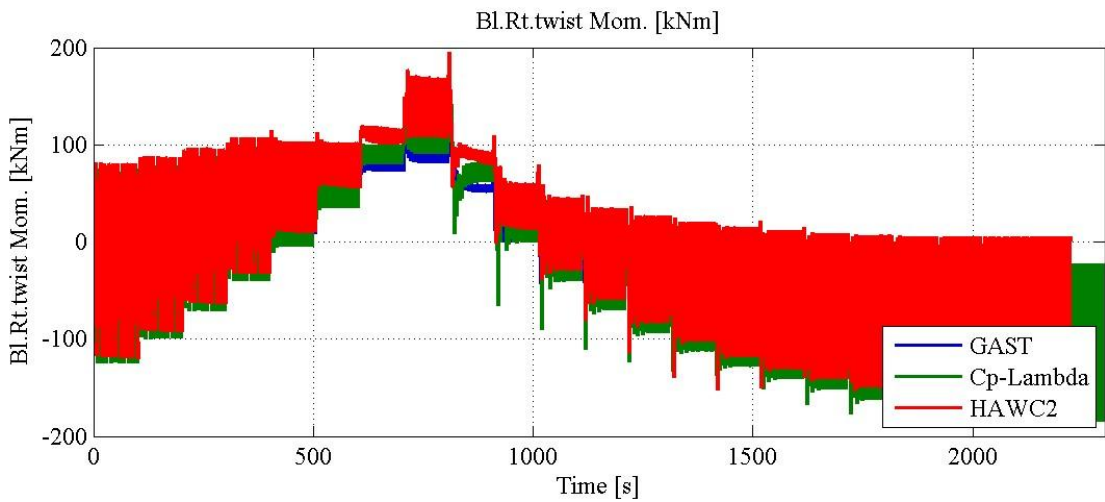
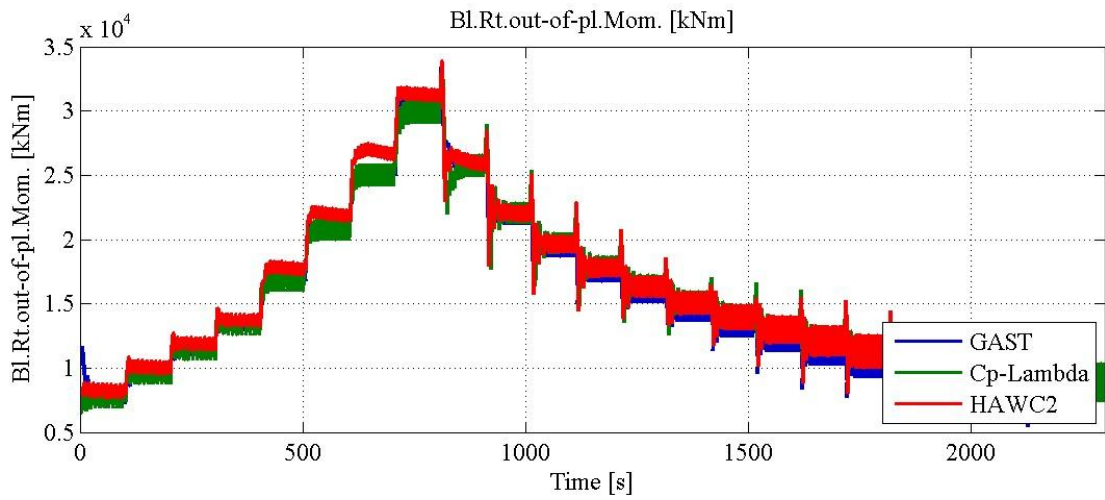
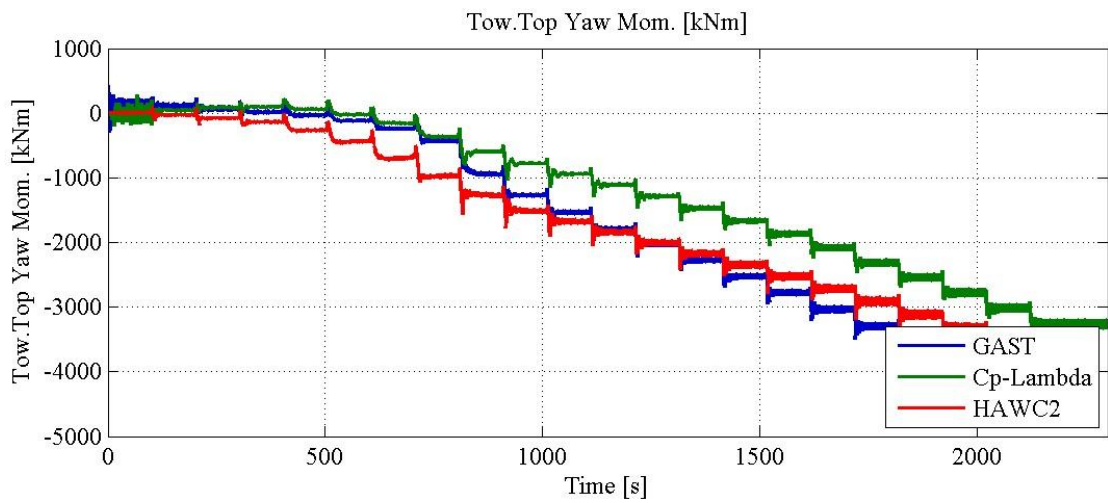
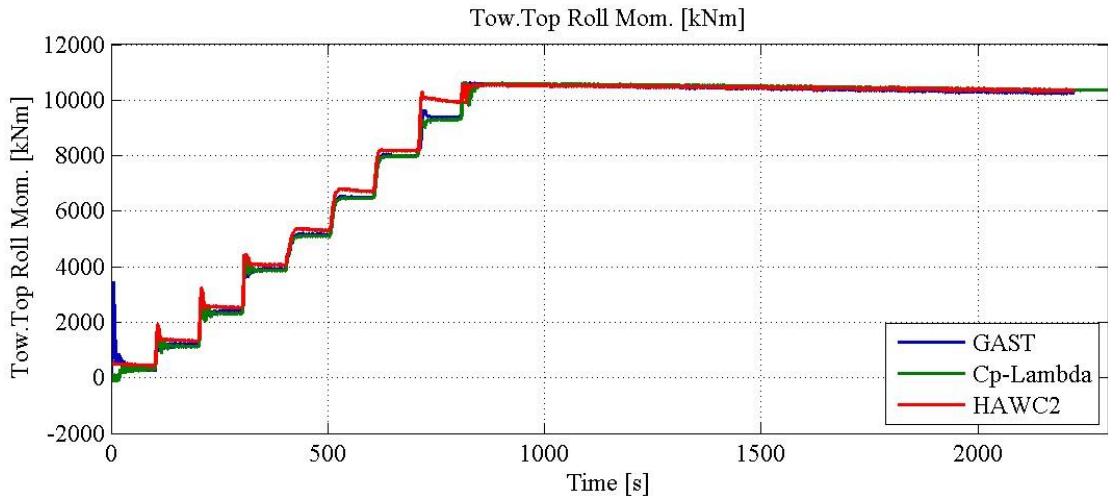
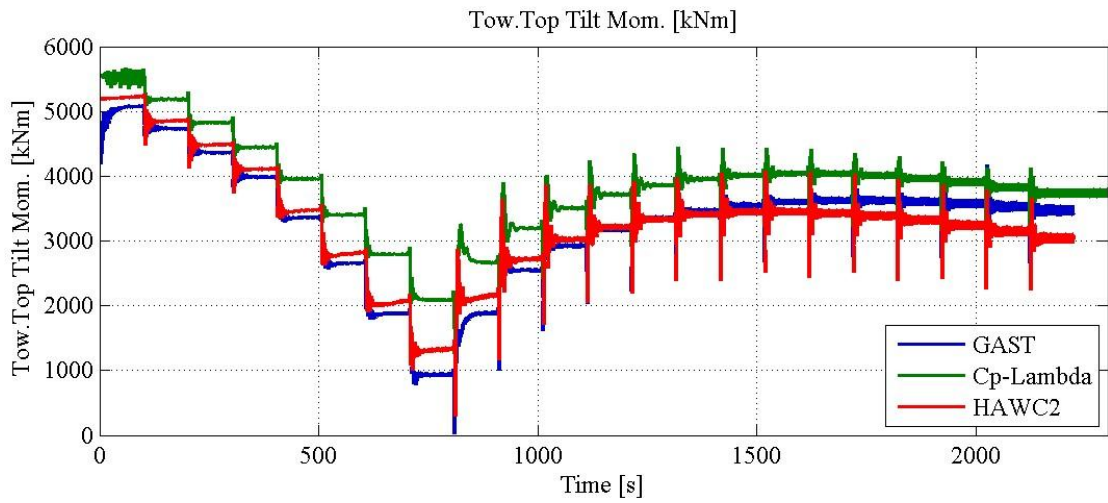


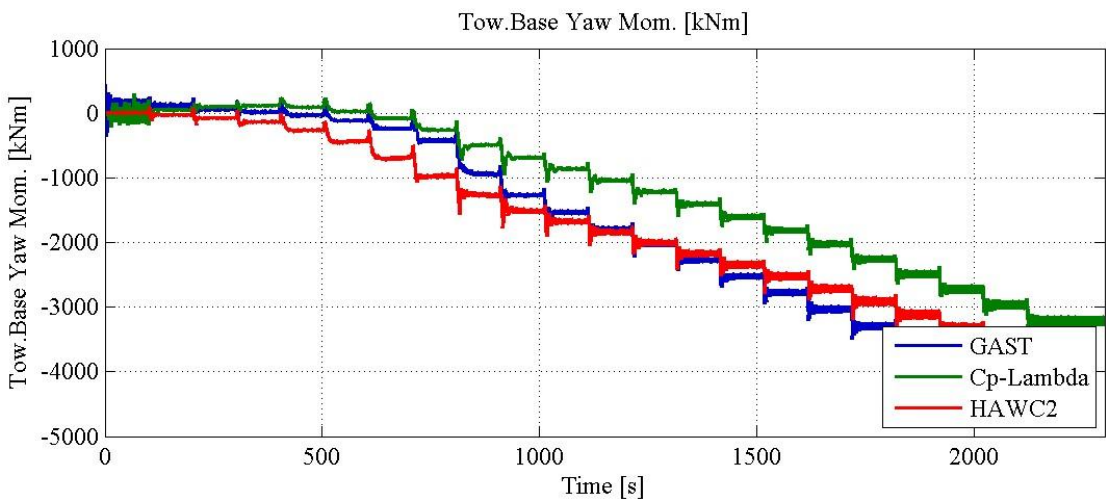
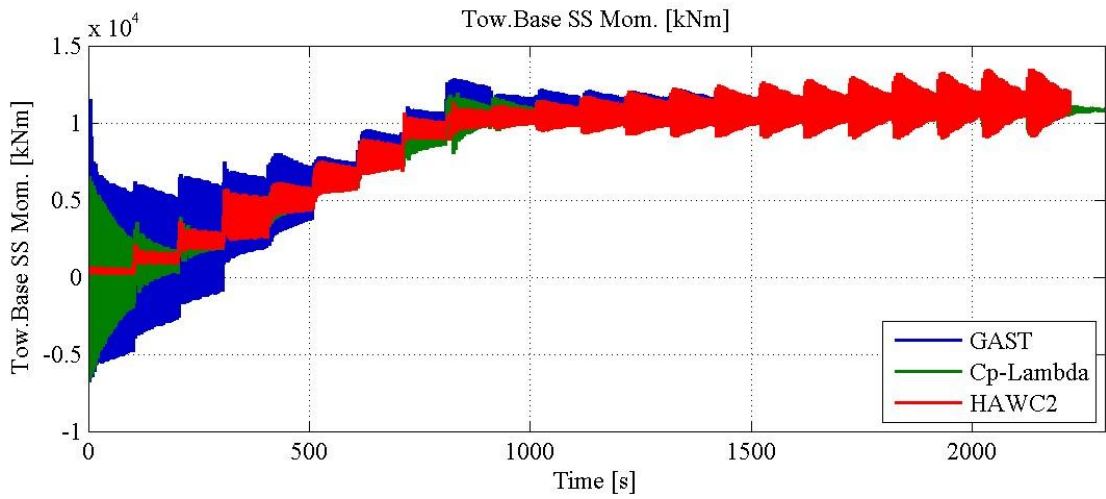
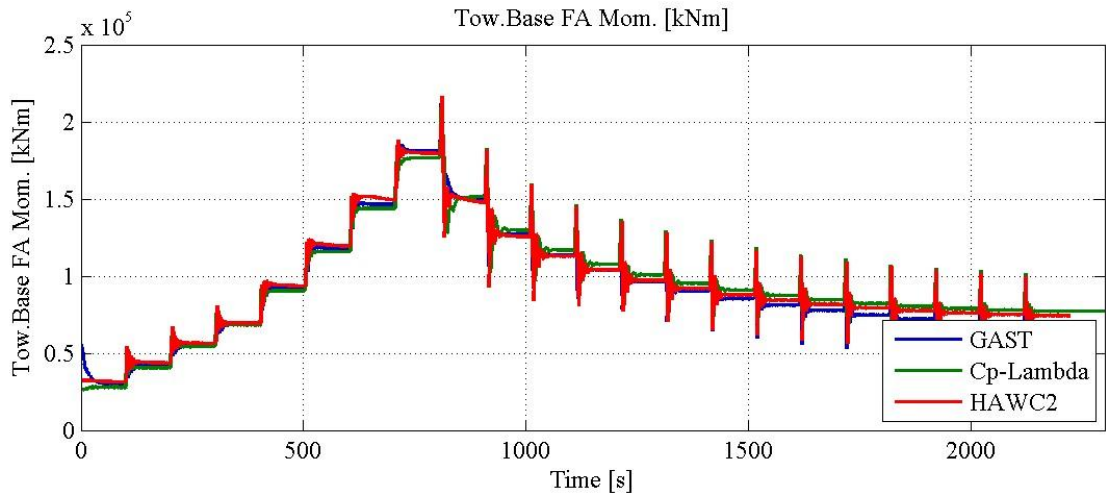
Figure 48: Step down rigid turbine

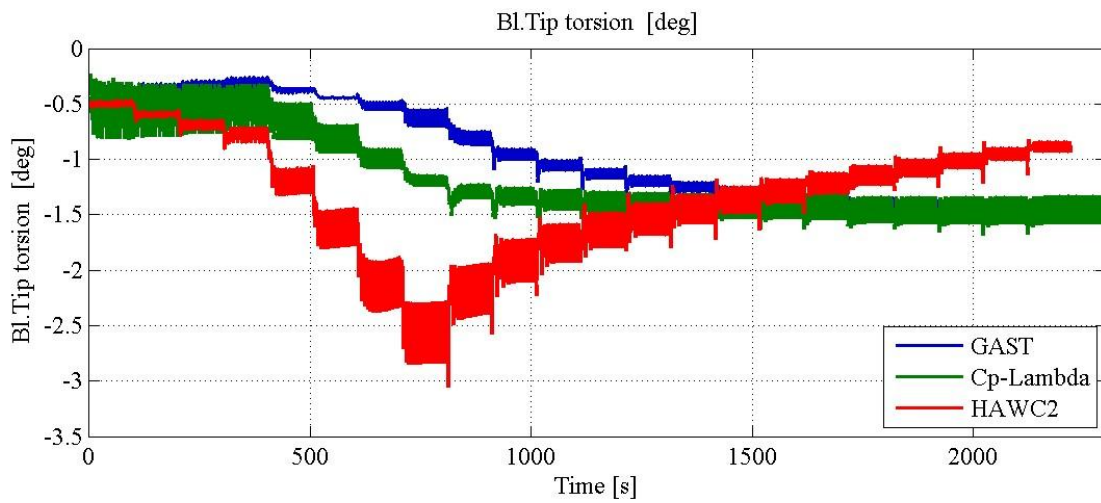
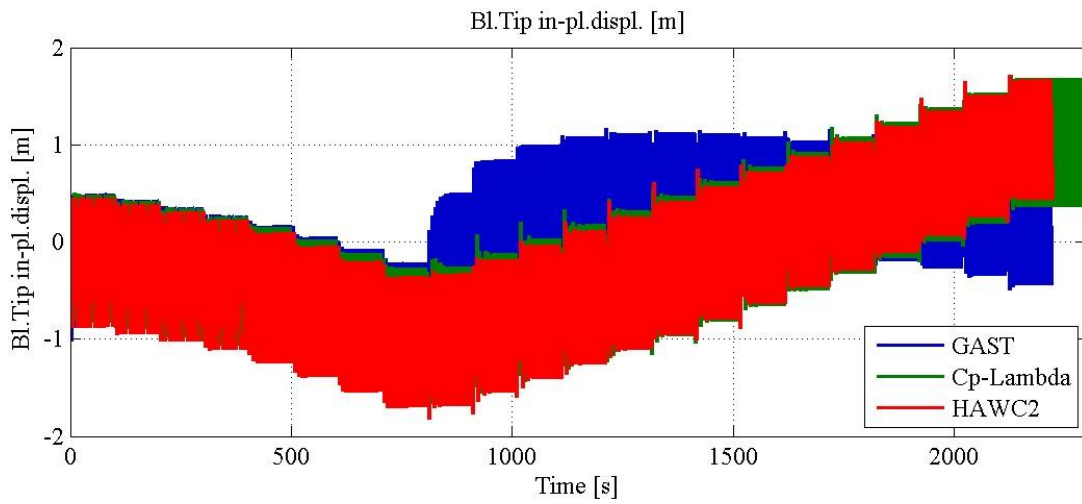
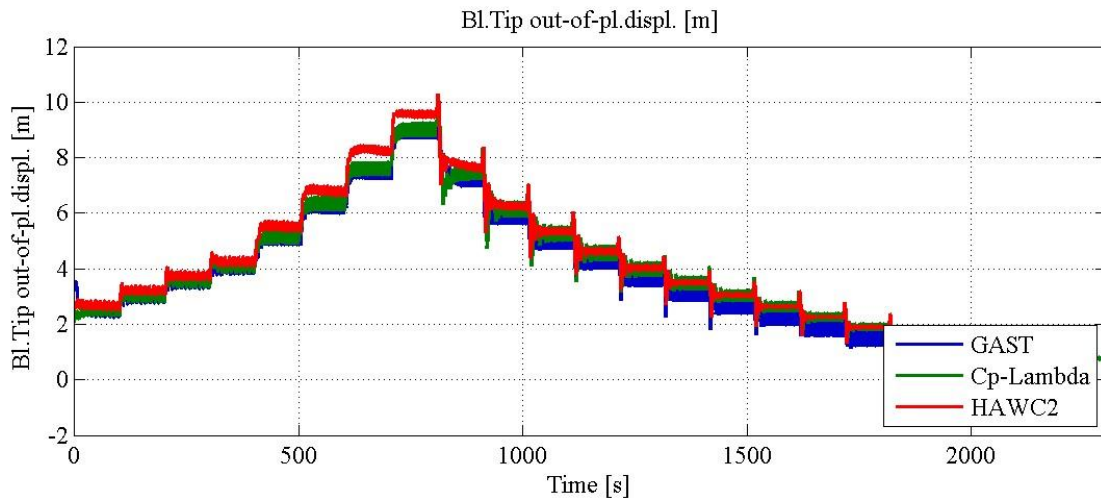
### Time series: flexible WT step-up case

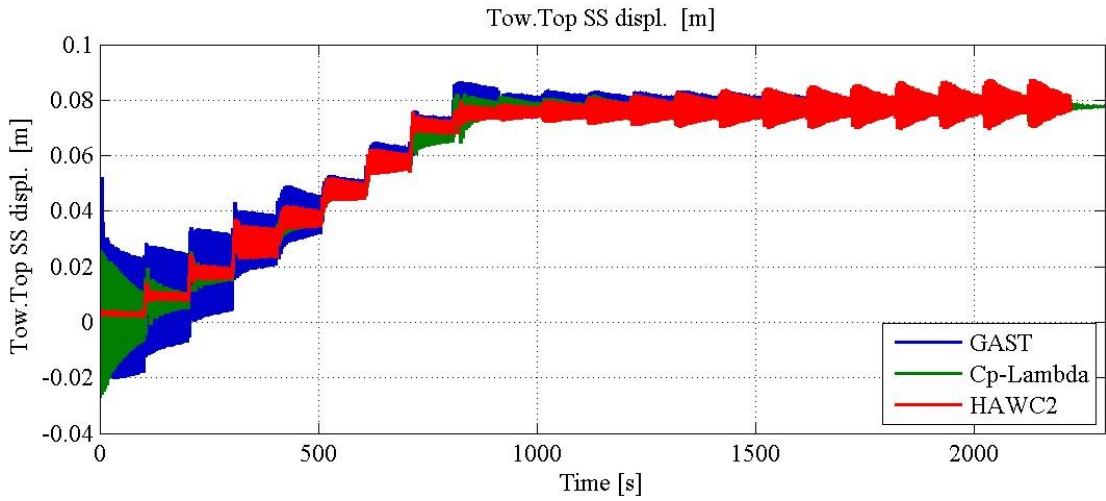
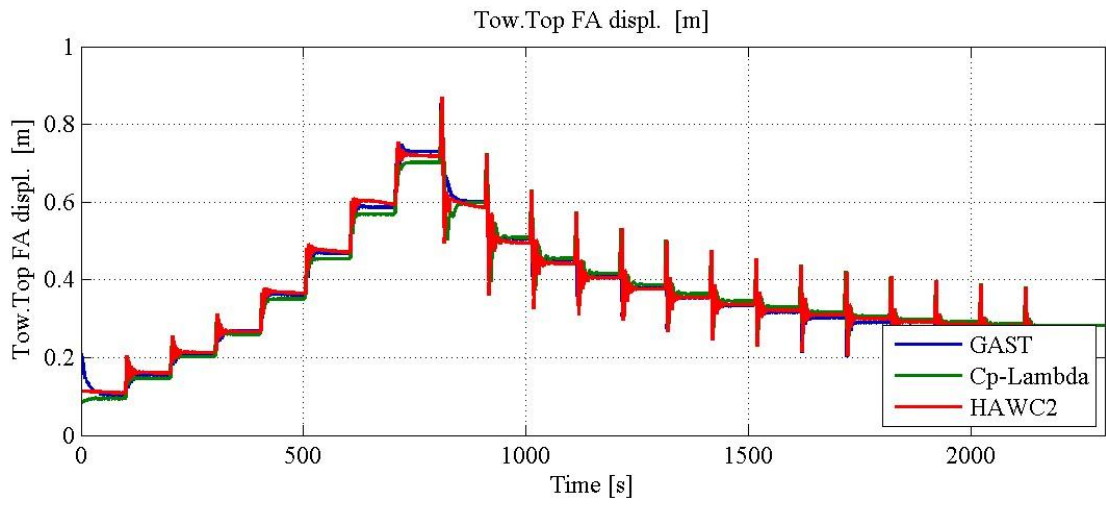












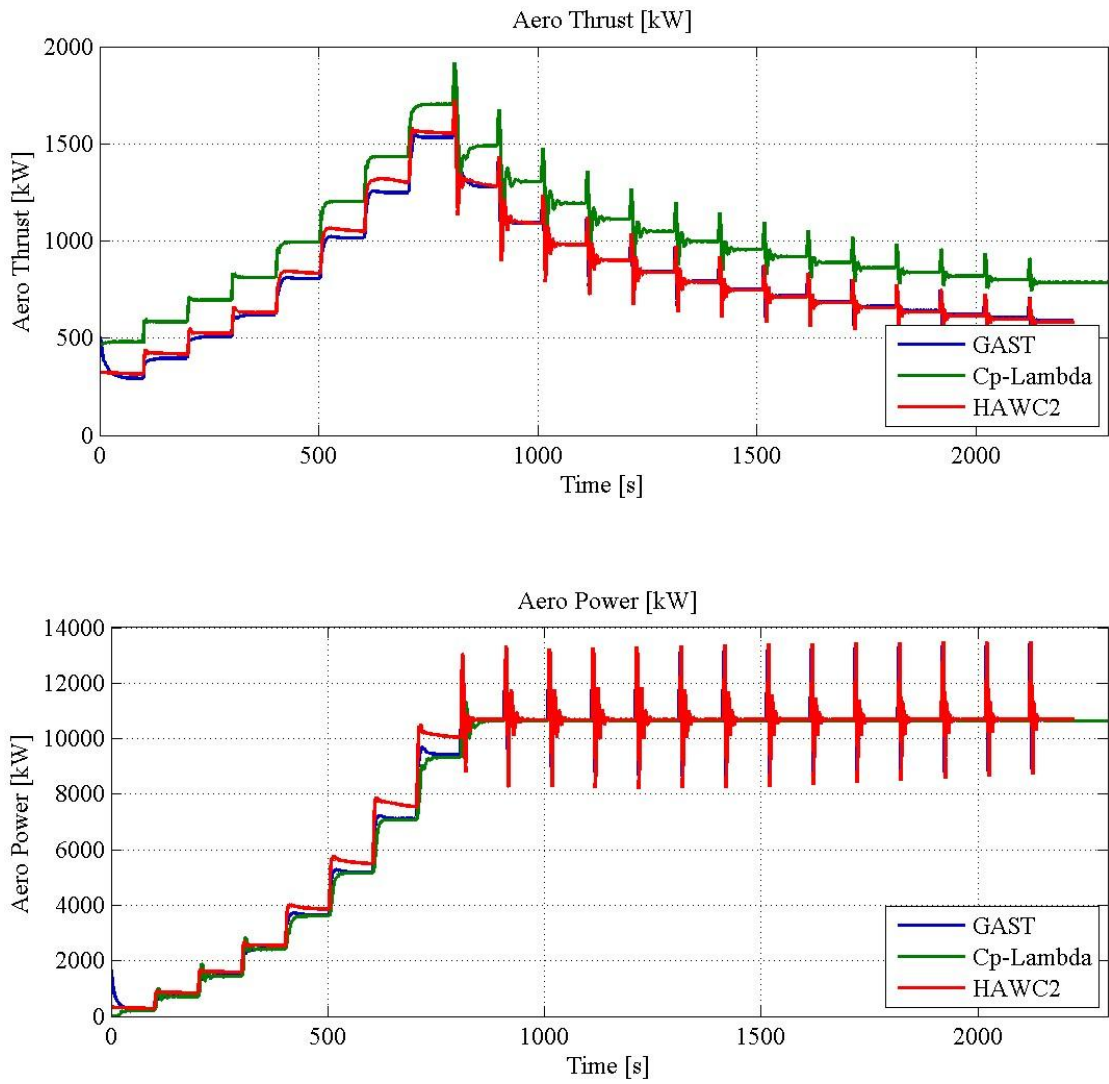
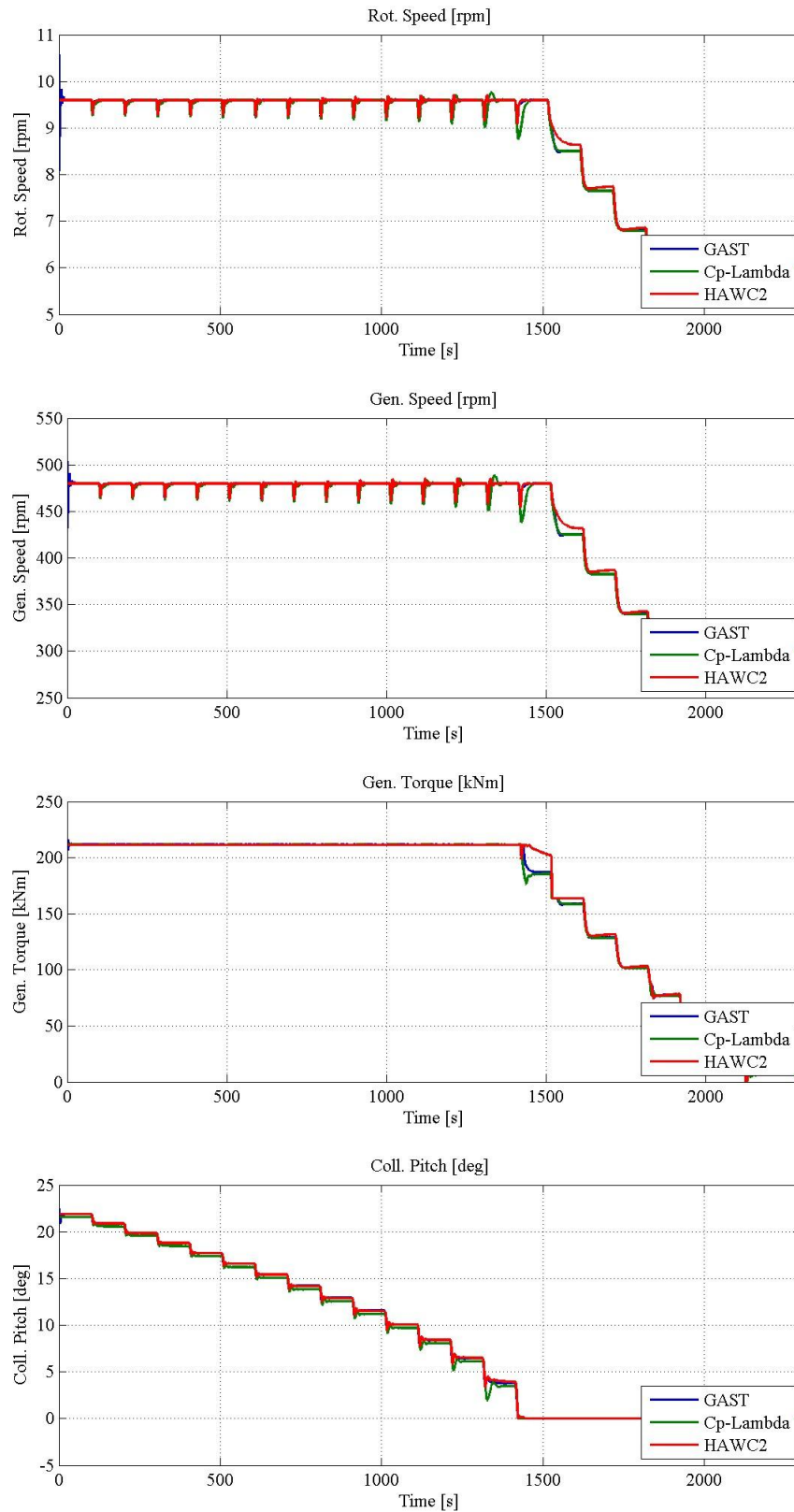
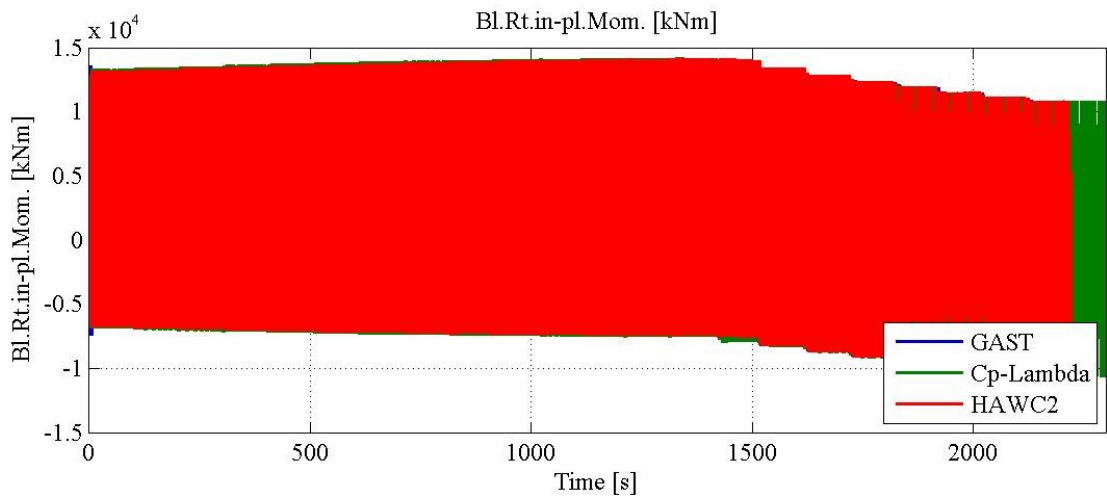
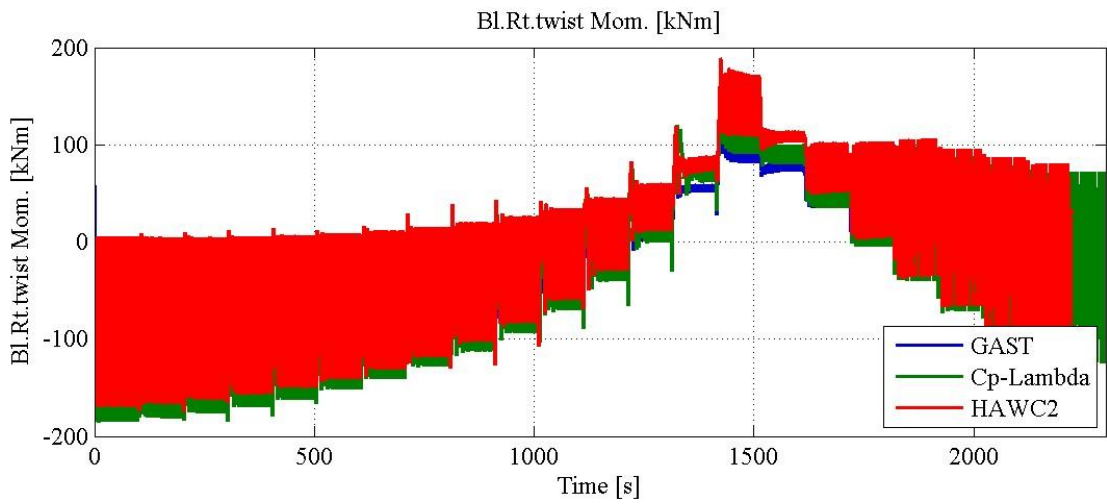
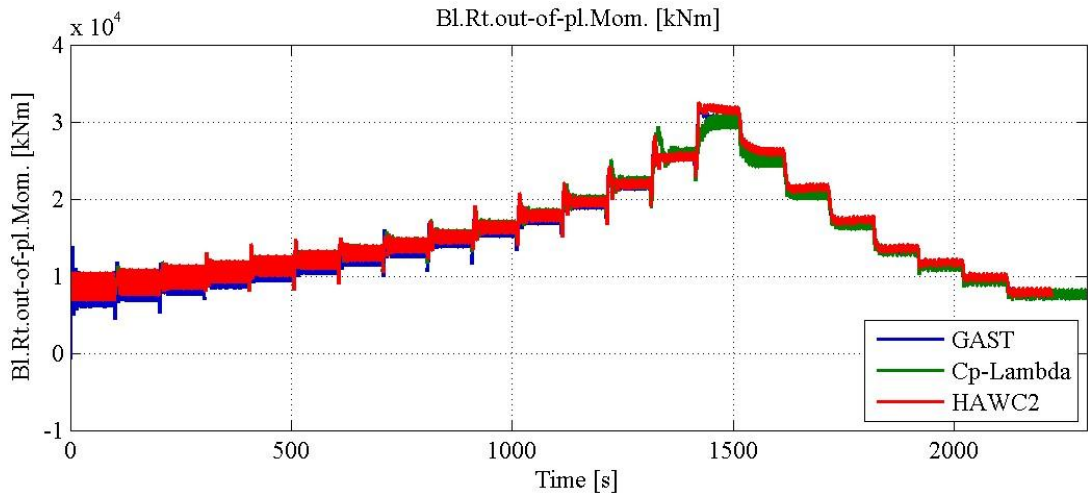
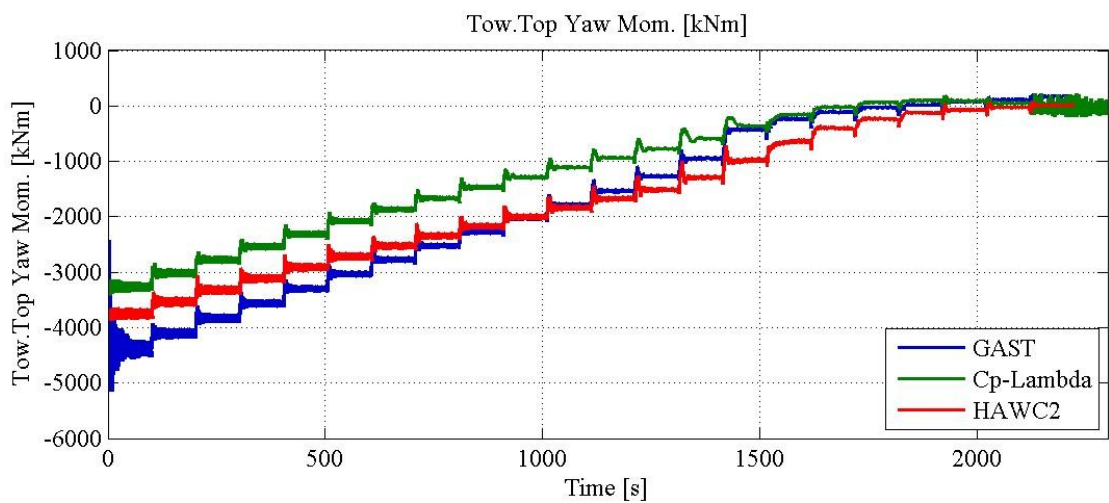
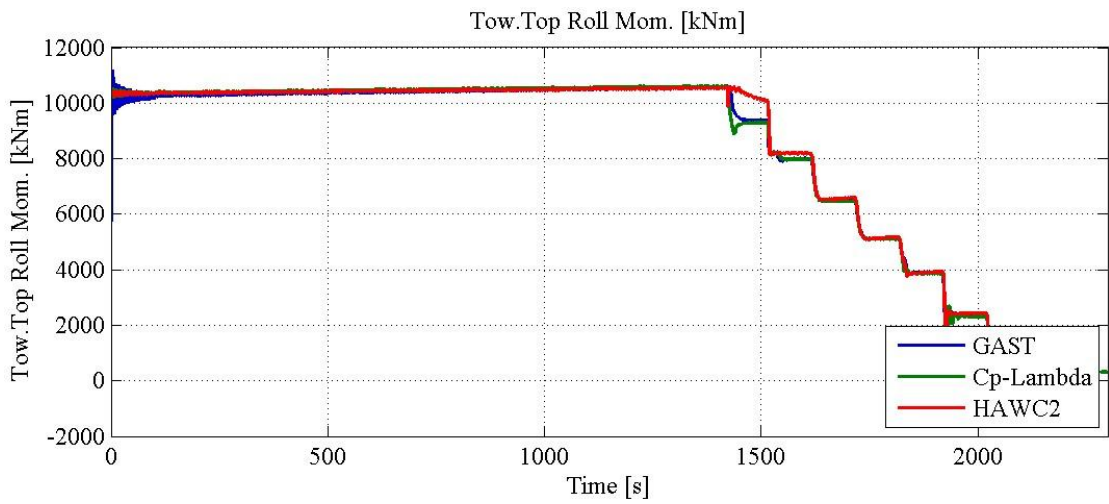
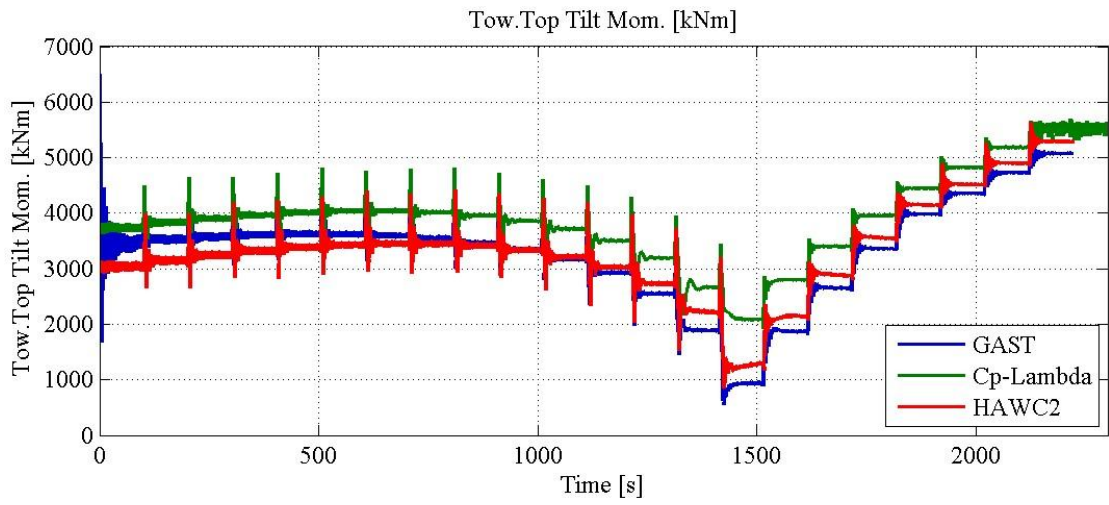


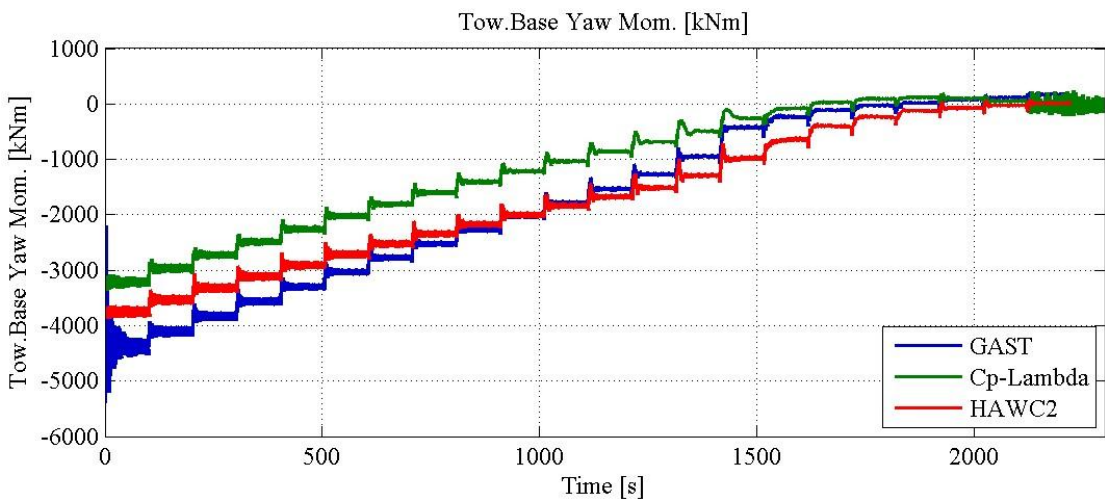
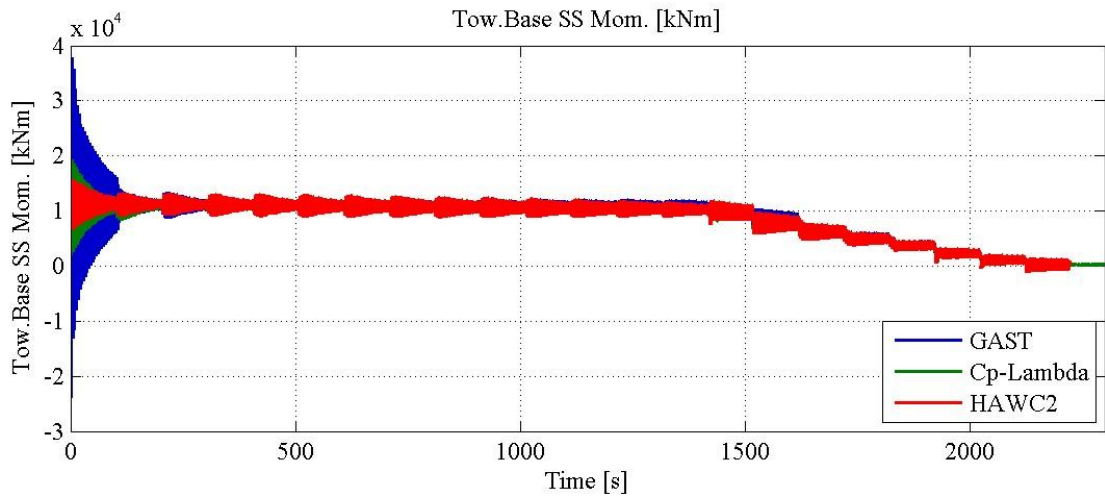
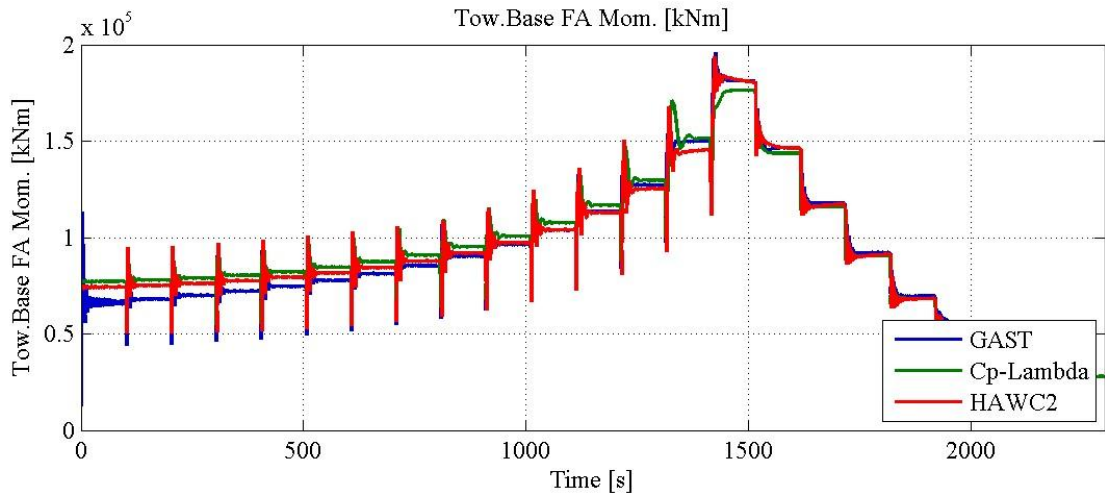
Figure 49: Step up flexible turbine- comparison of FEM codes

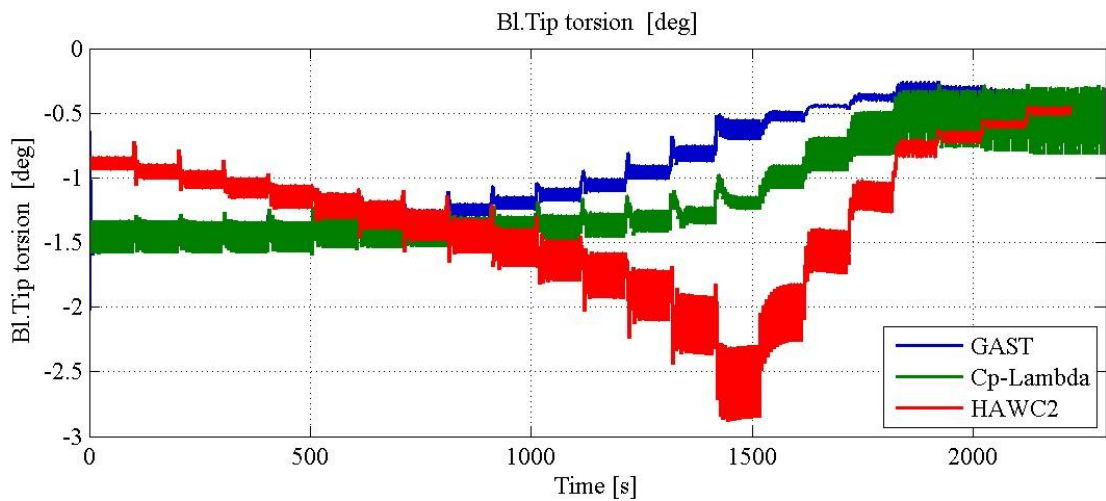
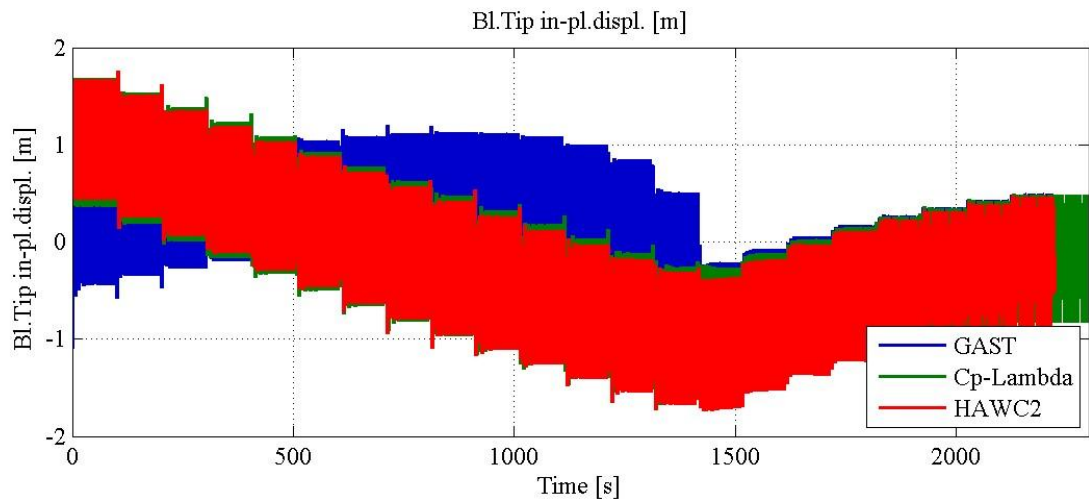
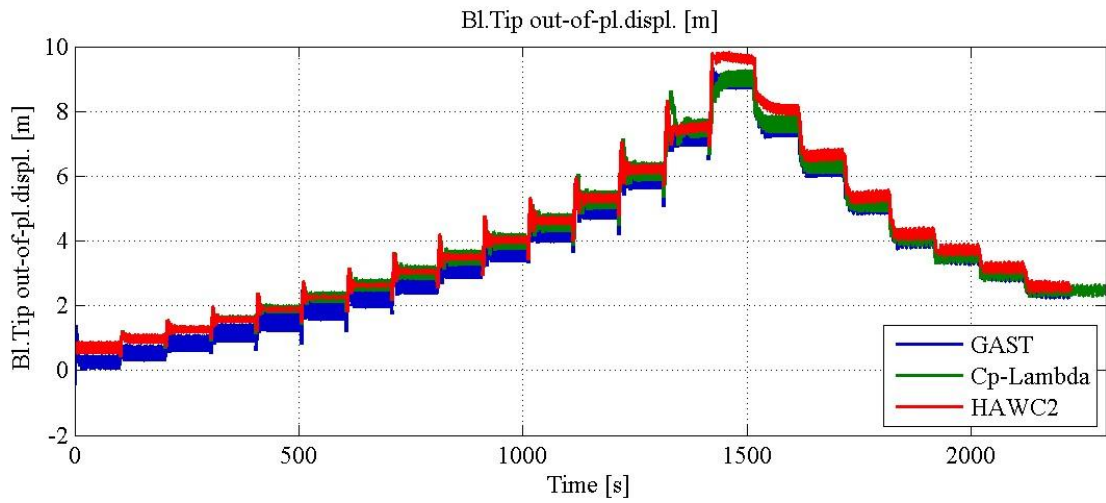
### Time series: flexible WT step-down case

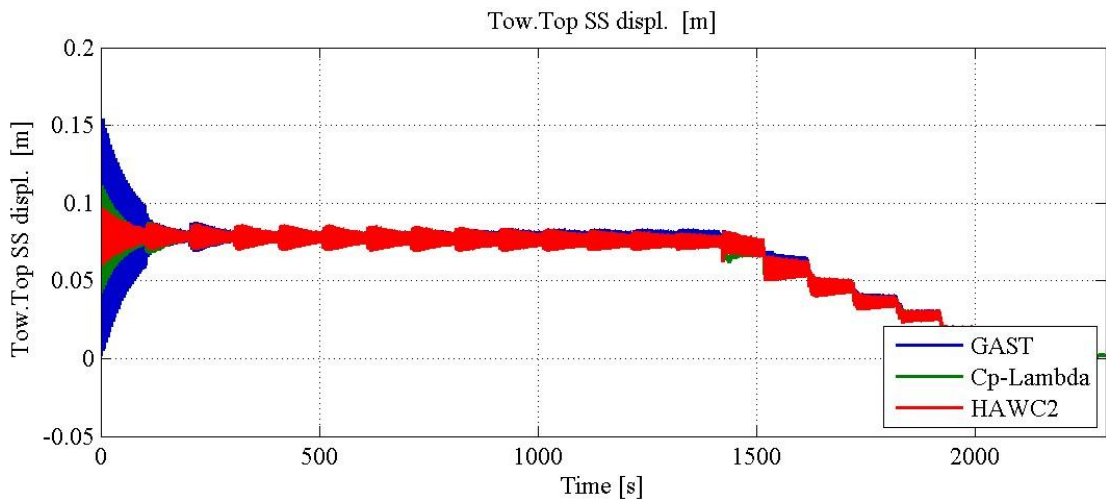
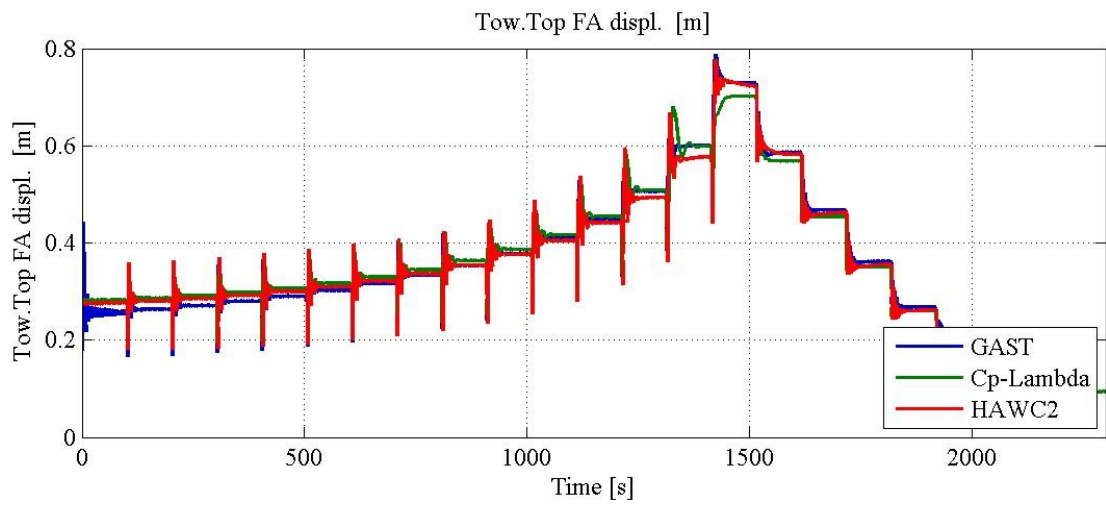












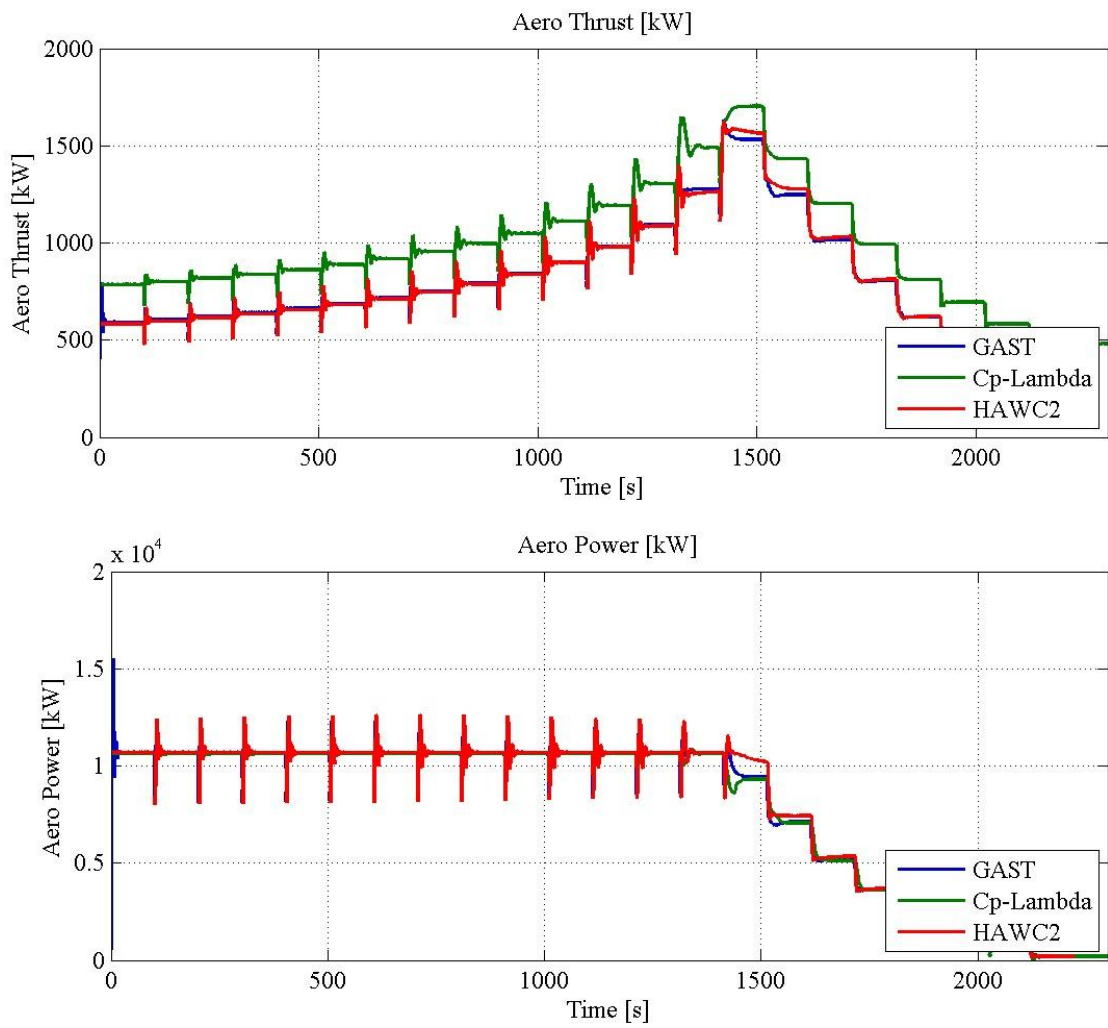
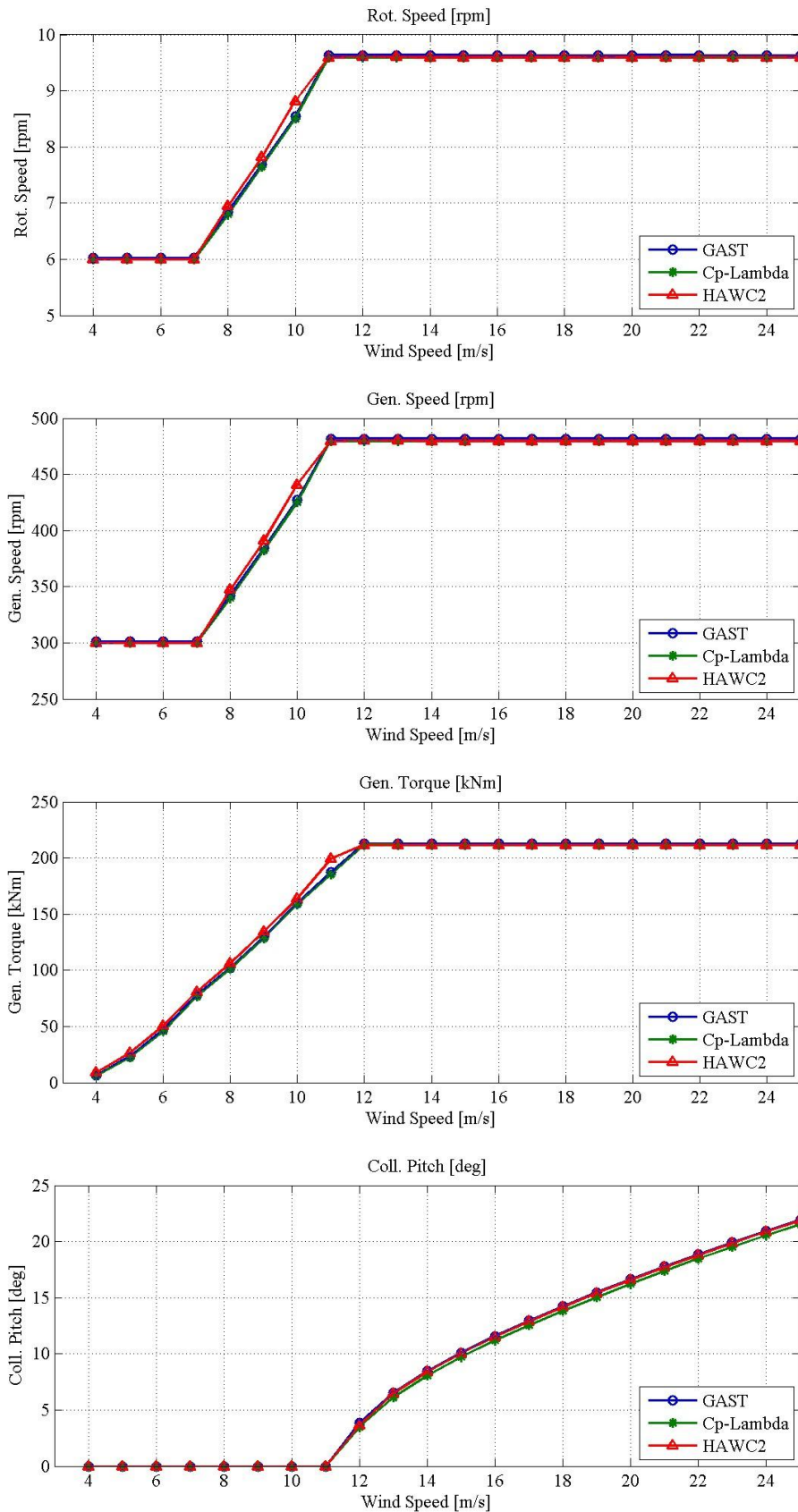
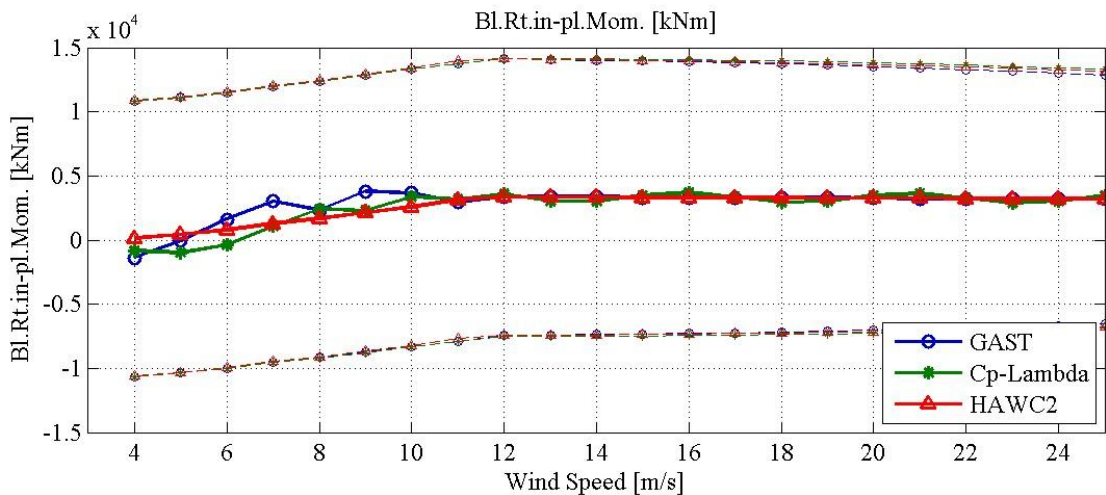
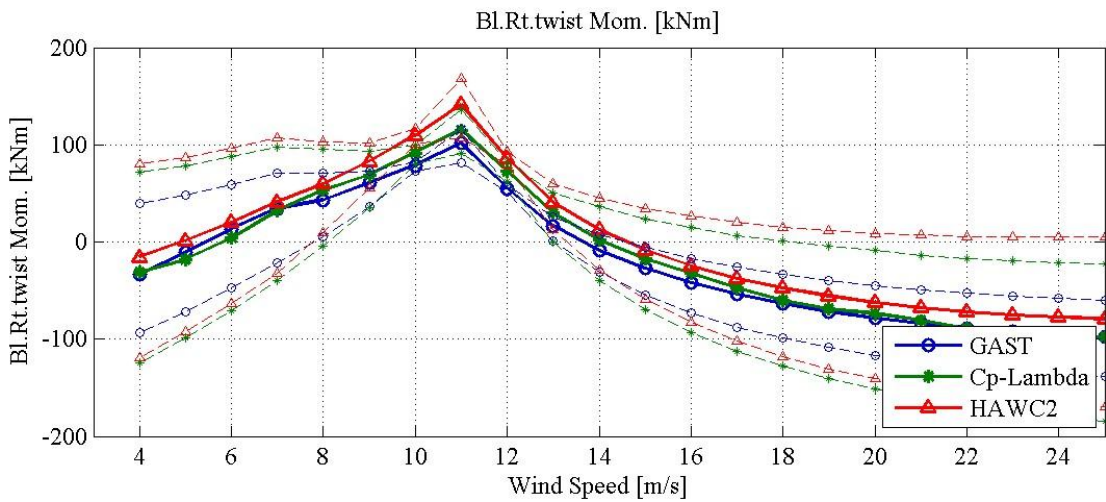
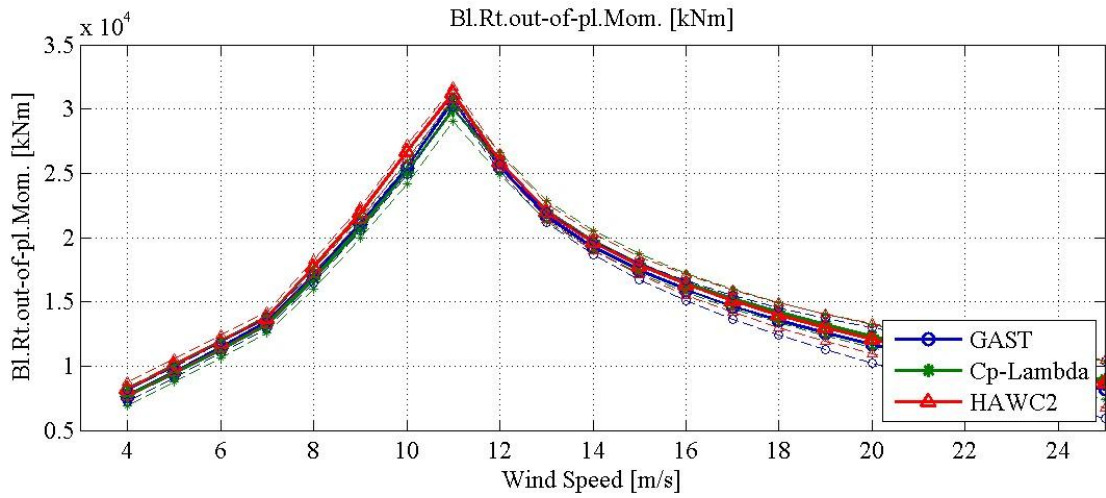
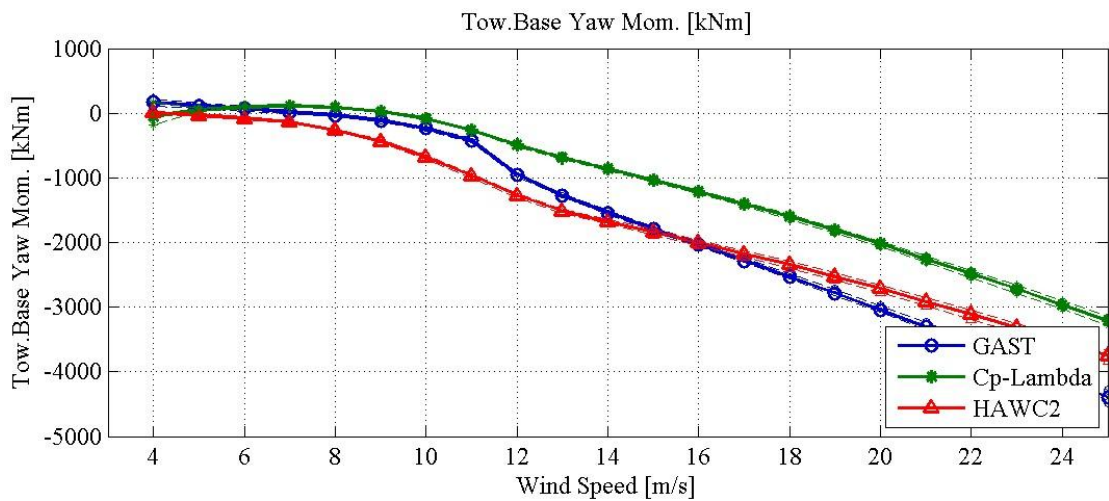
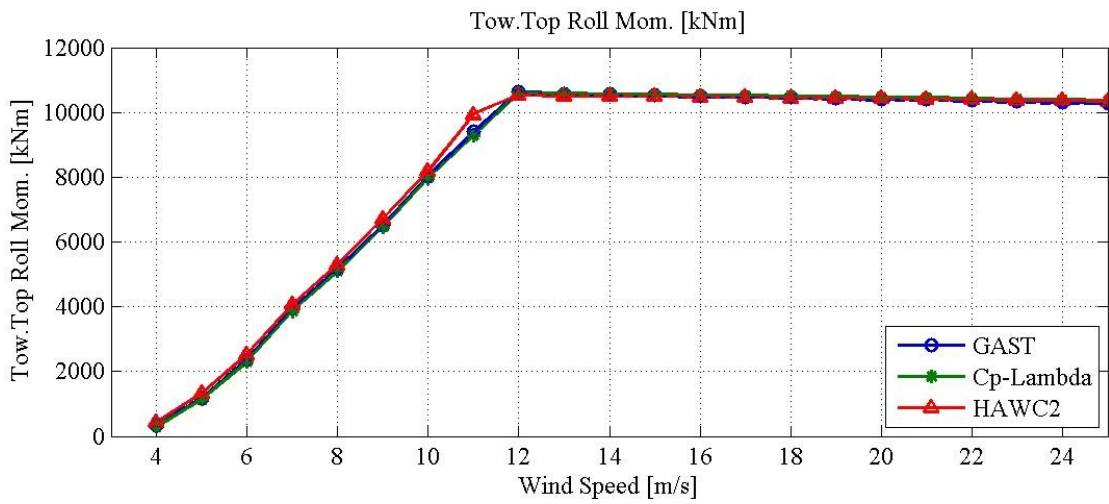
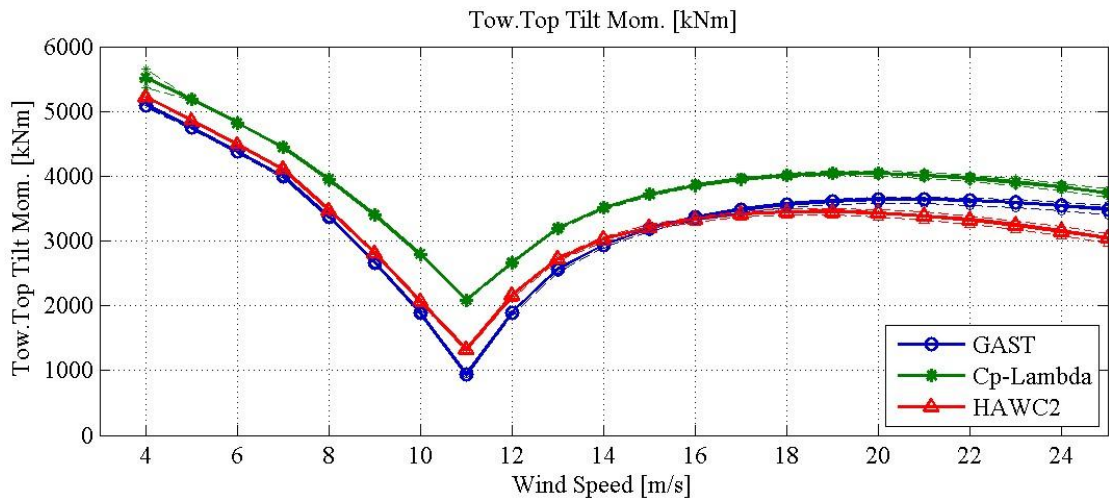


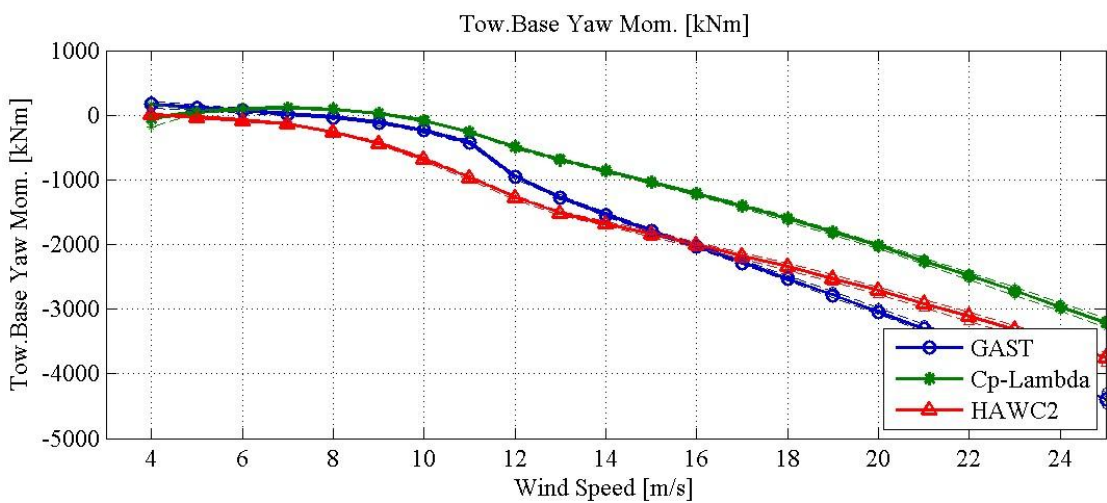
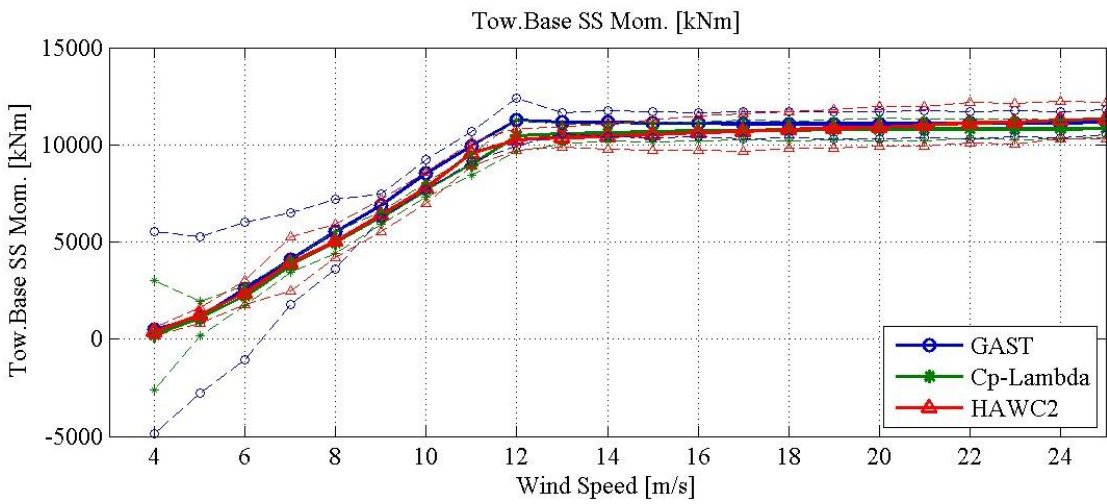
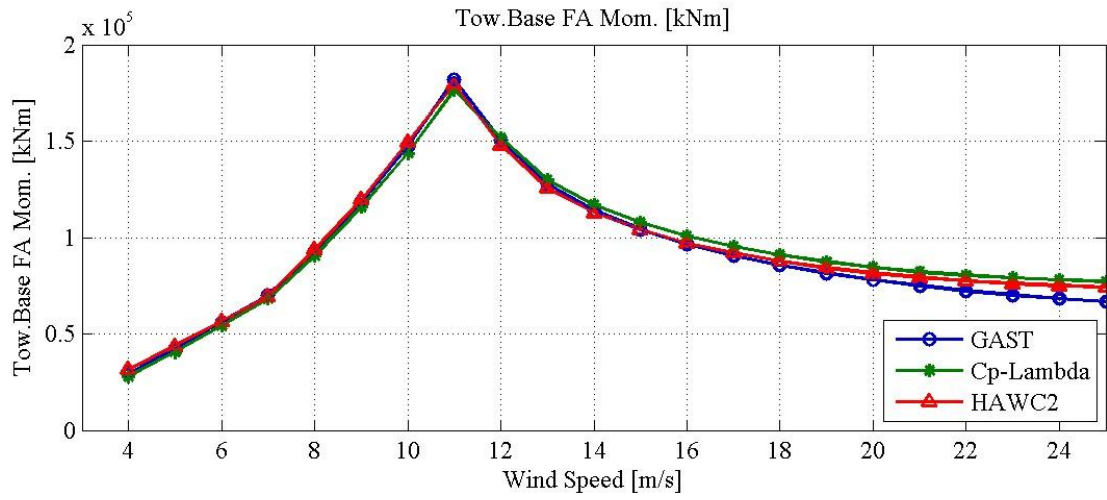
Figure 50: Step down flexible turbine- comparison of FEM codes

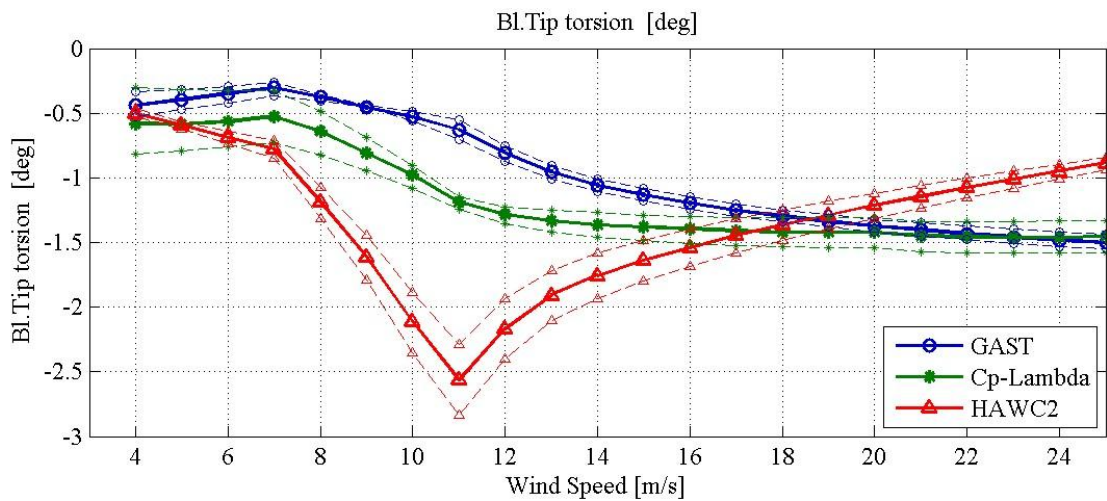
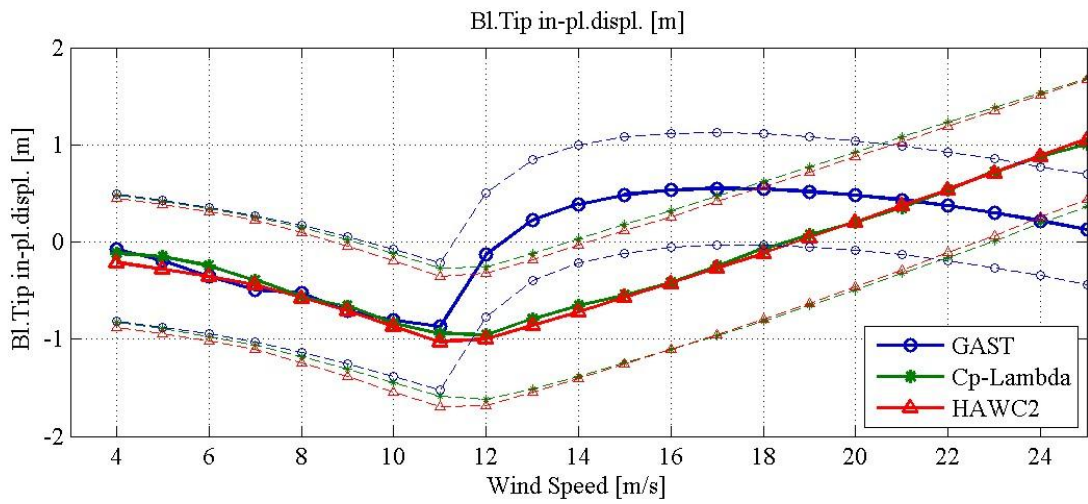
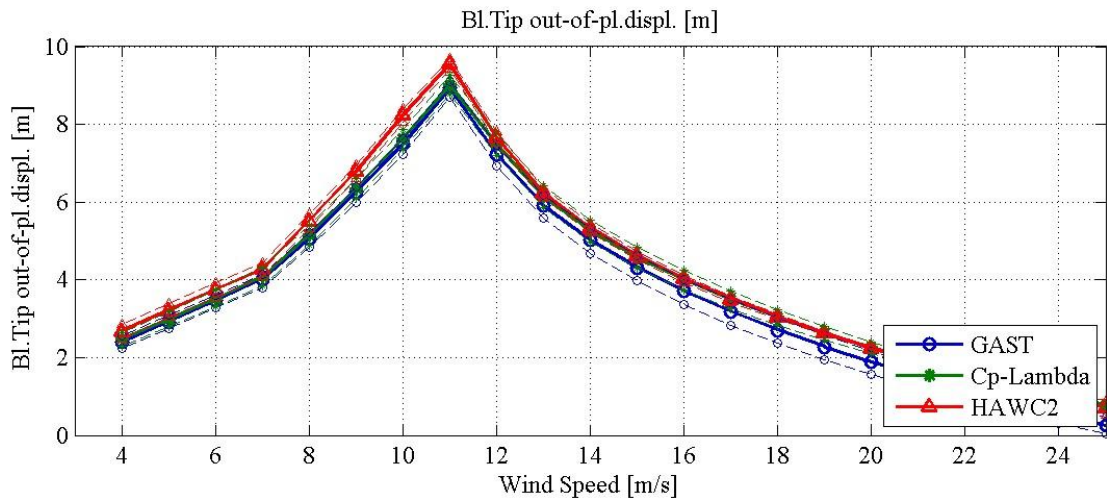
### Time series statistics vs. wind speed

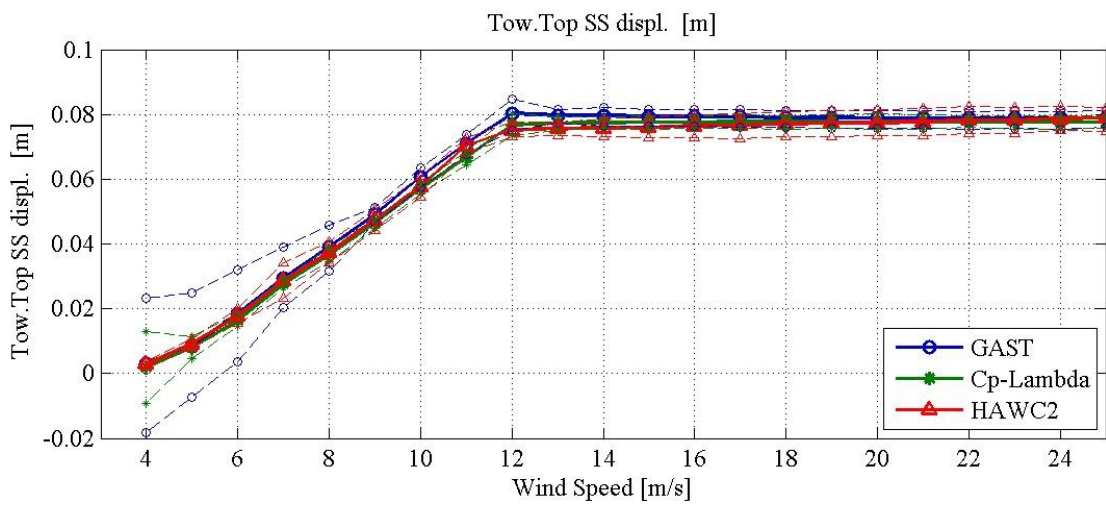
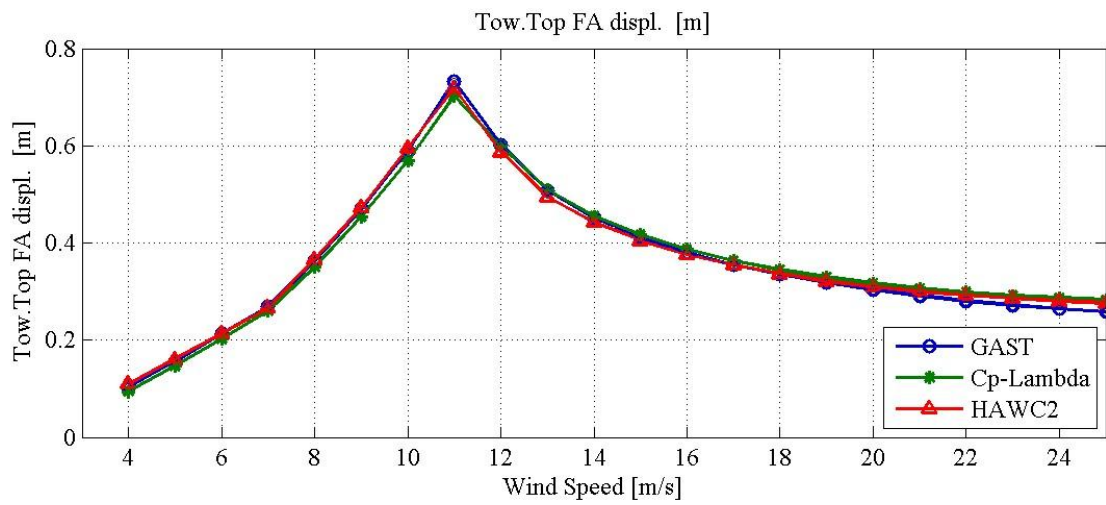












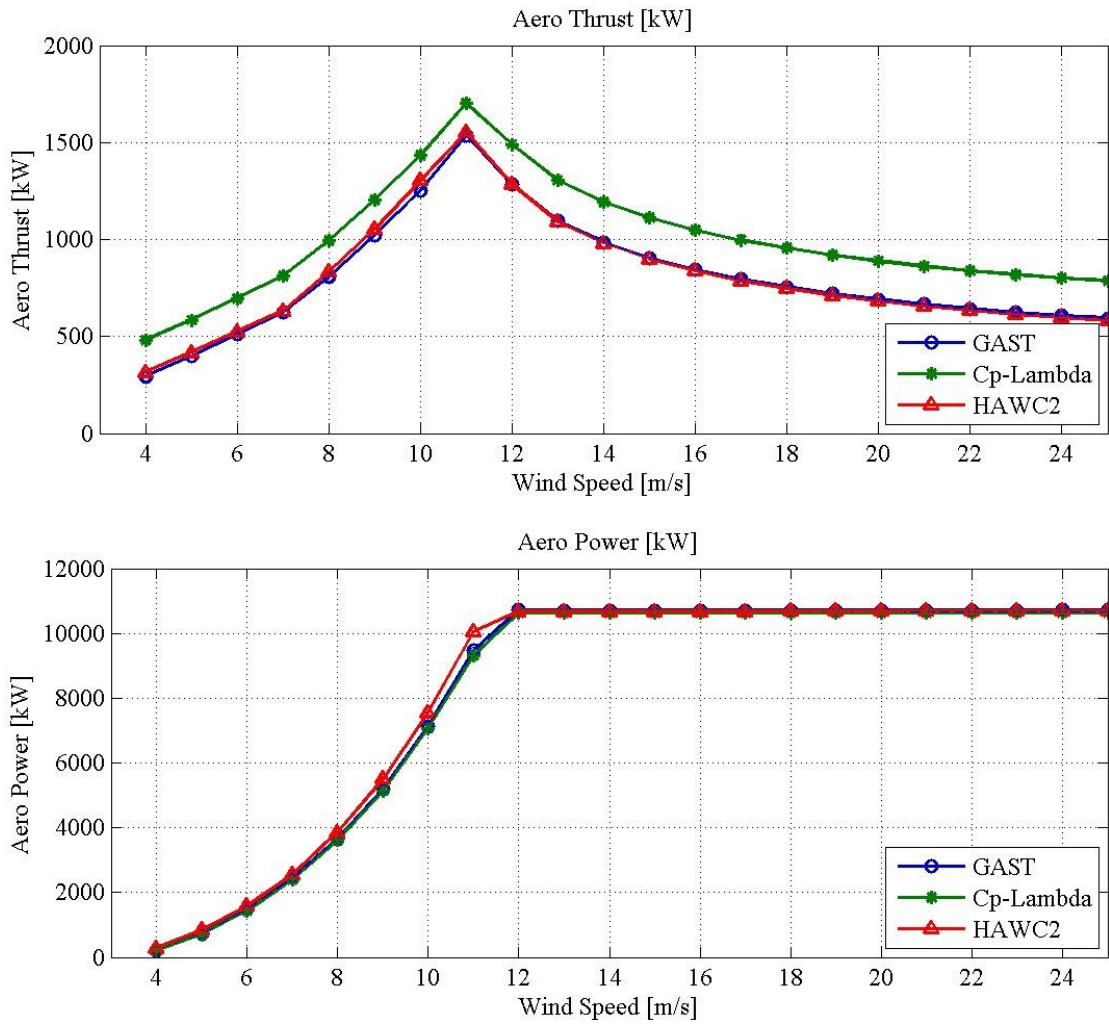
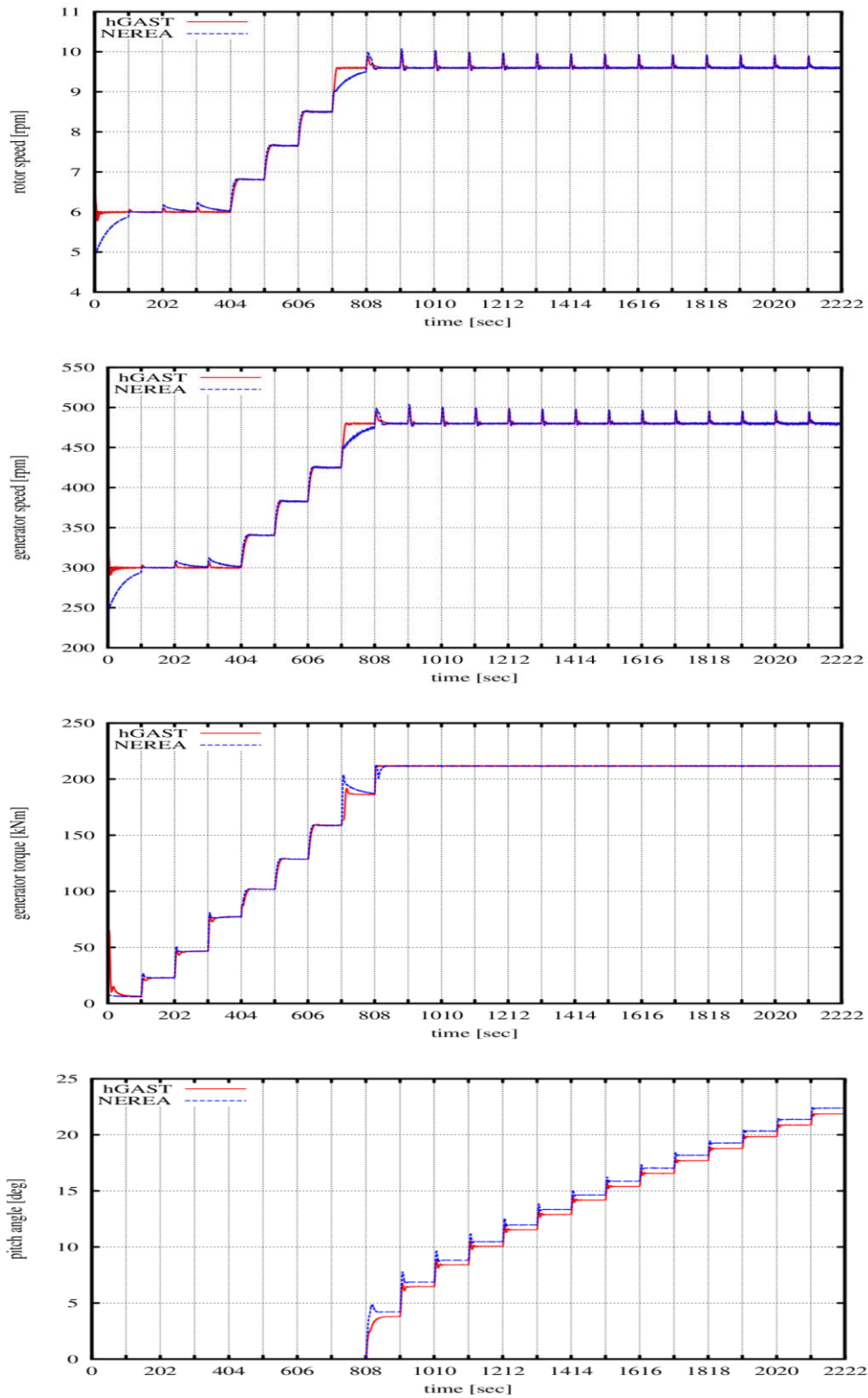
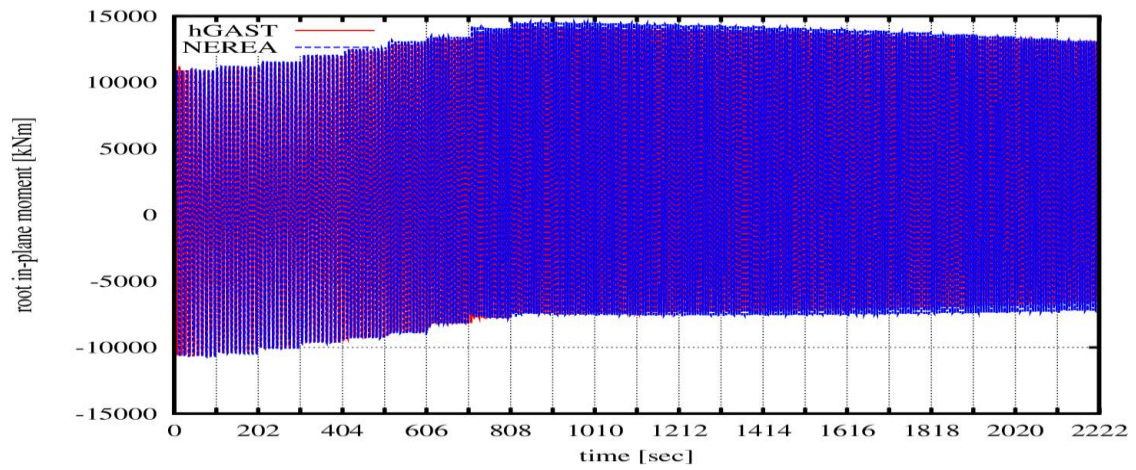
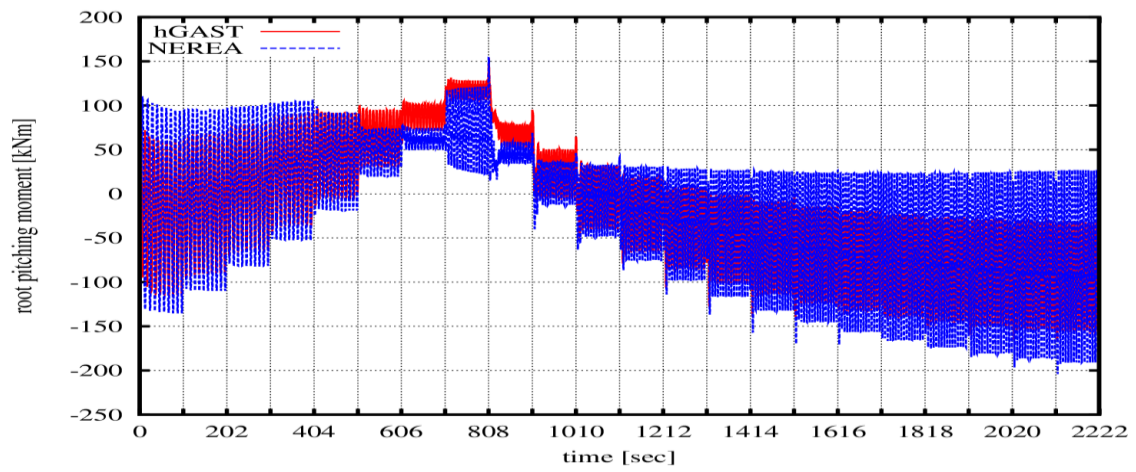
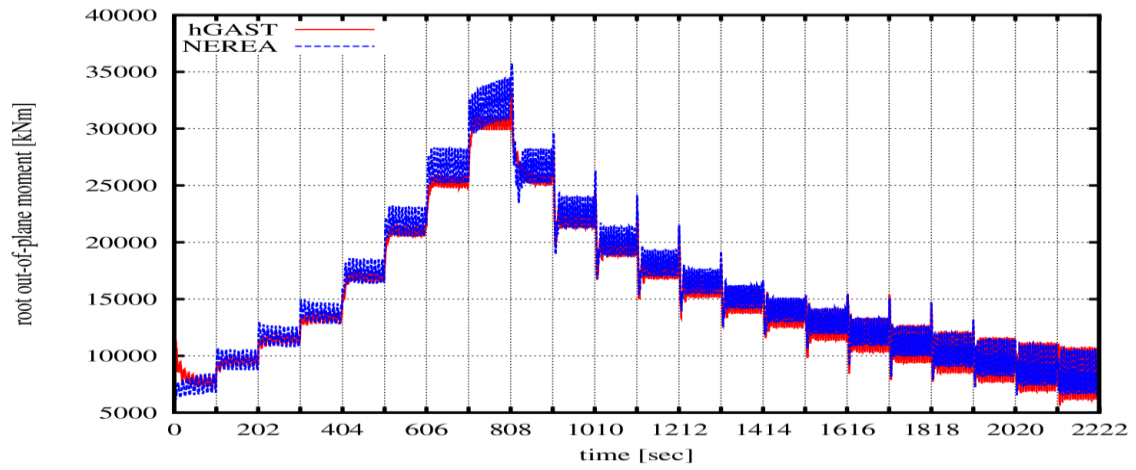
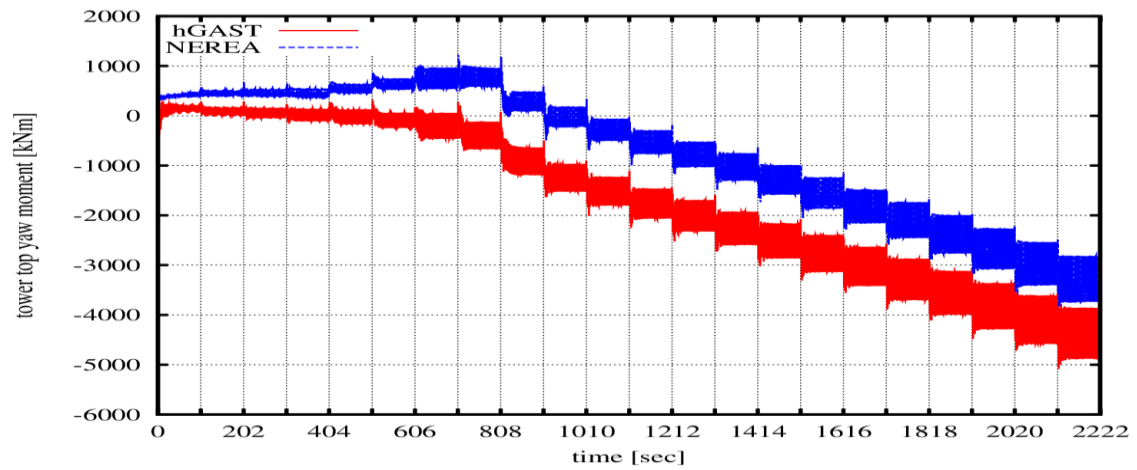
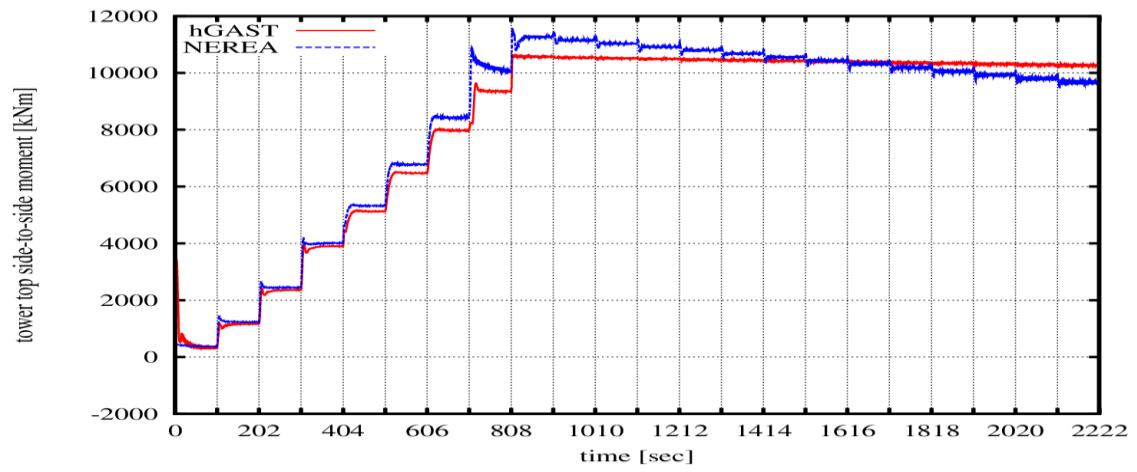
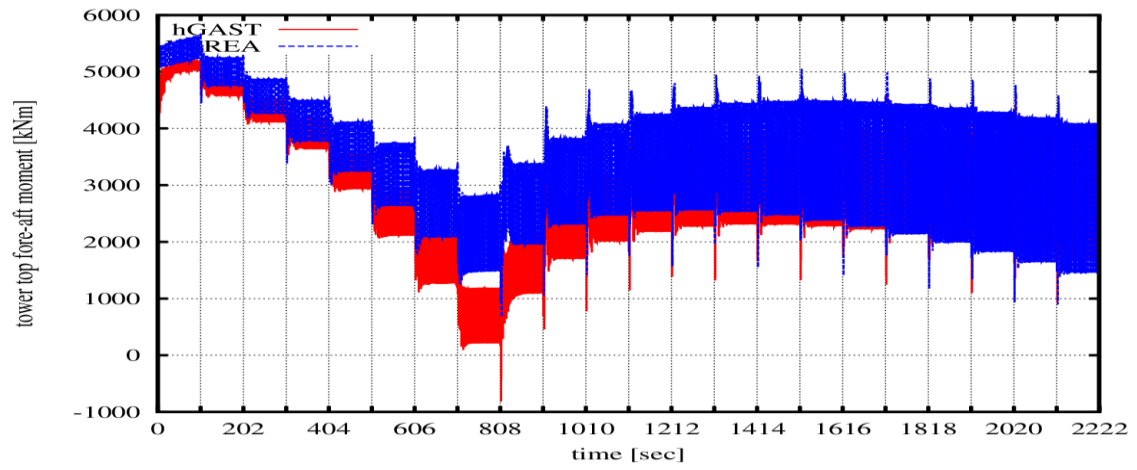


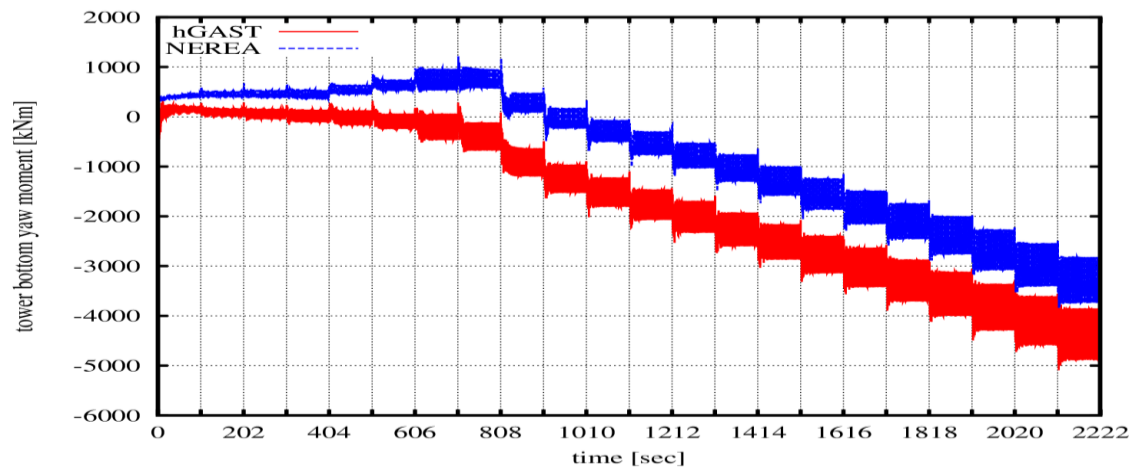
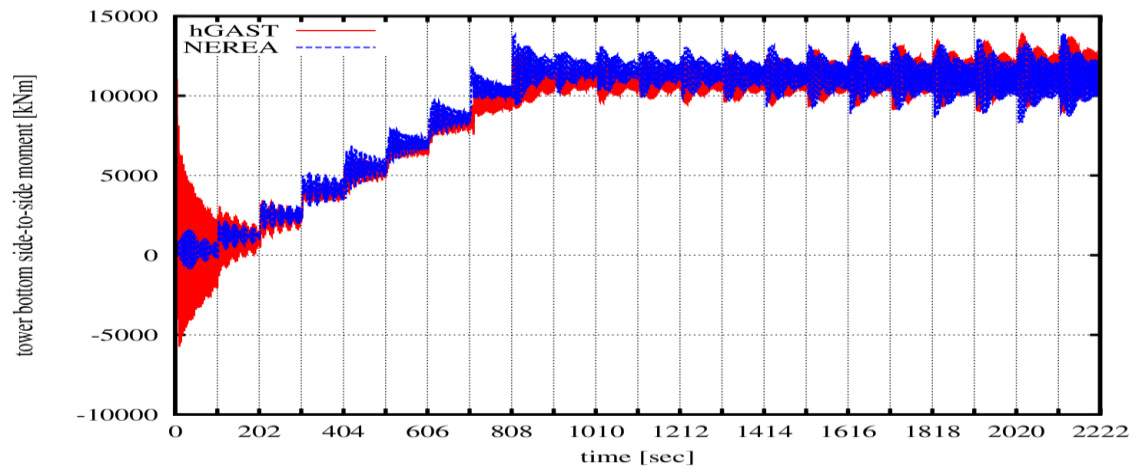
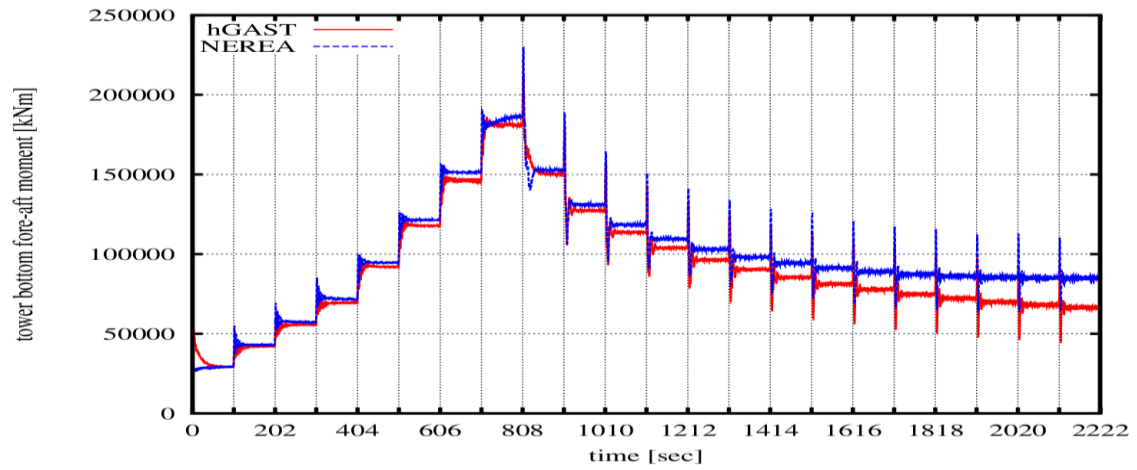
Figure 51: Statistics of the step-up case mean (solid lines) and min &max (dashed lines) values of the time series for the flexible WT.

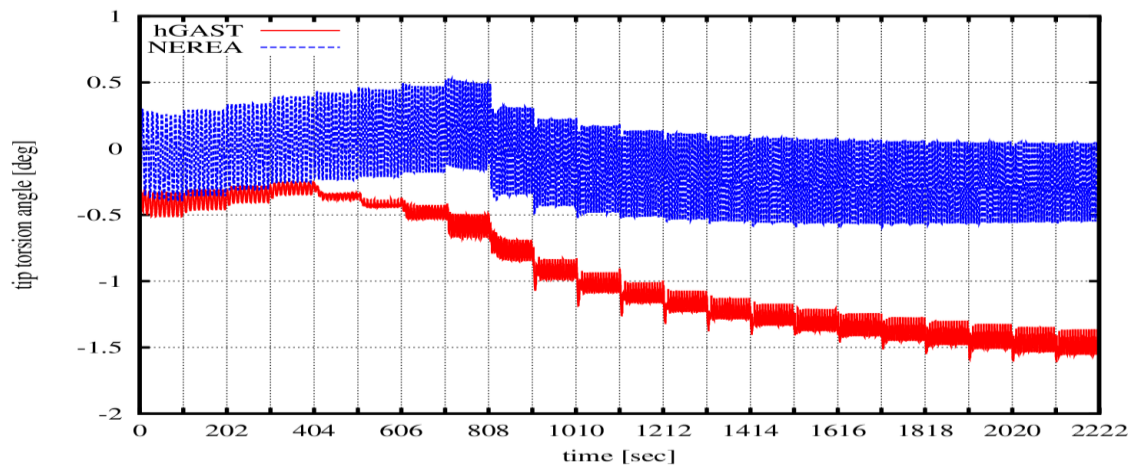
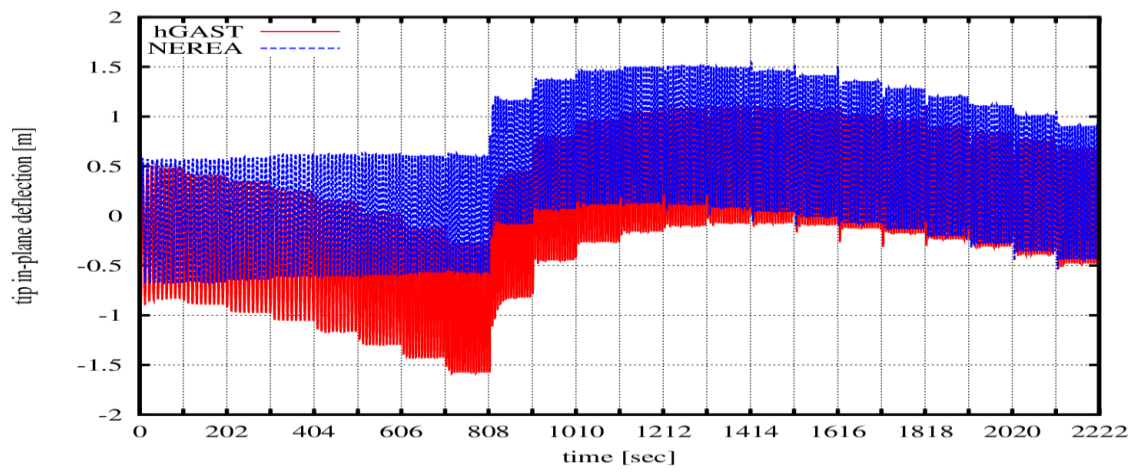
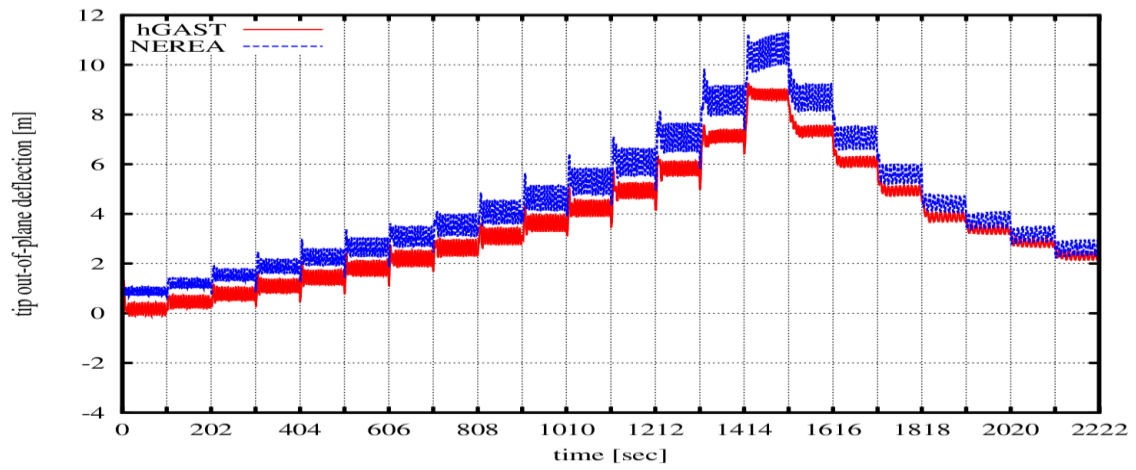
### Time series: flexible WT step-up case











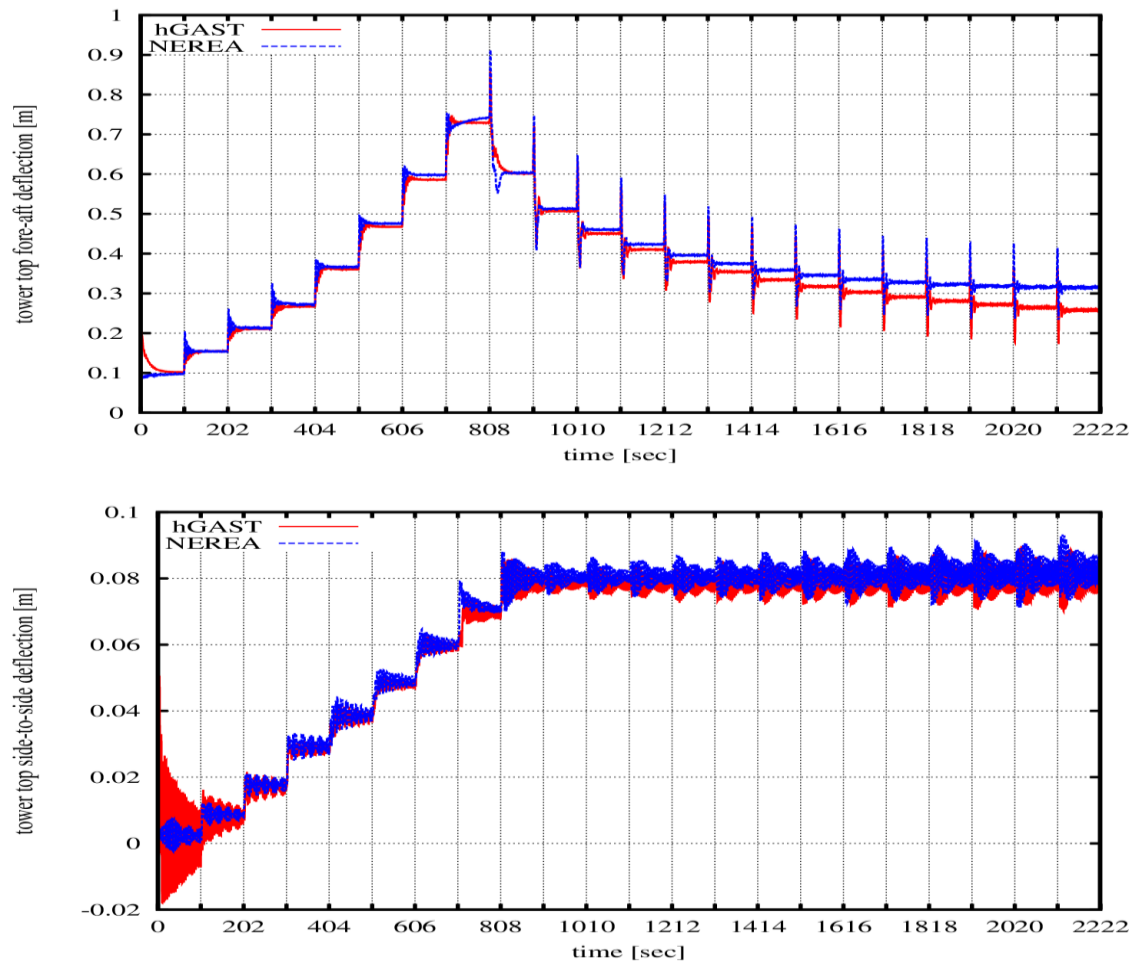
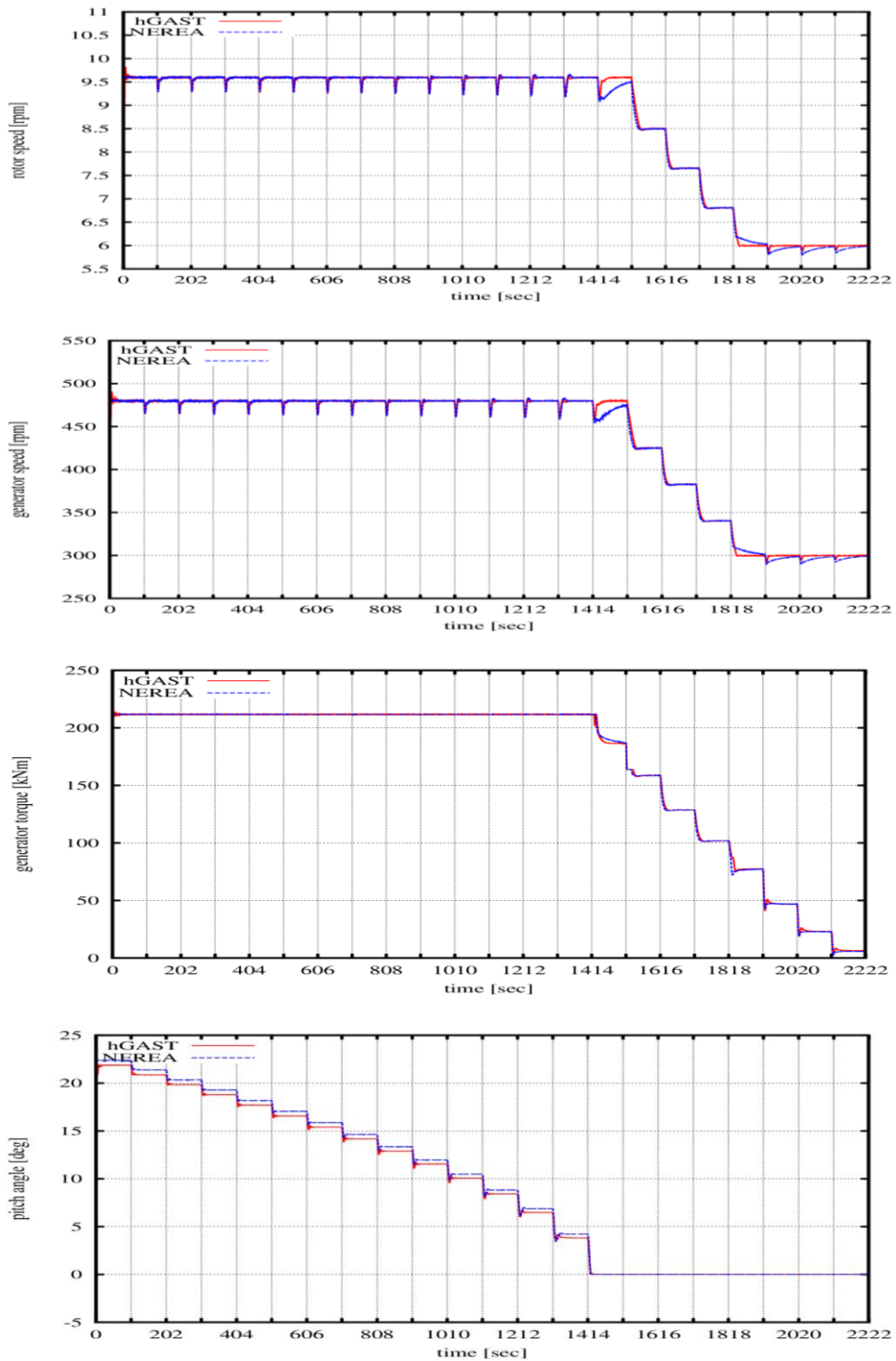
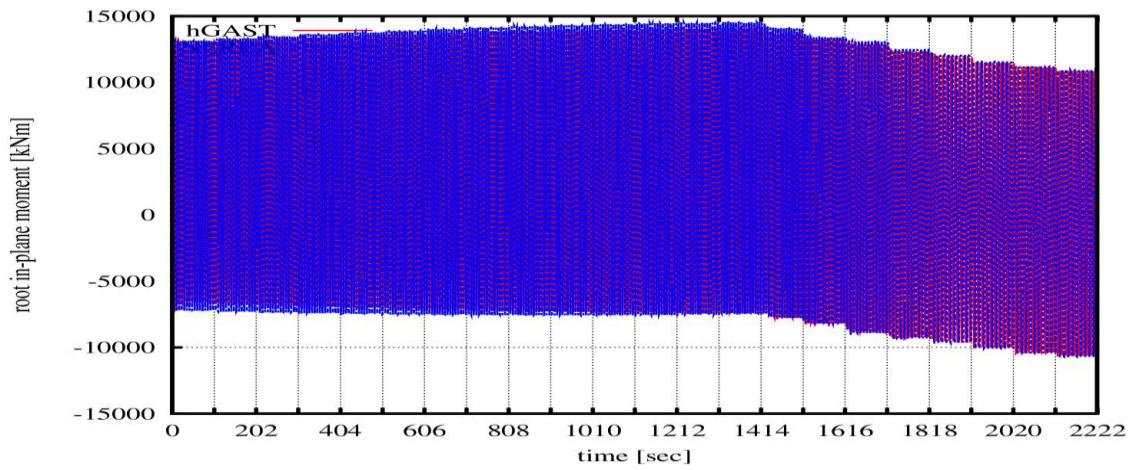
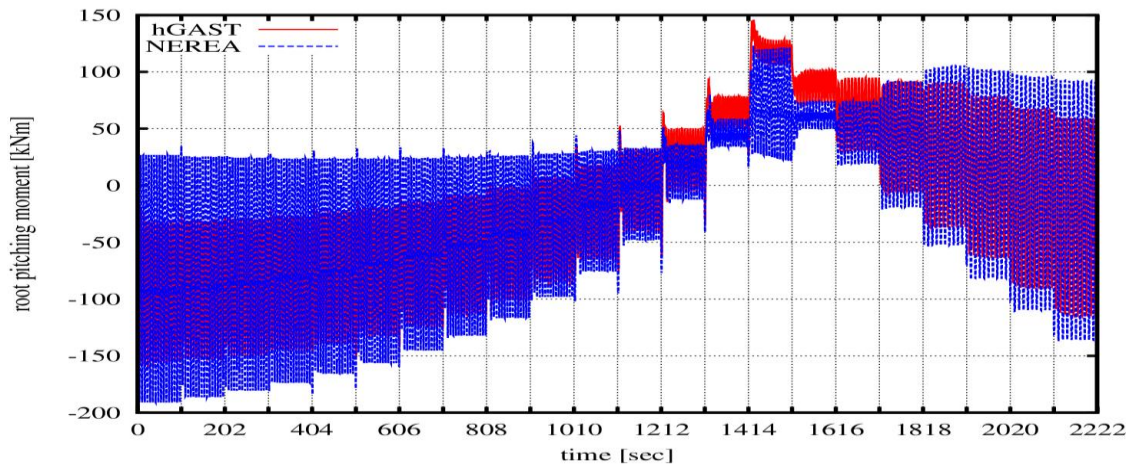
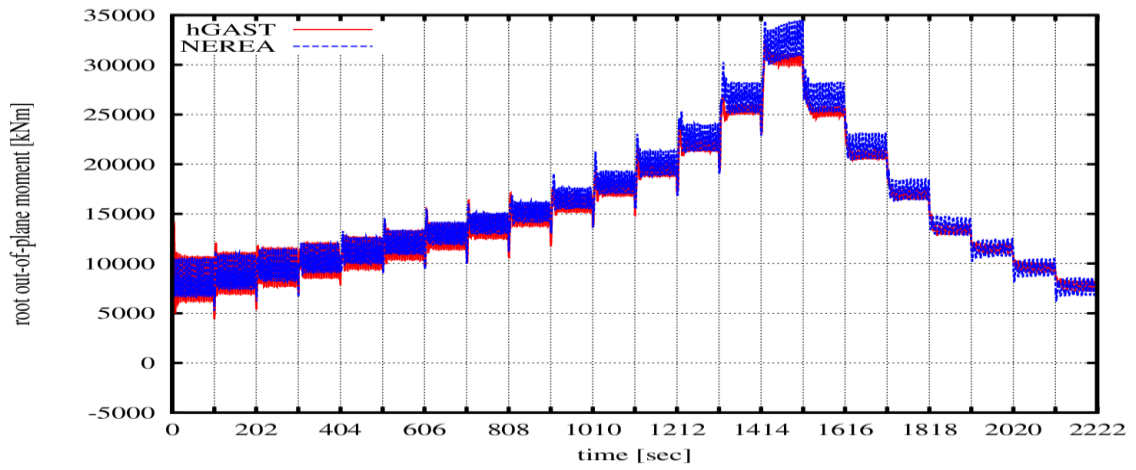
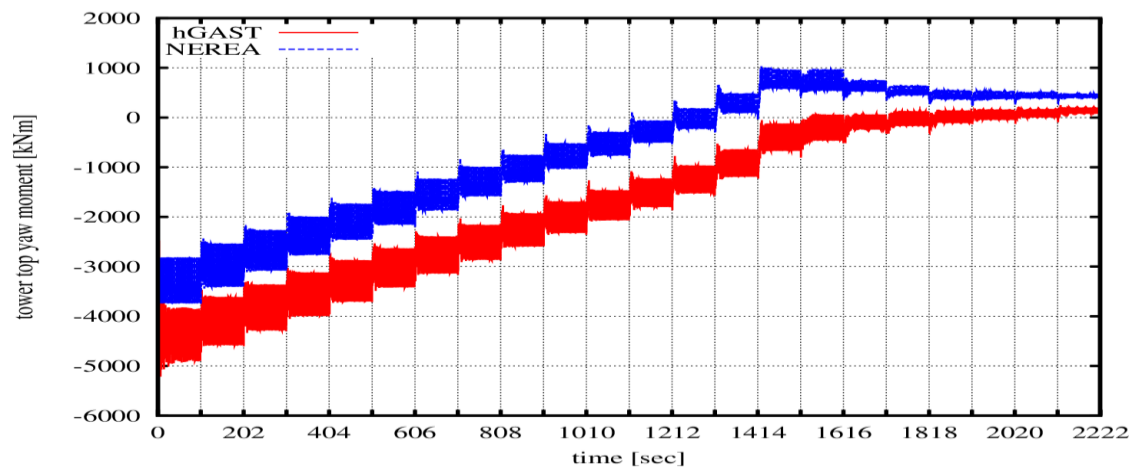
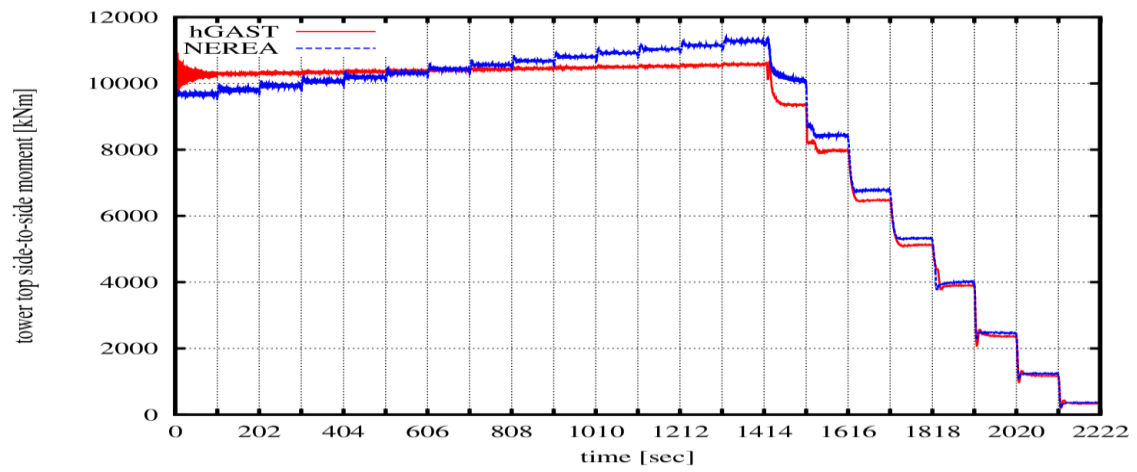
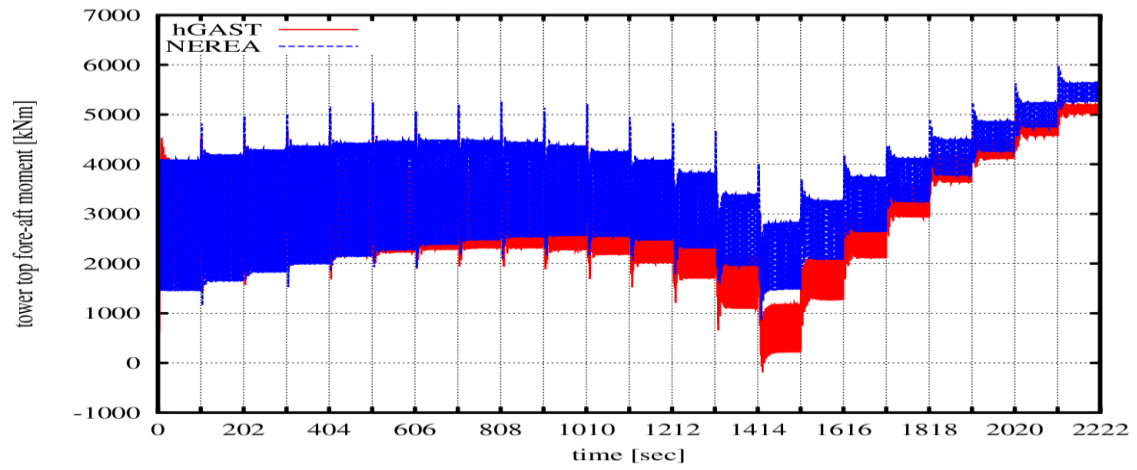


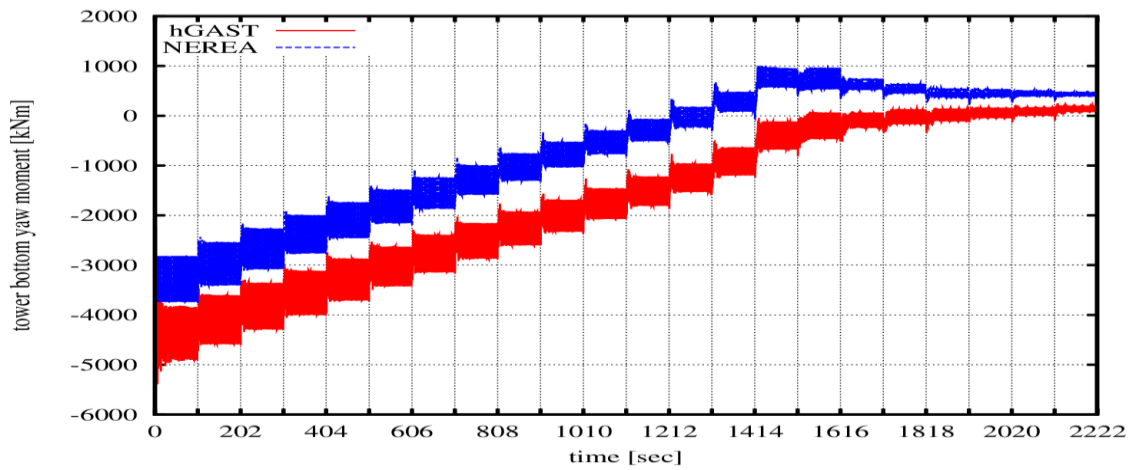
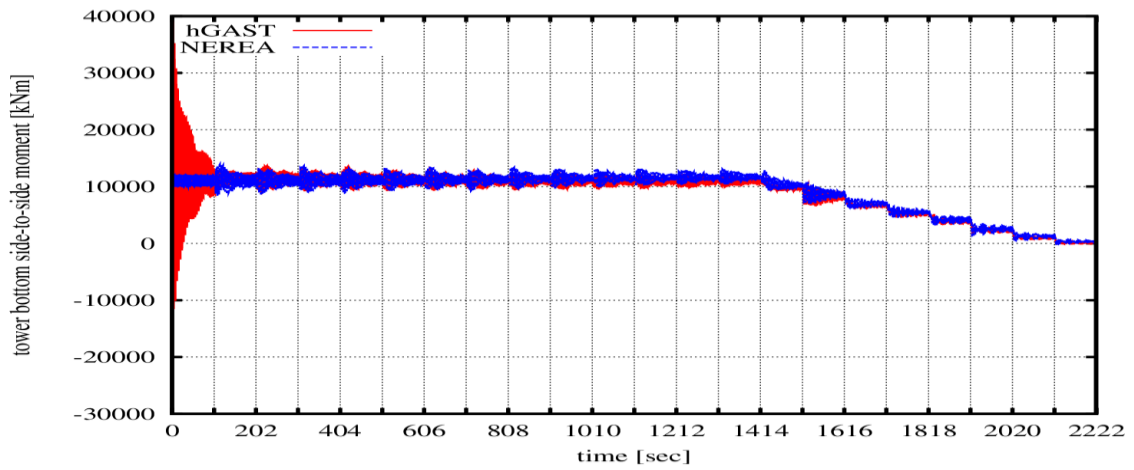
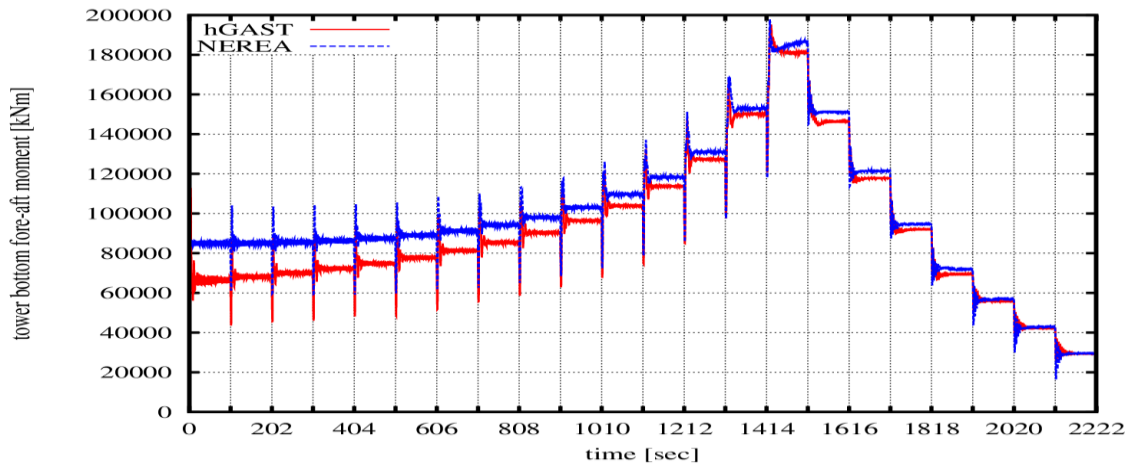
Figure 52: Step up flexible turbine- comparison of FEM (hGAST) against modal (NEREA) code

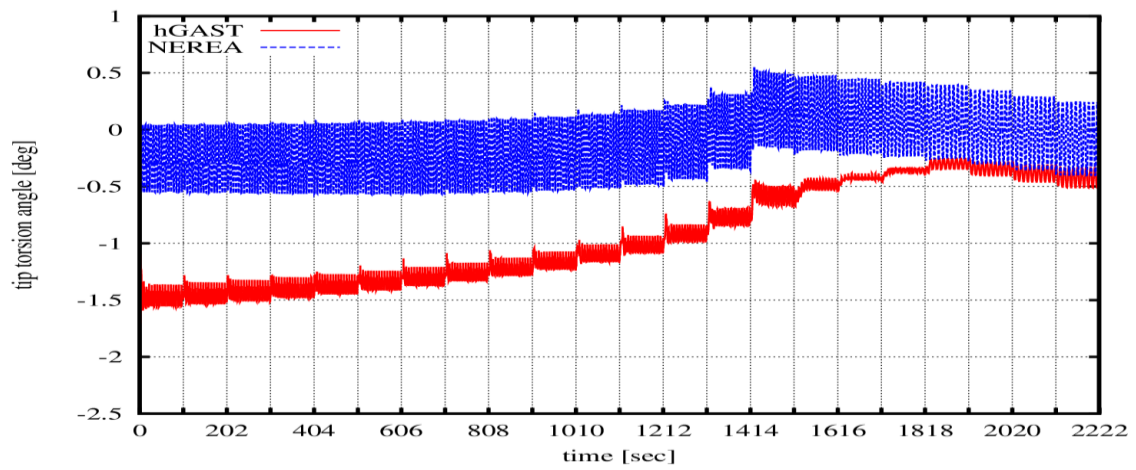
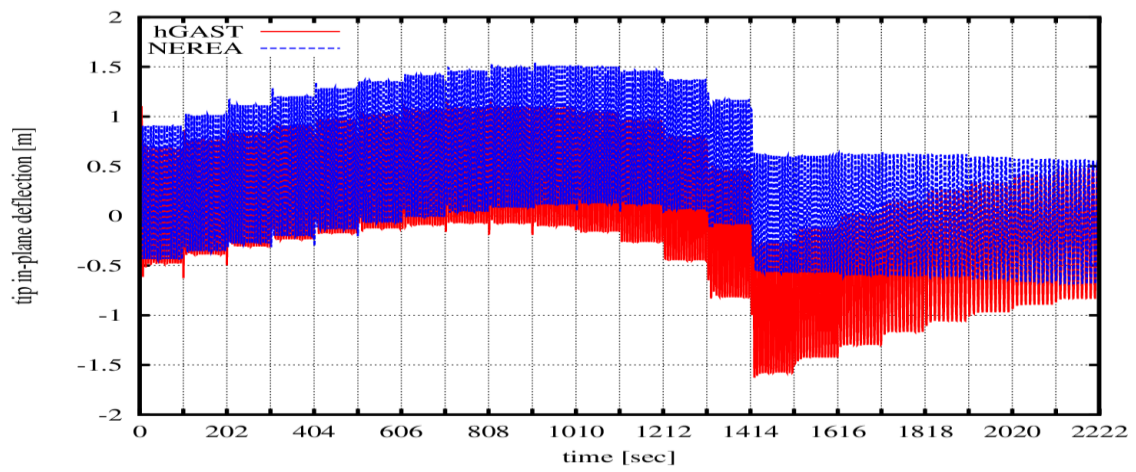
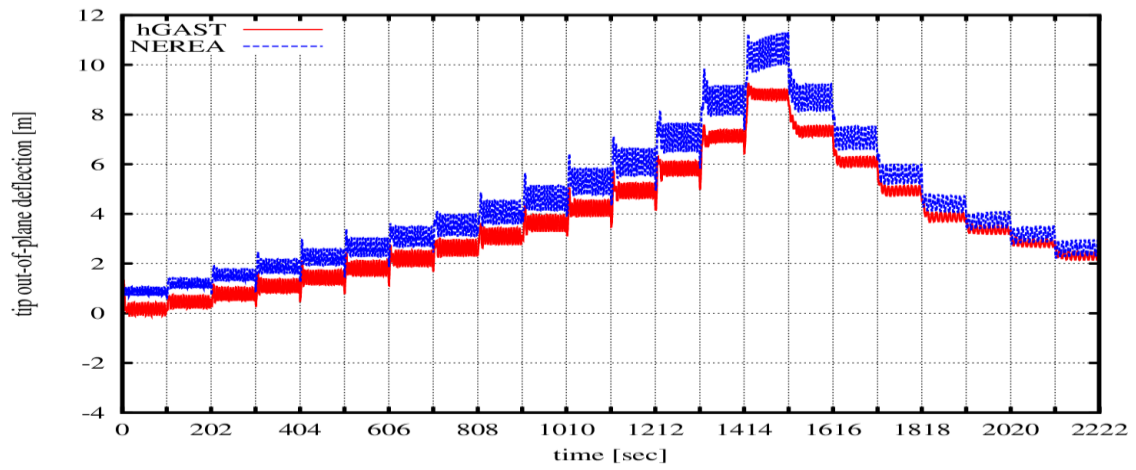
### Time series: flexible WT step-down case











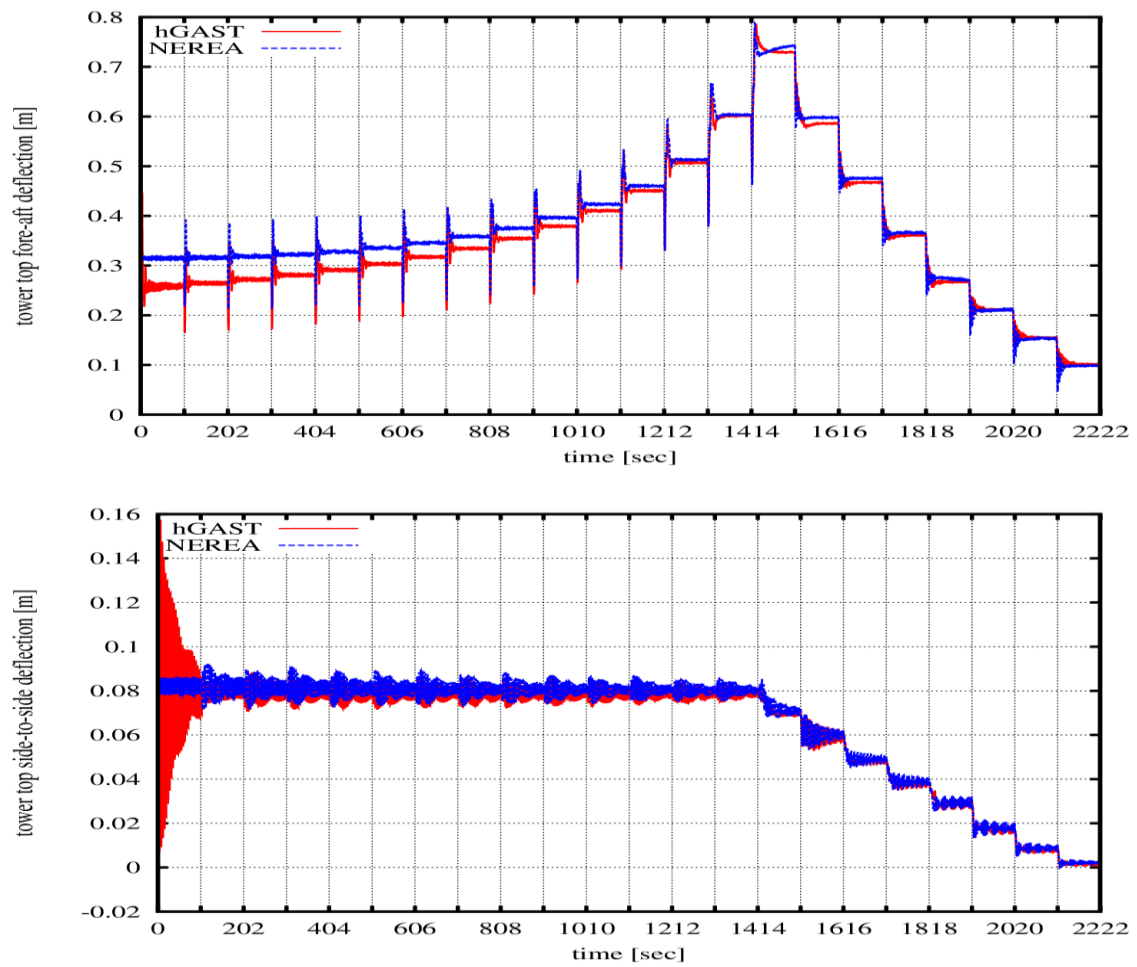


Figure 53: Step down flexible turbine- comparison of FEM (hGAST) against modal (NEREA) code

### 1.3.2 Turbulent wind cases at 8m/s (Mann model)

Turbulent wind simulations (10 min runs) have been performed at the wind speed of 8 m/s (partial load conditions). Results of Cp-Lambda, HAWC2 and hGAST are compared for the same turbulent wind box. The wind input to the various codes at the hub height position is compared in terms of time series, power spectral densities (PSD) and rainflow counting (RFC) in Figure 54-Figure 58. The turbulent wind velocities have been provided by DTU (Mann model) with respect to a fixed in space, rectangular grid which explains the almost perfect agreement between the various codes when referring to a fixed point in space (hub velocities). In Figure 59-Figure 63 the rotationally sampled wind velocities of hGAST and HAWC2 (constant rotational speed) at  $r=86.5$  m are compared. The agreement is fine, although the differences are increased compared to the fixed point velocities.

Aerodynamic models of various complexity are employed and compared in this section including standard BEM corrected for dynamic inflow effects (HAWC2-BEM, Cp-Lambda, hGAST-BEM), a near wake trailed vorticity model coupled to a standard BEM model (applied in HAWC2 - NW) and a free wake vortex particle model (applied in hGAST-gnvp).

The following simulation conditions have been defined:

**1 Stiff turbine**, no controller, no tower shadow, tilt=5°, pre-cone=2.5°, tip-prebend=3.3m, omega=6.423rpm, pitch=0°, Uwind=8m/s, shear exponent=0, wind yaw=0°, wind inclination=0°.

1.1 frozen wake, no unsteady airfoil aerodynamic model

1.2 frozen wake, plus unsteady airfoil aerodynamic model

1.3 dynamic inflow, unsteady airfoil aerodynamic model

**2 Flexible turbine**

2.3 **no controller**, no tower shadow, tilt=5°, pre-cone=2.5°, tip prebend=3.3m, omega=6.423rpm, pitch=0°, Uwind=8m/s, shear exponent=0, wind yaw=0°, wind inclination=0°

dynamic inflow, unsteady airfoil aerodynamic model

2.4 **closed loop**, tower shadow enabled, tilt=5°, pre-cone=2.5°, tip prebend=3.3m, Uwind=8m/s, shear exponent=0, wind yaw=0°, wind inclination=0°

dynamic inflow, unsteady airfoil aerodynamic model

PSD and RFC plots of the loads and deflections of the main components are presented in the sequel.

The following comments can be made for the stiff turbine simulations (Figure 64-Figure 67):

- A good agreement between HAWC2 & hGAST is obtained in case 1.1 (curves corresponding to dlc1.1 in Figure 64 and Figure 65).
- The effect of the unsteady airfoil aerodynamics is quite small in hGAST predictions (both ONERA (dlc1.2) and Beddoes/Leishman (dlc1.2b) models have been employed in hGAST). Especially in the aerodynamic torque the effect of the ONERA model is negligible. The effect of the unsteady aerodynamic model is much bigger in HAWC2 predictions (Beddoes model is used) (curves corresponding to dlc1.2 in Figure 64 and Figure 65).
- The effect of the dynamic inflow model is almost negligible in HAWC2 predictions. A much higher filtering of the load ranges is seen in hGAST results (curves corresponding to dlc1.3 in

Figure 64 and Figure 65). This is probably due to the simple cylindrical wake model employed in hGAST which overestimates significantly filtering effect due to dynamic induction on this 10 MW turbine. The uncertainty of the predictions is definitely linked to the increased azimuthal variation of the rotationally sampled inflow. For larger wind turbines more energy from the turbulent wind spectrum is concentrated to the 1P, 2P etc which imposes challenges to simplified cylindrical engineering BEM based models. A small difference in the delay effect predicted by the far wake dynamic inflow model and the shed vorticity unsteady airfoil aerodynamic model can lead to significantly different dynamic loads results.

- It is of particular interest that the free wake predictions lie between hGAST-BEM and HAWC2-BEM results. HAWC2-NW predictions (improved near wake model) seem to get closer to the free wake results (Figure 64 and Figure 65). As shown in Figure 66 and Figure 67 the free wake model under-estimates the level of the mean thrust. This is due to the fact that the inner part of the blade (root part) which contributes significantly to the thrust is not modeled in hGAST-gnvp code (the aerodynamic grid starts at  $R=18\text{m}$ ). Therefore, this difference is not expected to affect significantly shed vorticity of the outer blade part and thereby contribution to the overall thrust. However the dynamic response of the missing part of the blade will be missing in the rainflow counting. To some extent this explains the lower ranges predicted by hGAST-gnvp as compared to the HAWC2-NW.

The following comments can be made for the flexible turbine simulations in open loop (Figure 68-Figure 81):

- Overall hGAST predicts lower ranges of the flapwise bending moment as compared to HAWC2 and Cp-Lambda. As in the stiff turbine case hGAST-gnvp predictions lie between hGAST-BEM and HAWC2-BEM/Cp-Lambda results. It is noted that Cp-Lambda predicts lower ranges than the two other codes in the range of 150-700 cycles (Figure 68).
- A good agreement in the mean value prediction of the flapwise bending moment between hGAST-gnvp (free wake) and BEM based models results (Figure 69), which supports the previous comment that the level difference in the thrust is due to the contribution of the inner part of the blade (not modeled in hGAST-gnvp), which on the other hand does not influence significantly the root bending moment due to the small arm.
- The PSD plot of the flapwise moment shows that the differences in the ranges of the loads are mainly attributed to different prediction of the 1P and 2P peaks by the different codes. As discussed above this is mainly due to different implementation of the dynamic inflow model and partially due to the different unsteady airfoil aerodynamic models in the various codes (Figure 70).
- A good agreement between the various codes is obtained in the prediction of the edgewise moment (Figure 71). hGAST-BEM seems to slightly underestimate the damping of the 1<sup>st</sup> edgewise mode.
- In the PSD of the pitching moment at the root of the blade (Figure 72) all codes agree well in the prediction of the 1P peak which dominates the response. Also, all codes predict a peak at  $\sim 0.9\text{ Hz}$  that corresponds to the frequency of the first edgewise mode. Cross talking of the torsion with the edgewise direction takes place in this case as a result of the geometric torsion/bending coupling effect which gets more pronounced when high flapwise deflections take place.
- A difference in the prediction of the second symmetric edgewise mode between the models is noted in the PSD of the edgewise deflection most probably due to the bending-torsion geometric structural coupling (Figure 73).

- hGAST predicts lower ranges of the tower bottom side-side/fore-aft (Figure 75, Figure 78) bending moments most probably due to a higher structural damping. The corresponding loads at the top of the tower (Figure 74) are in much better agreement (consistent with the flapwise bending moment results). As seen in the PSD of the tower bottom bending moment (Figure 77) hGAST under-predicts (compared to HAWC2 and Cp-Lambda) the first tower frequency peak (due to higher structural damping). On the other hand Cp-Lambda seems to under-predict the 6P peak both of the tower top (Figure 76) and tower bottom moments (Figure 77).
- As shown in Figure 79 some tower vibrations in the lateral direction more pronounced by HAWC2 and Cp-Lambda partially explain the lower RFC prediction by hGAST (see Figure 78).
- In the PSD of the lateral (side-to-side) tower bending moment both at tower top and bottom (Figure 80, Figure 81) it is seen that the 0.5 Hz peak predicted by hGAST and HAWC2 which corresponds to the free-fixed drive train mode is shifted to 0.8 Hz in Cp-Lambda predictions probably due to a different boundary condition imposed at the generator side.

In Figure 82-Figure 93 the results of the flexible turbine in closed loop are shown. It can be noted that:

- As seen in the low speed shaft rotational speed (Figure 82) all codes properly model the controller operation (variable speed mode of operation).
- A slightly better agreement is seen in the ranges of the flapwise bending moment (Figure 83) as compared to the open loop case. This is probably because as a result of the variable speed operation less sharp 1P and 2P peaks are obtained (energy is spread to a wider frequency range) (Figure 84). As already noted differences in the flapwise bending moment are driven by the filtering of the azimuthal variation (1P and 2P) of the induction by the simpler dynamic inflow models and the differences of the unsteady airfoil aerodynamic models.
- The peak of the first edgewise mode in the edgewise bending moment at  $\sim 0.9$ Hz is under-predicted by Cp-Lambda (Figure 85)
- As in the open loop case a difference in the prediction of the second symmetric edgewise mode between the models is noted in the PSD of the edgewise deflection at tip of the blade (Figure 87). In the closed loop case the agreement between HAWC2 and Cp-Lambda is much closer (as compared to open loop (Figure 73)) while hGAST under-predicts the frequency. It is interesting to note that all models predict a lower frequency as compared to the open loop case. This indicates that a non-linear structural coupling dominated by the loading of the blade takes place.
- The tower loads are very similar to those of the open loop case (Figure 88 – Figure 93).

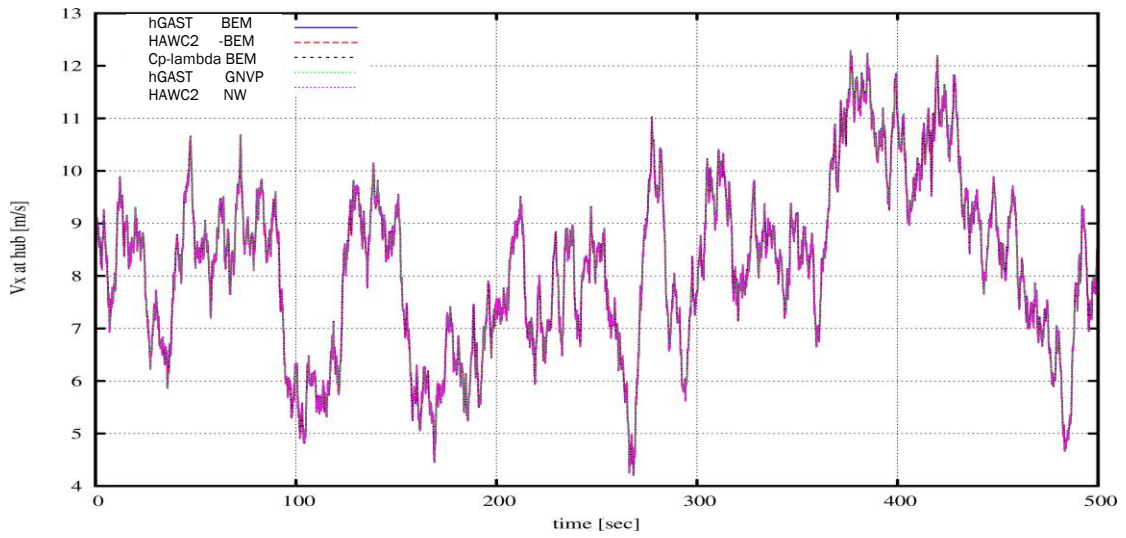


Figure 54: Time series of the axial wind velocity at the hub position (mean wind speed 8m/s).

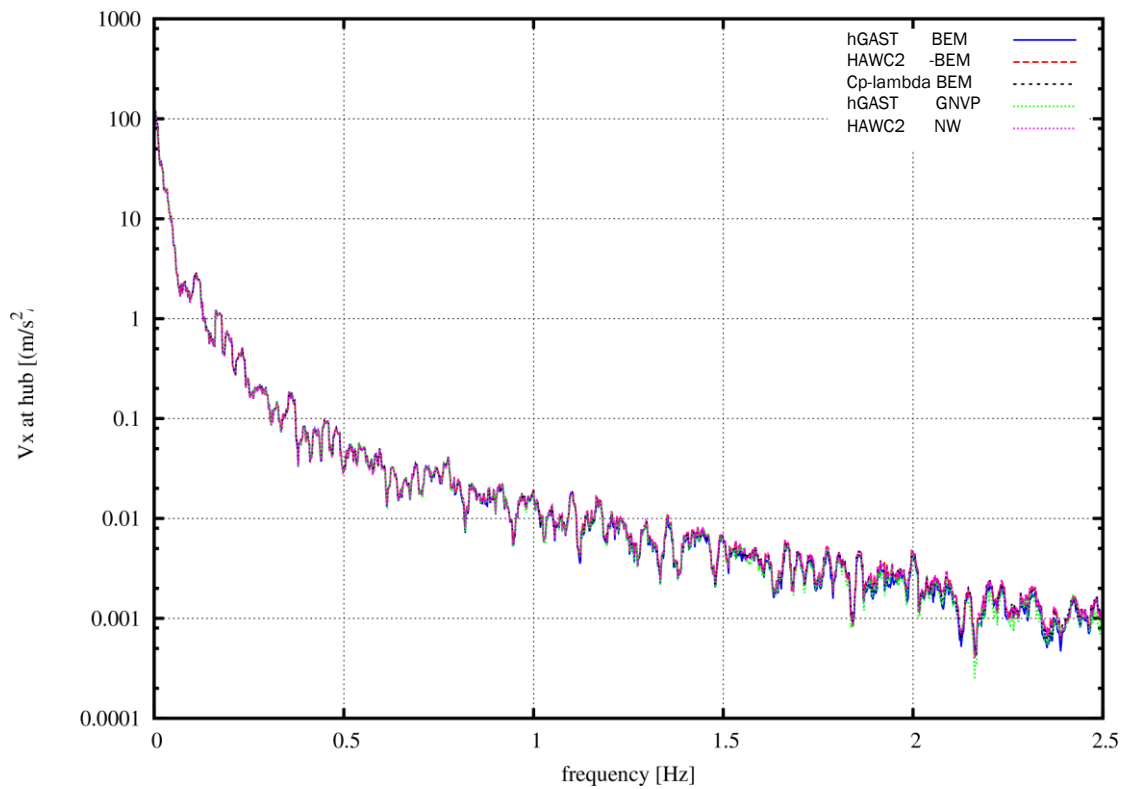


Figure 55: PSD of the axial wind velocity at the hub position (mean wind speed 8m/s).

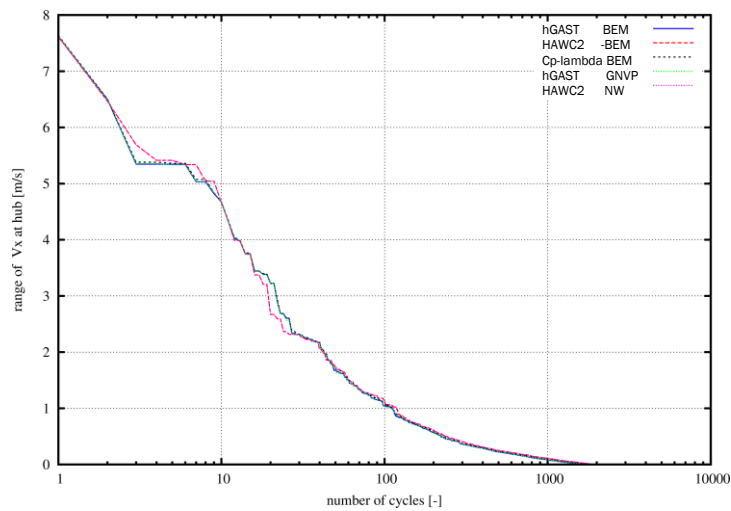


Figure 56: RFC of the axial wind velocity at the hub position (mean wind speed 8m/s).

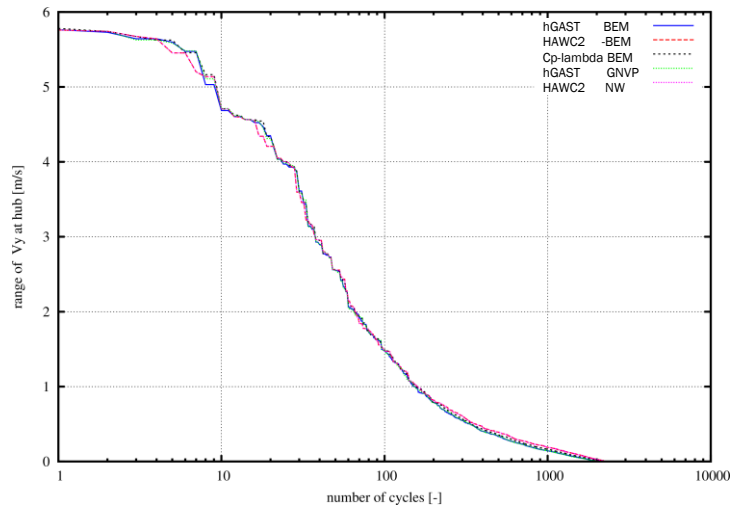


Figure 57: RFC of the horizontal wind velocity at the hub position (mean wind speed 8m/s).

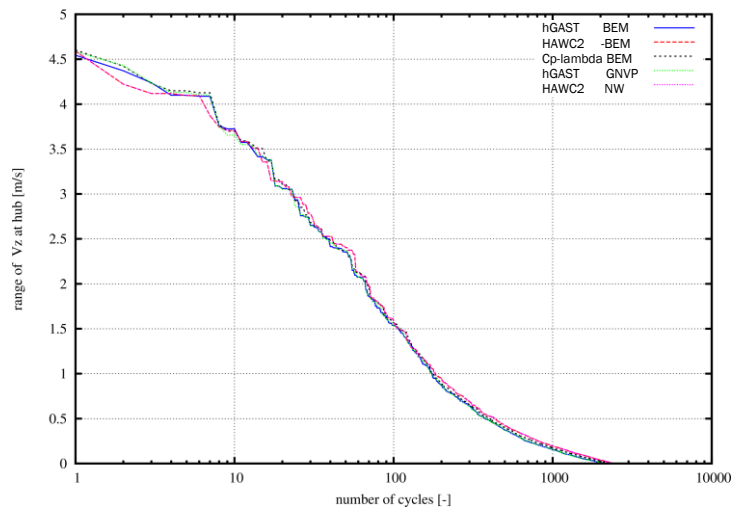


Figure 58: RFC of the vertical wind velocity at the hub position (mean wind speed 8m/s).

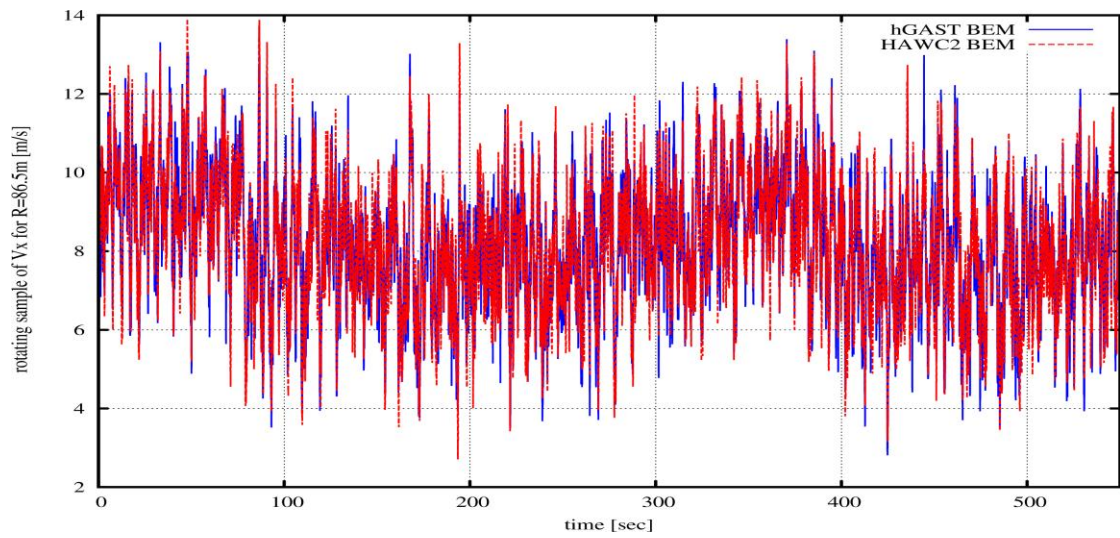


Figure 59: Time-series of the blade tip ( $r=86.5$  m) rotational sampled axial wind velocity (mean wind speed 8m/s).

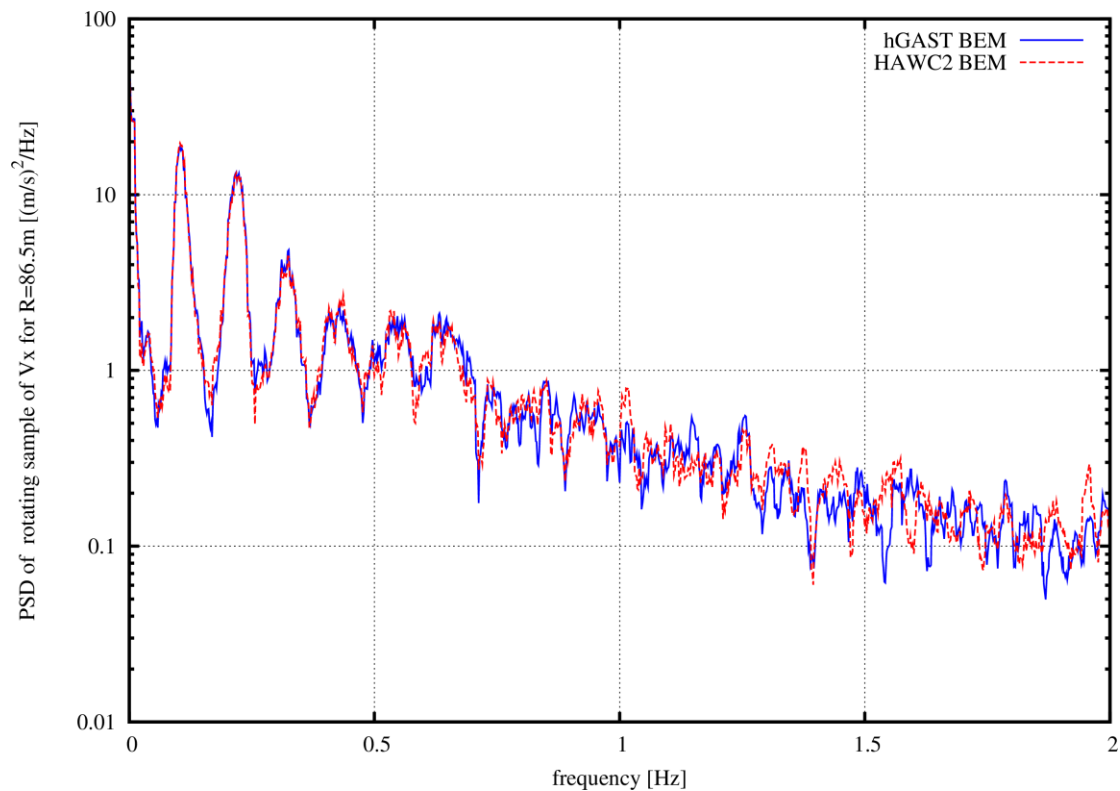


Figure 60: PSD of the blade tip ( $r=86.5$  m) rotational sampled axial wind velocity (mean wind speed 8m/s).

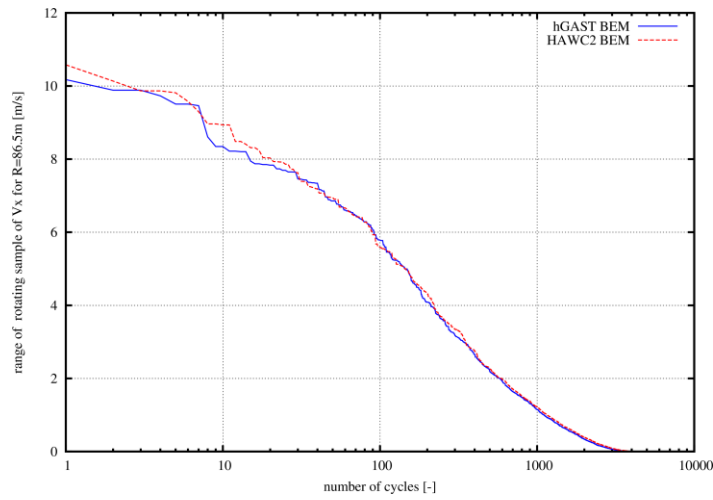


Figure 61: RFC of the blade tip ( $r=86.5$  m) rotational sampled axial wind velocity (mean wind speed 8m/s).

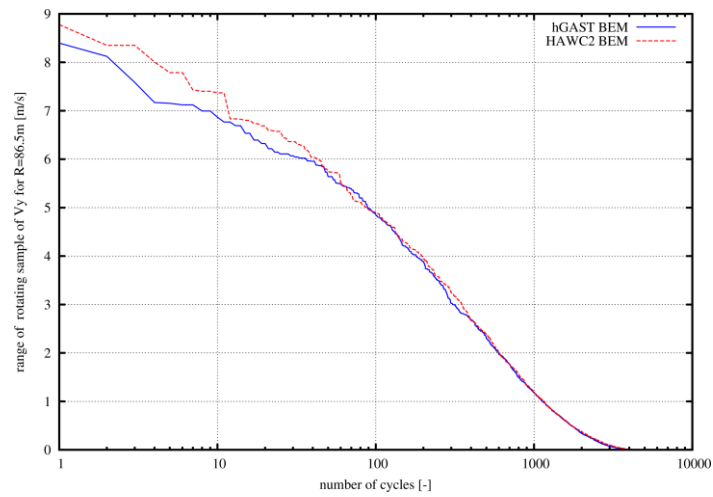


Figure 62: RFC of the blade tip ( $r=86.5$  m) rotational sampled horizontal wind velocity (mean wind speed 8m/s).

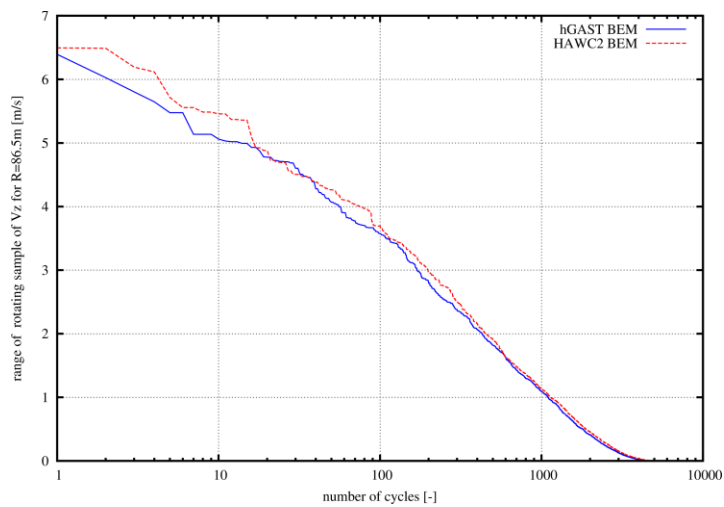


Figure 63: RFC of the blade tip ( $r=86.5$  m) rotational sampled vertical wind velocity (mean wind speed 8m/s).

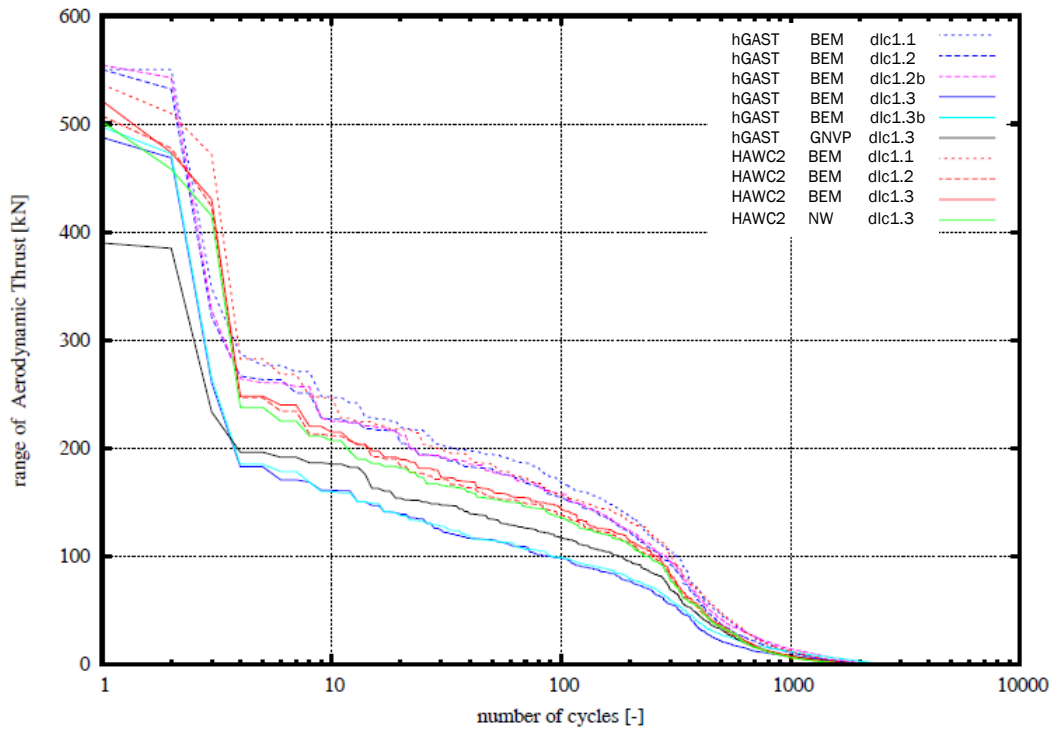


Figure 64: RFC of the aerodynamic thrust at the wind speed 8m/s (Case1: Stiff).

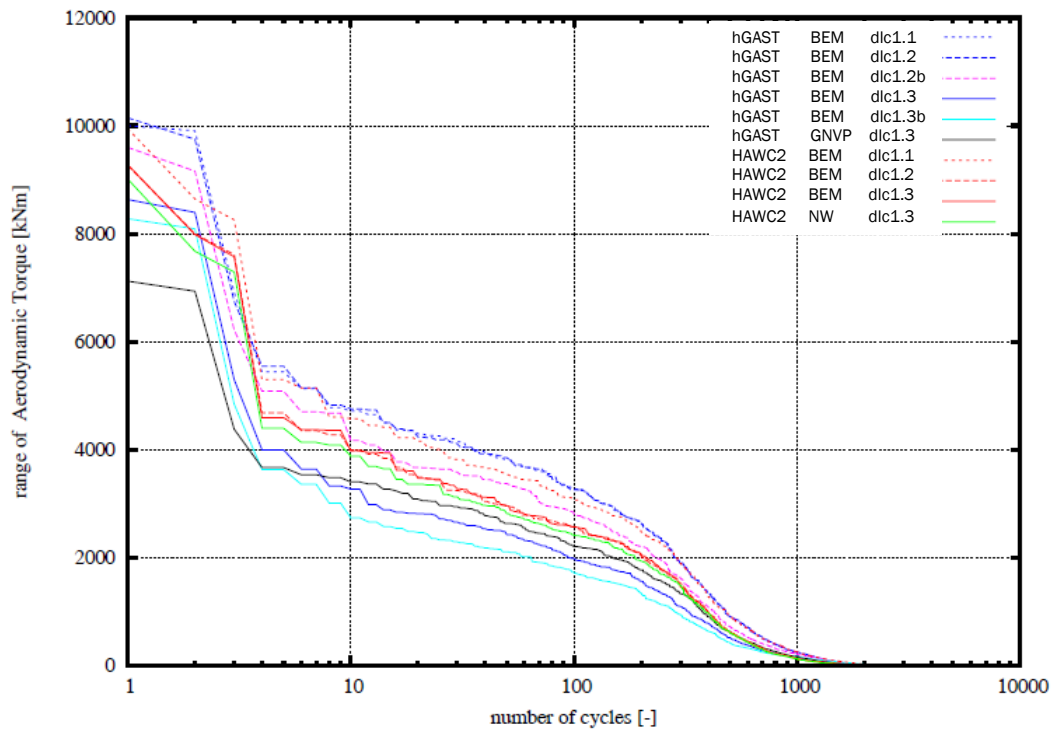


Figure 65: RFC of the aerodynamic torque at the wind speed 8m/s (Case1: Stiff).

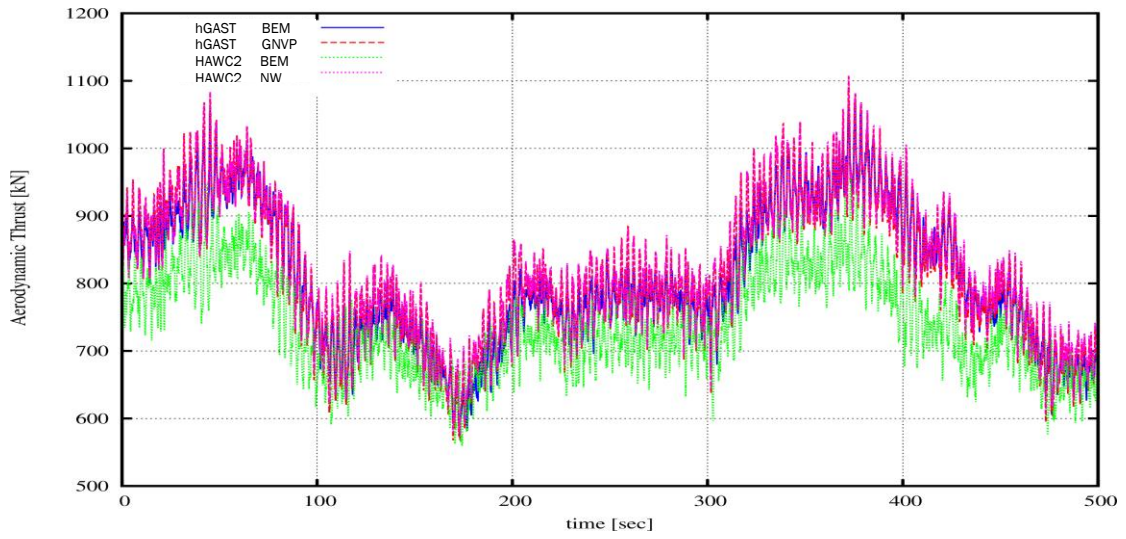


Figure 66: Time series of the aerodynamic thrust at the wind speed 8m/s (Case1.3: Stiff).

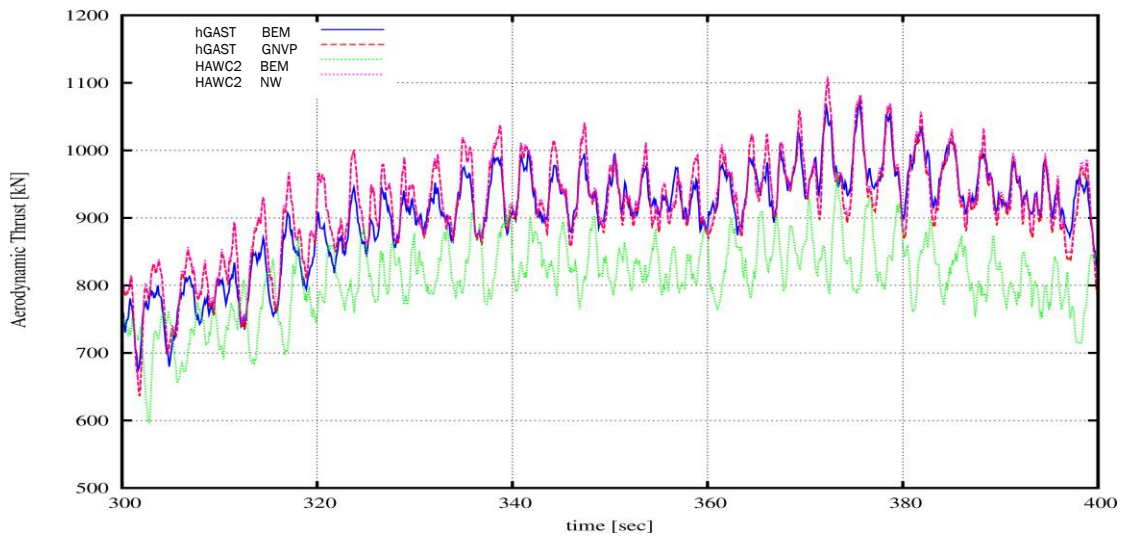


Figure 67: Time series of the aerodynamic thrust (100 s focus plot) at the wind speed 8m/s (Case1.3: Stiff).

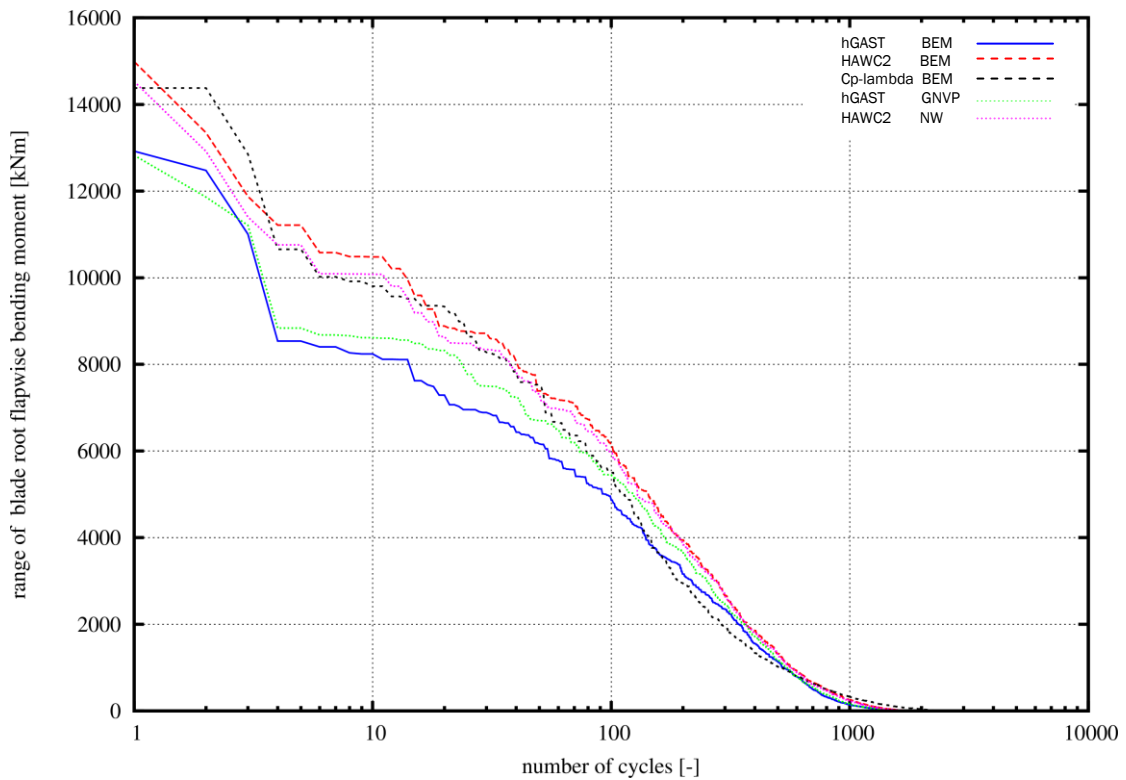


Figure 68: RFC of the blade root flapwise bending moment at the wind speed 8m/s (Case2.3: flexible turbine - open loop).

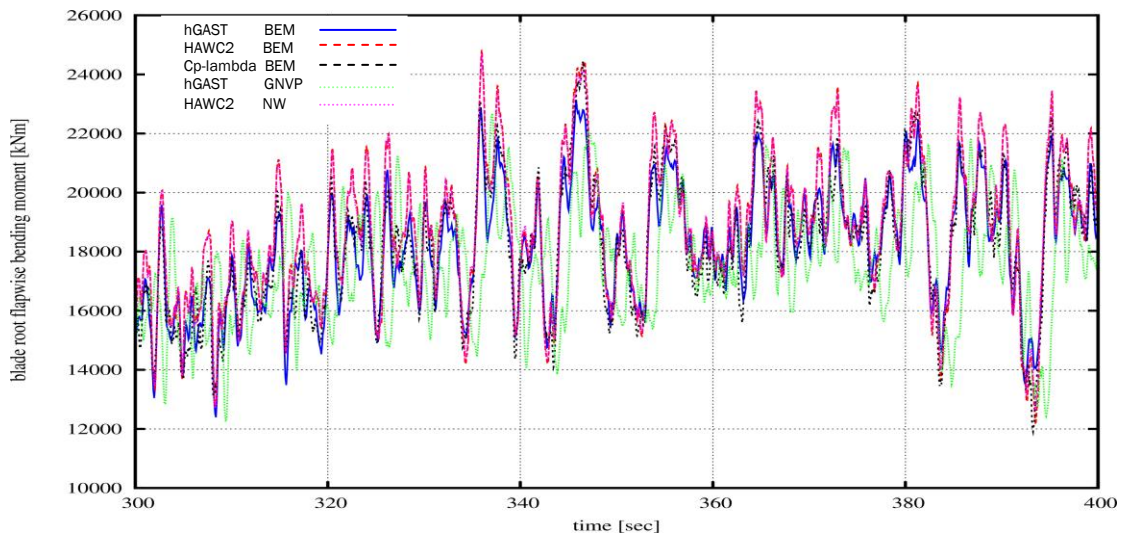


Figure 69: Time-series of the blade root flapwise bending moment at the wind speed 8m/s (Case2.3: flexible turbine - open loop).

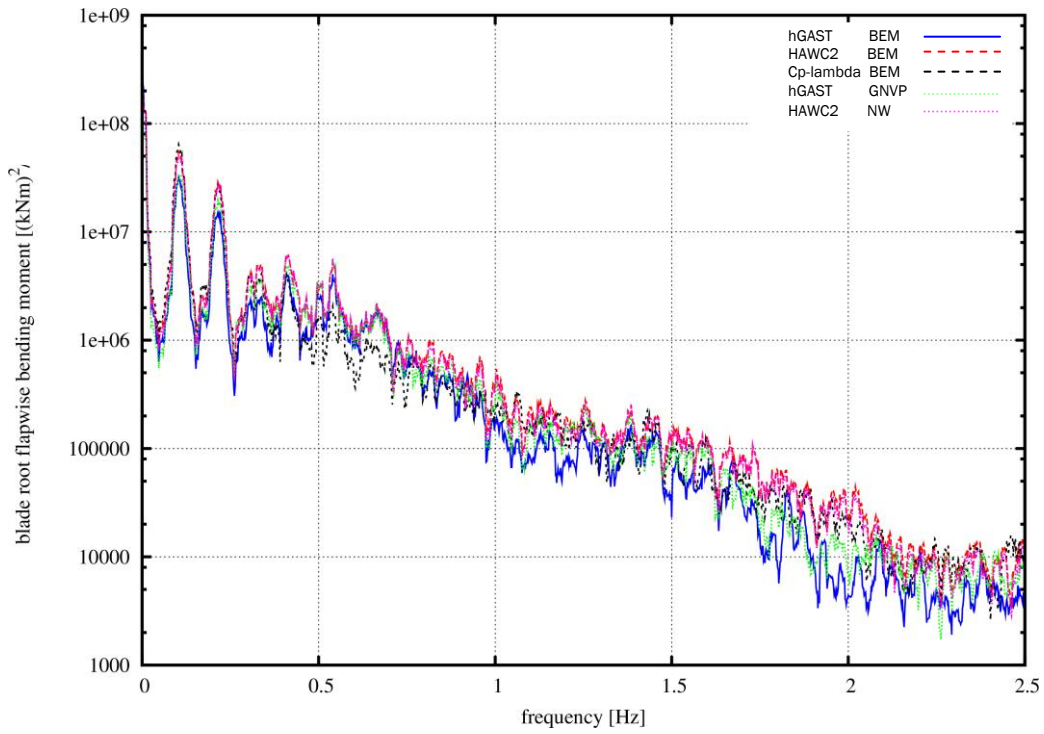


Figure 70: PSD of the blade root flapwise bending moment at the wind speed 8m/s (Case2.3: flexible turbine - open loop).

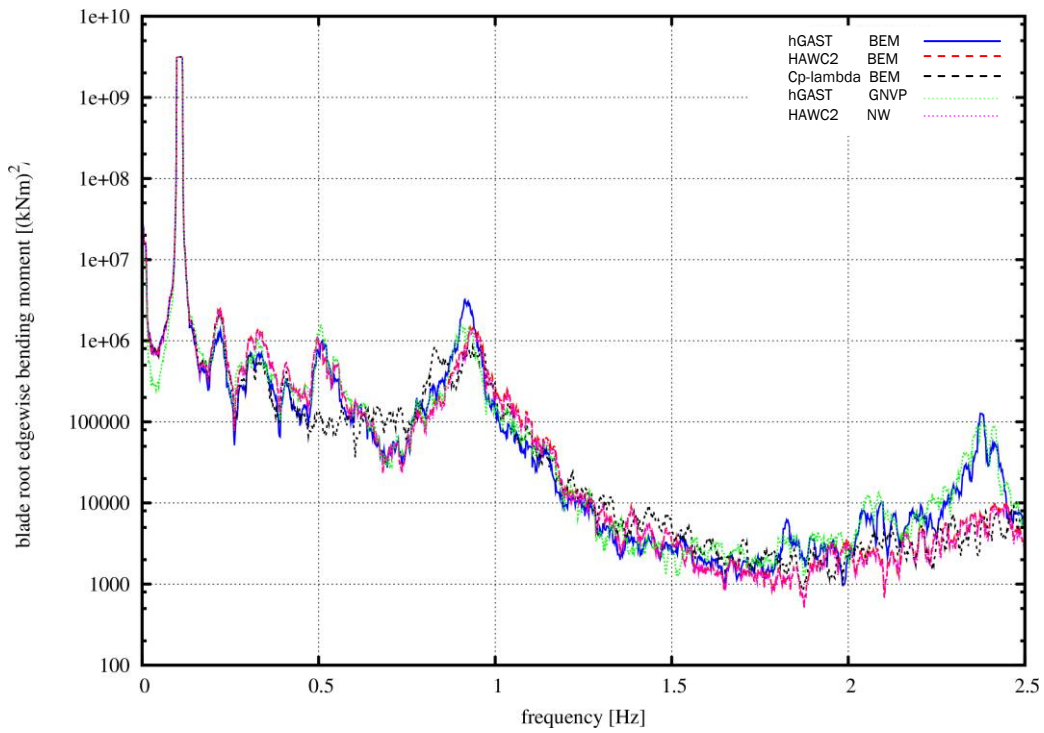


Figure 71: PSD of the blade root edgewise bending moment at the wind speed 8m/s (Case2.3: flexible turbine - open loop).

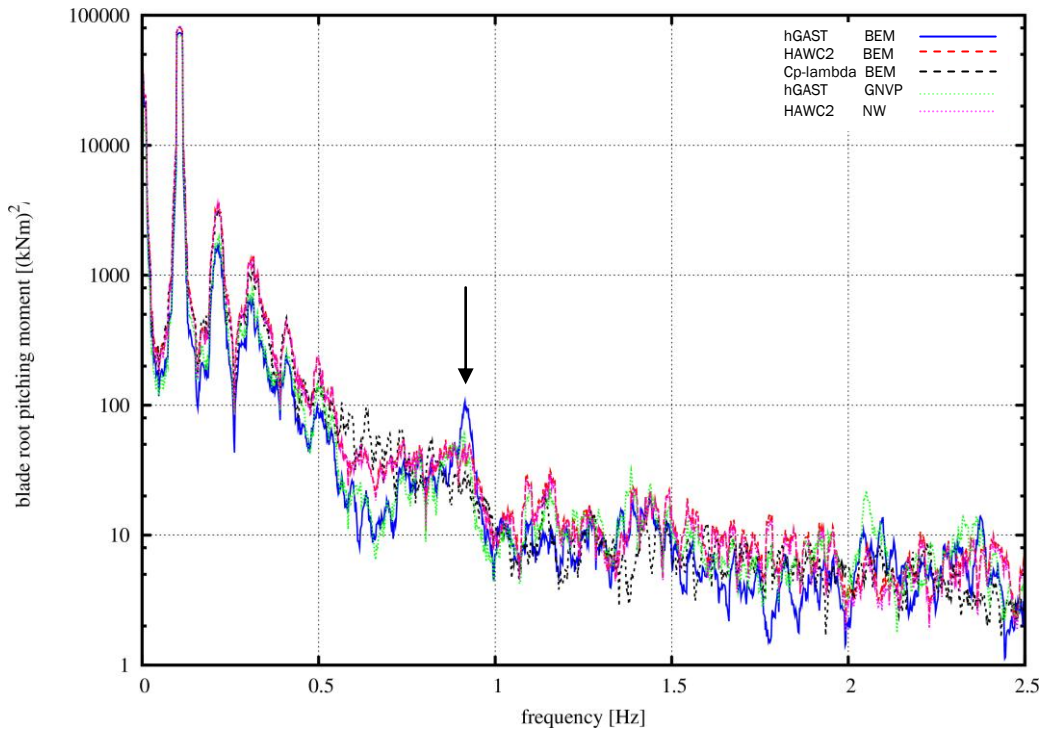


Figure 72: PSD of the blade root pitching moment at the wind speed 8m/s (Case2.3: flexible turbine - open loop).

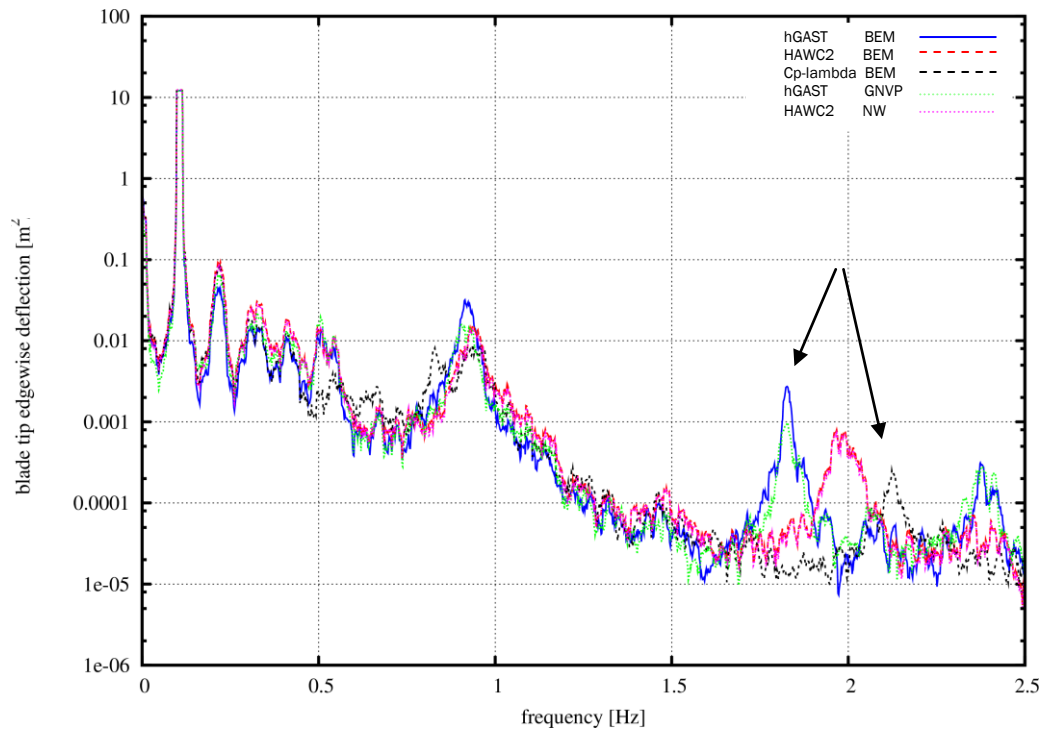


Figure 73: PSD of the blade tip edgewise deflection at the wind speed 8m/s (Case2.3: flexible turbine - open loop).

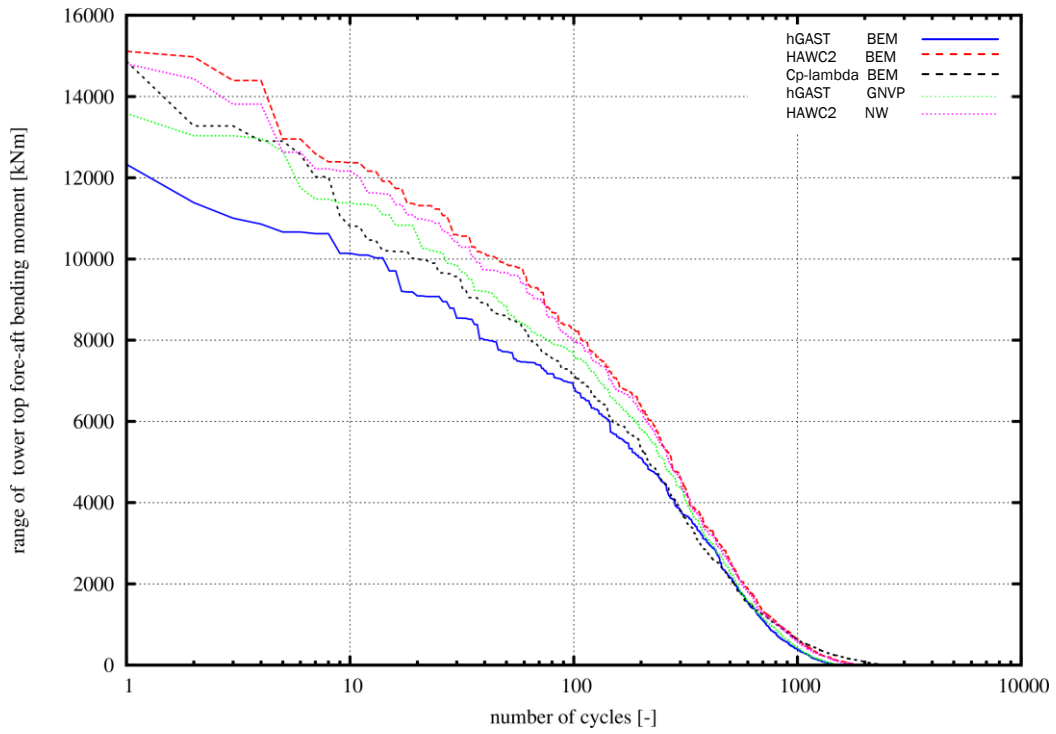


Figure 74: RFC of tower top fore-aft bending moment at the wind speed 8m/s (Case2.3: flexible turbine - open loop).

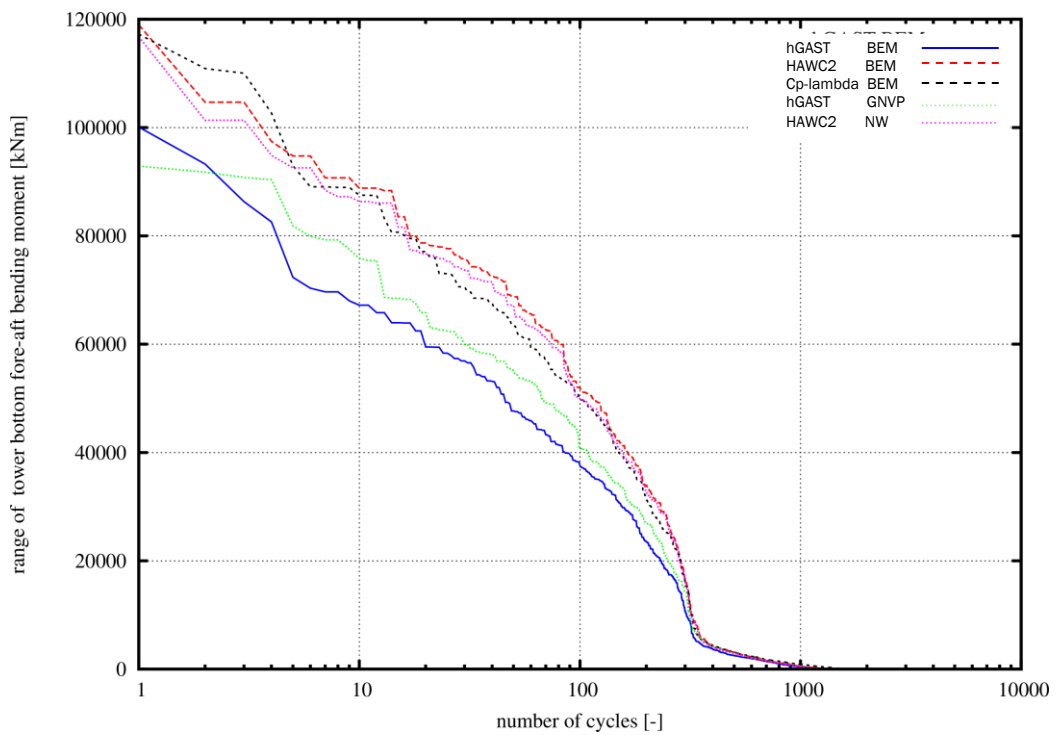


Figure 75: RFC of tower bottom fore-aft bending moment at the wind speed 8m/s (Case2.3: flexible turbine - open loop).

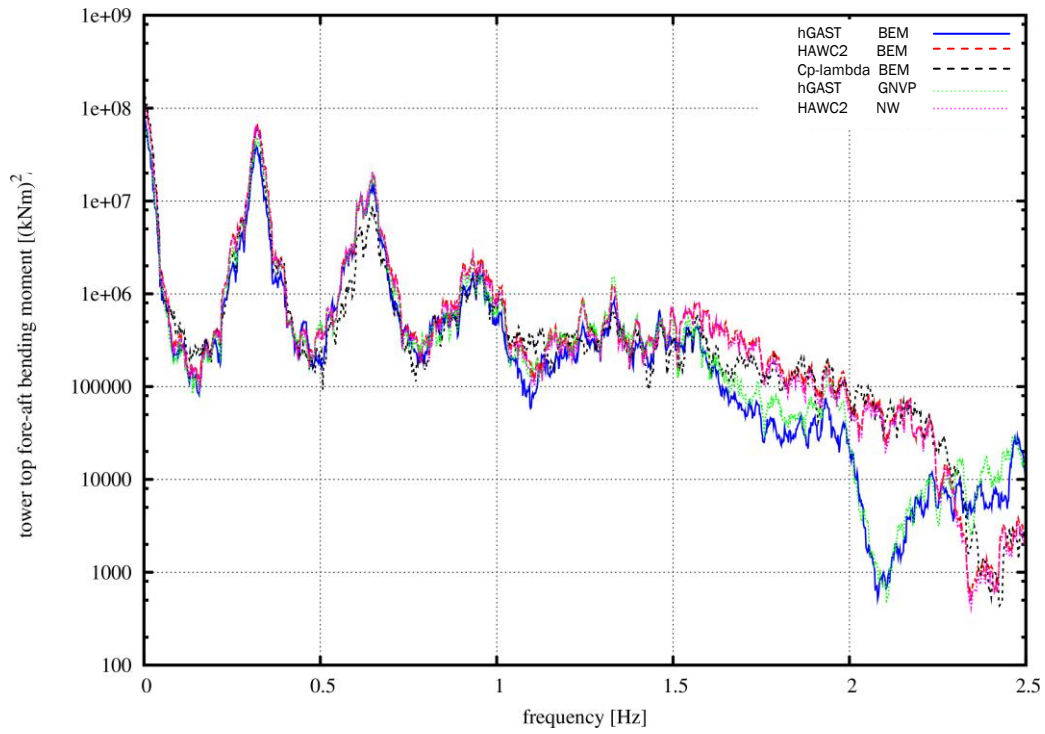


Figure 76: PSD of tower top fore-aft bending moment at the wind speed 8m/s (Case2.3: flexible turbine - open loop).

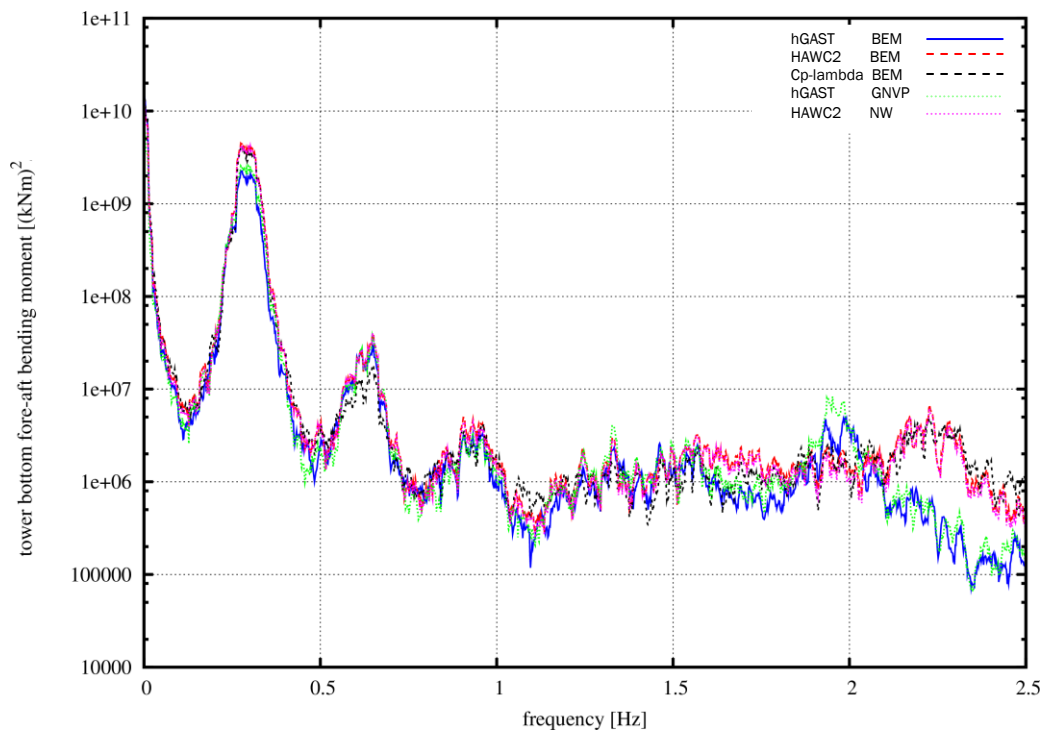


Figure 77: PSD of tower bottom fore-aft bending moment at the wind speed 8m/s (Case2.3: flexible turbine - open loop).

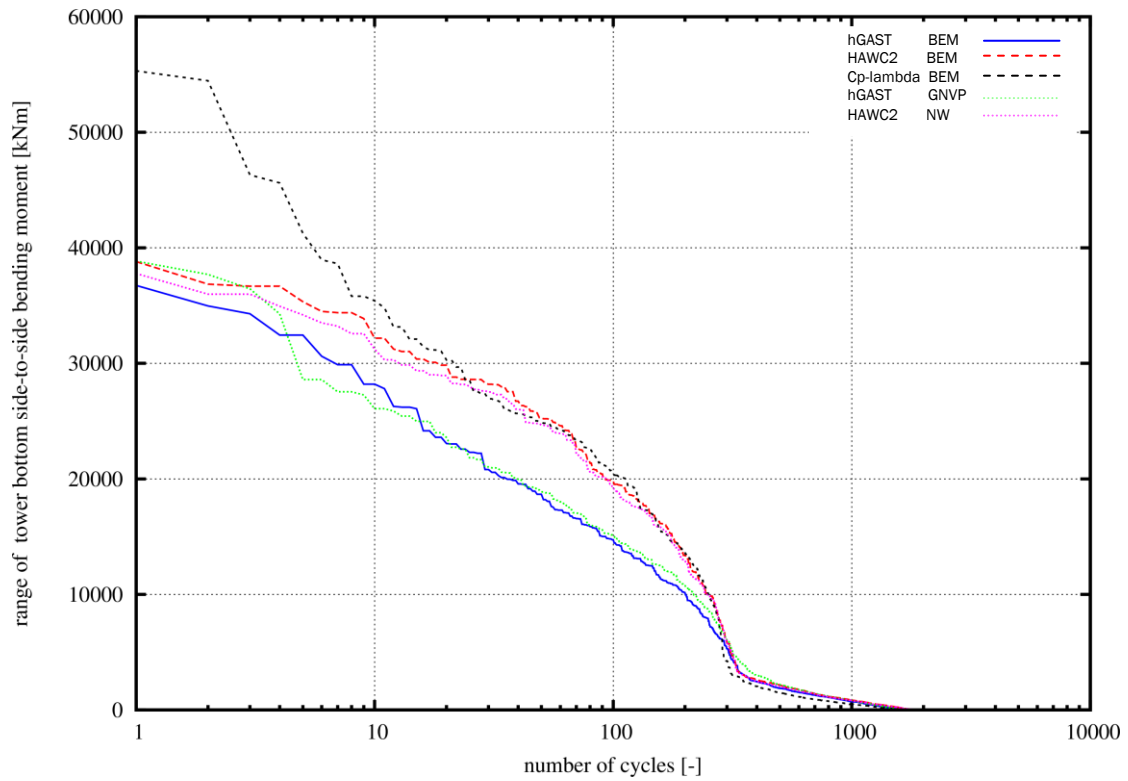


Figure 78: RFC of tower bottom side-to-side bending moment at the wind speed 8m/s (Case2.3: flexible turbine - open loop).

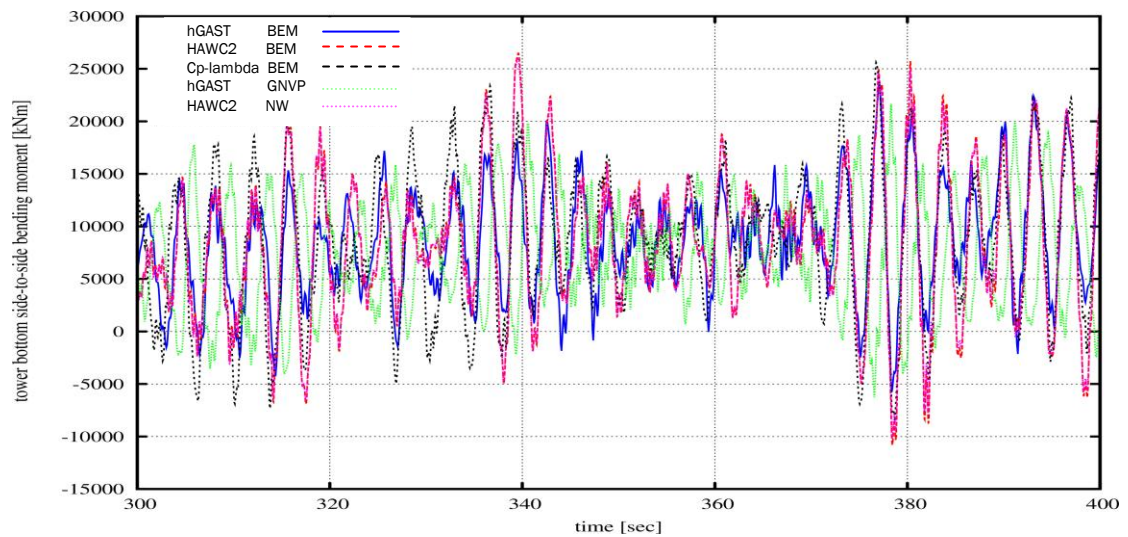


Figure 79: Time-series of tower bottom side-to-side bending moment at the wind speed 8m/s (Case2.3: flexible turbine - open loop).

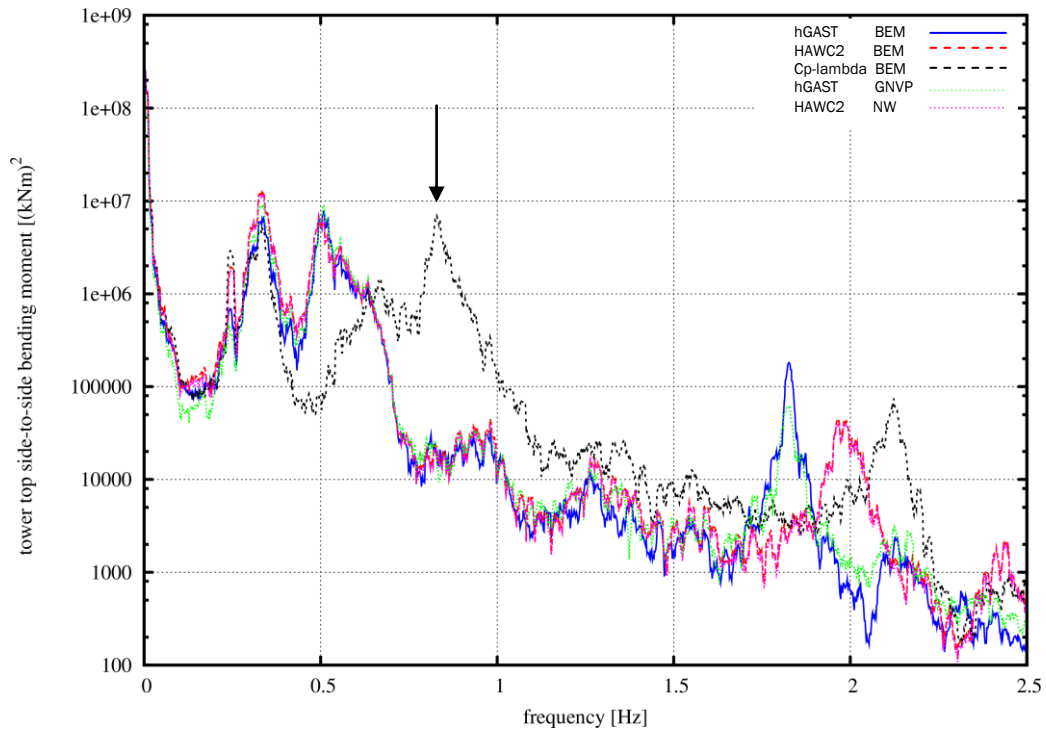


Figure 80: PSD of tower top side-to-side bending moment at the wind speed 8m/s (Case2.3: flexible turbine - open loop).

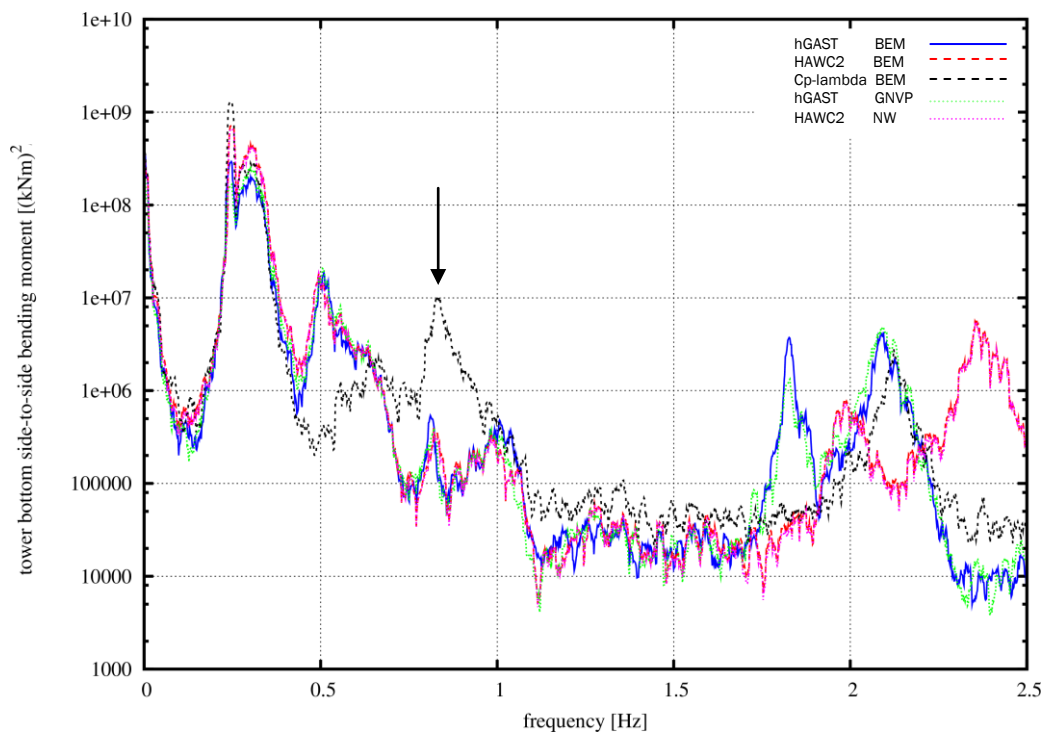


Figure 81: PSD of tower bottom side-to-side bending moment at the wind speed 8m/s (Case2.3: flexible turbine - open loop).

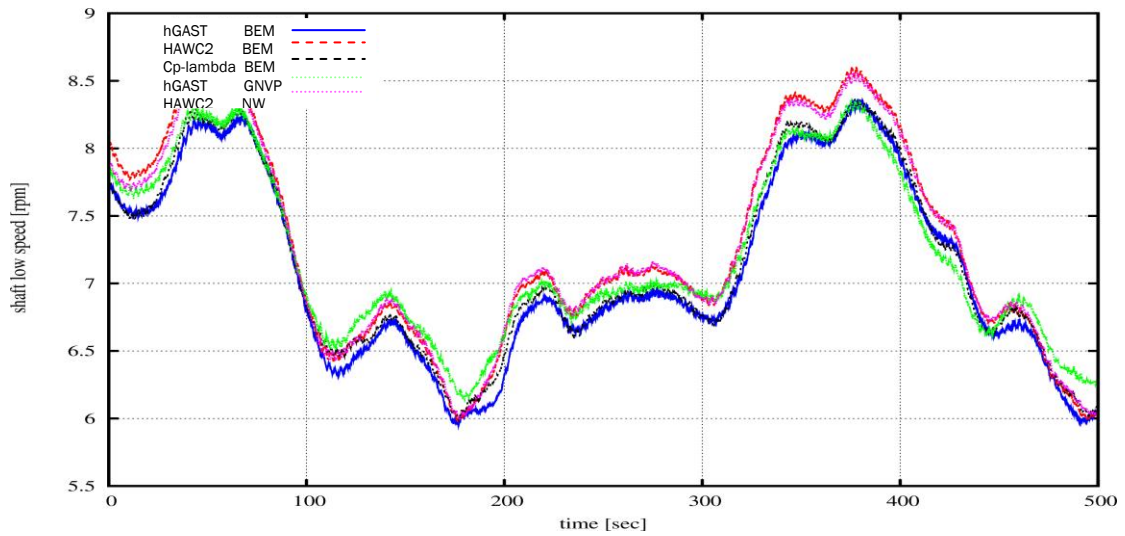


Figure 82: Time-series of low speed shaft speed at the wind speed 8m/s (Case2.4: flexible turbine - closed loop).

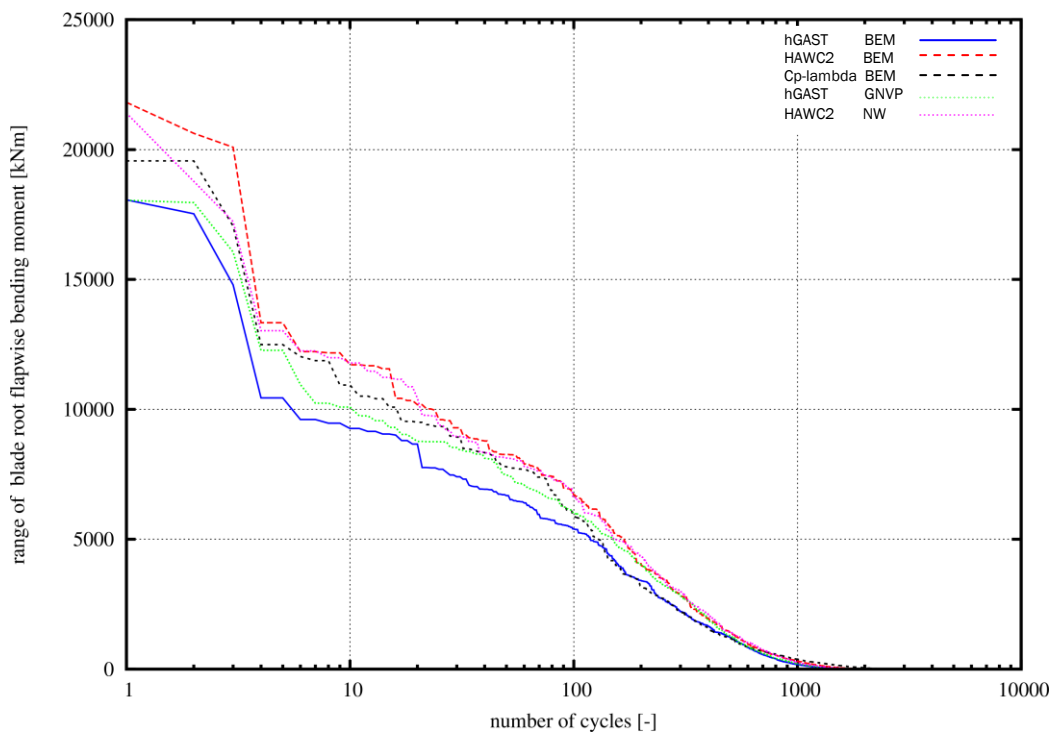


Figure 83: RFC of the blade root flapwise bending moment at the wind speed 8m/s (Case2.4: flexible turbine - closed loop).

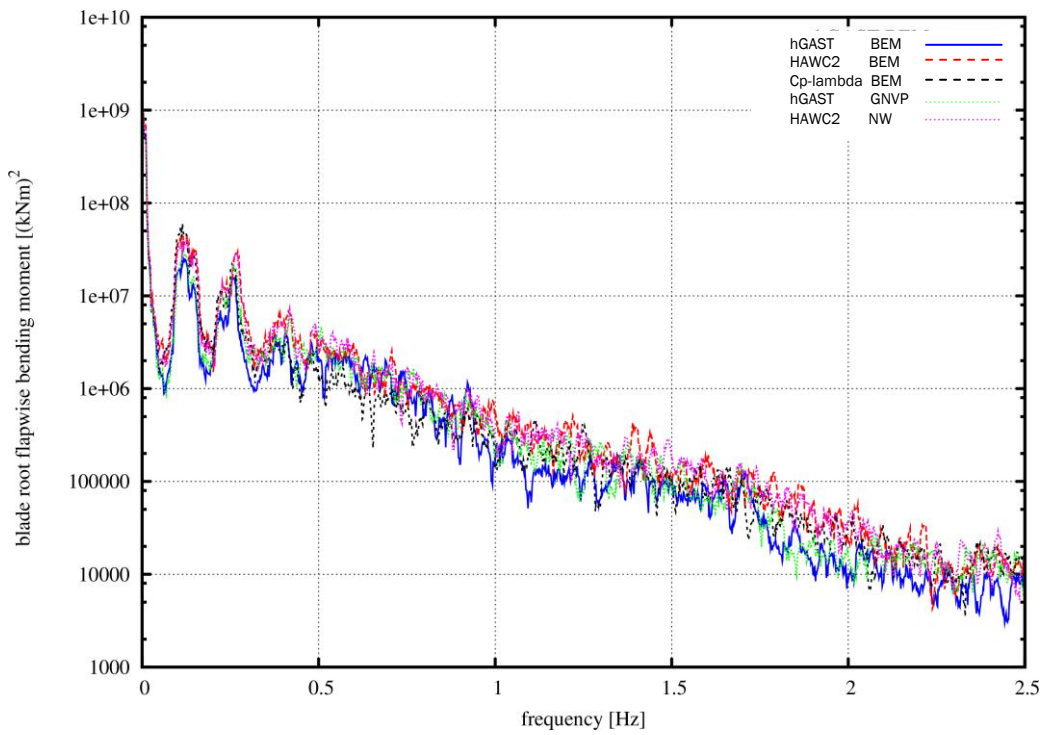


Figure 84: PSD of the blade root flapwise bending moment at the wind speed 8m/s (Case2.4: flexible turbine - closed loop).

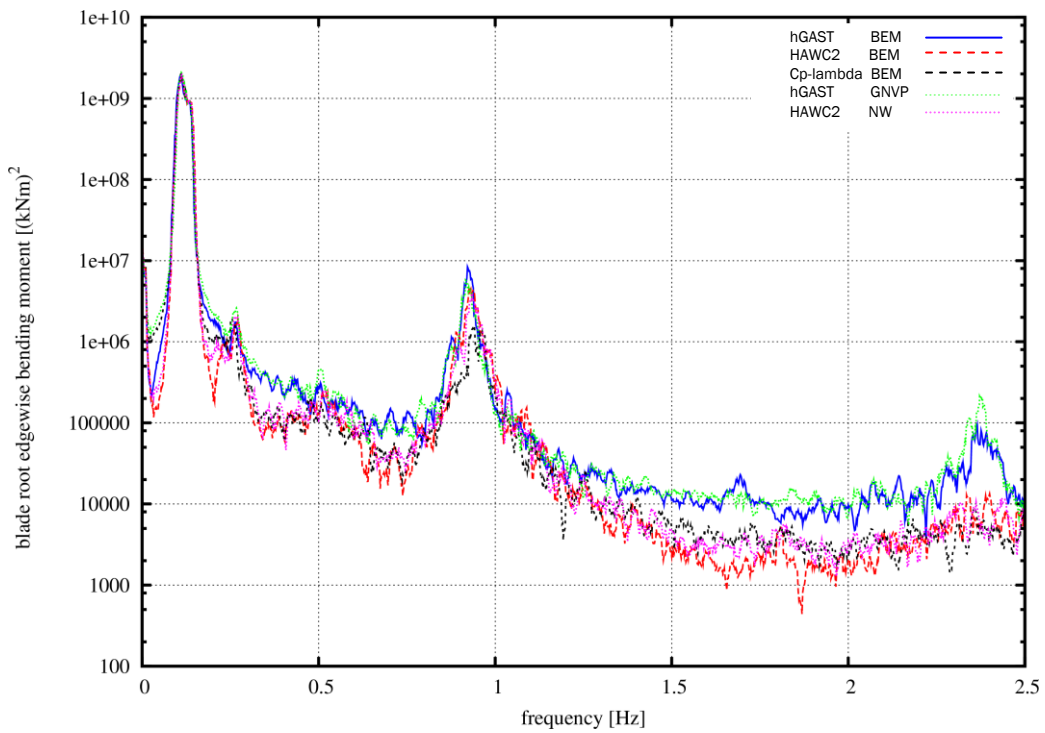


Figure 85: PSD of the blade root edgewise bending moment at the wind speed 8m/s (Case2.4: flexible turbine - closed loop).

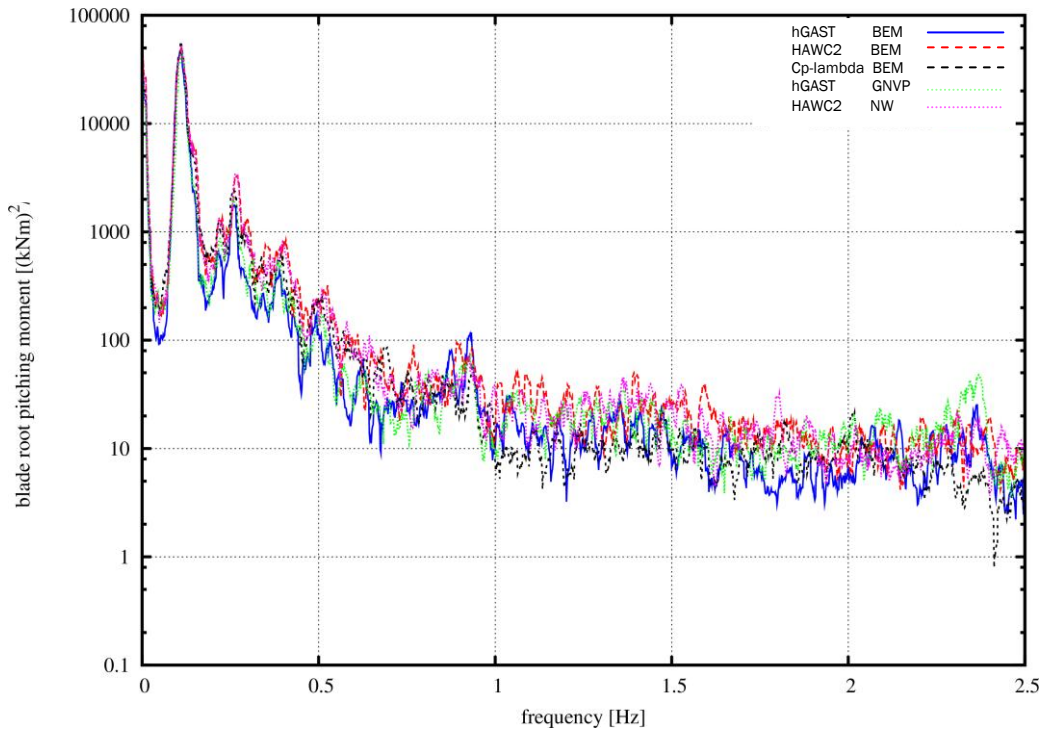


Figure 86: PSD of the blade root pitching moment at the wind speed 8m/s (Case2.4: flexible turbine - closed loop).

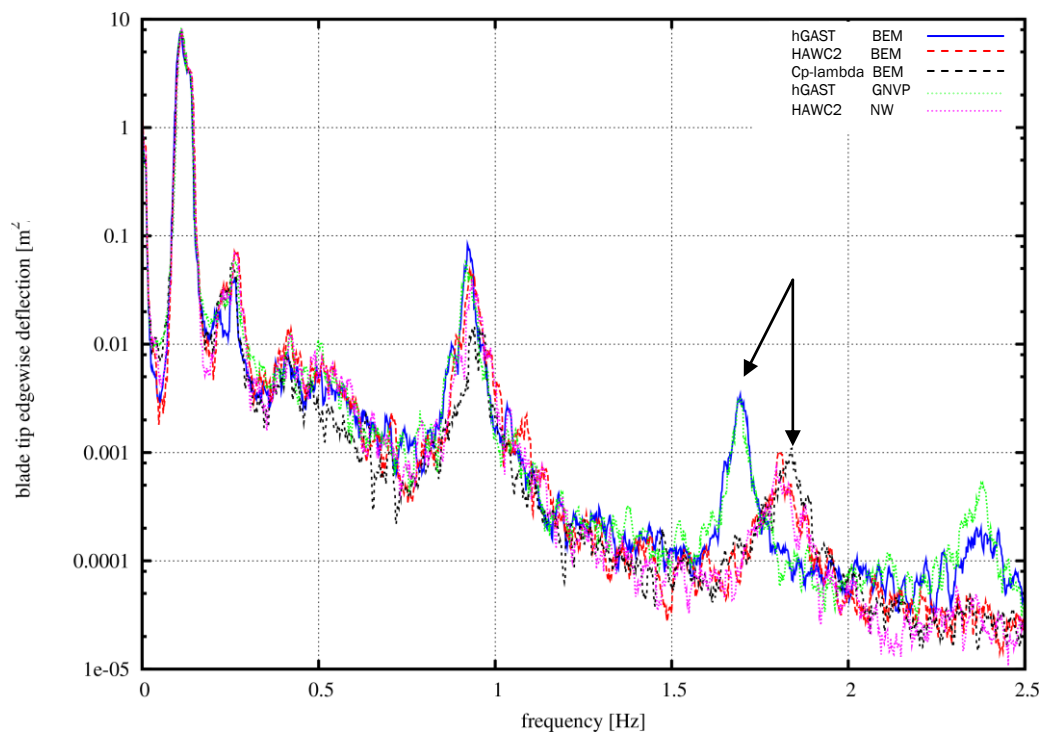


Figure 87: PSD of the blade tip edgewise deflection at the wind speed 8m/s (Case2.4: flexible turbine - closed loop).

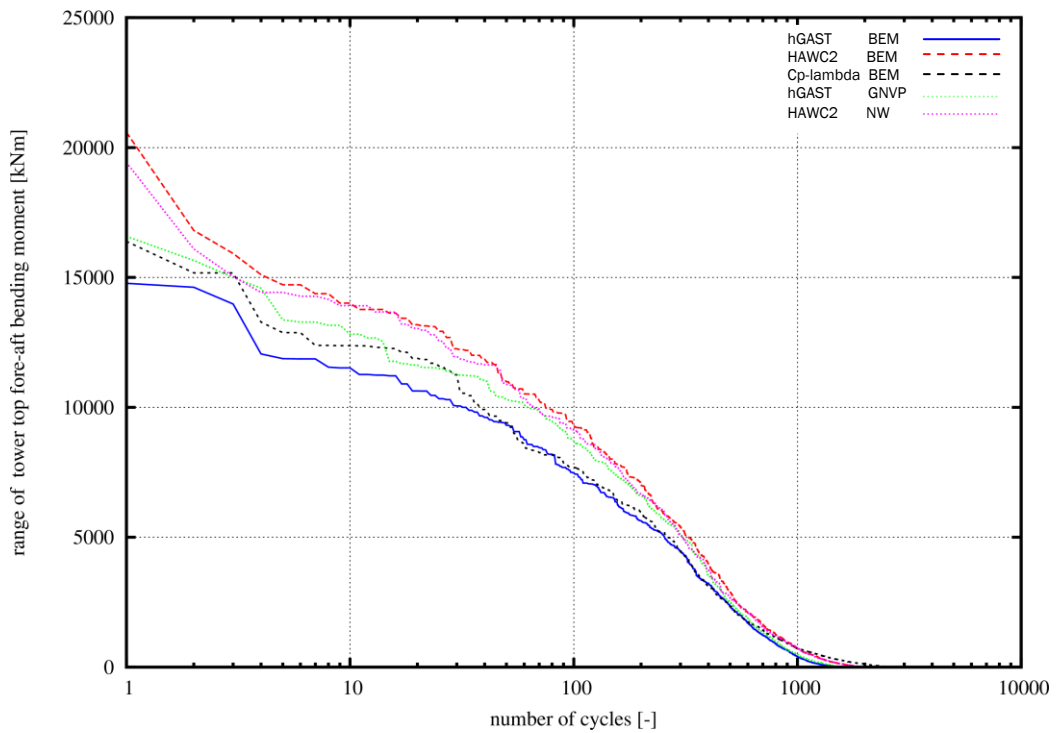


Figure 88: RFC of tower top fore-aft bending moment at the wind speed 8m/s (Case2.4: flexible turbine - closed loop).

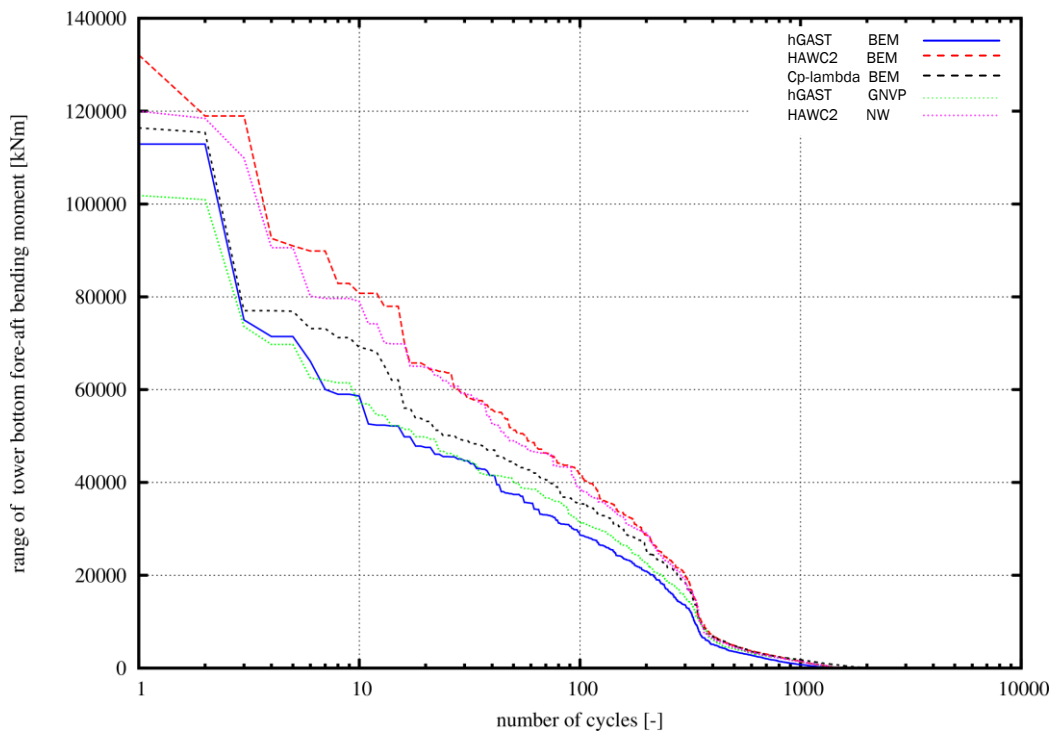


Figure 89: RFC of tower bottom fore-aft bending moment at the wind speed 8m/s (Case2.4 flexible turbine - closed loop).

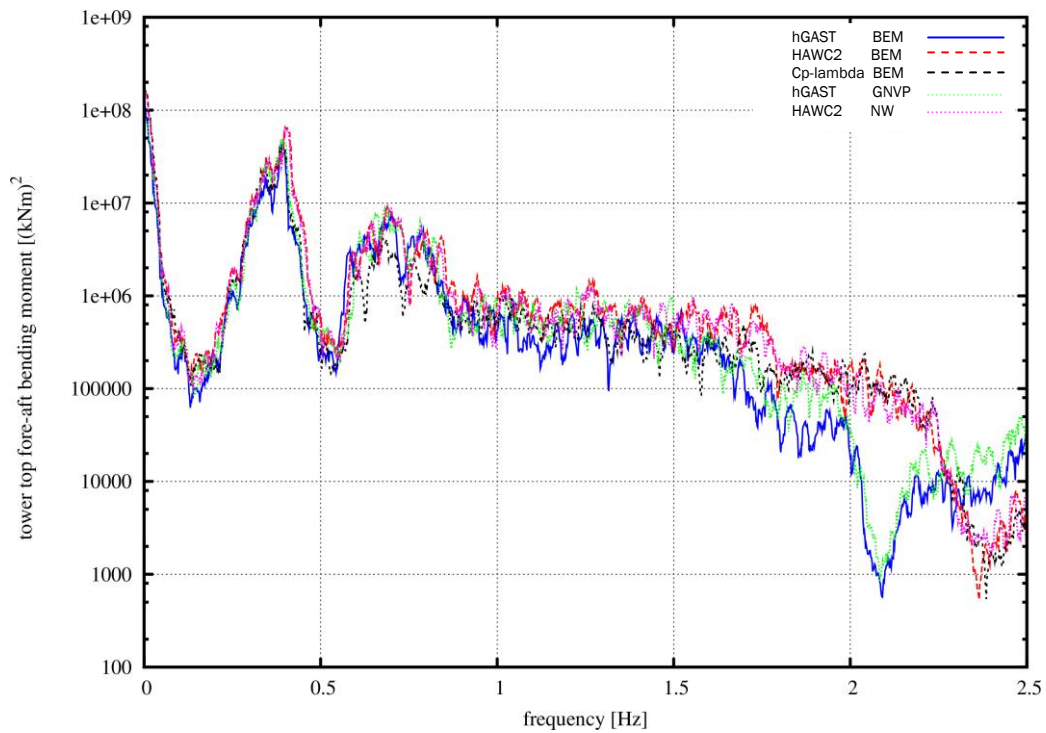


Figure 90: PSD of tower top fore-aft bending moment at the wind speed 8m/s (Case2.4: flexible turbine - closed loop).

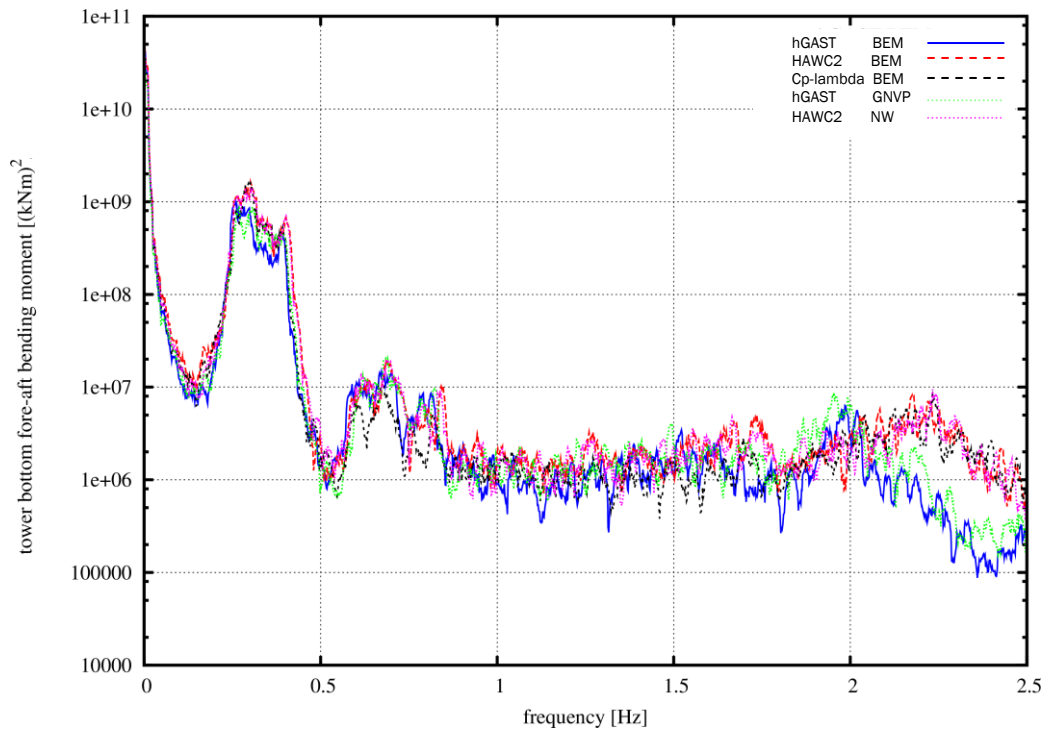


Figure 91: PSD of tower bottom fore-aft bending moment at the wind speed 8m/s (Case2.4: flexible turbine - closed loop).

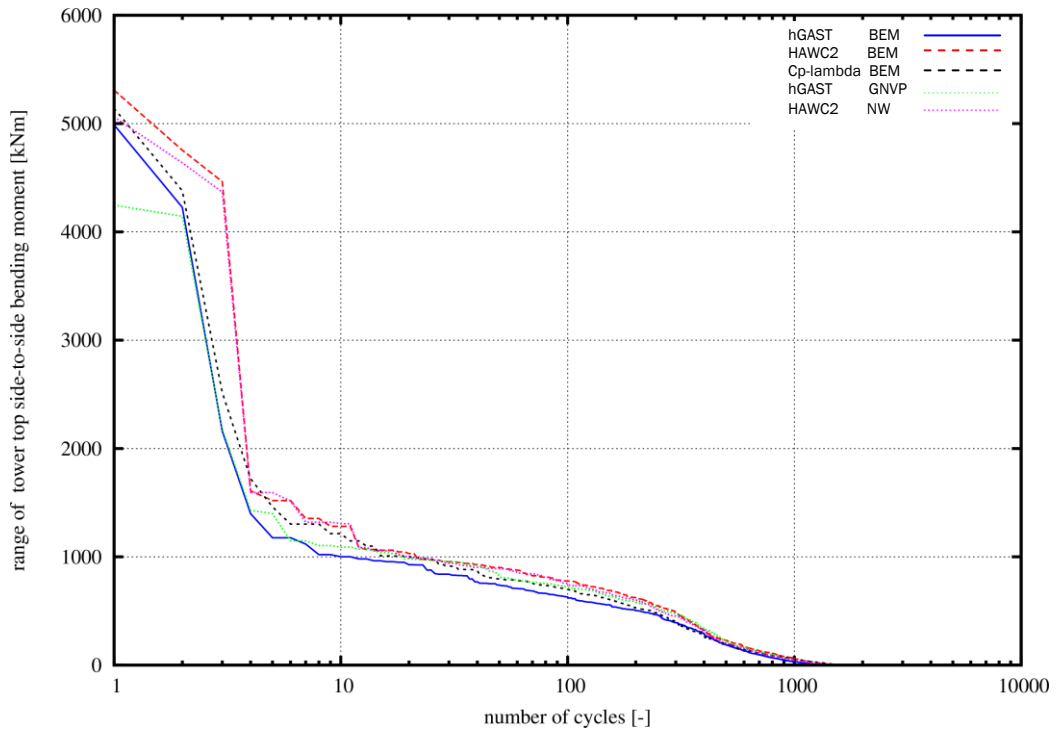


Figure 92: RFC of tower top side-to-side bending moment at the wind speed 8m/s (Case2.4: flexible turbine - closed loop).

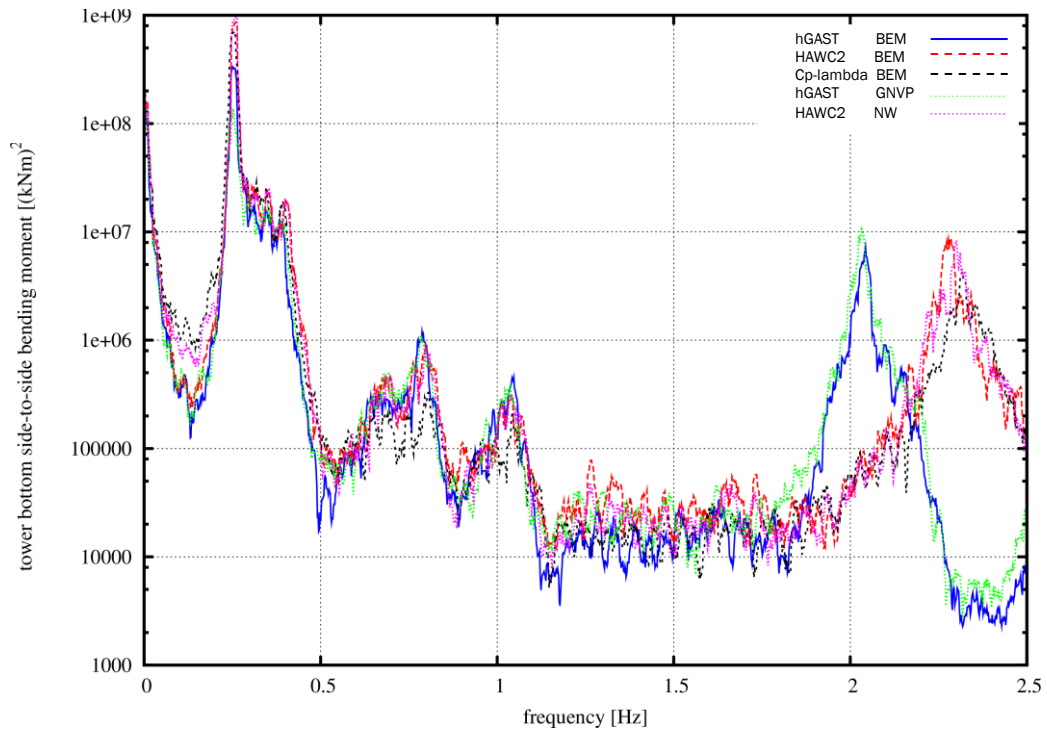


Figure 93: PSD of tower top side-to-side bending moment at the wind speed 8m/s (Case2.4: flexible turbine - closed loop).

### 1.3.3 Turbulent wind cases at 8m/s and 18m/s (Veers mode)

Turbulent wind simulations (10 min runs) have been performed at the wind speeds of 8 m/s (partial load conditions) and 18 m/s (full load conditions). Results of hGAST and NEREA modal code are compared for the same turbulent wind boxes. The turbulent wind velocities have been provided by NTUA (Veers model) with respect to a fixed in space and provided in a polar grid. NEREA (modal) represents the typical fast aeroelastic tool used by the industry while hGAST is a non-linear tool that accounts for geometric non-linearity effects.

The following simulation conditions are defined in the analysis below:

Flexible turbine

**closed loop operation**, tower shadow enabled, tilt=5°, pre-cone=2.5°, tip-prebend=3.3m, Uwind=8m/s, shear exponent=0, wind yaw=0°, wind inclination=0°

dynamic inflow, unsteady airfoil aerodynamic model

Time series results and Power Spectral Density (PSD) plots of the loads of the main components are presented in the sequel.

The following comments can be made for the abovementioned conditions (see Figure 94-Figure 109):

#### 8m/s case:

- As seen in the low speed shaft rotational speed (Figure 94) and the generator torque (Figure 95) the two codes properly model the controller operation (variable speed mode of operation).
- A notable difference is seen in the prediction of the 1P and 2P peaks of the flapwise bending moment at 8 m/s wind speed (Figure 97).
- Higher damping of the first edgewise mode is predicted by hGAST (see lower peak of the edgewise mode in the blade root edgewise moment in Figure 98).
- NEREA modal code does not predict the cross talking of the edge moment in the root pitching moment as all higher order models do (peak at 0.9 Hz predicted by all higher order models in the root pitching moment – compare Figure 86 against Figure 99)
- A good agreement is seen in the tower loads (Figure 100, Figure 101).

#### 18m/s case:

- As seen in the low speed shaft rotational speed (Figure 102) and the blade pitch angle (Figure 103) the two codes properly model the controller operation (full load operation). The almost 1° level difference in the pitch angle results is due to the fact that NEREA modal code neglects blade torsion d.o.f. As can be seen in Figure 51 the expected mean torsion angle at the tip of the blade at 18 m/s wind speed exceeds -1.5° (minus sign means nose down twisting).
- A better agreement of the flapwise bending moment is seen in the wind speed of 18 m/s (Figure 105). This is reasonable taking into account that the effect of the induction on loads is expected to be much lower at this high wind speed.
- Lower damping of the first edgewise mode is predicted by hGAST (see higher peak of the edgewise mode in the blade root edgewise moment in Figure 106) in this higher mean wind speed case.
- A less pronounced bending/torsion coupling is observed in this high mean wind speed case as a result of the lower mean flapwise deflections. This indicated by the lower edgewise mode peak in the blade root pitching moment seen in Figure 107.

- A good agreement is seen again in the tower loads at this high mean wind speed case (Figure 108, Figure 109). NEREA modal seems to over-predict the 3P peak at  $\sim 0.45\text{Hz}$  in the tower bottom fore-aft bending moment (Figure 109).

**8 m/s case (hGAST vs. NEREA modal – closed loop)**

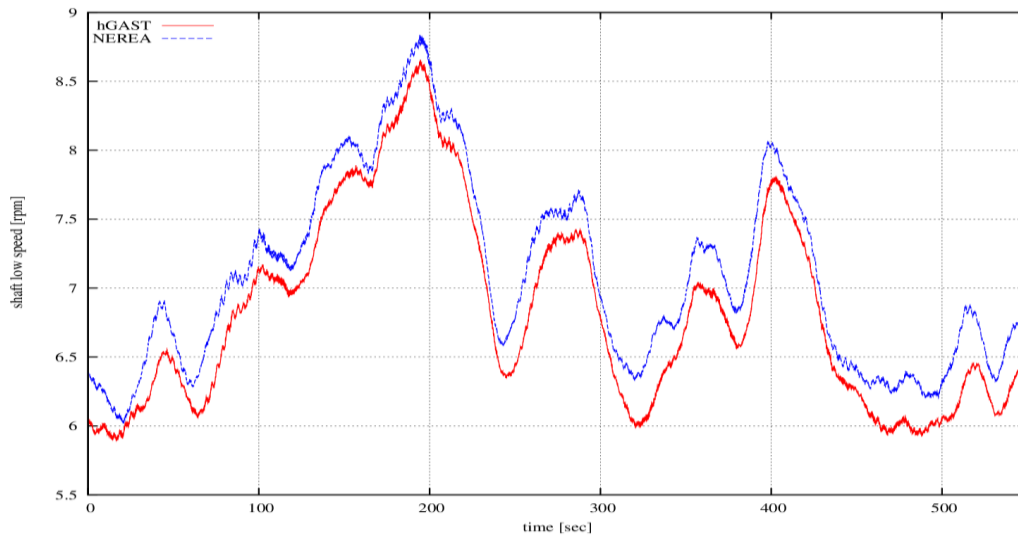


Figure 94: Time series of the rotor speed at 8m/s.

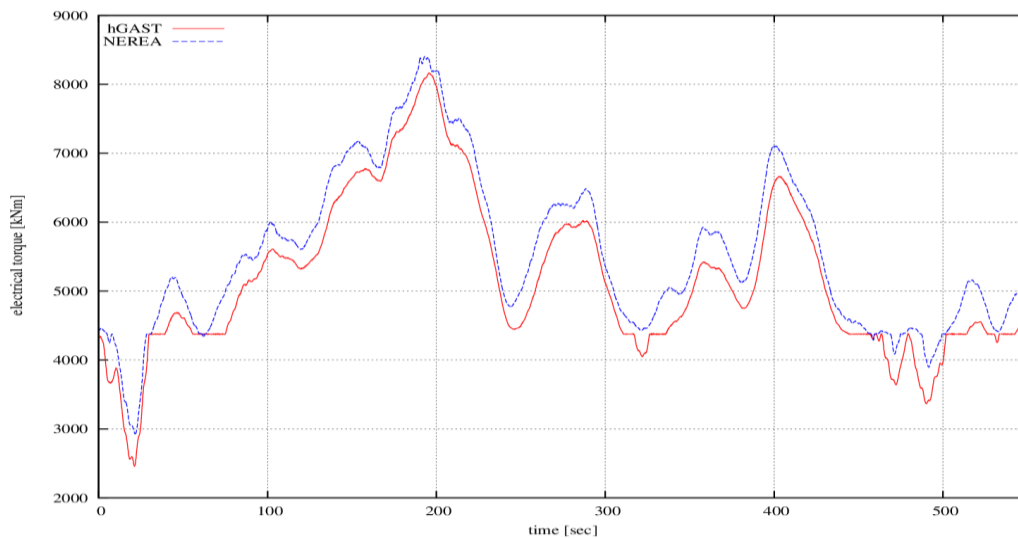


Figure 95: Time series of the generator torque at 8m/s.

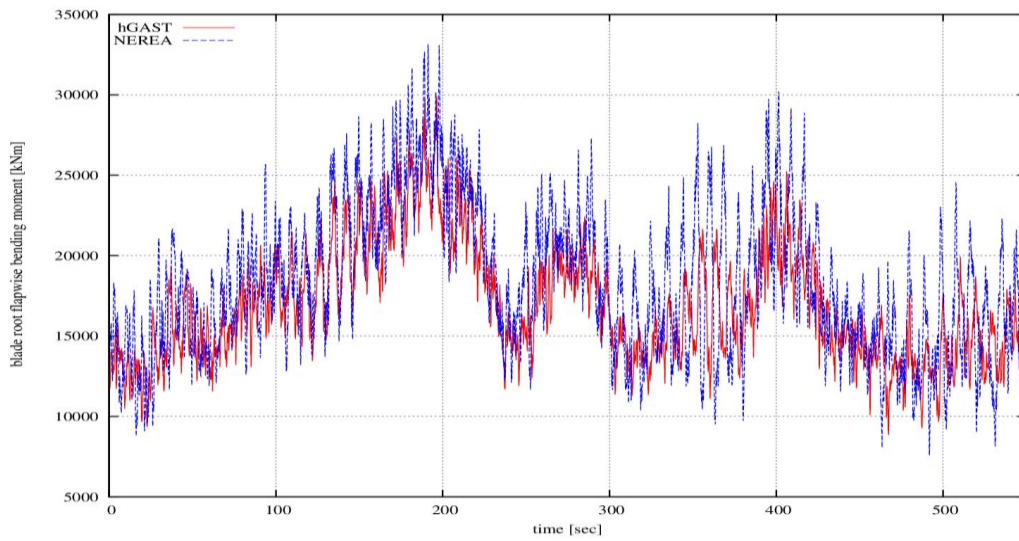


Figure 96: Time series of the flapwise bending moment at the root of the blade at 8m/s.

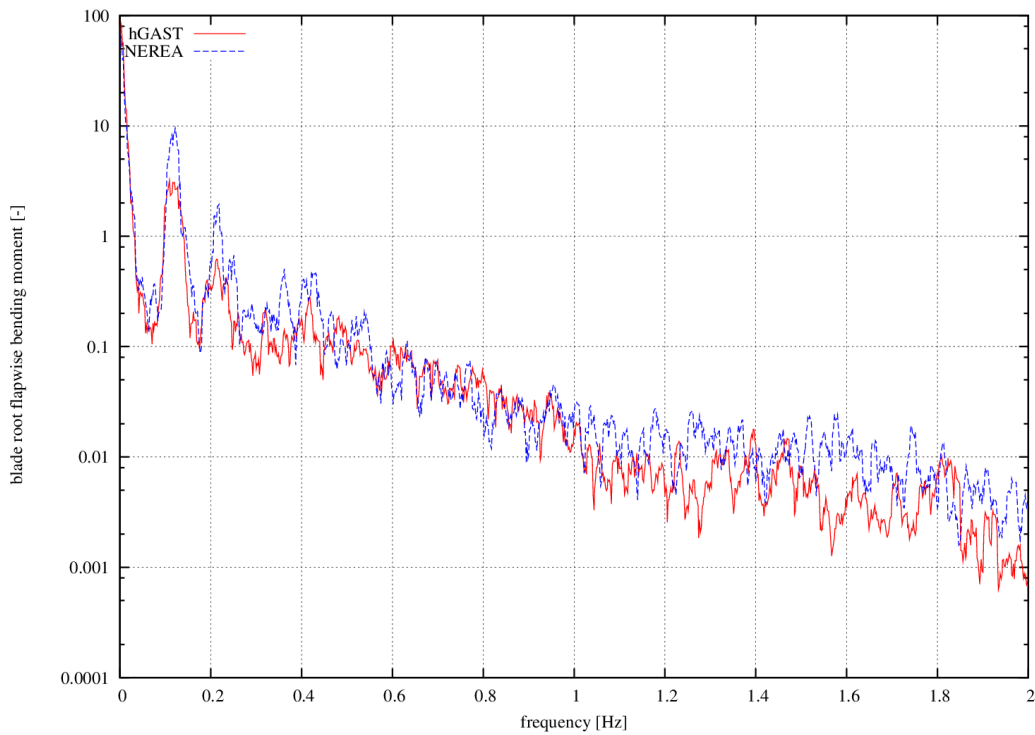


Figure 97: PSD of the flapwise bending moment at the root of the blade at 8m/s.

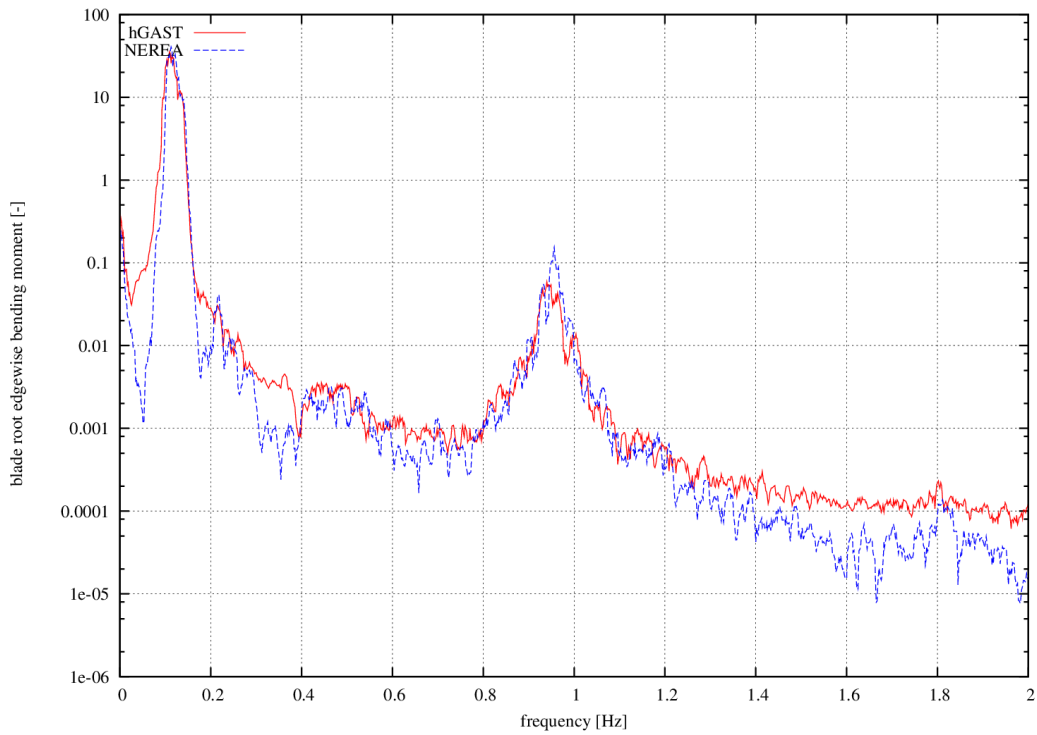


Figure 98: PSD of the edgewise bending moment at the root of the blade at 8m/s.

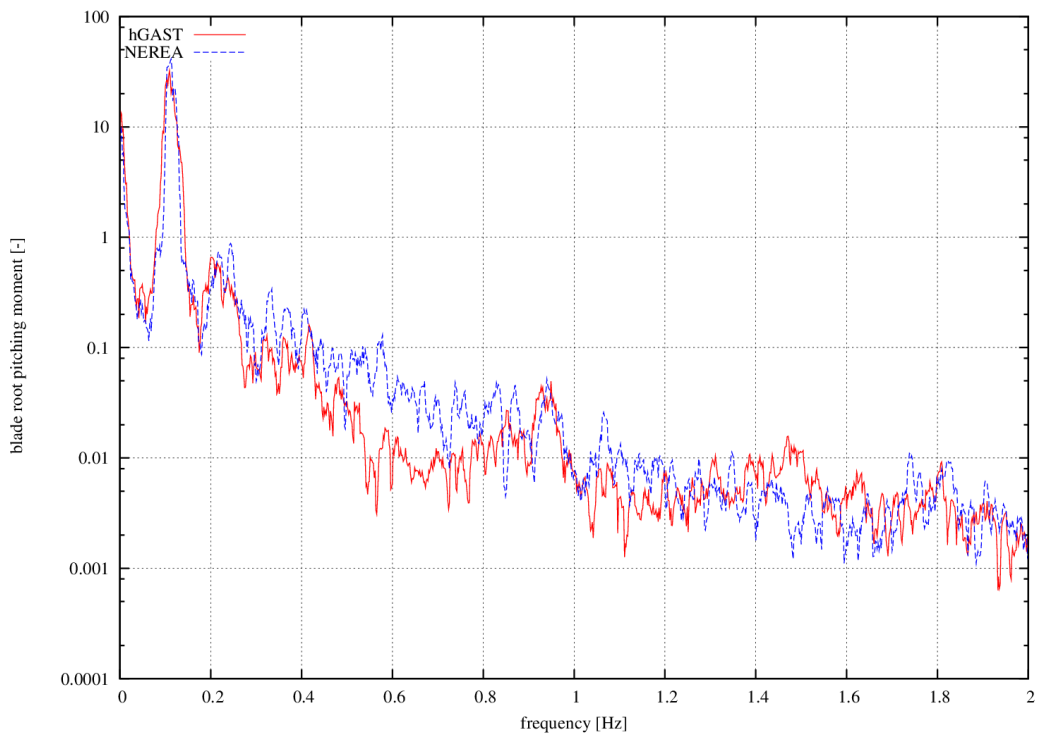


Figure 99: PSD of the pitching moment at the root of the blade at 8m/s.

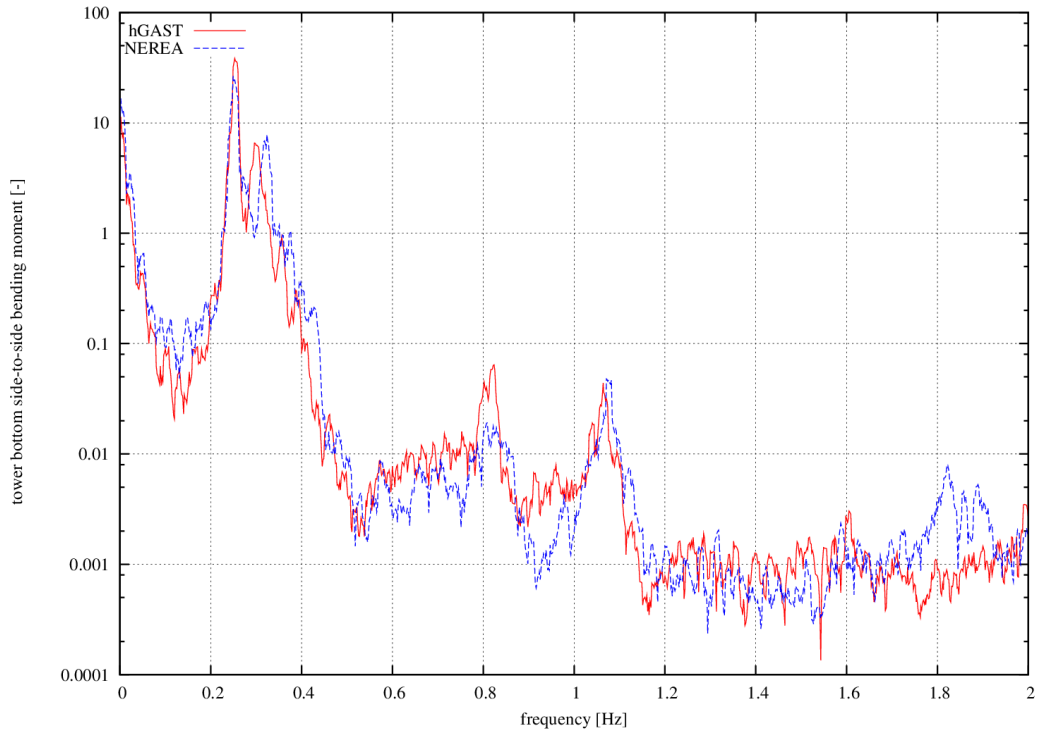


Figure 100: PSD of the tower bottom side to side bending moment at 8m/s.

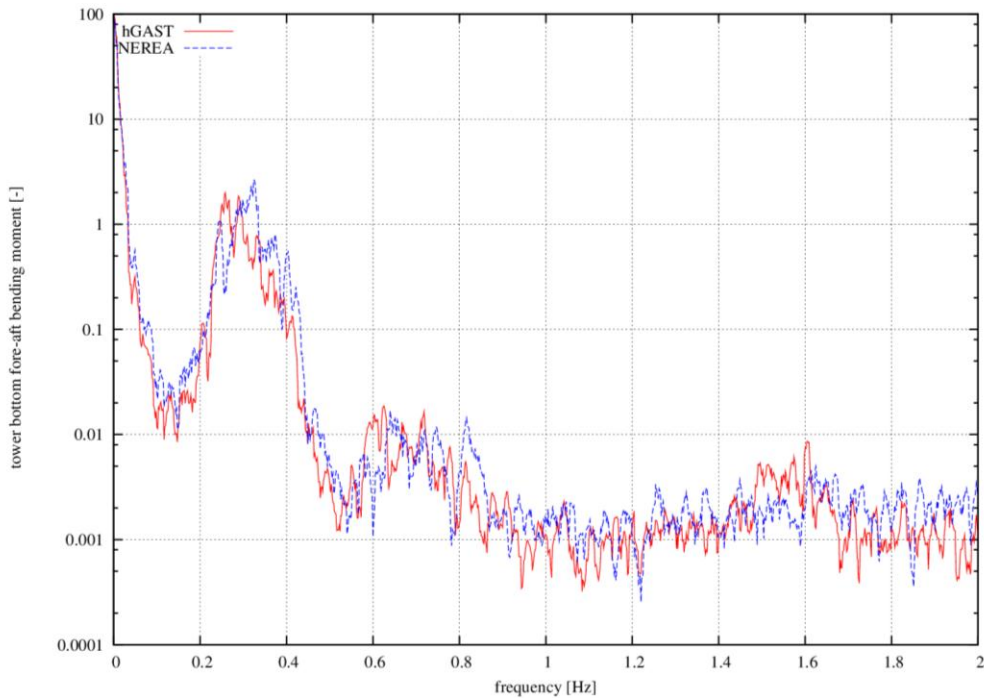
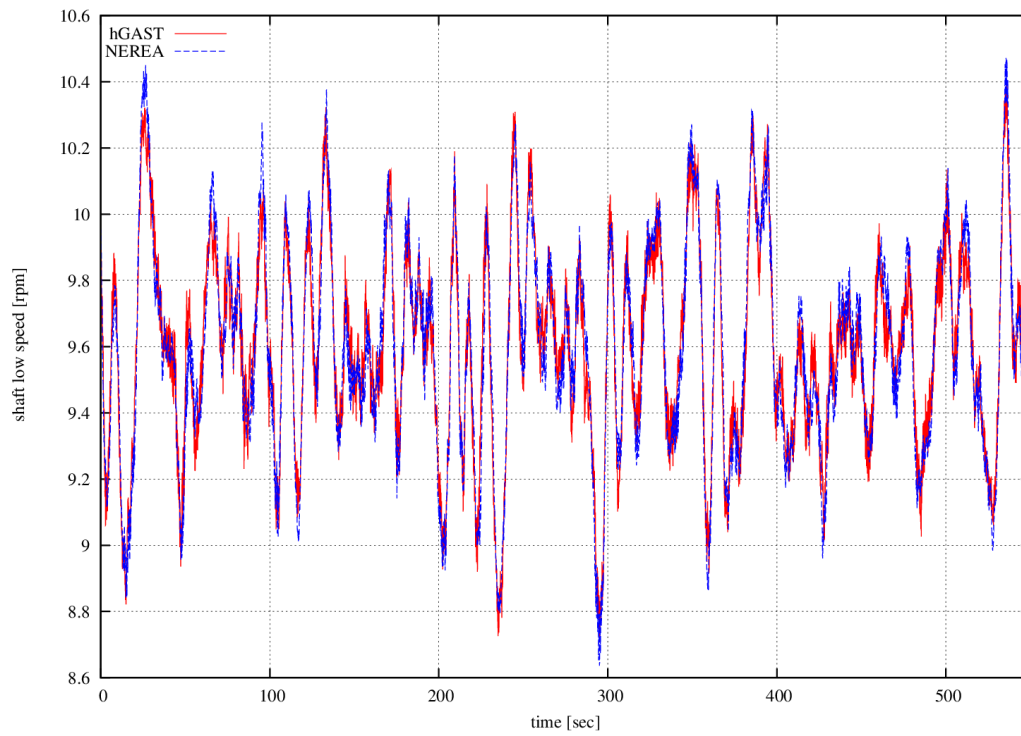
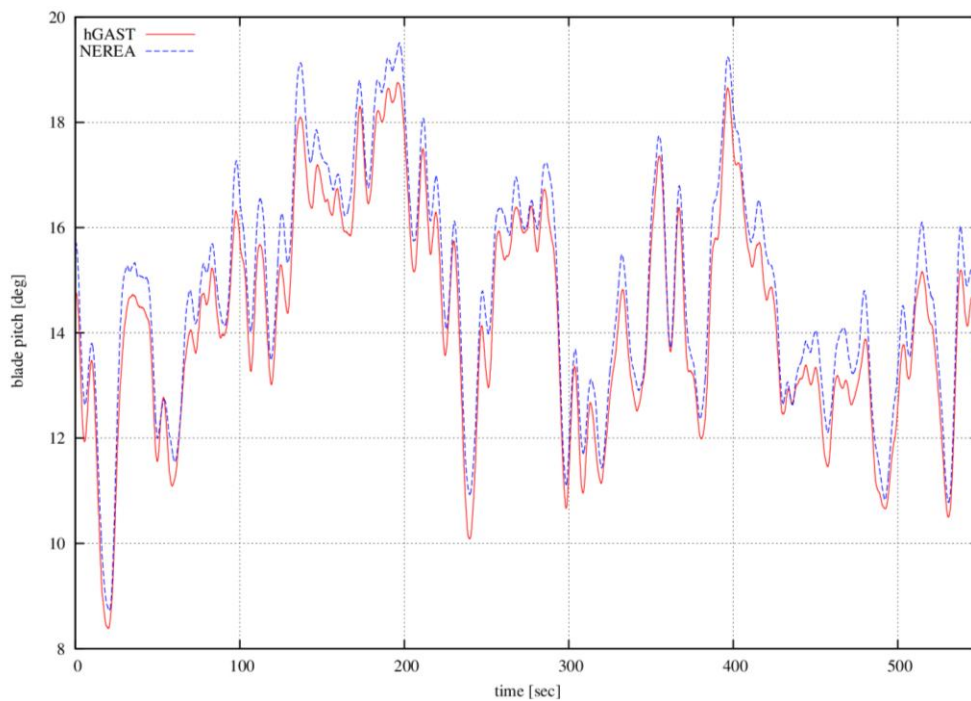


Figure 101: PSD of the tower bottom fore-aft bending moment at 8m/s.

**18 m/s case (hGAST vs. NEREA modal – closed loop)**



**Figure 102: Time series of the rotor speed at 8m/s.**



**Figure 103: Time series of the generator torque at 8m/s.**

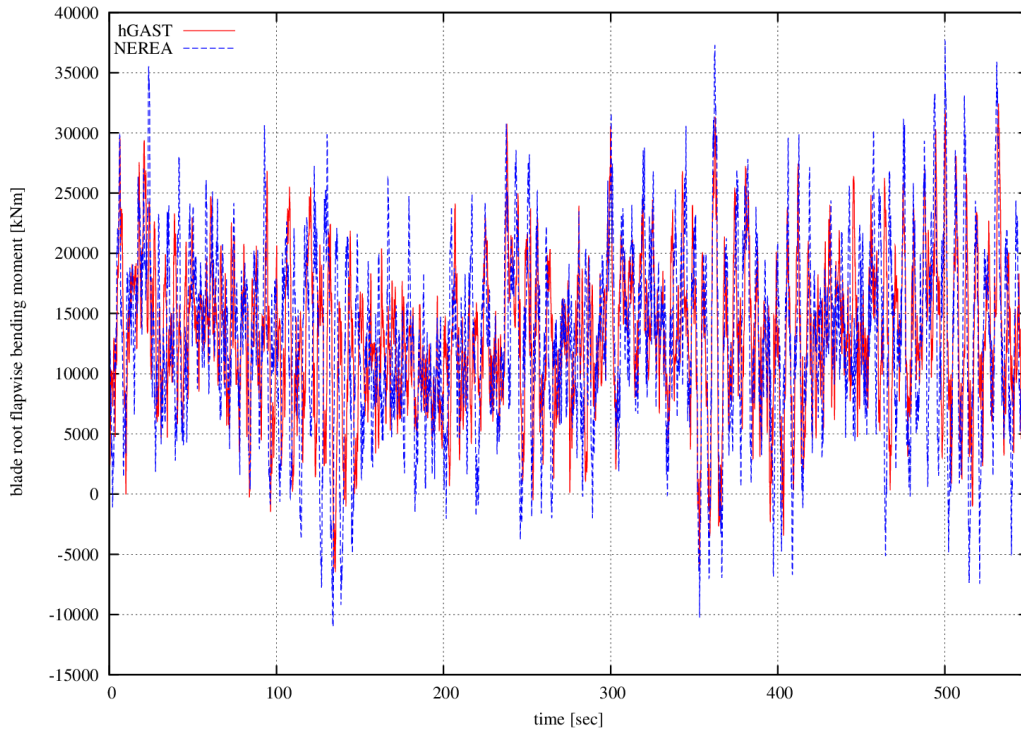


Figure 104: Time series of the flapwise bending moment at the root of the blade at 18m/s.

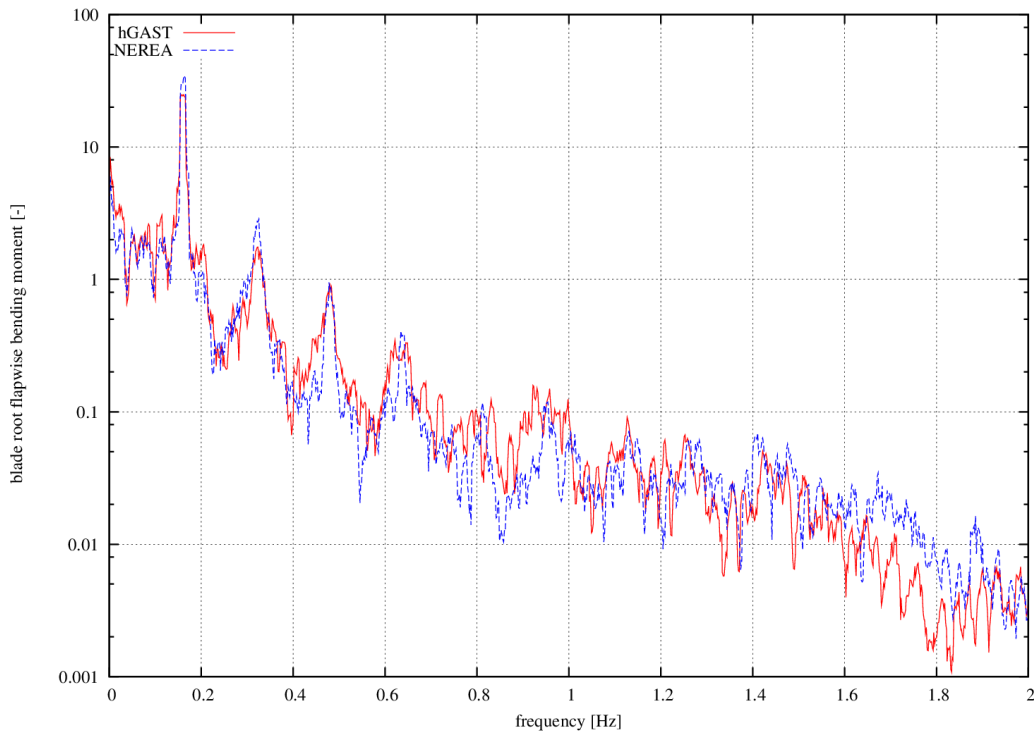


Figure 105: PSD of the flapwise bending moment at the root of the blade at 18 m/s.

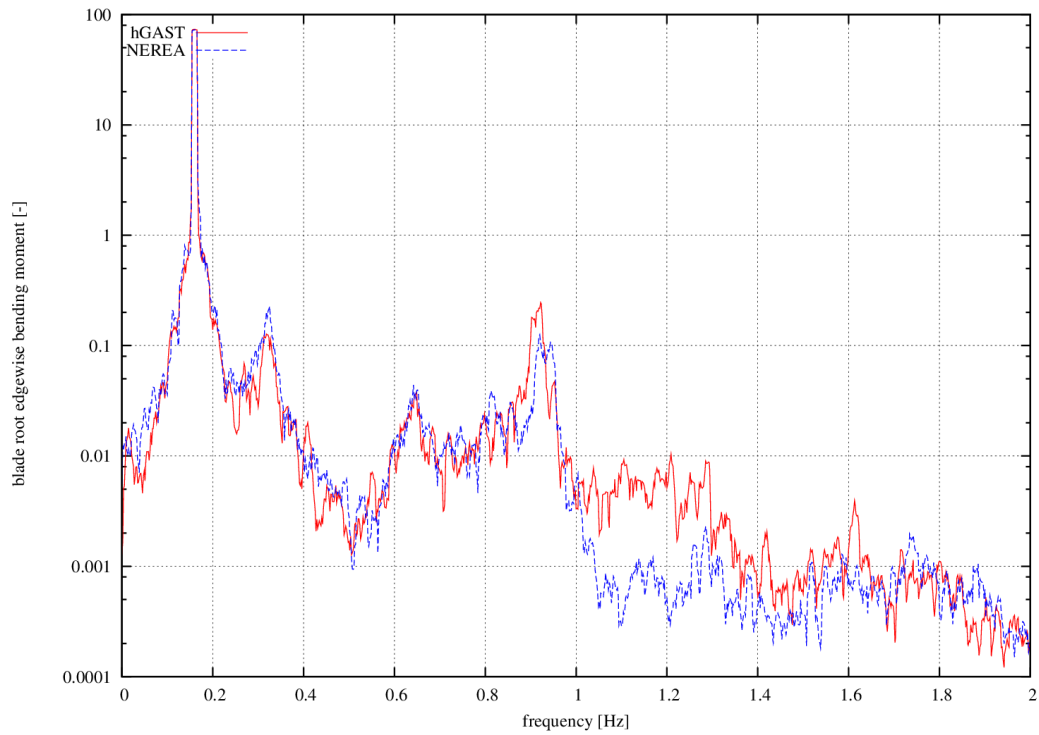


Figure 106: PSD of the edgewise bending moment at the root of the blade at 18m/s.

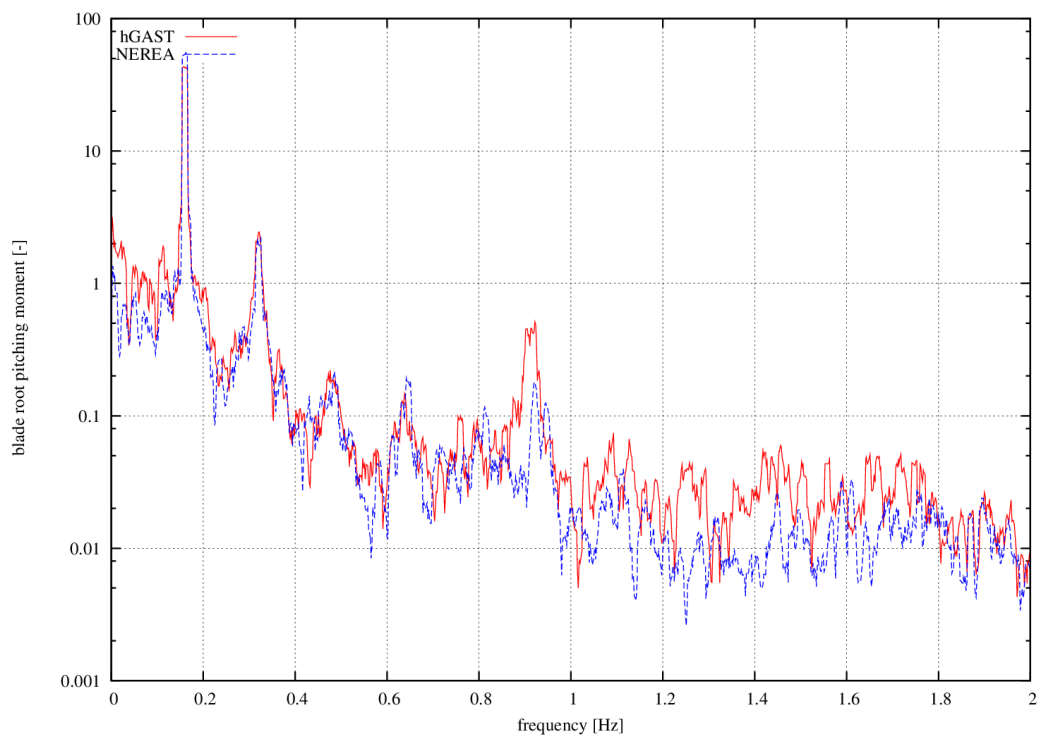


Figure 107: PSD of the pitching moment at the root of the blade at 18m/s.

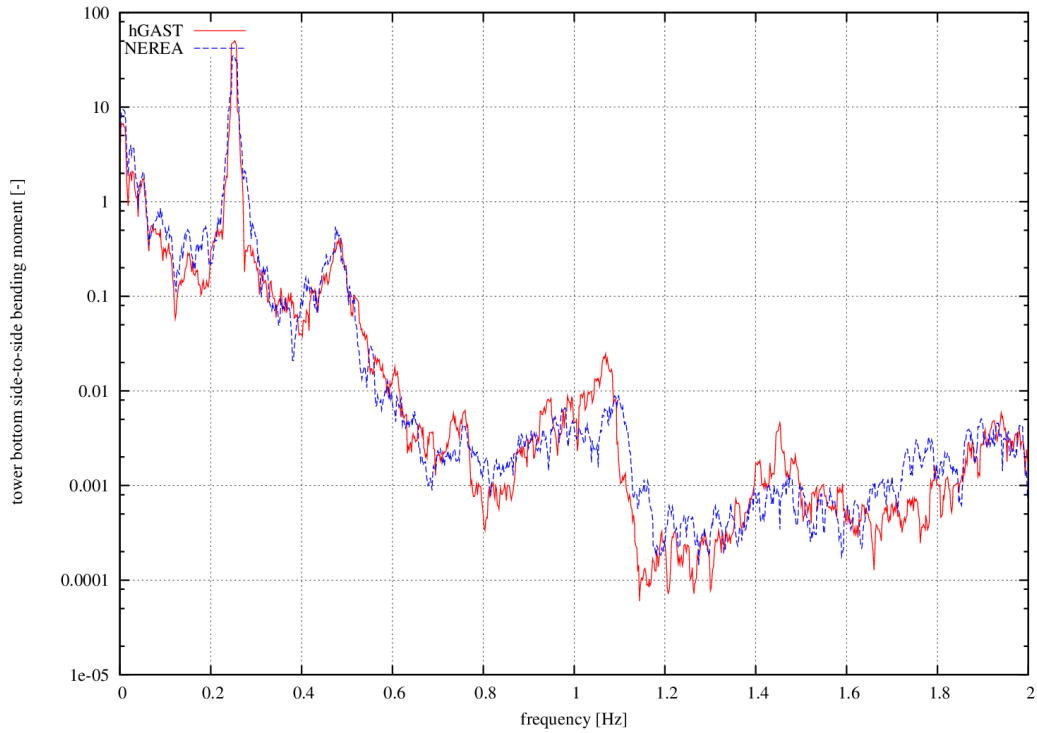


Figure 108: PSD of the tower bottom side to side bending moment at 18m/s.

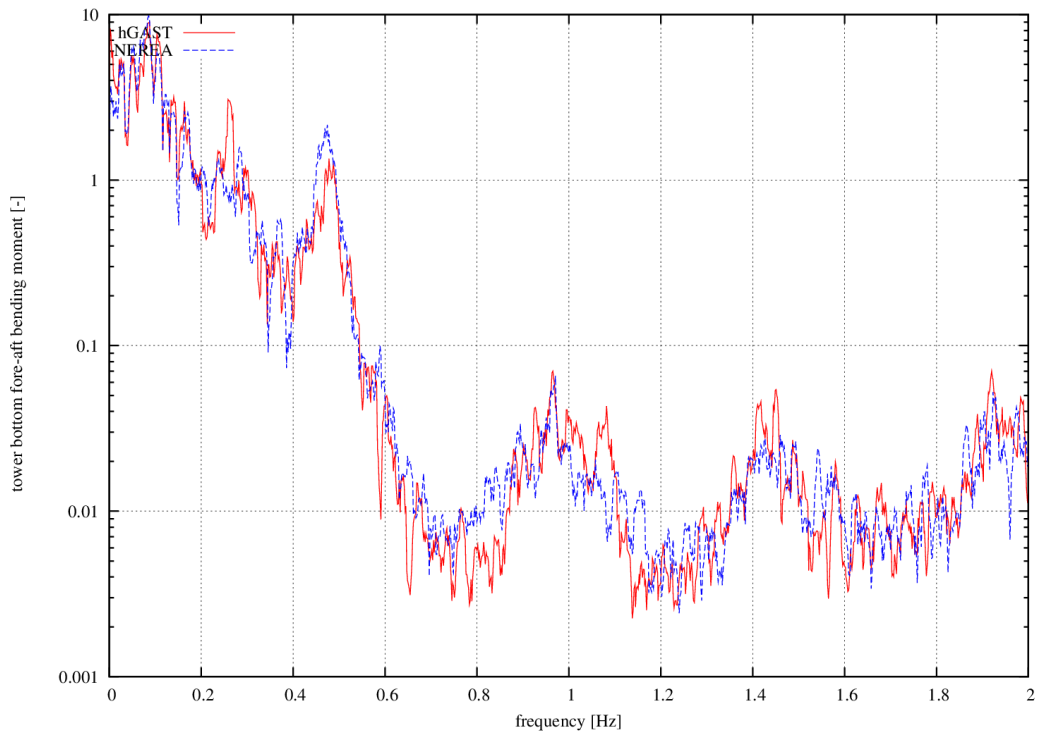


Figure 109: PSD of the tower bottom fore-aft bending moment at 18m/s.

## BIBLIOGRAPHY

- Bak, C. Z. (2013). *Description of the DTU 10 MW Reference Wind Turbine*. Report-I-0092.
- Bauchau, O., Botasso, C., & Nikishkov, Y. (2001). Modelling Rotorcraft Dynamics with Finite Element Multibody Procedures. *Math. Comput. Model.* 33, 1113-1137.
- Bossanyi, E. (2013). *Reference Wind Turbine Design, Reference Wind Turbine Controller Validation*. INN WIND.EU Deliverable D1.2.1 2013.
- Botasso, C., & A., C. (2006-2013). *Cp-Lambda: Users Manual*. Milano: Dipartimento di Ingegneria Aerospaziale, Politecnico di Milano.
- Bottasso, C. C. (2006-2015). *Cp-Lambda User's Manual*. Dipartimento di Scienze e Tecnologie Aerospaziali. Politecnico di Milano, Milano, Italy.
- Gérardin M., C. A. (2001). *Flexible Multibody Dynamics. A Finite Element Approach*. Chichester: John Wiley & Sons Ltd.
- Larsen T J, H. A. (2004). Aeroelastic effects of large blade deflections for wind turbines. *The Science of making Torque from Wind*, (pp. pp 238-246).
- Larsen, T., & Yde, A. (n.d.). Welcome to HAWC2! Retrieved 2013 йил 28-September from <http://hawc2.dk/>.
- Lekou, D. J., & Chortis, D. (2013). *Benchmarked aerodynamic-structural design methods, Part A: Results of the benchmark for blade structural models*. Innwind.EU Deliverable D2.21.
- Manolas D.I., R. V. (2014). Assessing the importance of geometric non-linear effects in the prediction of wind turbine blade loads. *Computational and Nonlinear Dynamics Journal*, Vol. 10, 041008.
- Peters, & He. (n.d.). Dynamic Inflow model.
- Pirrung, G. M. (2014). A Coupled Near and Far Wake Model for Wind Turbine Aerodynamics. *submitted to Wind Energy*.
- Riziotis, V., & Voutsinas, S. (1997). Gast: A General Aerodynamic and Structural Prediction Tool for Wind Turbines. *Proceedings of the EWEC`97*. Dublin, Ireland.
- Sieros, G. C. (2012). Upscaling wind turbines. Theoretical and practical aspects and their impact on the cost of energy. *Wind Energy*, vol15, issue 1, pp 3-17.
- Voutsinas, S. (2006). Vortex methods in aeronautics: how to make things work. *International Journal of Computational Fluid Dynamics*, Vol. 20, pp. 3-18.
- Zahle, F., Riziotis, V. A., Bergami, L., & Madsen, H. A. (2013). *Benchmarked aerodynamic-structural design methods, Part A: Results of the benchmark for blade structural models*. Innwind.EU Deliverable D2.21.

